# Modèles d'échanges ioniques dans le rein: théorie, analyse asymptotique et applications numériques

Magali Tournus

Laboratoire Jacques-Louis Lions, UMR 7598
Université Pierre et Marie Curie-Paris 6 & CNRS

Thèse de doctorat

# Modèles d'échanges ioniques dans le rein : théorie, analyse asymptotique et applications numériques

*Magali Tournus*

Sous la direction de (par ordre alphabétique) :
Aurélie Edwards, Benoit Perthame et Nicolas Seguin

*Rapporteurs* :

**Florence Hubert**
Professeur, Université Aix-Marseille

**Roberto Natalini**
Dirigente di Ricerca, CNR

*Soutenance le 3 juillet 2013 devant le jury* :

**Luis Almeida**
Directeur de recherche, CNRS

**Irene Gamba**
Professeur, Austin, Texas

**Benoît Perthame**
Professeur, Université Pierre et Marie Curie-Paris 6

**Randall S. Thomas**
Directeur de recherche, IGR, Evry

**Aurélie Edwards**
Directrice de recherche, CRC

**Florence Hubert**
Professeur, Université Aix-Marseille

**Nicolas Seguin**
Maître de conférence, Université Pierre et Marie Curie-Paris 6

*à Paulette*

# Remerciements

Merci à mes directeurs de thèse d'avoir bien voulu me prendre en thèse, et d'avoir construit un sujet de thèse aussi enthousiasmant. Je leur suis très reconnaissante pour leur soutien, pour la liberté qu'ils m'ont donnée, et pour leur aide de tous les jours.

Aurélie Edwards avec qui j'ai eu beaucoup de plaisir à travailler. J'ai beaucoup appris en l'observant, tant sur le plan scientifique qu'humain. Je vais essayer de m'inspirer de son exemple.

Benoit Perthame, qui malgré toutes ses responsabilités m'a consacré beaucoup de son temps. Je le remercie pour sa patience et pour ses conseils avisés, que je mettais souvent plusieurs semaines à comprendre. Je le remercie aussi de m'avoir fait voyager, me permettant ainsi de participer à des conférences dans le monde entier.

Nicolas Seguin, que je remercie lui aussi pour sa patience et pour m'avoir expliqué ce qu'étaient les mathématiques appliquées et la modélisation, en plus du reste.

Je remercie beaucoup Florence Hubert et Roberto Natalini d'avoir fait un rapport sur ma thèse.

Je remercie les membres du jury de me faire l'honneur d'être là. Irene Gamba, Luis Almeida, et Randall Thomas, qui grâce à son expérience des modèles du néphron nous a souvent aidés à interpréter des problèmes de code.

Je remercie Alain Doucet et son laboratoire de m'avoir accueillie pendant mon stage de M2 et une bonne partie de ma première année de thèse. J'ai été très impressionnée par le laboratoire de physiologie et physiopathologie rénale. Surtout par les réunions du vendredi. C'est comme ça que j'imaginais la recherche quand j'étais petite.

Je remercie Pascal Houillier pour les entrevues que nous avons eues.

Le laboratoire JLL est un cadre de travail exceptionnel qui m'a permis de côtoyer des chercheurs ausi exceptionnels. Merci à tous.

Merci à Lorette, toujours si enthousiaste. Surtout pour cette soirée, où, dans un bar de Londres, tu m'as annoncé que tu venais de comprendre qu'il fallait prendre $\sigma = 0$ dans les vasa recta pour avoir le bon gradient.

Merci à Ariane et Juliette pour leurs questions et leurs réponses.

Merci à mes frères et soeurs de thèse, comme on dit. Anne-Céline (ma jumelle), Thibaud, Sepideh et Pierre.

Merci à ceux qui se sont occupés de mon ordinateur portable quand il en avait besoin : Khashayar, Fabien et Thibaud.

Merci à Corentin Lacombe de rendre les démarches administratives si faciles et si claires.

Merci à tous ceux qui participent à la bonne ambiance du labo. Entre autres, les membres permanents et étendus du bureau de mon directeur, tous les thésards du LJLL. Un petit clin d'oeil particulier à mes co-bureaux : Benjamin et ses récits de voyage, Quang et ses questions surréalistes, et Wafaa, toujours si attentionnée. Et à mes anciens co-bureaux : André, Bang, Jean-Paul, Laurent, Malik, Nancy et Tobias. Merci à Christian David d'avoir imprimé et relié cette thèse.

Et... bravo aux pilotes de tous les avions que j'ai été amenée à prendre pendant ma thèse. Ils ont tous très bien conduit.

*Je ne sais pas si vous vous êtes déjà trouvés dans ce genre de situation où vous n'avez pas posé à temps la question qu'il aurait fallu poser. Si vous vous étiez pris à temps, personne n'aurait trouvé à redire. Mais voilà, vous avez attendu un peu trop, et si vous posez la question maintenant, les gens vont se demander pourquoi vous leur avez fait perdre leur temps en les laissant parler, alors que vous n'y compreniez rien.*

*R. Feynman*

## Résumé

Cette thèse de mathématiques appliquées traite de problèmes théoriques, numériques et asymptotiques en transport motivés par la physiologie rénale. Plus précisément, elle vise à comprendre et quantifier les échanges de solutés qui peuvent mener dans des cas pathologiques à des néphrocalcinoses, qui se caractérisent par des dépôts calciques dans le parenchyme rénal.

Le manuscrit est constitué de deux parties.

La première partie concerne le développement et l'analyse mathématique d'un modèle simplifié du rein. Il s'agit d'un système de 3 EDP hyperboliques à vitesses constantes, couplées par leur terme source non linéaire et assorti de conditions aux bords spécifiques. Le modèle rentre dans le cadre des modèles cinétiques avec un nombre fini de vitesses et des conditions aux bords de type réflexion. Nous montrons que ce système est bien posé, qu'il tend en temps grand vers un état stationnaire. On montre que le taux de convergence est exponentiel avec des éléments spectraux. Nous proposons l'étude du rôle de deux paramètres à travers une analyse asymptotique. L'une d'entre elles nous place dans le cadre de la relaxation hyperbolique vers une loi de conservation scalaire avec un flux hétérogène en espace sur un domaine borné.

La deuxième partie concerne le développement et l'analyse numérique d'un modèle réaliste du rein. Il s'agit d'un système de 27 équations aux dérivées partielles de type hyperboliques dont les vitesses sont les solutions de 8 équations différentielles non linéaires, et toutes ces équations sont couplées par leur terme source. Les conditions aux bords sont là aussi spécifiques au modèle. Nous interprétons ensuite les résultats obtenus d'un point de vue physiologique, en proposant des prédictions de profils de concentration calciques dans le rein, dans le cas normal et dans certains cas pathologiques.



## Abstract

This thesis of applied mathematics deals with theoretical, numerical and asymptotic questions in transport, motivated by the renal physiology.

More specifically, the purpose is to understand and quantify solute exchanges in physiological and pathological cases and to explain why nephrocalcinosis, i.e. the deposition of calcium salts in kidney tissue, arise.

The manuscript is divided in two parts.

The first part describes the development and the mathematical analysis of a simplified kidney model. It is a system of 3 hyperbolic PDE's with constant velocities, coupled by a non-linear source term and with specific boundary conditions. This model can be considered in the framework of kinetic models with a finite number of velocities and reflexion boundary conditions. We prove that the system is well posed and that it relaxes toward the unique stationary state for large time with an exponential rate of convergence. Thanks to a spectral analysis, we prove that the rate of convergence is exponential. We study the role of two parameters through an asymptotic analysis. One of these analyses is formulated in the framework of hyperbolic relaxation toward a scalar conservation law with an heterogeneous flux on a bounded domain.

The second part describes the development and the numerical analysis of a realistic kidney model. It is an hyperbolic system of 27 hyperbolic partial differential equations whose velocities are solutions to 8 non linear differential equations, all coupled by their source term. The boundary conditions are also very specific. We then interpret the results from a physiological point of view, by predicting calcium concentration profiles in the kidney, under normal conditions and in some specific pathological cases.

# Contents

# Chapitre 1

# Introduction générale

Ma thèse porte sur l'étude d'un modèle d'une partie du rein. J'ai effectué ma thèse sous la direction d'Aurélie Edwards (du Centre de Recherche des Cordeliers au laboratoire de Génomique, Physiologie et Physiopathologie Rénales dans le 6 ème arrondissemnt de Paris), de Benoît Perthame, et de Nicolas Seguin (du laboratoire Jacques Louis Lions de Paris 6), sur le site de Jussieu.

### Quelques mots sur le rein

Pour pouvoir survivre, les cellules du corps doivent baigner dans un environnement physico-électro-chimique à peu près constant. Certaines quantités physiques comme la température, la glycémie ou la concentration sanguine en certains ions doivent rester dans des intervalles étroits au cours du temps. Le rein est un organe qui a pour rôle de maintenir l'homéostasie du sang. En particulier, il garantit que le débit sanguin et la concentration sanguine en les solutés présents dans l'organisme restent constants malgré les variations extérieures. Les variations extérieures, ce sont en particuler les apports alimentaires qui changent en fonction de la saison, de l'heure de la journée, des habitudes culturelles, mais aussi d'autres facteurs (perturbations liées aux pathologies, au stress). En première approche, on peut considérer le rein comme une boîte noire qui en entrée reçoit le sang avec des concentrations de solutés qui peuvent être différentes de celles visées à l'équilibre, et qui rend en sortie d'une part du sang avec des concentrations en soluté optimales pour le bon fonctionnement de l'organisme, sang qui est réinjecté dans la circulation générale, et d'autre part un fluide qui est constitué du reste d'eau et de solutés. Ce fluide est destiné à devenir plus tard l'urine (Figure 1.1). En moyenne, le rein filtre 180 litres de sang par jour. Environ 179 litres sont réinjectés dans l'organisme, et 1,5 litre est excrété dans l'urine.

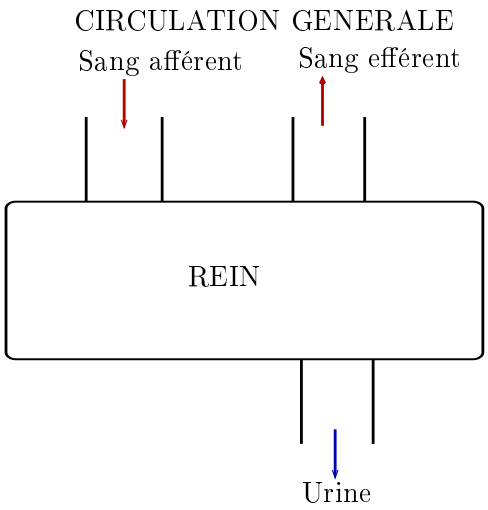


**Figure 1.1** – Représentation très schématique du rein

Si par exemple le sang qui arrive dans le rein est trop concentré en sodium, le rein va produire un filtrat plus concentré en sodium que le sang en entrée, et réinjecter dans la circulation générale du sang moins concentré en sodium. C'est le mécanisme de concentration urinaire. Pour la suite, on se placera toujours dans la situation où la concentration en sodium est trop élevée. Pour comprendre un peu mieux le mécanisme de concentration urinaire, nous allons rentrer un peu plus précisément dans l'architecture du rein.

Le rein est constituée de deux parties : le cortex et la médulla (Figure 1.2). Le cortex constitue la partie externe, la médulla la partie interne. La médulla est constituée de pyramides rénales et c'est au niveau de la pointe de chaque pyramide (appelée la papille) que le filtrat destiné à devenir l'urine est récolté. Chaque pyramide est constitué de tubes de différentes tailles dans lesquels circule un fluide (du sang dans les vasa recta, un filtrat dans les tubules). Le fluide dans lequel

sont dissous les solutés est transporté à contre courant dans les tubes (certains tubes sont dits "ascendants" , d'autres "descendants") et des échanges d'eau et de solutés se font entre les tubes à travers les parois, via l'interstitium. Il s'établit alors un "gradient de concentration", c'est à dire que la concentration d'un soluté donné croît en fonction de la profondeur dans chaque tube. Le mécanisme de concentration urinaire n'est encore pas complètement élucidé actuellement. Les modèles actuels parviennent à montrer la présence d'un gradient de concentration dans la partie haute de la médulla (la médulla externe). En revanche, rien ne permet d'expliquer pourquoi ce gradient continue d'exister dans la partie basse de la médulla (médulla interne). Précisons que la dénomination "tubes ascendants-tubes descendants" ne fait pas référence à l'habituel "haut-bas" défini grâce au champ gravitationnel. Le rein est un organe organisé autour d'un centre qui est défini comme "le bas" (Figure 1.2). Le haut est alors la partie corticale (i.e. : le cortex).

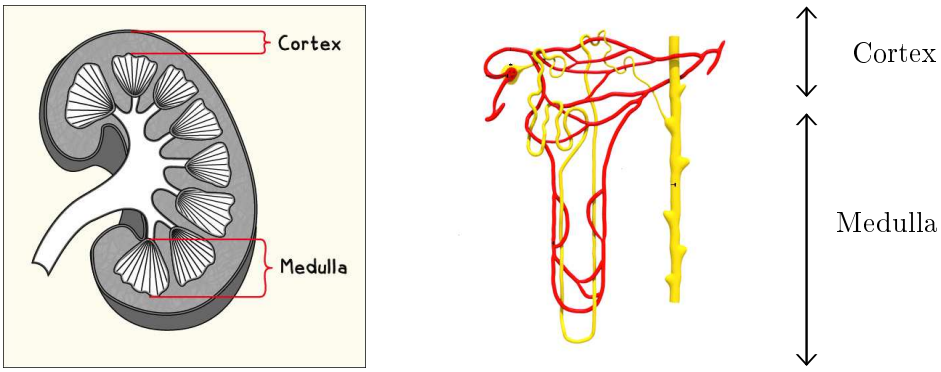


**Figure 1.2** – A gauche : Représentation d'un rein. On distingue deux zones : Le cortex et la médulla. Dans cette représentation, on dénombre 8 pyramides de Malpighi. A droite : Chaque unité de tubes constituée d'un tubule descendant, d'un tubule ascendant et d'un tube collecteur est appelée un néphron. En jaune, un néphron. En rouge, les vaisseaux sanguins appelés vasa recta descendants et ascendants.

### But du projet

Certaines pathologies rénales liées aux anomalies de transport de calcium, les néphrocalcinoses en particulier, demeurent très mal comprises [77]. Elles se caractérisent par des dépôts de $Ca^{2+}$ dans le parenchyme rénal, s'accompagnent fréquemment d'une hyper-calciurie (i.e., une concentration urinaire de $Ca^{2+}$ anormalement élevée) et évoluent souvent vers l'insuffisance rénale. Différents scénarios sont envisagés pour expliquer l'apparition des néphrocalcinoses. Un modèle mathématique qui intègre le transport de $Ca^{2+}$ à travers les différents segments tubulaires, vasculaires, et l'interstitium permettra de valider ou de réfuter certaines hypothèses. Plus précisément, le modèle développé a pour but : (1) de déterminer précisément les concentrations interstitielles, vasculaires, et tubulaires du $Ca^{2+}$ dans le rein dans le cas basal (par opposition à des cas pathologiques) (2) d'évaluer l'impact de mutations de protéines impliquées dans la réabsorption du $Ca^{2+}$ dans le rein afin de comprendre les mécanismes sous-jacents à l'hypercalciurie. Les concentrations calciques interstitielles n'ont encore jamais été déterminées, mais des mesures sont en cours au Centre de Recherche des Cordeliers et elles sont pour le moment en adéquation avec les prédictions du modèle.

### Les modèles existants

Le modèle macroscopique est unidimensionnel en espace. Les quantités qu'il nous intéresse de déterminer sont des concentrations ioniques ou moléculaires et des débits d'eau dans les néphrons et les vaisseaux sanguins. Le premier modèle mathématique du néphron a été développé dans les

années 50 dans le but d'expliquer le gradient de concentration [33]. C'est la première fois que le mécanisme de concentration urinaire est vu comme une simple conséquence du transport à contre courant et des échanges à travers les parois tubulaires. Un historique des modèles des années 50 aux années 90 peut être consulté dans [84]. Un peu plus tard, des considérations sur l'architecture globale du rein [55] ont montré que la répartition du nombre de tubes en fonction de la profondeur, qui donne la forme aux pyramides rénales, jouaient un rôle dans l'établissement du gradient de concentration. Jusqu'à présent, les modèles ont été développés afin de comprendre les mécanismes de concentration urinaire, ils ne concernent donc que les composants majoritaires de l'urine, à savoir l'eau, le chlorure de sodium et l'urée. Plusieurs modèles contenant des raffinements ont été étudiés numériquement dans le but de comprendre un peu mieux les facteurs intervenant dans le mécanisme de concentration urinaire. Pour la majorité, ce sont des modèles stationnaires qui consistent en un système d'équations différentielles couplées. Nous avons choisi de développer un modèle dynamique, d'une part pour l'intérêt propre d'avoir un modèle dynamique, ce qui nous permettra par la suite d'observer l'évolution des concentrations et des débits d'eau en fonction du temps et non pas seulement à l'équilibre, et d'autre part dans l'optique de faire converger ce modèle dynamique vers l'état stationnaire qui lui est associé. Il s'agit d'une stratégie numérique fréquemment utilisée pour calculer les solutions d'un système à l'équilibre. Le système différentiel n'est pas un problème de Cauchy, à cause des conditions aux bords qui lui sont associées, et on ne peut pas utiliser de méthodes de résolutions d'EDO classiques. C'est à notre connaissance le premier modèle dynamique qui prend à la fois en compte la répartition exponentielle du nombre du tubes en fonction de la profondeur, et qui inclut le transport de calcium.

## 1.1 Première prise en main du modèle

### 1.1.1 Quelques concepts de base sur le transport membranaire

Nous proposons ici un exposé des différentes expressions de flux à travers une membrane biologique [78]. Nous définissons également les coefficients qui caractérisent ce transport. On considère deux compartiments séparés par une membrane, contenant de l'eau dans laquelle est dissous un soluté. On appelle $\lambda$ la longueur de la membrane, et $C^A$ et $C^B$ les concentrations respectives du soluté dans les compartiments $A$ et $B$.

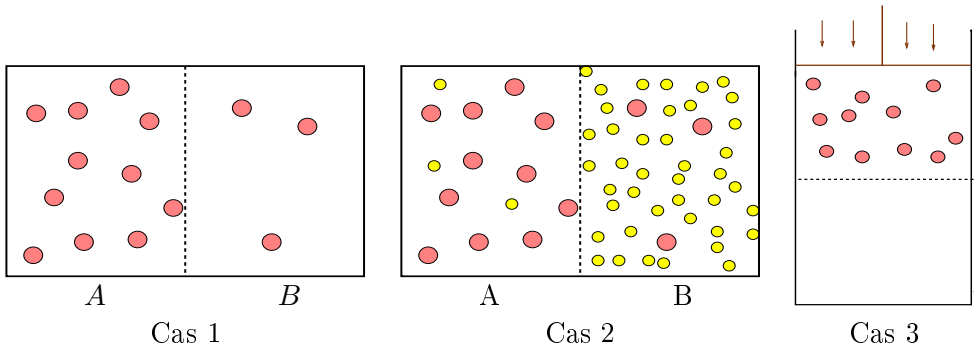


**Figure 1.3** – $A$ et $B$ sont deux compartiments de volume identique séparés par une membrane de longueur $\lambda$. Les petites boules jaunes et roses sont des solutés quelconques. Les molécules d'eau ne sont pas représentées.

#### Diffusion

Les solutés ne restent pas immobiles et ont des mouvements tantôt de droite à gauche et tantôt de gauche à droite avec même probabilité. Sur la Figure 1.3-Cas 1, il y a en moyenne plus de solutés situés du côté le plus concentré ($A$) qui traverseront la membrane que de solutés situés

du côté le moins concentré ($B$). On a alors un flux de diffusion net de solutés du côté $A$ vers le côté $B$. Le flux diffusif de soluté du compartiment $A$ vers le compartiment $B$ s'exprime en $mol.m^{-1}.s^{-1}$ est donné par

$$J_{diffusion} = P\lambda(C^B - C^A),$$

où $P$ est la perméabilité de la membrane au soluté en question, qui s'exprime en $m.s^{-1}$ et qui est proportionnelle à l'inverse de la taille du soluté, à l'inverse de l'épaisseur de la membrane, et au coefficient de partage du soluté entre l'eau et la membrane. La membrane, dans le cas des membranes biologiques, est constituée d'une couche de lipides, et le coefficient de partage est un coefficient qui mesure comment, à l'équilibre, le soluté se partage entre les deux solvants eau et couche lipidique. Si comme dans la Figure 1.3-Cas 2, plusieurs solutés sont en présence, et si les concentrations ne sont pas trop élevées, chaque soluté se diffuse indépendamment des autres.

**Osmose**

Les molécules d'eau elles aussi se diffusent. Sur la Figure 1.3-Cas 2, le côté $B$ qui contient plus de particules de solutés que le côté $A$ contient par conséquent moins de molécules d'eau. Il y a donc un flux net de diffusion d'eau du côté $A$ qui a une plus faible osmolarité, vers le côté $B$. On définit l'osmolarité d'une solution comme le nombre de moles de particules en solution dans 1 litre de solution.

$$Osm = \sum_{i=\text{solutés}} \Phi_i C_i$$

où $\Phi_i$ est le coefficient osmotique d'un soluté. Ce coefficient mesure la quantité de particules que va donner un soluté dans la solution. Par exemple, l'urée qui est un soluté qui ne se dissocie pas dans l'eau a un coefficient osmotique de 1. Par contre, le chlorure de sodium NaCl donne en solution deux ions $Na^+$ et $Cl^-$ avec une certaine constante de réaction. Son coefficient osmotique est alors compris entre 1 et 2. Il est de 1.82. Ce phénomène de diffusion de l'eau est simultané au phénomène de diffusion des solutés et dans le cas où la membrane est parfaitement perméable à l'eau comme au soluté, il n'y a de variation de volume dans aucun des deux compartiments. Si on se place dans le cas où la membrane de la Figure 1.3-Cas 2 est perméable à l'eau mais imperméable au soluté, seule l'eau pourra passer de $A$ vers $B$, et il y aura une modification du volume des deux compartiments. Supposons que seul le bord droit du compartiment $B$ soit mobile. On définit alors la pression osmotique comme la pression qu'il faudrait exercer sur le bord droit de $B$ pour empêcher tout mouvement d'eau de $A$ vers $B$, et s'exprime

$$\Pi = RT(Osm^B - Osm^A),$$

où $R$ est la constante des gaz parfaits et $T$ la température. Cette expression est valide uniquement dans le cas d'une membrane totalement imperméable au soluté. Pour s'approcher un peu plus de la réalité, on considère des membranes à la fois perméables au soluté et à l'eau. Cependant, la plupart des membranes biologiques ne laissent pas passer les solutés aussi bien que l'eau. Cette différence de perméabilité aux différentes espèces est due au niveau microscopique à la présence (ou à l'absence) de protéines membranaires (transporteurs ou tunnels) qui facilitent la diffusion. On mesure cette sélectivité membranaire en introduisant le coefficient de réflexion du soluté par rapport à la membrane noté $\sigma$. On considère une solution aqueuse (en haut sur la Figure 1.3-Cas 3), dans lequel est dissous le soluté avec une concentration $C^I$. On fait passer le soluté à l'aide d'un piston à travers la membrane, et on note $C^F$ la concentration en le soluté dans la solution aqueuse récupérée en bas. On définit le coefficient de réflexion du soluté comme

$$\sigma = 1 - \frac{C^F}{C^I}.$$

En particulier, si la membrane est imperméable au soluté, $C^F = 0$ et $\sigma = 1$. Les déterminants physiques du coefficient de réflexion d'un soluté par rapport à une membrane sont les voies à

travers lesquelles l'eau et le soluté traversent la membrane. Si tous les canaux qui laissent passer l'eau laissent également passer les solutés, $C^F = C^I$ et $\sigma = 0$. En tenant compte de la sélectivité membranaire, la pression osmotique s'écrit

$$\Pi = RT\Phi\sigma(C^B - C^A).$$

Le flux volumique du compartiment $B$ vers le compartiment $A$ dépend de la pression osmotique (on néglige la pression hydrostatique) et a pour expression

$$J_V = \lambda L_P RT\Phi\sigma(C^B - C^A)$$

où $L_P$ est la perméabilité de la membrane à l'eau. Dans la suite du manuscrit, puisque que l'eau est majoritaire devant les solutés, on parlera souvent par abus de langage de flux d'eau. Ce flux volumique, dû à la pression osmotique, a une conséquence sur le flux de soluté, appelée effet solvant ou convection des solutés. En effet, si un volume de solution bouge d'un compartiment à un autre, il contiendra de l'eau mais aussi des solutés. Dans le cas de la Figure 1.3-Cas 2,

$$J_{convection} = (1 - \sigma)J_V C^B,$$

La diffusion et l'osmose sont deux phénomènes passifs et uniquement dus à des mouvements statistiques. La convection dérive uniquement de phénomènes passifs, mais elle peut faire bouger les solutés à contre-gradient. Dans l'exemple de la figure 1.3-Cas 2, le soluté rose passe de gauche à droite par diffusion, mais est entraîné par le flux volumique et passe de droite à gauche par convection.

### Electro-diffusion

Notre modèle comporte un ion libre, l'ion $Ca^{2+}$. Il est soumis à un potentiel électrique que l'on considérera établi et stationnaire :

$$J_{electrodiffusion} = \frac{2F}{RT}\Delta V_{TE} C^\alpha,$$

où $F$ est la constante de Faraday, 2 est le nombre de charges de l'ion calcium, $\alpha = A$ ou $B$ selon le signe de $\Delta V_{TE}$ et $\Delta V_{TE}$ est la différence de potentiel entre les compartiments $A$ et $B$. Ce flux électro-diffusif entre également potentiellement en compétition avec les flux de diffusion et de convection.

### Transport actif

Les mécanismes décrits ci-dessus sont des mécanismes passifs, et ont tendance à homogénéiser les concentrations de part et d'autre de la membrane. Certaines membranes permettent le transport actif de solutés, c'est-à-dire qu'elles font passer les solutés contre leur gradient de potentiel électrochimique, via des pompes qui nécessitent de l'énergie. Le chlorure de sodium et le calcium sont concernés dans notre modèle par le transport actif. Macroscopiquement, on observe que les transporteurs sont en nombre limité, et qu'il peut ainsi y avoir saturation. Cela se traduit par une modélisation de type Michaelis-Menten [44]. L'approximation macroscopique du flux de transport actif est donné par

$$J_{pompe} = V_m \frac{C}{K_m + C}$$

où $V_m$ est le taux de transport maximal et $K_m$ est la concentration de substrat à laquelle le taux de transport est à la moitié du taux maximal.

### 1.1.2 L'architecture

#### Modèle à cinq tubes

Armés de ces quelques considérations de base sur le rein, nous décrivons à présent un premier modèle. Cette représentation minimale du rein contient 5 tubes, 3 trois d'entre eux représentant le néphron (en jaune sur la Figure 1.2) et les deux autres des vasa-recta (en rouge sur la Figure 1.2). Ce modèle comporte les 5 tubes de base du modèle réaliste étudié dans la partie II. Dans chacun de ces tubes circule un fluide de débit $F$ dans lequel sont dissous des solutés $i \in [1, I]$ avec une concentration $C_i$, $i = 1..I$. Chacun de ces 5 tubes baigne dans un interstitium commun et avec lequel ils peuvent échanger de l'eau et des solutés à travers la membrane tubulaire, à une profondeur donnée. En effet, les cellules interstitielles étant disposées en couches assez serrées, on considère qu'aucun transport ne se fait selon l'axe des $x$ dans l'espace interstitiel.

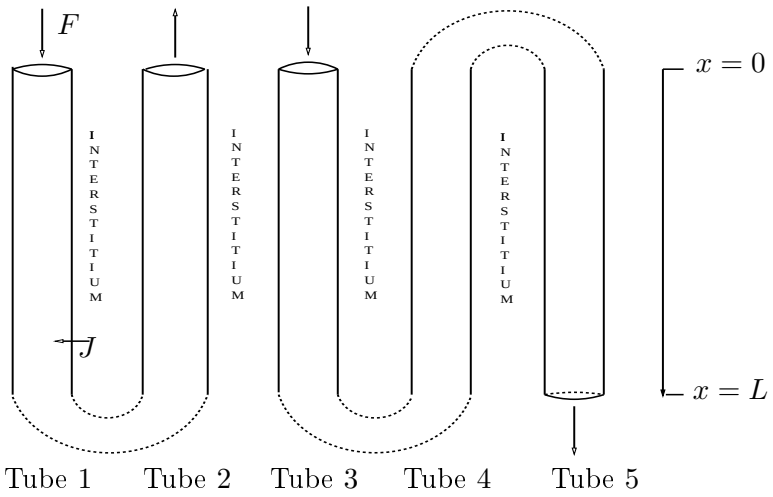


**FIGURE 1.4** – Représentation du modèle. Il est constitué de cinq tubes baignant dans l'interstitium.

Les paramètres ne dépendent que de $x \in [0, L]$ et les variables dépendent de $x$ et du temps $t$. En ce sens, c'est un modèle 1D. Les inconnues du modèles sont les quantités suivantes :

• $F^j(x,t)$ $(m^3.s^{-1})$ est le débit d'eau dans le tube $j$ à la profondeur $x$ au temps $t$. C'est le volume d'eau traversant la surface centrée en $x$ en 1 seconde.

• $J_V^j(x,t)$ $(m^2.s^{-1})$ est le flux d'eau à travers le tube $j$. Il représente la surface signée entrant dans le tube $j$ à la profondeur $x$ en 1 seconde.

• $C_i^j(x,t)(mol.m^{-3})$ est la concentration en le soluté $i$ dans le tube $j$ ($j = 1, ..., 5$ ou $j = int$). Le produit $F^j(x,t)C_i^j(x,t)(mol.s^{-1})$ représente le nombre de moles de soluté $i$ traversant la section à la profondeur $x$ en 1 seconde.

• $J_i^j(x,t)(mol.m^{-1}.s^{-1})$ est le flux de soluté $i$ entrant dans le tube $j$ ($j = 1, ..., 5, int$). Il représente le nombre de moles entrant dans le tube $j$ à la profondeur $x$ en 1 seconde.

### 1.1.3 Le système

Les variables sont reliées par des équations de bilan (conservation de l'eau et de la quantité de matière) pour $0 \leq x \leq L$ et $t > 0$

$$\begin{cases} \dfrac{\partial}{\partial x}F^j(x,t) = J_V^j(x,t), & j = 1,...,5, \\ \pi(R^j)^2(x)\dfrac{\partial}{\partial t}C_i^j(x,t) + \dfrac{\partial}{\partial x}\Big(F^j(x,t)C_i^j(x,t)\Big) = J_i^j(x,t), & j = 1,...,5, \quad i = 1,...,I, \\ \pi(R^{int})^2(x)\dfrac{\partial}{\partial t}C_i^{int}(x,t) = J_i^{int}(x,t), & i = 1,...,I. \end{cases} \tag{1.1}$$

Les flux volumiques sont donnés par

$$J_V^j = 2\pi R^j L_P^j RT \sum_{i=1}^{I} \sigma_i^j \Phi_i \Big(C_i^j - C_i^{int}\Big), \qquad j = 1,3,4,5. \tag{1.2}$$

Dans cette expression, la longueur de la membrane d'échange entre l'intérieur du tube et l'interstitium est de $2\pi R^j$, ce qui correspond au périmètre du tube $j$. Le tube 2 (qui représente les vasa recta ascendants) a une perméabilité à l'eau trop grande pour être mesurée, et le calcul du flux volumique entrant dans ce tube ne peut plus être obtenu par (1.2). On calcule alors $J_V^2$ en faisant l'hypothèse que l'interstitum est à parois rigides et ne peut pas changer de volume. On détermine $J_V^2$ grâce à la condition

$$\sum_{j=1}^{5} J_V^j(x,t) = 0 \qquad \forall t > 0, \qquad \forall x \in [0,L]. \tag{1.3}$$

Le flux de soluté (dans le cas d'un soluté électroneutre) tient compte de la diffusion, de la convection et du transport actif et est donné par

$$J_i^j = -2\pi R^j P_i^j \Big(C_i^j - C_i^{int}\Big) + J_V^j(1-\sigma_i^j)C_i^\alpha - 2\pi R^j V_m^j \frac{C_i^j}{K_m^j + C_i^j}, \tag{1.4}$$

avec

$$C_i^\alpha(x,t) = \begin{cases} C_i^{int}(x,t) & \text{pour } J_V^j(x,t) > 0, \\ C_i^j(x,t) & \text{pour } J_V^j(x,t) \leq 0. \end{cases} \tag{1.5}$$

La conservation des solutés conduit à la condition de fermeture

$$J_i^{int}(x,t) = -\sum_j J_i^j(x,t) \qquad \forall t > 0, \forall x \in [0,L]. \tag{1.6}$$

L'architecture des tubes (voir Figure 2.1) nous pousse à poser les conditions aux limites suivantes

$$\begin{cases} F_1(0) = F_1^0, & F_3(0) = F_3^0, & F_5(0) = -F_4(0), \\ C_1(0) = C_1^0, & C_3(0) = C_3^0, & C_5(0) = C_4(0), \\ F_2(L) = -F_1(L), & F_4(L) = -F_3(L), & \\ C_2(L) = C_1(L), & C_4(L) = C_3(L), & \end{cases} \tag{1.7}$$

où $F_1^0, F_3^0, C_1^0, C_3^0$ sont des constantes positives. En temps grand, la solution du système (1.1) converge vers la solution du problème stationnaire suivant

$$\begin{cases} \dfrac{\partial}{\partial x} F^j(x) = J_V^j(x), & j = 1, ..., 5, \\ \dfrac{\partial}{\partial x}\Big(F^j(x) C_i^j(x)\Big) = J_i^j(x), & j = 1, ..., 5, \qquad i = 1, ..., I. \end{cases} \tag{1.8}$$

Ce sont des variantes de ce dernier système qui sont étudiées dans la première partie du manuscrit.

**Ce qu'il manque à ce modèle simplifié**

- On n'a considéré dans ce modèle que des solutés neutres. En introduisant le calcium, le flux de soluté a un terme en plus qui correspond à l'électro-diffusion.
- L'architecture de base est beaucoup plus complexe dans le modèle plus réaliste. Entre autres, le haut du tube 4 n'est pas directement raccordé au tube 5, par la condition de transmission $C^4(0) = C^5(0)$ mais un tube appelé tube distal les relie. Ce tube distal baigne dans l'environnement cortical qui est considéré comme un bain infini avec des concentrations en tous les solutés fixées dès le départ et qui n'évoluent pas au cours du temps. Le cortex n'a pas non plus de limite de volume.
- Dans le modèle complet, il n'y a pas un seul tube de chaque type mais un continuum de tubes de chaque type avec des longueurs allant de 0 à $L$. On appelle $N^j(x)$ le nombre de tubes de type $j$ à la profondeur $x$, où $N$ est une fonction décroissante donnée. Il y a alors $-(N^j)'(x)$ tubes de type $j$ qui s'arrêtent à la profondeur $x$. On appelle $F(x, y, t)$ le débit volumique dans l'ensemble des tubes de type $j$ qui s'arrêtent à la profondeur $y$, calculé à la profondeur $x$. On fait l'hypothèse que $F(x, y, t)$ ne dépend pas de $y$, et on continue à le noter $F(x, t)$. Les équations de bilan que l'on dérive conservent les quantités $NF$ et $NFC$.

## 1.2 Les conclusions tirées du modèle réaliste

Le but de la seconde partie du manuscrit est de proposer des éléments qui aident à une compréhension des néphrocalcinoses. Dans cette optique nous avons développé un modèle dynamique qui tient compte

- de l'architecture complexe du rein,
- des différents échanges ioniques pouvant avoir lieu à travers les parois tubulaires, qui sont des membranes biologiques.

Nous ne ferons pas dans cette introduction une présentation détaillée du modèle, ceci faisant l'objet du Chapitre 7, mais nous en donnons un bref aperçu dans le but de présenter les résultats obtenus d'un point de vue physiologique.

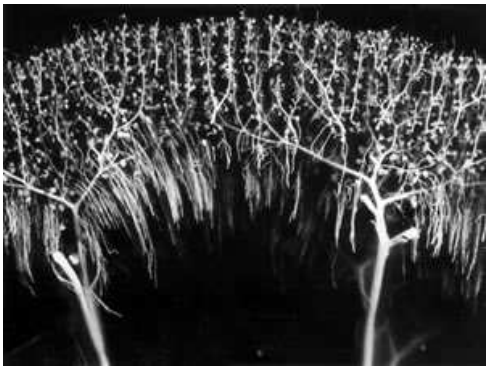

**Figure 1.5** – Cette photographie a été prise par Lise Bankir (CRC). Il s'agit de la vasculature d'un rein de lapin.

Les unités de base que l'on considère sont les néphrons (i.e. les tubules descendants, les tubules ascendants, les tubes distaux et les tubes collecteurs) et les vaisseaux sanguins (i.e les vaisseaux descendants et ascendants). Chaque rein est en réalité constitué de plusieurs dizaines de milliers de telles unités de base chez le rat (près de un million chez l'homme). On peut voir la vasculature d'un rein de lapin sur la photographie, Figure 1.5, ce qui donne une idée de l'architecture générale. Chaque tube $j$ a une taille qui lui est propre, certains s'arêtent avant la médullla, et d'autres vont jusqu'au bout (médulla qui mesure 6 mm chez le rat). C'est ce qui donne aux pyramides rénales leur structure. Notre modèle distingue les néphrons courts, c'est à dire ceux qui s'arrêtent à la frontière entre la médulla externe (partie haute de la médulla) et la médulla interne (partie basse de la médulla), des néphrons longs. A cause du caractère non-linéaire du modèle, ce n'est pas la même chose de considérer $N^{court}(x)$ néphrons courts et $N^{long}(x)$ néphrons longs que de considérer $(N^{court} + N^{long})(x)$ néphrons. Nous prenons en compte trois solutés : le chlorure de sodium, l'urée et l'ion calcium. Les variables sont les débits d'eau et les concentrations de solutés dans chaque type de tube. Nous avons ainsi un système de 27 EDP et 8 EDO couplées.

Les néphrocalcinoses sont des dépôts de calcium dans l'interstitum. Le mécanisme de calcification dans les tubules rénaux est encore méconnu, néanmoins, on sait que les néphrocalcinoses sont largement favorisées par l'hypercalciurie. Notre modèle actuel ne prend en compte que l'ion calcium (et pas l'élément calcium sous sa forme cristalline), et les quantités auxquelles on s'intéresse sont les concentrations calciques et les débit molaires calciques.

Pour décrire les concentrations, les débits molaires et les flux, nous avons adopté le point de vue des biologistes. Ils voient les choses comme suit : La partie interstitielle (interstitum sur les schémas) est considérée comme "l'intérieur" et l'intérieur des tubules est considéré comme "l'extérieur". On peut comprendre ce point de vue en se rappelant que ce qui est à l'intérieur des tubules est destiné à devenir l'urine, et donc à se retrouver à l'extérieur du corps. On emploiera également les terminologies suivantes :

**Définition 1.2.1.**
*Réabsorption : Un soluté est dit réabsorbé s'il passe à travers une membrane tubulaire en allant de l'extérieur vers l'intérieur (i.e. des tubules vers l'interstitum).*
*Sécrétion : Un soluté est dit sécrété s'il passe à travers une membrane tubulaire en allant de l'intérieur vers l'extérieur (i.e. de l'interstitium vers les tubules).*

Nous proposons dans la deuxième partie de ce manuscrit de prédire le gradient interstitiel calcique, la concentration calcique dans l'urine (pour savoir si le sujet est en hypercalciurie ou en hypocalciurie), et à quel endroit le calcium est réabsorbé ou sécrété, et dans quelles proportions. Nous proposons de faire ces prédictions dans un cas normal et dans des cas pathologiques et de déterminer quels sont les paramètres du modèle qui jouent un rôle important dans le bon fonctionnement du rein. Dans les cas pathologiques, nous déterminons également si des compensations peuvent avoir lieu, et si l'équilibre peut être rétabli.

Les paramètres du modèles proviennent d'estimations faites à partir de mesures chez le rat et trouvées dans la littérature. Les concentrations calciques interstitielles n'ont jamais été mesurées. En revanche, il existe des mesures de flux calciques, et la concentration est estimée en certains points stratégiques, ce qui nous permet de calibrer notre modèle et de vérifier sa pertinence a posteriori.

Nous rappelons qu'il s'agit d'un modèle de rein de rat, et que les conclusions que l'on en tire ne s'appliquent qu'à ce modèle de rein de rat.

## 1.3 Un modèle simplifié

Nous introduisons dans cette partie un modèle simplifié, qu'on analyse mathématiquement, dans le but de mieux comprendre le modèle plus complexe. En effet, il arrive parfois que certains

résultats exacts sur des modèles très simplifiés soient au moins aussi intéressants que des résultats numériques sur un modèle plus complexe qui peut-être sensible aux nombreux paramètres.

D'autre part, certaines analyses faites sur ce modèle rejoignent des problèmes rencontrés dans le cadre d'autres modèles étudiés en mathématiques, notamment les modèles cinétiques à deux vitesses.

### 1.3.1 Le modèle à trois tubes

La plus grosse simplification consiste à rendre les tubes imperméables à l'eau. De ce fait, le débit d'eau est constant dans chaque tube, et le terme de convection qui couple les solutés entre eux n'existe plus. On a aussi réduit le nombre de tubes et adapté les conditions aux limites à notre nouvelle architecture. Cette simplification a juste pour conséquence d'alléger les notations, mais on ne perd rien mathématiquement à enlever des tubes au modèle. Cependant, trois tubes est le nombre minimum de tubes à garder, parce qu'avec deux tubes seulement, on peut trouver des solutions analytiques et le comportement est qualitativement différent. Par exemple, la concentration croît exponentiellement en fonction du paramètre $V_m$.

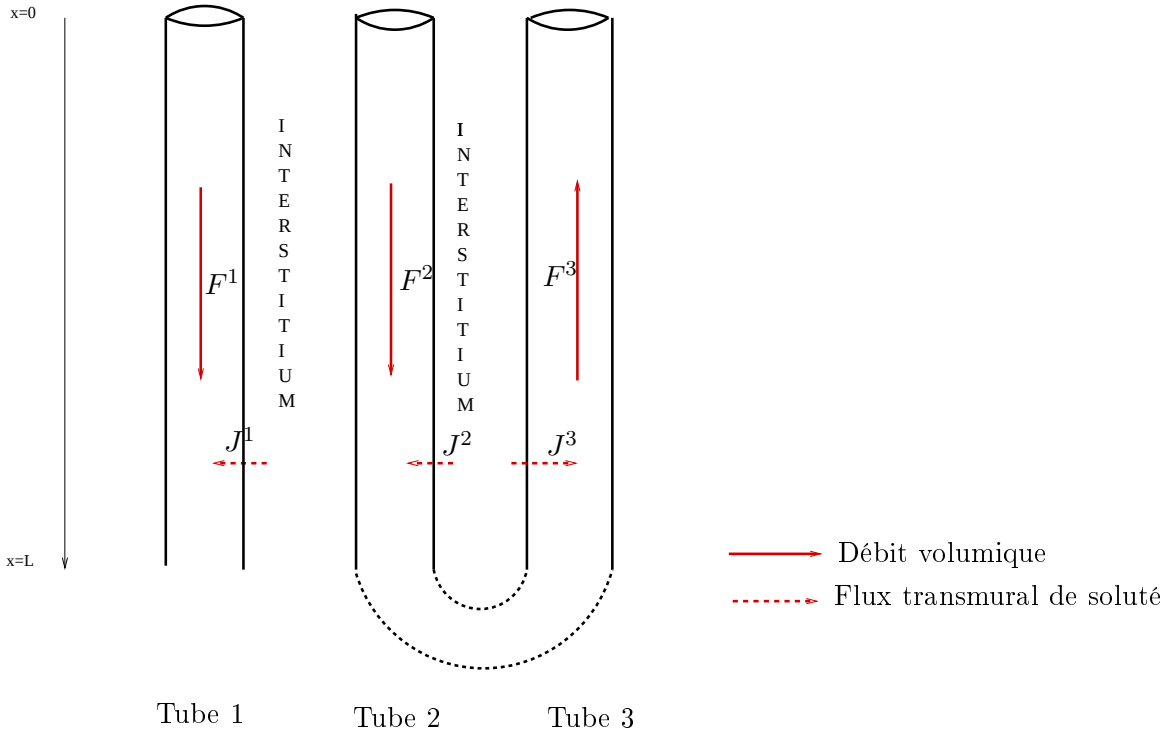


**Figure 1.6** – Modèle simplifié du néphron : Les tubes sont imperméables à l'eau mais peuvent échanger des solutés via l'interstitium

Chaque tube $j$ est imperméable à l'eau, le fluide circule ainsi à une vitesse constante $F^j$. A l'équilibre, la conservation de la matière s'écrit

$$\begin{cases} F^1 \dfrac{dC^1(x)}{dx} = J^1(x), & x \in [0, L], \\ F^2 \dfrac{dC^2(x)}{dx} = J^2(x), & x \in [0, L], \\ F^3 \dfrac{dC^3(x)}{dx} = J^3(x), & x \in [0, L], \\ C^1(0) = C_0^1, \quad C^2(0) = C_0^2, \quad C^3(L) = C^2(L), \end{cases} \tag{1.9}$$

où $C_0^1$ et $C_0^2$ sont deux constantes, et $J^j$ est le flux de soluté de l'interstitium vers le tube $j$. Les

flux de soluté ne contiennent plus de terme convectif et s'écrivent

$$\begin{cases} J^1(x) = 2\pi R^1(x)P^1(x)(C^{int}(x) - C^1(x)), \\ J^2(x) = 2\pi R^2(x)P^2(x)(C^{int}(x) - C^2(x)), \\ J^3(x) = 2\pi R^3(x)P^3(x)(C^{int}(x) - C^3(x)) - F(C^3(x), x), \end{cases} \tag{1.10}$$

où $F(C^3, x) > 0$ est un terme non linéaire représentant le transport actif. Pour cette étude, on fait les hypothèses suivantes sur $F$

$$F(C^3, x) \geq 0, \qquad F(0, x) = 0, \qquad 0 \leq \frac{\partial F}{\partial C}(C^3, x) \leq \mu(x) \leq \mu_M. \tag{1.11}$$

Ces hypothèses traduisent le fait que (1) le transport actif se fait toujours de l'intérieur du tube vers l'interstitium, (2) s'il n'y pas de matière dans le tube, il n'y pas de transport actif et (3) plus il y a des solutés dans le tube, plus le transport est important, mais le transport peut arriver à saturation. Ce phénomène de saturation apparaît quand toutes les pompes sont occupés. Dans le modèle réaliste, on choisit le cas particulier et habituel d'une non linéarité de type Michaëlis-Menten.

$$F(C^3, x) = V_m(x)\frac{C^3}{1 + C^3}. \tag{1.12}$$

On prendra tous les paramètres égaux à 1, ce qui est l'ordre de grandeur obtenu après adimensionnement. Dans ce modèle simplifié, le soluté ne peut pas s'accumuler dans l'interstitium ($J^{int} = 0$). En reportant dans (1.6) a donc la condition de fermeture

$$J^1(x) + J^2(x) + J^3(x) = 0. \tag{1.13}$$

Cette condition nous permet de calculer explicitement la concentration interstitielle

$$\forall x \in [0, L], \qquad C^{int}(x) = \frac{1}{3}\Big[C^1(x) + C^2(x) + C^3(x) + F(C^3(x), x)\Big].$$

En remplaçant $C^{int}$ par son expression, on arrive au système pour $x \in [0, L]$

$$\begin{cases} \dfrac{dC^1(x)}{dx} = \dfrac{1}{3}\Big[C^1(x) + C^2(x) + C^3(x) + F(C^3(x), x)\Big] - C^1(x), \\ \dfrac{dC^2(x)}{dx} = \dfrac{1}{3}\Big[C^1(x) + C^2(x) + C^3(x) + F(C^3(x), x)\Big] - C^2(x), \\ -\dfrac{dC^3(x)}{dx} = \dfrac{1}{3}\Big[C^1(x) + C^2(x) + C^3(x) + F(C^3(x), x)\Big] - C^3(x) - F(C^3(x), x), \\ C^1(0) = C_0^1, \qquad C^2(0) = C_0^2, \qquad C^3(L) = C^2(L). \end{cases} \tag{1.14}$$

Et on écrit le système dynamique sous la forme : Pour $t \geq 0$ et $x \in [0, L]$

$$\begin{cases} \dfrac{\partial C^1}{\partial t}(x,t) + \dfrac{\partial C^1}{\partial x}(x,t) = \dfrac{1}{3}\Big[C^1(x,t) + C^2(x,t) + C_3(x,t) + F(C^3(x,t), x)\Big] \\ \qquad\qquad - C^1(x,t), \\ \dfrac{\partial C^2}{\partial t}(x,t) + \dfrac{\partial C^2}{\partial x}(x,t) = \dfrac{1}{3}\Big[C^1(x,t) + C^2(x,t) + C^3(x,t) + F(C^3(x,t), x)\Big] \\ \qquad\qquad - C^2(x,t), \\ \dfrac{\partial C^3}{\partial t}(x,t) - \dfrac{\partial C^3}{\partial x}(x,t) = \dfrac{1}{3}\Big[C^1(x,t) + C^2(x,t) + C^3(x,t) + F\big(C^3(x,t), x\big)\Big] \\ \qquad\qquad - C^3(x,t) - F(C^3(x,t), x), \\ C^1(0,t) = C_0^1, \qquad C^2(0,t) = C_0^2, \qquad C^3(L,t) = C^2(L,t), \qquad t > 0, \\ C^1(x,0), \qquad C^2(x,0), \qquad C^3(x,0), \qquad x \in [0, L]. \end{cases} \tag{1.15}$$

On notera parfois $C$ le vecteur $(C^1, C^2, C^3)$.

## 1.4 Les problèmes mathématiques

### 1.4.1 Le caractère bien posé

A cause des conditions aux bords, le système stationnaire n'est pas un problème de Cauchy. Pour montrer l'existence de solutions, on utilise un argument de point fixe combiné avec une méthode de tir. Pour ce faire, on remplace le système (1.14) par le même système assorti des conditions aux bords

$$C^1(0) = C_0^1, \qquad C^2(0) = C_0^2, \qquad C^3(L) = C_L^3, \tag{1.16}$$

où $C_L^3$ est une constante positive donnée. Avec ces nouvelles conditions aux bords, on n'est toujours pas en présence d'un problème de Cauchy, mais on peut montrer par un argument de point fixe de Banach que le système admet une solution pour tout choix de la constante $C_L^3$. On introduit ensuite l'application

$$g : C_L^3 \mapsto C^2(L) - C^3(L)$$

où $C^2, C^3$ sont les solutions de (1.14) avec les conditions aux bords (1.16). On montre que cette application s'annule au moins une fois sur $\mathbb{R}^+$, ce qui nous permet de conclure à l'existence de solutions au système (1.14).

**Théorème 1.4.1** (Existence du problème stationnaire)**.** *Sous les hypothèses* (1.11)*, il existe une solution faible au système* (1.14)*, et cette solution est de classe* $\mathcal{C}^1$ *et positive.*

La méthode de démonstration adoptée pour ce théorème nous conduit naturellement à déterminer numériquement une solution stationnaire en combinant une méthode de résolution des problèmes de Cauchy avec une méthode de tir. Cependant, cette méthode devient peu robuste dès qu'on complexifie un peu le modèle parce que comme toute méthode de type Newton, elle nécessite de supposer qu'on est déjà dans le voisinage d'une solution stationnaire. Pour l'existence du problème dynamique (1.15), on utilise une méthode perturbative en approchant le système continu par un système d'équations différentielles ordinaires dont les solutions sont bornées. L'unicité des solutions au système (1.15) est basée sur un argument de contraction.

**Théorème 1.4.2** (Existence et unicité du problème dynamique)**.** *Sous les hypothèses* (1.11) *et sous des hypothèses de régularité sur la condition initiale, il existe une unique solution au système* (1.15)*, et cette solution appartient à* $BV([0,L]\times[0,T])$*. Par ailleurs, deux solution faibles* $C$ *et* $\widetilde{C}$ *pour des données initiales différentes* $C(x,0)$ *et* $\widetilde{C}(x,0)$*, vérifient le principe de contraction*

$$\begin{aligned}\int_0^L \big[\, |C^1 - \widetilde{C}^1| + |C^2 - \widetilde{C}^2| + |C^3 - \widetilde{C}^3| \,\big](x,t)dx \\ \leq \int_0^L \big[\, |C^1 - \widetilde{C}^1| + |C^2 - \widetilde{C}^2| + |C^3 - \widetilde{C}^3| \,\big](x,0)dx,\end{aligned} \tag{1.17}$$

On montre ensuite que le système dynamique converge en temps long vers toute solution stationnaire par une méthode de sur- et sous-solutions, montrant ainsi l'unicité de (1.14) et justifiant le fait d'utiliser un schéma dynamique pour atteindre l'équilibre décrit par (1.14).

**Théorème 1.4.3** (Comportement en temps long et unicité du problème stationnaire)**.** *La solution* $C$ *au système* (1.15) *converge vers l'unique solution* $\overline{C}$ *du système* (1.14) *dans* $L^1\Big([0,L]\Big)$*,*

$$\|C(x,t) - \overline{C}(x)\|_{L^1} \underset{t\to\infty}{\searrow} 0.$$

Grâce à des arguments de théorie spectrale, on peut aussi prouver la convergence avec un taux exponentiel de la solution dynamique vers l'état stationnaire.

### 1.4.2 Le rôle de la pompe

Qualitativement, on observe que si $V_m$ est suffisamment grand, les fonctions $C^1$, $C^2$ et $C^3$ sont croissantes en fonction de la profondeur. Physiologiquement, cela signifie que dans les zones plus profondes ($x = L$), le fluide sera plus concentré que dans les zones superficielles ($x = 0$), et ce à cause du transport actif.

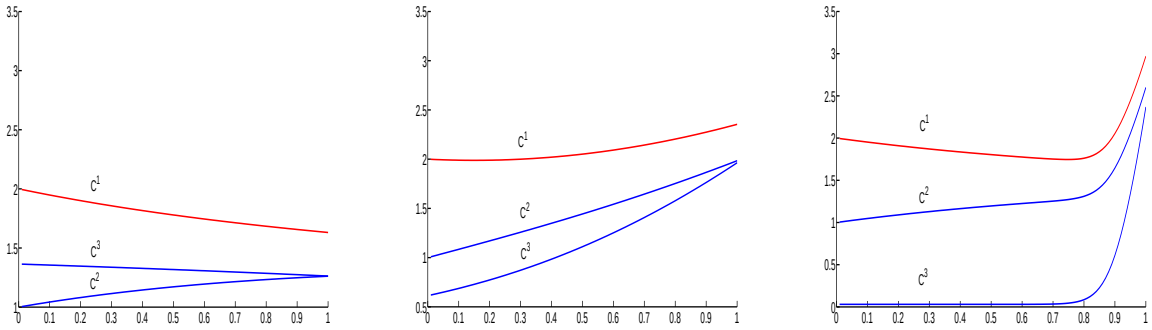


**FIGURE 1.7** – Profils $C^1, C^2$ et $C^3$ en fonction de la profondeur $x$ pour $V_m = 0$ (à gauche), $V_m = 5$ (au milieu), et $V_m = 50$ (à droite). Les données aux bords sont $C_0^1 = 2$ et $C_0^2 = 1$.

On s'est alors interrogé sur le rôle de la pompe et donc du paramètre $V_m$. On montre qu'asymptotiquement, le profil $C$ converge vers un profil limite, borné dans $L^\infty[0, L]$, et que la dérivée de $C$ converge vers un profil dans l'espace des mesures. Pour toutes les composantes de $C = (C^1, C^2, C^3)$, ce profil comporte une partie analytique, et une masse de Dirac en $x = L$.

**Théorème 1.4.4** (Asymptotique). *Les solutions au système* (1.14) *satisfont*

$$(C^1_{V_m}, C^2_{V_m}, C^3_{V_m}) \underset{V_m \longrightarrow +\infty}{\longrightarrow} (C^1, C^2, C^3) \qquad L^p (1 \leq p < \infty),\ p.p.,$$
$$(\frac{dC^1_{V_m}}{dx}, \frac{dC^2_{V_m}}{dx}, \frac{dC^3_{V_m}}{dx}) \underset{V_m \longrightarrow +\infty}{\longrightarrow} (\mu^1, \mu^2, \mu^3) \qquad M^1[0, L],$$

avec

$$\begin{cases} C^1(x) = \dfrac{C_0^1 + C_0^2}{2} + \dfrac{C_0^1 - C_0^2}{2} e^{-x}, \\ C^2(x) = \dfrac{C_0^1 + C_0^2}{2} + \dfrac{C_0^2 - C_0^1}{2} e^{-x}, \\ C^3(x) = 0. \end{cases} \qquad \begin{cases} \mu^1 = \dfrac{1}{2}\Big[(C_0^2 - C_0^1)e^{-x} + B\delta_L\Big], \\ \mu^2 = \dfrac{1}{2}\Big[(C_0^1 - C_0^2)e^{-x} + B\delta_L\Big], \\ \mu^3 = B\delta_L. \end{cases}$$

où

$$B = \lim_{V_m \to \infty} C^3_{V_m}(L).$$

Physiologiquement, cela signifie que la concentration urinaire de notre modèle simplifié ne peut augmenter infiniment, et que la pompe a tendance à conserver une valeur élevée de le concentration liquide au voisinage de $x = L$, qui est l'endroit auquel est déterminé la concentration urinaire.

### 1.4.3 Pourquoi 3 tubes et pas 2 ?

On a choisi d'étudier un modèle à trois tubes. On justifie à postériori ce choix par le fait que le système à deux tubes se comporte de façon différente du système à trois tubes ou plus, par exemple vis-à-vis du comportement de le pompe.

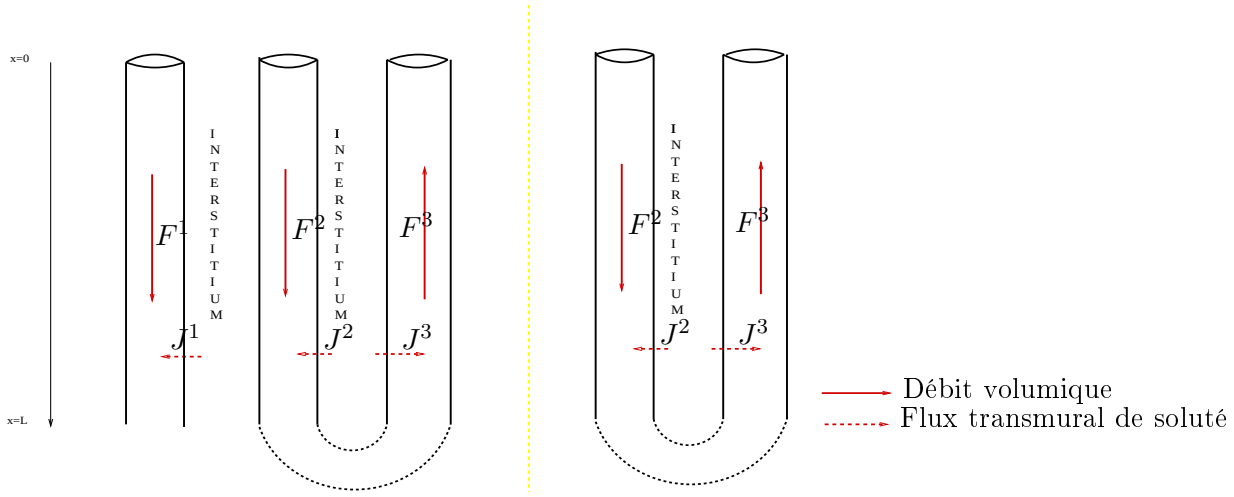


**FIGURE 1.8** – Deux architectures possibles pour notre modèle simplifié.

Le système à deux tube s'écrit

$$\begin{cases} \dfrac{dC^2_{V_m}(x)}{dx} = \dfrac{1}{2}\Big[C^3_{V_m}(x) + V_m \dfrac{C^3_{V_m}(x)}{1+C^3_{V_m}(x)} - C^2_{V_m}(x)\Big], \\ -\dfrac{dC^3_{V_m}(x)}{dx} = \dfrac{1}{2}\Big[C^2_{V_m}(x) - C^3_{V_m}(x) - V_m \dfrac{C^3_{V_m}(x)}{1+C^3_{V_m}(x)}\Big], \\ C^2_{V_m}(0) = C^2_0, \qquad C^3_{V_m}(L) = C^2_{V_m}(L). \end{cases} \tag{1.18}$$

Le comportment qualitatif du système (1.18) est différent du système (1.15). En effet, en sommant les deux lignes de (1.18), on obtient $C^2_{V_m} - C^3_{V_m} = K(V_m)$, où $K(V_m)$ est une constante qui ne dépend pas de $x$. Les conditions aux bords nous donnent $K(V_m) = 0$. Ainsi, $C^3_{V_m}$ et $C^2_{V_m}$ satisfont les équations

$$\begin{cases} \dfrac{dC^2_{V_m}(x)}{dx} = \dfrac{1}{2}\Big[V_m \dfrac{C^2_{V_m}(x)}{1+C^2_{V_m}(x)}\Big], \\ C^2_{V_m}(0) = C^2_0, \\ C^3_{V_m}(x) = C^2_{V_m}(x), \qquad x \in [0, L]. \end{cases} \tag{1.19}$$

Ainsi, les $C^i_{V_m}$ ne sont pas bornées uniformément en $V_m$. En effet, si c'était le cas, on aurait $C^2_{V_m} \leq M$, donc en reportant dans (1.19), $\dfrac{dC^2_{V_m}(x)}{dx} \geq \dfrac{1}{2}\Big[V_m \dfrac{C^2_{V_m}(x)}{1+M}\Big]$, et alors $C^2_{V_m}$ croîtrait exponentiellement $V_m$, ce qui entre en contradiction avec le caractère borné en $V_m$. Physiologiquement, la concentration urinaire ne peut pas augmenter indéfiniment, le modèle à deux tubes n'a donc pas un comportement acceptable dans ce cas-là.

### 1.4.4 Relaxation hyperbolique

On rappelle ici quelques notions sur les formulations entropiques des lois de conservation scalaire.

#### Formulation entropique d'une loi de conservation scalaire

On considère l'équation scalaire

$$\frac{\partial}{\partial t}\rho + \frac{\partial}{\partial x}f(\rho, x) = 0, \qquad t > 0,\ x \in \mathbb{R}, \tag{1.20}$$

$$\rho(x, 0) = \rho^0(x) \in L^\infty(\mathbb{R}). \tag{1.21}$$

Dès que $f$ est non linéaire en $\rho$, on peut trouver une condition initiale $\rho^0$ et un temps $T > 0$ tels qu'il n'existe pas de solution continue à (1.20) sur $[0, T] \times \mathbb{R}$. On travaille alors avec des solutions faibles, obtenues en multipliant l'équation (1.20) par une fonction test $\phi$ de classe $\mathcal{C}^1$ et en intégrant par parties. La formulation faible permet d'obtenir l'existence de solutions à (1.20), (1.21), mais ne détermine pas la solution de façon unique. La formulation entropique est une formulation plus stricte que la formulation faible et qui permet de sélectionner une seule des solutions faibles, celle qui provient du passage à la limite quand $\varepsilon \to 0$ de la solution à l'équation parabolique suivante

$$\frac{\partial}{\partial t}\rho_\varepsilon + \frac{\partial}{\partial x}f(\rho_\varepsilon, x) = \epsilon\Delta\rho_\varepsilon. \tag{1.22}$$

La formulation entropique ne fait pas intervenir le paramètre $\varepsilon$. En 1970, Kružkov propose la définition suivante [?]

**Définition 1.4.5** (Solution entropique de Kružkov)**.** *Une fonction $\rho \in L^\infty([0, T] \times \mathbb{R})$ est appelée solution entropique de Kružkov du problème* (1.20), (1.21) *sur $[0, T] \times \mathbb{R}$ si pour toute constante $k \in \mathbb{R}$, et pour toute fonction test $\phi \geq 0$ de classe $C^1$ à support compact sur $[0, T[\times\mathbb{R}$ , on a*

$$\begin{aligned}\int_0^T \int_{\mathbb{R}} |\rho(x,t) - k|\phi_t + \operatorname{sign}(\rho(x,t) - k)[f(\rho(x,t), x) - f(k, x)]\phi_x \\ - \operatorname{sign}(\rho(x,t) - k) f_x(k, x)\phi dx dt + \int_0^L \phi(x, 0)\rho^0(x)dx \geq 0.\end{aligned} \tag{1.23}$$

Les quantités $(|\rho - k|)_{k\in\mathbb{R}}$ sont appelées les entropies de Kružkov. Pour déterminer la solution à (1.20), on a remplacé le passage à la limite de la solution $\rho_\varepsilon$ de (1.22) par une inégalité qui doit être vérifiée pour un continuum de paramètres. Cela permet également de définir un schéma numérique pour trouver la solution entropique, sans passer par le processus de passage à la limite. La solution discrète entropique est construite de sorte à vérifier un continuum d'inégalités. A cause du terme $f_x$, cette définition n'a de sens que pour des fonctions $f$ dérivables en espace. En 2005, Audusse et Perthame [3] proposent dans le cas des flux monotones en $\rho$ mais discontinus en $x$ une formulation équivalente dans le sens où la solution qu'ils définissent coïncide avec la solution de Kružkov quand le flux $f$ est suffisamment régulier en $x$. Leurs hypothèses sont les suivantes

- Le flux $f(.,.)$ est continu, sauf sur un ensemble de mesure nulle en $x$.
- Pour tout $x$ hors de cet ensemble de mesure nulle, $f(., x)$ est localement Lipschitzienne et inversible.
- Il existe deux fonctions continues $f_-, f_+$ strictement positives, sauf peut-être en zéro où elles peuvent s'annuler, avec $f(\pm\infty) = +\infty$, et telles que pour tout $x \in \mathbb{R}$, $f_-(\rho) \leq |f(\rho, x)| \leq f_+(\rho)$.

Les entropies de Audusse-Perthame sont définies par $(|\rho - k_p(x)|)_{p\in\mathbb{R}}$ où $k_p$ est l'unique solution de

$$f(k_p(x), x) = p \qquad p.p.\ \ x \in \mathbb{R}. \tag{1.24}$$

Pour faire le lien avec les entropies de Kružkov, on remarque que les fonctions $k_p$ sont les solutions du problème stationnaire

$$\frac{d}{dx}f(k_p, x) = 0.$$

Si $f$ ne dépend pas de $x$, on retombe sur les constantes.

**Définition 1.4.6** (Solution entropique de Audusse-Perthame). *Une fonction* $\rho \in L^\infty([0,T]\times\mathbb{R})\cap\mathcal{C}^0\Big([0,T],L^1_{loc}(\mathbb{R})\Big)$ *est appelée solution entropique de Audusse-Perthame du problème* (1.20), (1.21) *sur* $[0,T]\times\mathbb{R}$ *si pour toute fonction* $k_p$ *vérifiant* (1.24) *et pour toute fonction test* $\phi\geq 0$ *de classe* $C^1$ *à support compact sur* $[0,T[\times\mathbb{R}$, *on a*

$$\begin{aligned}\int_0^T\int_{\mathbb{R}} |\rho(x,t)-k_p(x)|\phi_t + \operatorname{sign}(\rho(x,t)-k_p(x))[f(\rho(x,t),x)-f(k_p(x),x)]\phi_x dxdt \\ + \int_0^L \phi(x,0)\rho^0(x)dx \geq 0.\end{aligned} \tag{1.25}$$

Ces deux formulations entropiques sont valables pour des équations posées sur $\mathbb{R}$. Dans notre étude, on s'intéresse aux domaines bornés.

$$\begin{aligned}\frac{\partial}{\partial t}\rho + \frac{\partial}{\partial x}f(\rho,x) = 0, \qquad t>0,\ x\in[0,L], \\ \rho(x,0)=\rho^0(x) \qquad \rho^0\in L^\infty([0,L]),\end{aligned} \tag{1.26}$$

$$\rho(0,t)=\rho_0, \qquad \rho(L,t)=\rho_L. \tag{1.27}$$

En 1979, Bardos, Leroux et Nédélec généralisent la formulation de Kružkov aux domaines bornés. Ils donnent une caractérisation de la solution de viscosité obtenue comme la limite (1.22) assorti des conditions aux bords $\rho_\varepsilon(0,t)=\rho_0,\ \rho_\varepsilon(L,t)=\rho_L$ quand $\varepsilon\to 0$. Ils se placent dans un cadre $BV$ pour avoir l'existence de traces. On peut généraliser leur formulation au cadre $L^\infty$ dans le cas où $f$ est non dégénérée au sens où elle n'est linéaire sur aucun intervalle [71], puisque l'on a également existence de traces dans ce cas [93]. On appelle respectivement $\rho(0,t)$ et $\rho(L,t)$ la trace de $\rho$ en 0 et $L$.

**Définition 1.4.7** (Solution entropique de Bardos-Leroux-Nedélec). *Une fonction* $\rho\in BV([0,T]\times[0,L])$ *est appelée solution entropique de Kružkov-BLN du problème* (1.20), (1.21) *sur* $[0,T]\times[0,L]$ *si pour toute constante* $k$, *et pour toute fonction test* $\phi\geq 0$ $C^1$ *à support compact sur* $[0,T[\times[0,L]$, *on a*

$$\begin{aligned}\int_0^T\int_{\mathbb{R}} |\rho(x,t)-k|\phi_t + \operatorname{sign}(\rho(x,t)-k)[f(\rho(x,t),x)-f(k,x)]\phi_x \\ - \operatorname{sign}(\rho(x,t)-k)\phi_x(k,x)dxdt - \int_0^T \operatorname{sign}(\rho_L-k)\Big(f(\rho(t,L),L)-f(k,L)\Big) \\ + \int_0^T \operatorname{sign}(\rho_0-k)\Big(f(\rho(0,t),0)-f(k,0)\Big) + \int_0^L \phi(x,0)\rho^0(x)dx \geq 0.\end{aligned} \tag{1.28}$$

En combinant avec la Définition 1.4.6, on écrit la formulation suivante. C'est cette formulation que l'on utilisera dans le manuscrit.

**Définition 1.4.8** (Solution entropique de Bardos-Leroux-Nedélec adaptée). *Une fonction* $\rho\in BV([0,T]\times[0,L])$ *est appelée solution entropique du problème* (1.20), (1.21) *sur* $[0,T]\times[0,L]$ *si pour toute fonction* $k_p$ *vérifiant* (1.24), *et pour toute fonction test* $\phi\geq 0$ $C^1$ *à support compact*

*sur* $[0,T[\times[0,L]$ *, on a*

$$\begin{aligned}\int_0^T \int_{\mathbb{R}} &|\rho(x,t)-k_p(x)|\phi_t + \operatorname{sign}(\rho(x,t)-k_p(x))[f(\rho(x,t),x)-f(k_p(x),x)]\phi_x \\ &- \operatorname{sign}(\rho(x,t)-k)\phi_x(k,x)dxdt \\ &- \int_0^T \operatorname{sign}(\rho_L - k_p(L))\Big(f(\rho(L,t),L)-f(k_p(L),L)\Big) \\ &+ \int_0^T \operatorname{sign}(\rho_0 - k_p(0))\Big(f(\rho(0,t),0)-f(k_p(0),0)\Big) \\ &+ \int_0^L \phi(x,0)\rho^0(x)dx \geq 0.\end{aligned} \tag{1.29}$$

**La relaxation hyperbolique - Principe**

On peut faire apparaître des systèmes hyperboliques avec un terme de relaxation dans différents contextes de modélisation tels que les trafics routiers [4], la chromatographie [36], la théorie cinétique [13], où certains modèles contiennent "naturellement" un terme qui peut être très petit dans certains régimes, ou lorsque le modèle est étudié en temps asymptotiquement long via le changement de variable $(\frac{x}{\varepsilon},\frac{t}{\varepsilon})$. Un des premiers travaux rigoureux dans ce domaine est l'étude de la relaxation d'un système visco-élastique vers un système élastodynamique [23]. Une revue sur le sujet peut être consultée dans [49].

Plus récemment, les systèmes de relaxations hyperboliques ont été utilisés comme une perturbation d'une loi de conservation scalaire donnée, dans le but d'approcher les solutions discontinues. Le premier pas dans cette direction a été fait par [59] où les auteurs s'intéressent à la relaxation du modèle cinétique avec un continuum de vitesses suivant

$$\frac{\partial}{\partial t}g(x,t,\xi) + a(\xi)\frac{\partial}{\partial x}g(x,t,\xi) = \frac{1}{\varepsilon}\Big[M\Big(\int_\xi g(x,t,\xi)d\xi\Big) - g(x,t,\xi)\Big],$$

avec

$$\int_\xi M(\rho,\xi)d\xi = \rho, \qquad \int_\xi a(\xi)M(\rho,\xi)d\xi = f(\rho)$$

vers la loi de conservation (1.20) Ceci sert de justification théorique à l'utilisation de schémas cinétiques [9]. Plus tard, Jin et Xin [42] ont développé un système hyperbolique linéaire $2\times 2$ destiné à approcher une loi de conservation scalaire générique. Le système de Jin et Xin peut être vu comme un modèle cinétique à deux vitesses et s'écrit

$$\begin{cases} \dfrac{\partial z_\epsilon}{\partial t}(x,t) + \dfrac{\partial w_\epsilon}{\partial x}(x,t) = 0, \\ \dfrac{\partial w_\epsilon}{\partial t}(x,t) + a^2\dfrac{\partial z_\epsilon}{\partial x}(x,t) = \dfrac{1}{\epsilon}\Big[f(z_\epsilon(x,t)) - w_\epsilon(x,t)\Big], \end{cases} \tag{1.30}$$

où $a\in\mathbb{R}$ et $f$ est une fonction $\mathcal{C}^1$. On s'attend à ce que la quantité $z_\varepsilon$ converge vers la solution $\rho$ de la loi de conservation (1.20). Le problème est de montrer rigoureusement que la solution $(z_\varepsilon, w_\varepsilon)$ converge vers $(\rho, f(\rho))$ où $\rho$ est la solution faible entropique de (1.20). Une condition nécessaire pour que les solutions soient stables est la condition de Whitham [98], ou condition sous-caractéristique, et s'écrit

$$\forall z\in\mathbb{R} \qquad |f'(z)| \leq a.$$

On trouve cette condition par exemple en dérivant formellement l'équation scalaire sur $z$ à l'ordre 2 en $\epsilon$. On retombe alors sur une approximation parabolique de (1.20) dont le terme devant le laplacien est exactement $\varepsilon(f'(z)-a)$. L'équation parabolique est alors stable si $|f'(z)|\leq a$.

**La relaxation hyperbolique - Méthodes de compacité**

A cause de la non-linéarité de la formulation entropique, la convergence faible ne suffit pas à passer à la limite. Il faut des estimations fortes sur les quantités $z_\varepsilon$ et $w_\varepsilon$. Différentes techniques ont été utilisées pour contrôler les solutions. On peut citer la compacité par compensation [45] et les lemmes de moyenne [10, 26]. Dans le cas des domaines bornés, il faut aussi s'occuper de la convergence des valeurs aux bord. Pour la grande majorité, les auteurs se placent sur $[0, +\infty]$ et considèrent les conditions aux limites $z_\varepsilon(0,t) = z_0,\ w_\varepsilon(0,t) = f(z_0)$, qui sont compatibles avec l'équilibre $w = f(z)$. Dans [67], les auteurs, en se restreignant au cas où les conditions initiales et les conditions aux bords sont à l'équilibre, montrent des estimations BV. De nombreuses variations sur ce thème ont ensuite été publiées. Par exemple, les auteurs de [101] s'intéressent au cas où la loi de conservation contient un terme source $q(x,t)$ et utilisent les mêmes arguments que [67] . Quand les conditions aux bords ne sont pas à l'équilibre, une couche limite apparaît [94]. La couche limite en $x = 0$ est décrite dans [68, 100], dans le cadre des solutions régulières.

Dans le cas de notre étude, la relaxation a un sens physique et les conditions aux bord du système relaxé sont imposées. Comme aternative au système $3 \times 3$ (1.14), dans l'objectif d'avoir des notations plus légères et de façon à mettre en évidence la proximité de notre étude avec les études relatives au sytème (1.30), on introduit lors de cette analyse un système intermédiaire entre les systèmes (1.14) et (1.18). Ce système ne modélise que deux tubes, mais les conditions aux bords sont légèrement modifiées, de sorte qu'une partie seulement du fluide du tube descendant soit réinjectée dans le tube ascendant. La système que l'on étudie s'écrit pour $t \geq 0$ et $x \in [0, L]$,

$$\begin{cases} \dfrac{\partial u_\epsilon}{\partial t}(x,t) + \dfrac{\partial u_\epsilon}{\partial x}(x,t) = \dfrac{1}{\epsilon}\Big[h(v_\epsilon(x,t),x)) - u_\epsilon(x,t)\Big], \\ \dfrac{\partial v_\epsilon}{\partial t}(x,t) - \dfrac{\partial v_\epsilon}{\partial x}(x,t) = \dfrac{1}{\epsilon}\Big[u_\epsilon(x,t) - h(v_\epsilon(x,t),x))\Big], \\ u_\epsilon(0,t) = u_0, \qquad v_\epsilon(L,t) = \alpha u_\epsilon(L,t), \qquad \alpha \in (0,1), \\ u(x,0) = u_\varepsilon^0(x), \qquad v_\varepsilon(x,0) = v^0(x). \end{cases} \tag{1.31}$$

et on fait les hypothèses

$$\begin{aligned} h(0,x) = 0, \qquad 1 < \beta \leq \frac{\partial h}{\partial v}(v,x) \leq \mu, \\ \sup_v \int_0^L |\frac{\partial h}{\partial x}(v,x)|dx \leq C, \qquad h(.,x) \text{ n'est affine sur aucun intervalle,} \end{aligned} \tag{1.32}$$

Ce système a l'avantage d'avoir un comportement similaire au système (1.14), mais il a l'inconvénient de ne pas distinguer les 3 tubes. Si on omet dans un premier temps la dépendance spatiale de la fonction $h$, en faisant le changement de variable $u + v = z,\ u - v = w$, on obtient le système,

$$\begin{cases} \dfrac{\partial z_\epsilon}{\partial t} + \dfrac{\partial w_\epsilon}{\partial x} = 0, \\ \dfrac{\partial v_\epsilon}{\partial t} - \dfrac{\partial v_\epsilon}{\partial x}(x,t) = \dfrac{2}{\epsilon}\Big[h(\dfrac{z_\epsilon - w_\varepsilon}{2}) - \dfrac{z_\varepsilon + w_\varepsilon}{2}\Big], \end{cases}$$

qui n'est pas exactement le système de Jin et Xin.

**Proposition 1.4.9.** *Il existe une fonction $v \in L^\infty([0,L] \times [0,T])$ telle que la solution $u_\varepsilon, v_\varepsilon$ de (1.31) vérifie*

$$u_\epsilon(x,t) \underset{\epsilon \to 0}{\longrightarrow} h(v(x,t),x), \qquad v_\epsilon(x,t) \underset{\epsilon \to 0}{\longrightarrow} v(x,t),\ p.p.$$

Le système de Jin et Xin a été construit dans le but d'approcher d'une équation scalaire non linéaire donnée par un système perturbé linéaire, et la plupart des études sur ce système ont été

effectuées dans cette optique. Les variables choisies $(z_\varepsilon, w_\varepsilon)$ relaxent vers $(\rho, f(\rho))$ et les conditions aux bord sont choisies à l'équilibre, c'est à dire que $z_\varepsilon(0,t) = z_0(t)$ et $w_\varepsilon(0,t) = f(z_0(t))$. Ainsi, on s'attend à ce que $\rho(0,t) = z_0(t)$. Dans le cas du système (1.31), l'identification des conditions au bord $\rho(t,0)$ et $\rho(t,L)$ est moins immédiate.

On définit $\rho$ et $A$ comme

$$\rho(x,t) := h(v(x,t),x) + v(x,t), \qquad A(\rho,t) := h(v(x,t),x) - v(x,t), \tag{1.33}$$

Le principal résultat est le théorème

**Théorème 1.4.10** (Limite $\varepsilon \to 0$)**.** *La quantité $\rho(x,t)$ est une solution entropique (selon la définition 1.4.8) à la loi de conservation scalaire*

$$\begin{cases} \dfrac{\partial}{\partial t}\rho(x,t) + \dfrac{\partial}{\partial x}A(\rho(x,t),x) = 0, \qquad t>0,\ x\in[0,L], \\ \rho(0,t) = h^{-1}(u_0,0) + u_0, \qquad t>0, \\ \rho(x,0) = \rho^0(x), \qquad \rho^0(x) := v^0(x) + h(v^0(x),x), \qquad x\in[0,L]. \end{cases} \tag{1.34}$$

La démonstration se fait en deux temps. On commence par montrer la convergence sur l'intérieur du domaine domaine. Pour contrôler les solutions $u_\varepsilon$ et $v_\varepsilon$, sous l'hypothèse de conditions initiales à l'équilibre, on peut adapter la preuve de [67] et dériver des estimations BV en temps. En revanche, nous n'avons pas d'estimations BV en espace à cause de la dépendance spatiale du terme source. On propose une méthode alternative pour montrer la compacité des solutions dans ce cas, sans passer par des estimations BV. Pour avoir un résultat sans contrainte sur les conditions initiales, on rédige une preuve utilisant compacité par compensation en s'inspirant de [36]. On identifie ensuite les conditions aux bords, et on les démontre rigoureusement. La nouveauté de ce travail réside donc dans (1) les conditions aux limites de type réflexion et surtout (2) la dépendance en $x$ du terme source, ce qui nous empêche d'appliquer les estimations BV classiquement dérivées et ce qui donne lieu à la limite à une loi de conservation scalaire dont le flux discontinu dépend de $x$, nous amenant à utiliser la formulation entropique de la Définition 1.4.8.

### 1.4.5 Un schéma numérique qui préserve l'asymptotique

Dans le but d'illustrer la convergence de (1.31) vers (1.34) (respectivement notés $S_\varepsilon$ et $S$ pour l'occasion), on construit dans le Chapitre 4 un schéma numérique qui préserve l'asymptotique (schéma AP). Cela signifie que l'on construit un schéma $S_{\varepsilon,\Delta}$, qui converge quand $\Delta = (\Delta t, \Delta x)$ tend vers 0 vers la solution de $S_\varepsilon$, et tel que la limite quand $\varepsilon$ tend vers 0 est un schéma $S_\Delta$ admissible pour l'équation $S$ (voir Figure 1.9).

Une condition nécessaire pour que le schéma $\Delta = (\Delta t, \Delta x)$ soit AP est que la condition CFL de stabilité soit minorée indépendamment de $\varepsilon$. Le schéma numérique construit dans le chapitre 4 vérifie toutes les propriétés d'un schéma AP, mais on note l'apparition d'une couche limite au voisinage de $x = L$ quand $\varepsilon$ est petit. On interprète cette couche limite en remarquant que les conditions à ce bord $v_\varepsilon = \alpha u_\varepsilon$ ne sont en général pas compatibles avec l'équilibre $h(u) = v$, mais ce sont ces conditions qui sont imposées dans le schéma. Puisque $h(.,x)$ est croissante, le système limite $S$ est une équation de transport à vitesse positive. Le schéma limite $S_\Delta$ que l'on obtient pour l'équation $S$ est un schéma très diffusif. Par conséquent, les conditions que l'on impose sur le bord droit diffusent à l'intérieur du domaine. Pour éliminer cette couche limite, qui est une réminiscence du modèle $S_\varepsilon$ mais qui n'a plus de sens pour le modèle $S$, on a décidé de construire un schéma AP $S_{\varepsilon,\Delta}$ en faisant en sorte que le schéma limite $S_\Delta$ soit le schéma décentré amont classique.

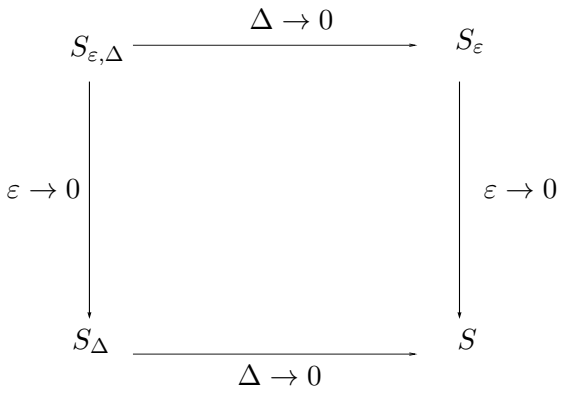


**Figure 1.9** – Principe des schémas AP

La problématique des schémas AP dépasse largement les équations hyperboliques, et un des premiers schémas AP modélisaient un transport de neutron en régime diffusif [48] [47]. Une revue sur les schémas AP peut être consultée dans [41].

Dans le cadre des équations hyperboliques, il ressort essentiellement deux stratégies pour construire des schémas AP. La première est basée sur le splitting d'opérateurs. Le terme de transport et le terme source sont traités indépendamment, et pour ne pas être limité par la condition CFL, le terme source est implicité. Sur l'exemple du système (1.30), on peut citer par exemple le schéma développé dans [20]. La preuve rigoureuse du caractère AP est détaillée dans [21].

La deuxième méthode a été développée dans [28] et utilise la technique des schémas équilibre [31]. Le principe opposé au principe de la méthode de splitting, dans le sens où la discrétisation du terme source est intimement liée à la discrétisation de la partie transport. La plupart des schémas AP ont été construits sur ce principe. Dans [8] cependant, les auteurs se sont intéressés au problème de trouver un schéma AP pour le système (1.30) en ayant des contraintes sur le schéma limite $S_\Delta$. Ils ont résolu le problème en utilisant un schéma adapté de Gosse-Toscani [29] [30]. Le schémas équilibres sont adaptés pour résoudre de tels problèmes, puisque le choix sur la discrétisation du terme source constitue un degré de liberté qui peut être exploité pour imposer la discrétisation du flux dans l'équation limite.

Dans le chapitre (6), on développe une méthode pour construire un schéma AP basée sur la technique des schémas équilibres. C'est une méthode alternative à la méthode proposée par [8]

On considère un maillage de $N$ cellules disjointes. On appelle $\Delta x$ la taille d'une cellule et $\Delta t$ la taille d'un intervalle de temps. Le temps final est noté $T$, et le nombre d'itérations à l'étape courante $n$. On obtient le résultat suivant

**Proposition 1.4.11.** *Il existe une classe de schémas AP $(S_\varepsilon)$ paramétrés par $1 \leq b \leq \beta$ dont le schéma limite $(S)$ coïncide avec le schéma décentré amont. Ces schémas s'écrivent*

$$\begin{cases} \dfrac{u_k^{n+1}-u_k^n}{\Delta t} + \dfrac{u_k^n - u_{k-1}^n}{\Delta x} = \dfrac{1}{\varepsilon + \Delta x}\Big(h(v_{k-1}^n) - u_{k-1}^n + bv_k^n - bv_{k-1}^n\Big), \\ \dfrac{v_k^{n+1}-v_k^n}{\Delta t} + \dfrac{v_k^n - v_{k+1}^n}{\Delta x} = -\dfrac{1}{\varepsilon + \Delta x}\Big(h(v_k^n) - u_k^n + v_{k+1}^n + (b-2)v_k^n + (1-b)v_{k-1}^n\Big), \\ u_0^n = u_0, \qquad v_0^n = h^{-1}(u_0), \qquad v_{N+1}^n = \alpha u_N^n. \end{cases} \tag{1.35}$$

## Structure de la thèse

Le manuscrit est divisé en deux parties. La première partie est consacrée à l'étude mathématique du modèle décrit dans la partie 1 de l'introduction.

- Le chapitre 2 développe pourquoi le modèle simplifié est bien posé. On y montre l'existence et l'unicité de solutions faibles pour les problèmes dynamique et stationnaire, et la relaxation en temps grand du problème dynamique vers l'équilibre. On estime la vitesse de convergence grâce à des éléments spectraux. Il reprend le travail de l'article [91].
- Dans le chapitre 3, on réalise une étude asymptotique en le paramètre $V_m$, et on identifie les profils limites analytiquement. On étudie aussi la forme des couches limites. Il reprend le travail de l'article [90].
- Les chapitres 4 et l'appendice 5 concernent l'adimensionnement hyperbolique du modèle simplifié. On travaille d'abord sur un modèle à deux tubes, dans le but d'avoir des notations moins lourdes, puis on modifie les résultats obtenus pour les appliquer au système à 3 tubes. Le chapitre 4 va donner lieu à un article, encore en cours d'écriture.
- Le chapitre 6 contient une description et une preuve de la stabilité de l'asymptotic targeting scheme.

La seconde partie est consacrée à l'étude du modèle plus réaliste. Elle s'inspire des articles [34] [92] et [18].

- On commence par décrire précisément le modèle dans le chapitre 7.
- Dans le chapitre 8, on décrit le schéma volume fini que l'on a développé pour la résolution du modèle.
- Le chapitre 9 est consacré à exposer les résultats obtenus, d'un point de vue physiologique.

# Part I

# Mathematical analysis of reduced models

# Chapter 2

# Well posedness and relaxation toward equilibrium of a simplified kidney model

This chapter is taken from the paper

M. Tournus, A. Edwards, N. Seguin, and B. Perthame. Analysis of a simplified model of the urine concentration mechanism. *Network Heterogeneous Media*, 7:989 – 1018, 2012.

*We study a nonlinear stationary system of transport equations with specific boundary conditions describing the transport of solutes dissolved in a fluid circulating in a countercurrent tubular architecture, which constitutes a simplified model of a kidney nephron. We prove that for every Lipschitz and monotonic nonlinearity (which stems from active transport across the ascending limb), the dynamic system, a PDE which we study through contraction properties, relaxes toward the unique stationary state. A study of the linearized stationary operator enables us, using eigenelements, to further show that under certain conditions regarding the nonlinearity, the relaxation is exponential. We also describe a finite volume scheme which allows us to efficiently approach the numerical solution to the stationary system. Finally, we apply this numerical method to illustrate how the countercurrent arrangement of tubes enhances the axial concentration gradient, thereby favoring the production of highly concentrated urine.*

## 2.1 Introduction

The main role of the kidney is to maintain fluid and electrolyte homeostasis, by regulating the volume and composition of blood so that it remains clean and chemically balanced. Kidneys receive blood from the renal artery, filter it, and return it to the body via the renal vein while excreting unwanted substances in the urine. The functional units of the kidney, known as nephrons, each consist of several segments arranged in a countercurrent manner so as to maximize the production of concentrated urine.

Our purpose is to develop a simplified mathematical model predicated on a steady state model describing solute transport in nephrons, to prove that the solution to the dynamic model we defined relaxes toward the solution to the steady state model, and to compute this solution. In this simplified representation, the nephron consists of 3 water-impermeable tubes that exchange solutes via a common interstitium, as illustrated in Figure 2.1. There have been other simplified models of renal function based on similar hypotheses [38].

Here, we only consider one generic uncharged solute (e.g., NaCl), whose transport across walls is driven by diffusion and "active" pumps (which require metabolic energy to carry the solute against its concentration gradient). If the tubes were permeable to water, convection would also contribute to solute transport. In other words, by assuming that there is no water movement across the walls, we are neglecting the convective part of the solute flux. However, the latter is negligible in most renal tubules.

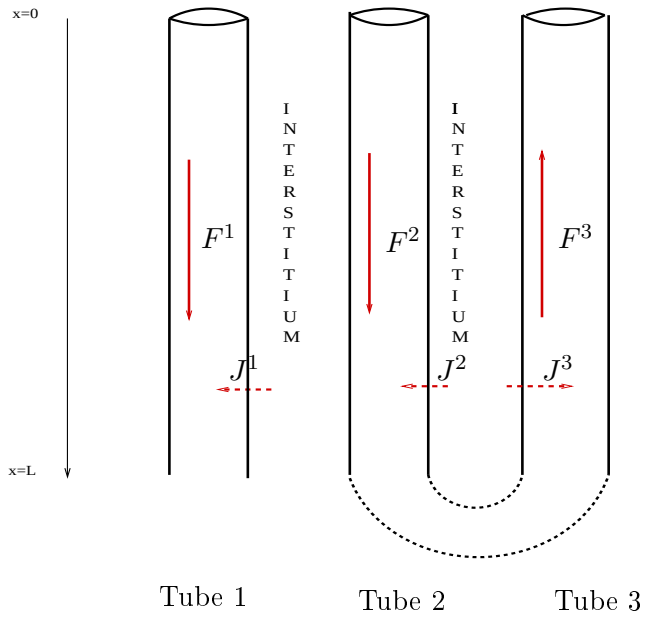


**Figure 2.1:** Simplified model of a nephron. Tubes are water-impermeable but can exchange solutes with the interstitium. These exchanges are quantified by the transmural fluxes $J$.

Models that account for the presence of blood vessels usually consider at least 5 tubes (i.e., tubules and vessels). We choose to only represent 3 here so as to keep the presentation and analysis tractable, but the problem formulation and the mathematical methods described herein apply to any number $\geq 3$.

Given the solute concentration (denoted $C$) at the inlet of tubes 1 and 2, and knowing that $C^3(L) = C^2(L)$ by continuity, our objective is to determine concentration profiles in the three tubes, as well as in the surrounding interstitium.

In each tube $i$, the fluid (mostly water) is assumed to flow at a constant rate $F^i$. At steady

state, conservation of solute in each tube can be expressed as

$$\begin{cases} F^1 \dfrac{dC^1(x)}{dx} = J^1(x), & x \in [0, L], \\ F^2 \dfrac{dC^2(x)}{dx} = J^2(x), & x \in [0, L], \\ F^3 \dfrac{dC^3(x)}{dx} = J^3(x), & x \in [0, L], \\ C^1(0) = C_0^1, \qquad C^2(0) = C_0^2, \qquad C^3(L) = C^2(L), \end{cases} \tag{2.1}$$

where $C_0^1$ and $C_0^2$ are two given nonnegative values, $F^i$ is the water flow rate in tube $i$ and $J^i$ is the transmural flux from the interstitium into tube $i$. What makes this system specific and mathematically challenging is its unusual boundary conditions.

In the absence of transversal water movement, the main driving force for the transport of an uncharged solute is passive diffusion. In some kidney tubules there is also active transport, mediated by energy-consuming pumps that carry some solutes against their concentration gradient. We assume the presence of such a pump in only tube 3 (which is meant to represent the thick ascending limb), so that

$$\begin{cases} J^1(x) = 2\pi R^1(x) P^1(x)(C^{int}(x) - C^1(x)), \\ J^2(x) = 2\pi R^2(x) P^2(x)(C^{int}(x) - C^2(x)), \\ J^3(x) = 2\pi R^3(x) P^3(x)(C^{int}(x) - C^3(x)) - F(C^3(x), x), \end{cases} \tag{2.2}$$

where $R^i$ and $P^i$ respectively denote the radius and solute permeability of tube $i$, $C^{int}$ is the interstitial concentration, and $F(C^3, x) > 0$ is a nonlinear term representing active transport, which is usually described using Michaelis-Menten kinetics

$$F(C^3, x) = V_m(x) \frac{C^3}{1 + C^3}. \tag{2.3}$$

Summarized in Table 2.1 are symbol definitions.

**Table 2.1:** Definition of frequently used symbols

| Parameter | Description | order of magnitude (in rats) |
|---|---|---|
| $C^i(x)$ | Solute concentration in tube $i$ at depth $x$ | $5\ mol.m^{-3}$ |
| $C^{int}(x)$ | Solute concentration in the interstitium at depth $x$ | $5\ mol.m^{-3}$ |
| $C_0^1$, $C_0^2$ | Concentrations at the inlet of tubes 1 and 2 (assumed to be known) | $5\ mol.m^{-3}$ |
| $L$ | Length of the tubes | $6.10^{-3}m$ |
| $F^i(x)$ | Water flow rate in tube $i$ at depth $x$ | $10^{-13}m^3.s^{-1}$ |
| $R^i(x)$ | Radius of tube $i$ at depth $x$ | $5.10^{-5}.m$ |
| $P^i(x)$ | Solute permeability of the wall of tube $i$ at depth $x$ | $10^{-5}m.s^{-1}$ |
| $V_m$ | Rate of the active transport | $10^{-7}mol.m^{-1}.s^{-1}$ |
| $J^i(x)$ | Transmural flux of solute through the wall of tube $i$ at depth $x$ | |

We then proceed to make the system non-dimensional. We define the dimensionless form of a generic variable $A$ as:

$$\overline{A} = \frac{A}{A^0}$$

where $A^0$ is a constant on the same order of magnitude as $A$ (see Table 2.1). We have

$$\overline{x} = \frac{x}{L^0},\ \overline{C} = \frac{C}{C^0},\ \overline{F^i} = \frac{F^i}{F^0},\ \overline{R} = \frac{R}{R^0},\ \overline{P} = \frac{P}{P^0},$$

with $L^0$ to be defined.

Combining (2.1) with (2.2), we write for $\overline{x} \in [0, \frac{L}{L^0}]$

$$\begin{cases} F^0\overline{F^1}\dfrac{d(C^0\overline{C}^1)(x)}{L^0 d\overline{x}} = 2\pi R^0\overline{R}^1(x)P^0\overline{P}^1(x)C^0(\overline{C}^{int}(x) - \overline{C}^1(x)), \\ F^0\overline{F^2}\dfrac{d(C^0\overline{C}^2)(x)}{L^0 d\overline{x}} = 2\pi R^0\overline{R}^2(x)P^0\overline{P}^2(x)C^0(\overline{C}^{int}(x) - \overline{C}^2(x)), \\ F^0\overline{F^3}\dfrac{d(C^0\overline{C}^3)(x)}{L^0 d\overline{x}} = 2\pi R^0\overline{R}^3(x)P^0\overline{P}^3(x)C^0(\overline{C}^{int}(x) - \overline{C}^3(x)) - F(\overline{C}^3(\overline{x}), \\ \qquad \overline{C}^1(0) = \overline{C}^1_0, \qquad \overline{C}^2(0) = \overline{C}^2_0, \qquad \overline{C}^3(\dfrac{L}{L^0}) = \overline{C}^2(\dfrac{L}{L^0}), \end{cases} \tag{2.4}$$

To simplify the notation, we now drop the overbars ($\overline{A}$) and simply denote dimensionless variables as $A$. In addition, we assume that the radii, permeabilities, and flow rates are equal in all three tubes. Note that the flow is in the opposite direction in tube 3. We thus obtain

$$\begin{cases} \dfrac{dC^1(x)}{dx} = P_s(C^{int}(x) - C^1(x)), \qquad x \in [0, \dfrac{L}{L^0}], \\ \dfrac{dC^2(x)}{dx} = P_s(C^{int}(x) - C^1(x)), \qquad x \in [0, \dfrac{L}{L^0}], \\ \dfrac{dC^3(x)}{dx} = P_s(C^{int}(x) - C^3(x)) - F(C^3(x), x) \qquad x \in [0, \dfrac{L}{L^0}], \\ C^1(0) = C^1_0, \qquad C^2(0) = C^2_0, \qquad C^3(\dfrac{L}{L^0}) = C^2(\dfrac{L}{L^0}), \end{cases} \tag{2.5}$$

where

$$P_s = \frac{2\pi L^0 R^0 P^0}{F^0} \tag{2.6}$$

is a dimensionless effective solute permeability. We now choose $L^0$ so that $P_s = 1$. The nondimensional parameter $\frac{L}{L^0}$ (which is subsequently denoted $L$) is then about 200, and the nondimensional rate of active transport (that we still call $V_m$) is on the order of $\frac{L^0 V_m}{C^0 F^0} = \frac{(3.10^{-5}).10^{-7}}{5.10^{-13}} \approx 5$. We then choose $F$ such that $\frac{\partial F}{\partial C}(C \approx 5$ Axial convection and diffusion are thought to be negligible in the renal interstitium. Since there is no accumulation of solute therein at steady state, we have

$$J^1(x) + J^2(x) + J^3(x) = 0. \tag{2.7}$$

This condition enables us to calculate the interstitial concentration explicitly

$$\forall x \in [0, L], \qquad C^{int}(x) = \frac{1}{3}\Big[C^1(x) + C^2(x) + C^3(x) + F(C^3(x), x)\Big].$$

The goal of the study is to analyze and solve the following nonlinear boundary value problem set for $x \in [0, L]$

$$\begin{cases} \dfrac{dC^1(x)}{dx} = \dfrac{1}{3}\Big[C^1(x) + C^2(x) + C^3(x) + F(C^3(x), x)\Big] - C^1(x), \\ \dfrac{dC^2(x)}{dx} = \dfrac{1}{3}\Big[C^1(x) + C^2(x) + C^3(x) + F(C^3(x), x)\Big] - C^2(x), \\ -\dfrac{dC^3(x)}{dx} = \dfrac{1}{3}\Big[C^1(x) + C^2(x) + C^3(x) + F(C^3(x), x)\Big] - C^3(x) - F(C^3(x), x), \\ C^1(0) = C^1_0, \qquad C^2(0) = C^2_0, \qquad C^3(L) = C^2(L). \end{cases} \tag{2.8}$$

This system represents the steady-state formulation of the standard dynamic problem [63] set for $t \geq 0$ and $x \in [0, L]$

$$\begin{cases} \dfrac{\partial C^1}{\partial t}(x,t) + \dfrac{\partial C^1}{\partial x}(x,t) = \dfrac{1}{3}\Big[(C^1+C^2+C^3)(x,t) + F(C^3(x,t),x)\Big] - C^1(x,t), \\ \dfrac{\partial C^2}{\partial t}(x,t) + \dfrac{\partial C^2}{\partial x}(x,t) = \dfrac{1}{3}\Big[(C^1+C^2+C^3)(x,t) + F(C^3(x,t),x)\Big] - C^2(x,t), \\ \dfrac{\partial C^3}{\partial t}(x,t) - \dfrac{\partial C^3}{\partial x}(x,t) = \dfrac{1}{3}\Big[(C^1+C^2+C^3)(x,t) + F\big(C^3(x,t),x\big)\Big] \\ \qquad\qquad\qquad - C^3(x,t) - F(C^3(x,t),x), \\ C^1(0,t) = C_0^1, \qquad C^2(0,t) = C_0^2, \qquad C^3(L,t) = C^2(L,t), \qquad t > 0. \end{cases} \tag{2.9}$$

which we complete with nonnegative initial concentrations $C^1(x,0)$, $C^2(x,0)$, $C^3(x,0)$. Implicit in this dynamic system is the assumption that the interstitium equilibrates immediately with its surroundings. In this study, we first prove that the solution to (2.9) converges, as $t$ tends to $\infty$, to the solution to (2.8) and that, under certain conditions, the convergence is exponential. We then use a finite volume scheme to solve (2.9) and thus approach the solution to (2.8). The numerical solution is subsequently employed to examine the effects of the countercurrent architecture on concentration gradients.

We study a nonlinear stationary system of transport equations with specific boundary conditions describing the transport of solutes dissolved in a fluid circulating in a countercurrent tubular architecture, which constitutes a simplified model of a kidney nephron. We prove that for every Lipschitz and monotonic nonlinearity (which stems from active transport across the ascending limb), the dynamic system, a PDE which we study through contraction properties, relaxes toward the unique stationary state. A study of the linearized stationary operator enables us, using eigenelements, to further show that under certain conditions regarding the nonlinearity, the relaxation is exponential. We also describe a finite volume scheme which allows us to efficiently approach the numerical solution to the stationary system. Finally, we apply this numerical method to illustrate how the countercurrent arrangement of tubes enhances the axial concentration gradient, thereby favoring the production of highly concentrated urine.

## 2.2 Main Results

The main objective of this section is to study the long time convergence of the dynamic solution to the stationary solution. For this purpose, we describe the mathematical structure of the dynamic and stationary systems, state the natural properties of the dynamic solution, and infer a priori bounds for the latter solution which are time-independent. The proofs of the theorems outlined below are given in Section 2.3. We follow the approach generally used to study relaxation systems, as in [43, 65], albeit with novel boundary conditions. We use the notation $C$ for the vector function $(C^1, C^2, C^3)$.

### 2.2.1 Existence, uniqueness and a priori bounds

To ensure that the dynamic solution exists, we must make some assumptions regarding the nonlinear term representing active transport. We assume that the (smooth) function $F$ satisfies for some (smooth) function $\mu(x) \geq 0$

$$F(C^3, x) \geq 0, \qquad F(0,x) = 0, \qquad 0 \leq \frac{\partial F}{\partial C}(C^3, x) \leq \mu(x) \leq \mu_M. \tag{2.10}$$

The Michaelis-Menten equation (2.3) which is generally used to represent active transport in the thick ascending limb can readily be shown to satisfy these 3 assumptions. The first one

means that the pump can only transport the solute in one direction, from the lumen of the thick ascending limb toward the interstitium. The second one describes the fact that there is no transport in the absence of solute. Lastly, the third assumption expresses the fact that the pump can be saturated because the number of carriers is limited.

Initial ($t = 0$) solute concentrations are positive. We further assume that, for $i = 1$, 2 or 3,

$$C^i(t=0) \geq 0, \qquad C^i(t=0) \in L^1(0,L), \qquad \frac{d}{dx}C^i(t=0) \in L^1(0,L). \tag{2.11}$$

Another possible assumption is that the initial data are 'well-prepared', that is to say they match the boundary conditions

$$C^1(0,t=0) = C_0^1, \qquad C^2(0,t=0) = C_0^2, \qquad C^3(L,t=0) = C^2(L,t=0).$$

We do not use this assumption and thus handle possibly discontinuous solutions.

**Theorem 2.2.1** (Existence and uniqueness of the dynamic problem solution)**.** *With assumptions* (2.10) *and* (2.11)*, there is a weak solution (defined in Appendix A) to the initial value problem* (2.9)*, which lies in* $BV([0,L]\times[0,T])$*. For two initial data* $C(x,0)$ *and* $\widetilde{C}(x,0)$*, the weak solutions satisfy the weak contraction property and the comparison principle*

$$\begin{aligned}\int_0^L \big[\, |C^1-\widetilde{C}^1| + |C^2-\widetilde{C}^2| + |C^3-\widetilde{C}^3| \,\big](x,t)dx \\ \leq \int_0^L \big[\, |C^1-\widetilde{C}^1| + |C^2-\widetilde{C}^2| + |C^3-\widetilde{C}^3| \,\big](x,0)dx,\end{aligned} \tag{2.12}$$

$$\begin{aligned}\int_0^L \big[\, |C^1-\widetilde{C}^1|_+ + |C^2-\widetilde{C}^2|_+ + |C^3-\widetilde{C}^3|_+ \,\big](x,t)dx \\ \leq \int_0^L \big[\, |C^1-\widetilde{C}^1|_+ + |C^2-\widetilde{C}^2|_+ + |C^3-\widetilde{C}^3|_+ \,\big](x,0)dx.\end{aligned} \tag{2.13}$$

*For the latter inequality, we can assume that* $\widetilde{C}$ *is only a supersolution. The contraction property implies the uniqueness of the solution.*

**Theorem 2.2.2** (Stationary supersolution)**.** *There is a family of supersolutions to* (2.8)*, as large as needed, that are continuous functions* $U$ *such that*

$$\begin{cases} \dfrac{dU^1(x)}{dx} + \dfrac{2}{3}U^1(x) - \dfrac{1}{3}\Big[U^2(x)+U^3(x)\Big] - \dfrac{1}{3}F(U^3(x),x) \geq 0, & (i) \\ \dfrac{dU^2(x)}{dx} + \dfrac{2}{3}U^2(x) - \dfrac{1}{3}\Big[U^1(x)+U^3(x)\Big] - \dfrac{1}{3}F(U^3(x),x) \geq 0, & (ii) \\ -\dfrac{dU^3(x)}{dx} + \dfrac{2}{3}U^3(x) + \dfrac{2}{3}F(U^3(x),x) - \dfrac{1}{3}\Big[U^1(x)+U^2(x)\Big] \geq 0, & (iii) \\ U^1(0) \geq C_0^1, \qquad U^2(0) \geq C_0^2, \qquad U^3(L) \geq U^2(L). \end{cases} \tag{2.14}$$

*For initial data* $C^i(x,0) \leq U^i(x)$*, then* $C^i(x,t) \leq U^i(x)$ *for all* $t \geq 0$*.*

**Theorem 2.2.3** (Uniform a priori estimates)**.** *The weak solution to* (2.9) *satisfies*

$$\int_0^L \big[\, |\frac{\partial}{\partial t}C^1| + |\frac{\partial}{\partial t}C^2| + |\frac{\partial}{\partial t}C^3| \,\big](x,t)dx \leq A^0, \tag{2.15}$$

$$\sup_{0\leq x\leq L} [C^1+C^2+C^3](x,t) \leq A^1, \tag{2.16}$$

$$\int_0^L \big[\, |\frac{\partial}{\partial x}C^1| + |\frac{\partial}{\partial x}C^2| + |\frac{\partial}{\partial x}C^3| \,\big](x,t)dx \leq A^2, \tag{2.17}$$

*for some constants* $A^i$ *depending only on the initial values* $C^i(0,x)$ *and their derivatives but not on* $t$*.*

### 2.2.2 Long time behavior. Stationary problem

Our next results concern the problem we are interested in, that is the steady state and its stability. We begin with the

**Theorem 2.2.4** (Existence of the stationary problem solution)**.** *With assumptions* (2.10)*, there is a unique solution to* (2.8) *which is* $C^1$ *and nonnegative.*

With the uniform bounds in Theorem 2.2.3, we can study the time convergence to this steady state.

**Theorem 2.2.5** (Long time behavior and uniqueness of the stationary problem solution)**.** *With assumptions* (2.10)*,* (2.11)*, the solution* $C$ *to* (2.9) *converges to the unique solution* $\overline{C}$ *to* (2.8) *in* $L^1$*,*

$$\|C(x,t) - \overline{C}(x)\|_{L^1} \underset{t\to\infty}{\searrow} 0.$$

Physiologically, this means that, whatever the initial solute concentrations, the system reaches the same steady state, that is, stationary concentration profiles are independent of initial values.

We can go further and study the rate of convergence toward the stationary solution. This requires some further notations and assumptions. For $\mu(x)$ defined in (2.10), we use the notations in Appendix C for the eigenelements $\phi = (\phi^1, \phi^2, \phi^3)$, $k(\mu)$ and $\lambda(\mu)$. We assume

$$\sup_{x\in[0,L]} \big(2 - k(\mu)\big)_+ [\mu(x) - \frac{\partial F}{\partial C}(C,x)] < \lambda(\mu). \tag{2.18}$$

When $F(C,x) = \mu(x)C$, this condition is obviously satisfied and thus expresses a smallness condition on the second derivative in $C$.

When $F(C^3,x) = V_m(x)\frac{C^3}{1+C^3}$, the condition simplifies to

$$\sup_{x\in[0,L]} \big(2 - k(V_m)\big)_+ V_m(x) < \lambda(V_m), \tag{2.19}$$

which is a smallness condition on $V_m$ since $\lambda(0) > 0$.

With this assumption, we can state the

**Theorem 2.2.6** (Exponential convergence)**.** *With assumptions* (2.10)*,* (2.11) *and* (2.18)*, the solution to the problem* (2.9) *converges exponentially with* $t$ *to the unique solution to* (2.8) *in the space*

$$L^1(\phi) = \left\{ f : [0,L] \to \mathbb{R}^3,\ \int_{[0,L]} \Big( |f^1(x)|\phi^1(x) + |f^2(x)|\phi^2(x) + |f^3(x)|\phi^3(x) \Big) dx < \infty \right\}.$$

*that is to say:*

$$\|C(x,t) - \overline{C}(x)\|_{L^1(\phi)} \le e^{-\mu t} \|C(x,0) - \overline{C}(x)\|_{L^1(\phi)}.$$

This theorem expresses a narrower result: if the maximal pump velocity $V_m$ is small enough, the system reaches steady state at an exponential rate which depends on $V_m$. It is proved in Appendix C.

## 2.3 Proof of existence and a priori bounds

Because it is closely related to our numerical algorithm, and in order to introduce some basic concepts, we choose an approach based on the semi-discrete scheme.

### 2.3.1 Existence of a solution to the semi-discrete problem

Consider a discretisation parameter $\Delta x = L/N > 0$ with $N$ an integer. The semi-discrete scheme associated with (2.9) is defined, for $k \in [1, N]$, as

$$\begin{cases} \dfrac{dC_k^1}{dt}(t) + \dfrac{C_k^1(t) - C_{k-1}^1(t)}{\Delta x} = \dfrac{1}{3}\Big[C_k^1(t) + C_k^2(t) + C_k^3(t) + F(C_k^3(t))\Big] - C_k^1(t), \\ \dfrac{dC_k^2}{dt}(t) + \dfrac{C_k^2(t) - C_{k-1}^2(t)}{\Delta x} = \dfrac{1}{3}\Big[C_k^1(t) + C_k^2(t) + C_k^3(t) + F(C_k^3(t))\Big] - C_k^2(t), \\ \dfrac{dC_k^3}{dt}(t) - \dfrac{C_{k+1}^3(t) - C_k^3(t)}{\Delta x} = \dfrac{1}{3}\Big[C_k^1(t) + C_k^2(t) + C_k^3(t) + F(C_k^3(t))\Big] \\ \qquad\qquad - C_k^3(t) - F(C_k^3(t)), \end{cases} \tag{2.20}$$

with the boundary conditions $C_0^1 > 0$ and $C_0^2 > 0$ given in (2.9) and $C_{N+1}^3 = C_N^2$. We also choose the initial data

$$C_k^i(0) = \frac{1}{\Delta x}\int_{(k-1)\Delta x}^{k\Delta x} C^i(x,0)dx, \quad i = 1,\ 2,\ 3, \quad k = 1, ..., N. \tag{2.21}$$

Because (2.20) is a system of differential equations, it has a unique smooth solution and it is nonnegative. Indeed, if there exists $(i, k, t)$ (for instance $i = 1$ without loss of generality) where

$$t = \inf\{s \text{ such that } \exists (k, i) \text{ satisfying } C_k^i(s) = 0\},$$

then,

$$\frac{dC_k^1}{dt}(t) = \frac{C_{k-1}^1(t)}{\Delta x} + \frac{1}{3}\Big(C_k^2(t) + C_k^3(t) + F(C_k^3(t))\Big) \geq 0.$$

So, $C_k^1(t)$ cannot become negative.

In order to link the continuous model to this discrete equation, we reconstruct three piecewise constant functions $C_{\Delta x}^i(x,t)$, from the discrete values, as

$$C_{\Delta x}^i(x,t) = C_k^i(t), \quad \text{for} \quad x \in ((k-1)\Delta x, k\Delta x), \quad i = 1,\ 2,\ 3. \tag{2.22}$$

To simplify the notation, we sometimes merely write $C$ instead of $C_{\Delta x}$. We next prove that $C_{\Delta x}$ converges to the continuous solution.

Our proof is divided in several steps. We first recall some preliminary estimates on $C_k^i(0)$. Secondly we derive several uniform (in $\Delta x$) a priori bounds on the semi-discrete solutions. Thirdly, we use these estimates to prove that the solution converges when $\Delta x$ goes to 0 to a weak solution to (2.9). Then, still using a priori bounds, we find some additional properties of the solution. These are enough to pass to the limit and recover a weak solution to (2.9).

**First step. Preliminary controls.** Given our assumptions (2.11), we derive using a classic approach (see [9, 25, 58]) the following initial bounds at the discrete level

$$\|C_{\Delta x}(t=0)\|_{L^1} \leq K^0 := \sum_{i=1}^{3} \|C^i(t=0)\|_{L^1}, \tag{2.23}$$

$$\sum_{i=1}^{3}\sum_{k=1}^{N} \|C_k^i(t=0) - C_{k-1}^i(t=0)\|_{L^1} \leq K^1 := \sum_{i=1}^{3} \|\frac{d}{dx}C^i(t=0)\|_{M^1}, \tag{2.24}$$

$$\|\frac{d}{dt}C_{\Delta x}(t=0)\|_{L^1} \leq K^2, \tag{2.25}$$

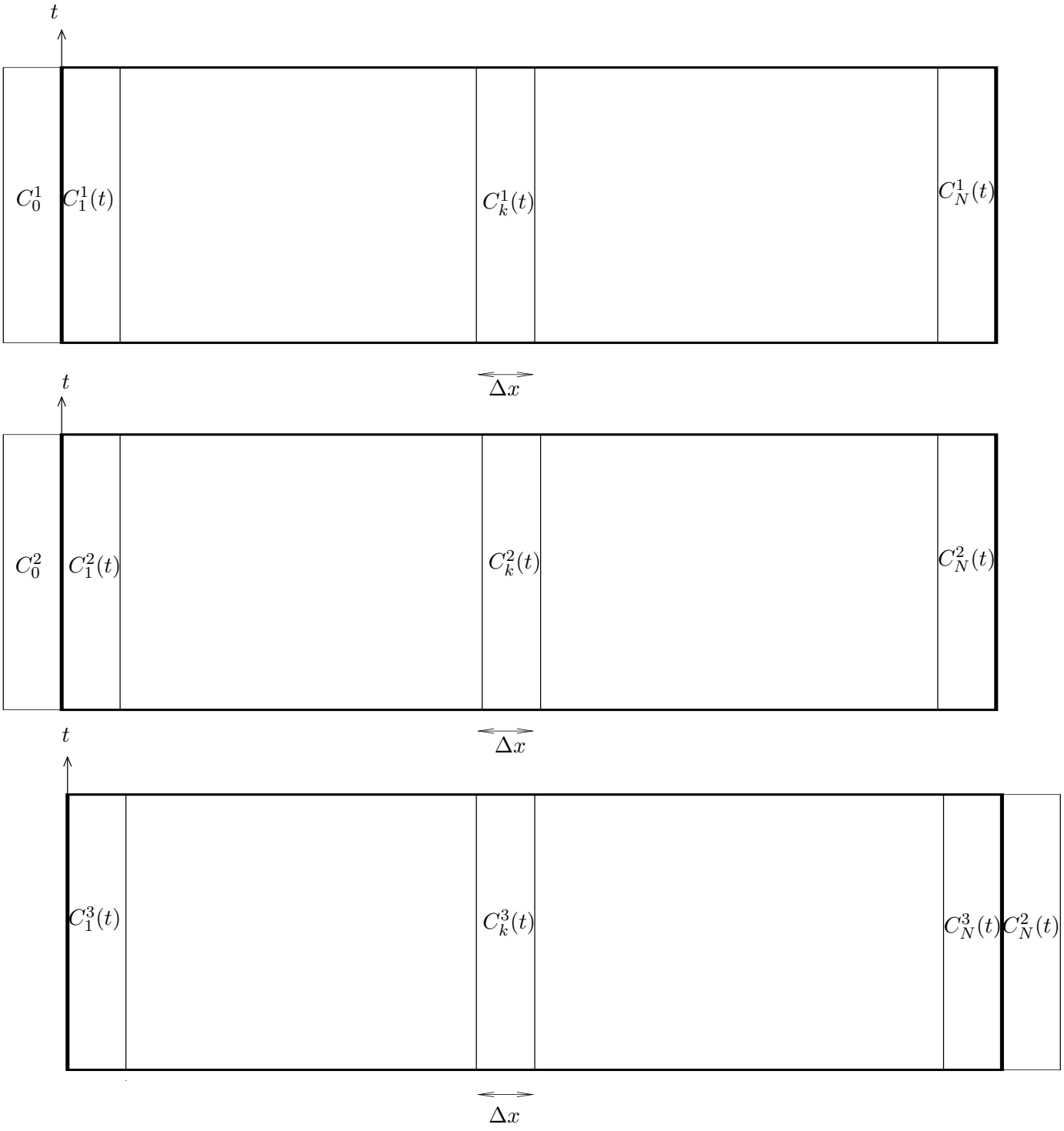


**Figure 2.2:** The 3 discretization grids correspond to the 3 concentrations $C^i, i = 1, 2, 3$. In abscissa : the discrete space $k \in [1, N]$. In ordinate : time evolves continuously. We denote by $C_k^i(t)$ the solution of (2.20) taken at time $t$ in cell $k$, $k \in [1, N]$. The cells numbered by $k = 0$ and $k = N + 1$ stock the boundary conditions

for a constant $K^2$, obtained from the equation and using (2.23)–(2.24), which only depends on the initial data but not on $\Delta x$. Here, $M^1$ is the Banach space of bounded measures. Indeed, from (2.20), we deduce that we have

$$\begin{aligned}\|\frac{dC}{dt}(0)\|_{L^1} \leq &\sum_{k=1}^{N}|C_k^1(0)-C_{k-1}^1(0)|+\sum_{k=1}^{N}|C_k^2(0)-C_{k-1}^2(0)|\\ &+\sum_{k=1}^{N}|C_k^3(0)-C_{k+1}^3(0)|+\frac{4}{3}(\mu_M+1)\|C(0)\|_{L^1}\end{aligned} \tag{2.26}$$

because $\mu$ is bounded on $[0,L]$ by $\mu_M$.

On the other hand (2.24) holds true. The notation $\|\cdot\|_{M^1}$ includes a Dirac mass at $x=0$ for $i=1$, 2, when the initial data do not match the boundary condition. Indeed, applying (2.11) to $C^1$, and based upon (2.21), we can write

$$\begin{aligned}\sum_{k=1}^{N}|C_k^1(0)-C_{k-1}^1(0)| =&\frac{1}{\Delta x}\Big[\sum_{k=2}^{N}\Big|\int_{(k-1)\Delta x}^{k\Delta x}C^1(x,0)dx-\int_{(k-2)\Delta x}^{(k-1)\Delta x}C^1(x,0)dx\Big|\\ &+\Big|\int_0^{\Delta x}(C^1(x,0)-C_0^1)dx\Big|\Big],\end{aligned}$$

$$\begin{aligned}\sum_{k=1}^{N}|C_k^1(0)-C_{k-1}^1(0)| &= \frac{1}{\Delta x}\Big[\sum_{k=2}^{N}\Big|\int_{(k-1)\Delta x}^{k\Delta x}[C^1(x,0)-C^1(x-\Delta x,0)]dx\Big|+\Big|\int_0^{\Delta x}(C^1(x,0)-C_0^1)dx\Big|\Big]\\ &= \frac{1}{\Delta x}\Big[\sum_{k=2}^{N}\Big|\int_{(k-1)\Delta x}^{k\Delta x}\int_{x-\Delta x}^{x}\frac{d}{dx}C^1(z,0)dzdx\Big|+\Big|\int_0^{\Delta x}\int_0^{x}\frac{d}{dx}C^1(z,0)dzdx\Big|\Big]\\ &\leq \frac{1}{\Delta x}\Big[\sum_{k=2}^{N}\int_{(k-1)\Delta x}^{k\Delta x}\int_0^{\Delta x}\Big|\frac{d}{dx}C^1(x+u-\Delta x,0)\Big|dudx+\int_0^{\Delta x}\int_0^{x}\Big|\frac{d}{dx}C^1(z,0)\Big|dzdx\Big]\\ &\leq \frac{1}{\Delta x}\Big[\int_0^{\Delta x}\int_{\Delta x}^{L}\Big|\frac{d}{dx}C^1(x+u-\Delta x,0)\Big|dx\,du+\int_0^{\Delta x}\int_0^{x}\Big|\frac{d}{dx}C^1(z,0)\Big|dzdx\Big]\\ &\leq \frac{1}{\Delta x}\Big[\int_0^{\Delta x}\int_{x}^{L+x-\Delta x}\Big|\frac{d}{dx}C^1(z,0)\Big|dz\,dx+\int_0^{\Delta x}\int_0^{x}\Big|\frac{d}{dx}C^1(z,0)\Big|dzdx\Big]\\ &\leq \frac{1}{\Delta x}\int_0^{\Delta x}\int_0^{L+x-\Delta x}\Big|\frac{d}{dx}C^1(z,0)\Big|dz\,dx\\ &\leq \|\frac{d}{dx}C^1(t=0)\|_{L^1}.\end{aligned}$$

□

**Second step. Control in time.** We first prove a uniform control on time derivatives

$$\|\frac{dC_{\Delta x}}{dt}(t)\|_{L^1}\leq\|\frac{dC_{\Delta x}}{dt}(0)\|_{L^1}\leq K^2,\qquad\forall t>0. \tag{2.27}$$

To prove this, we differentiate (2.20) with respect to $t$, we multiply each line $i$ by $\mathrm{sign}(\frac{d}{dt}C_k^i)$ and find

$$\begin{cases}\frac{d}{dt}\Big|\frac{dC_k^1(t)}{dt}\Big|+\frac{1}{\Delta x}\Big[\Big|\frac{d}{dt}C_k^1(t)\Big|-\Big|\frac{d}{dt}C_{k-1}^1(t)\Big|\Big]\leq-\frac{2}{3}\Big|\frac{d}{dt}C_k^1\Big|+\frac{1}{3}\Big|\frac{d}{dt}C_k^2\Big|+\frac{1}{3}\Big|\frac{d}{dt}C_k^3\Big|+\frac{1}{3}\Big|\frac{d}{dt}C_k^3\Big|\frac{\partial F}{\partial C},\\ \frac{d}{dt}\Big|\frac{dC_k^2(t)}{dt}\Big|+\frac{1}{\Delta x}\Big[\Big|\frac{d}{dt}C_k^2(t)\Big|-\Big|\frac{d}{dt}C_{k-1}^2(t)\Big|\Big]\leq\frac{1}{3}\Big|\frac{d}{dt}C_k^1\Big|-\frac{2}{3}\Big|\frac{d}{dt}C_k^2\Big|+\frac{1}{3}\Big|\frac{d}{dt}C_k^3\Big|+\frac{1}{3}\Big|\frac{d}{dt}C_k^3\Big|\frac{\partial F}{\partial C},\\ \frac{d}{dt}\Big|\frac{dC_k^3(t)}{dt}\Big|+\frac{1}{\Delta x}\Big[\Big|\frac{d}{dt}C_k^3(t)\Big|-\Big|\frac{d}{dt}C_{k+1}^3(t)\Big|\Big]\leq\frac{1}{3}\Big|\frac{d}{dt}C_k^1\Big|+\frac{1}{3}\Big|\frac{d}{dt}C_k^2\Big|-\frac{2}{3}\Big|\frac{d}{dt}C_k^3\Big|-\frac{2}{3}\Big|\frac{d}{dt}C_k^3\Big|\frac{\partial F}{\partial C}.\end{cases}$$

We sum on the lines and on the indices $k$ to obtain

$$\frac{d}{dt}\sum_{k=1}^{N}\sum_{i=1}^{3}\Delta x|\frac{d}{dt}C_k^i(t)| \le -|\frac{d}{dt}C_N^1(t)| + |\frac{d}{dt}C_0^1| - |\frac{d}{dt}C_N^2(t)| + |\frac{d}{dt}C_0^2| + |\frac{d}{dt}C_{N+1}^3(t)| - |\frac{d}{dt}C_1^3|. \tag{2.28}$$

Knowing that $C_0^1$ and $C_0^2$ are independent of $t$, we have $\frac{d}{dt}C_0^1 = 0$, $\frac{d}{dt}C_0^2 = 0$. In addition, since $C_{N+1}^3(t) = C_N^2(t)$, we have $\frac{d}{dt}C_{N+1}^3(t) = \frac{d}{dt}C_N^2(t)$. Altogether, we arrive at

$$\frac{d}{dt}\sum_{k=1}^{N}\Delta x\Big[|\frac{d}{dt}C_k^1(t)| + |\frac{d}{dt}C_k^2(t)| + |\frac{d}{dt}C_k^3(t)|\Big] \le 0. \tag{2.29}$$

That proves our first estimate (2.27).

**Third step. Bounds on $C_{\Delta x}$.** Our purpose here is to prove that we also have for all $t \ge 0$

$$\|C_{\Delta x}(t)\|_{L^1} \le K^0 + K^3 t, \qquad \text{with } \; K^3 = C_0^1 + C_0^2. \tag{2.30}$$

To do so, using (2.20), we sum on the lines and on the indices and find

$$\frac{d}{dt}\sum_{k=1}^{N}\Delta x\Big[C_k^1(t) + C_k^2(t) + C_k^3(t)\Big] \le C_0^2 + C_0^1 \tag{2.31}$$

and the result follows.

**Fourth step. Uniform bounded variations on $C_{\Delta x}$.** We want to prove the uniform $BV$ control

$$\sum_{k=1}^{N}|C_k - C_{k-1}|(t) \le K^4(1+t) \qquad \forall t > 0. \tag{2.32}$$

Note that an uniform bound follows directly from this $BV$ control. For all $t \ge 0$,

$$C_k^i \le C_0^i + K^4(1+t),\ i = 1,\ 2, \qquad C_k^3 \le C_0^2 + 2K^4(1+t). \tag{2.33}$$

We prove it for $C^1$ only. We deduce from (2.20) that

$$\begin{aligned}\sum_{k=1}^{N}|C_k^1 - C_{k-1}^1|(t) &\le \sum_{k=1}^{N}\Delta x|\frac{d}{dt}C_k^1(t)| + \sum_{k=1}^{N}\frac{\Delta x}{3}\Big[2|C_k^1| + |C_k^2| + (1+\mu_M)|C_k^3|\Big](t)\\ &\le K^4(1+t)\end{aligned}$$

using the estimates (2.30) and (2.27).

**Fifth step. Convergence of the semi-discrete solution.** Because we have proved that $C_{\Delta x}$ is uniformly bounded in $BV([0,T]\times[0,L])$, according to the Rellich-Kondrachov compactness theorem (see [16,19]), there is a subsequence which converges in $L^1\big((0,T)\times(0,L)\big)$ to a function $C(x,t) \in L^1\big((0,T)\times(0,L)\big)$. Then, after further extracting a subsequence we obtain

$$C_{\Delta x}(x,t) \underset{\Delta x\to 0}{\longrightarrow} C(x,t), \qquad a.e.$$

Consequently we also have, because $F$ is continuous in $C^3$,

$$F(C_{\Delta x}^3(x,t),x) \underset{\Delta x\to 0}{\longrightarrow} F(C^3(x,t),x).$$

To check that this limit is a weak solution to (2.9), we introduce the set $V$ of test-functions

$$V = \left\{ \Phi \in \left( C^1(\mathbb{R}^+ \times [0,L]) \right)^3, \qquad \Phi^1(L,t) = \Phi^3(0,t) = 0, \qquad \Phi^3(L,t) = \Phi^2(L,t) \right\}. \quad (2.34)$$

It is easy to pass to the limit in the zero order terms because, using the dominated convergence theorem, we have, for all $\Phi \in V$

$$\int_0^T \int_0^L C^j_{\Delta x}(x,t)\Phi^j(x,t)dxdt \underset{\Delta x \to 0}{\longrightarrow} \int_0^T \int_0^L C^j(x,t)\Phi^j(x,t)dxdt,$$

$$\int_0^T \int_0^L F(C^3_{\Delta x}(x,t),x)\Phi^j(x,t)dxdt \underset{\Delta x \to 0}{\longrightarrow} \int_0^T \int_0^L F(C^3(x,t),x)\Phi^j(x,t)dxdt.$$

To recover the terms with $x$-derivatives is more difficult. After a change of variable, we write

$$\int_0^T \int_{\Delta x}^L \frac{C^1_{\Delta x}(x,t) - C^1_{\Delta x}(x-\Delta x,t)}{\Delta x}\Phi^1(x,t)dxdt$$

$$= \int_0^T \int_{\Delta x}^L \frac{C^1_{\Delta x}(x,t)}{\Delta x}\Phi^1(x,t)dxdt - \int_0^T \int_0^{L-\Delta x} \frac{C^1_{\Delta x}(x,t)}{\Delta x}\Phi^1(x+\Delta x,t)dxdt$$

$$= -\int_0^T \int_0^{\Delta x} \frac{C^1_{\Delta x}(x,t)}{\Delta x}\Phi^1(x,t)dxdt + \int_0^T \int_0^{L-\Delta x} C^1_{\Delta x}(x,t)\frac{\Phi^1(x,t) - \Phi^1(x+\Delta x,t)}{\Delta x}dxdt$$

$$+ \int_0^T \int_{L-\Delta x}^L \frac{C^1_{\Delta x}(x,t)}{\Delta x}\Phi^1(x,t)dxdt.$$

Using again the dominated convergence theorem, we have

$$\int_0^T \int_{\Delta x}^{L-\Delta x} C^1_{\Delta x}(x,t)\frac{\Phi^1(x,t) - \Phi^1(x+\Delta x,t)}{\Delta x}dxdt \underset{\Delta x \to 0}{\longrightarrow} -\int_0^T \int_0^L C^1(x,t)\frac{\partial \Phi^1(x,t)}{\partial x}dxdt,$$

$$-\int_0^T \int_0^{\Delta x} \frac{C^1_{\Delta x}(x,t)}{\Delta x}\Phi^1(x+\Delta x,t)dxdt \underset{\Delta x \to 0}{\longrightarrow} -\int_0^T \Phi^1(0,t)C^1(0,t),$$

$$\int_0^T \int_{L-\Delta x}^L \frac{C^1_{\Delta x}(x,t)}{\Delta x}\Phi^1(x,t)dxdt \underset{\Delta x \to 0}{\longrightarrow} \int_0^T \Phi^1(L,t)C^1(L,t) = 0.$$

Integrating by part, we obtain

$$\int_0^T \int_0^L \frac{\partial C^1_{\Delta x}(x,t)}{\partial t}\Phi^1(x,t)dxdt = \underset{\Delta x \to 0}{\longrightarrow} -\int_0^T \int_0^L C^1(x,t)\frac{\partial \Phi^1(x,t)}{\partial t}dxdt$$

$$+ \int_0^L \Phi^1(x,T)C^1(x,T)dx - \int_0^L \Phi^1(x,0)C^1(x,0)dx.$$

We are now ready to pass to the limit in the equations. We treat each component of the system independently. The equation satisfied by $C^1_{\Delta x}$ is

$$\begin{cases} \dfrac{\partial C^1_{\Delta x}}{\partial t}(x,t) + \dfrac{C^1_{\Delta x}(x,t) - C^1_{\Delta x}(x-\Delta x,t)}{\Delta x} = -\dfrac{2}{3}C^1_{\Delta x}(x,t) \\ \qquad\qquad + \dfrac{1}{3}\Big[C^2_{\Delta x}(x,t) + C^3_{\Delta x}(x,t) + F(C^3_{\Delta x}(x,t),x)\Big], \ x \in ]\Delta x, L], \\ \dfrac{\partial C^1_{\Delta x}}{\partial t}(x,t) + \dfrac{C^1_{\Delta x}(x,t) - C^1_0}{\Delta x} = -\dfrac{2}{3}C^1_{\Delta x}(x,t) \\ \qquad\qquad + \dfrac{1}{3}\Big[C^2_{\Delta x}(x,t) + C^3_{\Delta x}(x,t) + F(C^3_{\Delta x}(x,t),x)\Big], \quad x \in ]0, \Delta x], \\ C^1_{\Delta x}(0,t) = C^1_0, \qquad\qquad x = 0. \end{cases} \quad (2.35)$$

The equations for $C^2$ and $C^3$ are treated similarly, because the boundary conditions are related and cancel out when adding the equations. Thus, we prove that $C$ satisfies the following weak formulation.

We subsequently prove that the first line of (2.35) converges to a weak equation, and deduce the weak equation satisfied by $C$.

### 2.3.2 Properties of limit

In the limit process, we keep the a priori bounds that we record here from (2.27), (2.30), (2.32)

$$\int_0^L [C^1 + C^2 + C^3](x,t)dx \leq K^0 + K^3 t, \qquad \forall t \geq 0, \tag{2.36}$$

$$\int_0^L \big[\, |\frac{\partial}{\partial t}C^1| + |\frac{\partial}{\partial t}C^2| + |\frac{\partial}{\partial t}C^3| \,\big](x,t)dx \leq K^2, \qquad \forall t \geq 0, \tag{2.37}$$

$$\|\frac{\partial C}{\partial x}(t)\|_{L^1[0,L]} \leq K^4(1+t) \qquad \forall t \geq 0. \tag{2.38}$$

Moreover, we can prove that $C$ is uniformly continuous in time. Indeed, $\forall t > 0, h > 0$,

$$\begin{aligned}\|C(x,t+h) - C(x,t)\|_{L^1[0,L]} &\leq \int_0^L \Big| \int_0^h \frac{\partial}{\partial t} C(x,t+s)ds \Big| dx \\ &\leq \int_0^h \|\frac{d}{dt}C(x,t+s)\|_{L^1[0,L]}ds \leq K^0 h. \qquad \square\end{aligned}$$

This proves that for all $T > 0$ the regularity holds also

$$C^i \in C\Big([0,T]; L^1[0,L]\Big) \cap BV\Big([0,T] \times [0,L]\Big).$$

The drawback of estimates (2.36) and (2.38) is that they are time-dependent. This is improved in Section 2.3.4.

### 2.3.3 The contraction property and the comparison principle

We continue this section with the contraction property (2.12). We use the notations

$$d^i(x,t) := |C^i(x,t) - \widetilde{C}^i(x,t)|, \qquad i = 1,\ 2,\ 3.$$

$$G(x,t) := |F\big(C^3(x,t),x\big) - F\big(\widetilde{C^3}(x,t),x\big)| \leq \mu(x)\ d^3(x,t).$$

We substract the lines $i$ in (2.9) for $C$ and $\widetilde{C}$. We multiply them by sign $\big(C^i(x,t) - \widetilde{C^i}(x,t)\big)$, (see [1, 72] and the references therein). We obtain the inequalities

$$\begin{cases} \dfrac{\partial d^1}{\partial t} + \dfrac{\partial d^1}{\partial x} \leq -\dfrac{2}{3}d^1 + \dfrac{1}{3}(d^2 + d^3 + G), \\ \dfrac{\partial d^2}{\partial t} + \dfrac{\partial d^2}{\partial x} \leq -\dfrac{2}{3}d^2 + \dfrac{1}{3}(d^1 + d^3 + G), \\ \dfrac{\partial d^3}{\partial t} - \dfrac{\partial d^3}{\partial x} \leq -\dfrac{2}{3}(d^3 + G) + \dfrac{1}{3}(d^2 + d^1). \end{cases} \tag{2.39}$$

The third line uses the fact that, because we assume $F$ is nondecreasing in $C$ (assumption (2.10))

$$\text{sign}\,\big(C^3(x,t) - \widetilde{C^3}(x)\big)\,\Big[F\big(C^3(x,t),x\big) - F\big(\widetilde{C^3}(x),x\big)\Big] = \Big|F\big(C^3(x,t),x\big) - F\big(\widetilde{C^3}(x),x\big)\Big|.$$

From these inequalities we conclude that

$$\frac{d}{dt}\int_0^L [d^1+d^2+d^3]dx \le -d^1(L,t)-d^3(0,t)\le 0, \tag{2.40}$$

which implies

$$\int_0^L [d^1(x,t)+d^2(x,t)+d^3(x,t)]dx \le \int_0^L [d^1(x,0)+d^2(x,0)+d^3(x,0)]dx. \tag{2.41}$$

This is the contraction property (2.12). □

The variant (2.13) can be proved following the same calculation, multiplying line $i$ by $\mathrm{sign}_+\Big(\widetilde{C}^i(x,t)-C^i(x,t)\Big)$, defined by $\mathrm{sign}_+(f)=\mathrm{sign}\Big(\max(f,0)\Big)$. Because $\mathrm{sign}_+$ is increasing, it is enough to work with a supersolution $\widetilde{C}^i(x,t)$.

### 2.3.4 Proof of Theorem 2.2.3 and supersolution

We first build the family of stationary supersolutions, then we derive the uniform bounds on $C(x,t)$.

**First step. A family of supersolution to** (2.8)**.** Our goal is to build nonnegative functions $U^1$, $U^2$, $U^3$ such that $U^3(x)=U^1(x)+U^2(x)$ and $U^1$, $U^2$ satisfy

$$\begin{cases} \dfrac{dU^1(x)}{dx}+\dfrac{1}{3}U^1(x)-\dfrac{2}{3}U^2(x)-\dfrac{1}{3}F(U^1(x)+U^2(x),x)=0,\\ \dfrac{dU^2(x)}{dx}+\dfrac{1}{3}U^2(x)-\dfrac{2}{3}U^1(x)-\dfrac{1}{3}F(U^1(x)+U^2(x),x)=0,\\ U^1(0)\ge C_0^1, \qquad U^2(0)\ge C_0^2. \end{cases} \tag{2.42}$$

which is clearly sufficient to have a supersolution to (2.8).

For $U^3$, summing the equations on $U^1$ and $U^2$, we obtain

$$\frac{d}{dx}\Big[U^1(x)+U^2(x)\Big]-\frac{1}{3}\Big[U^1(x)+U^2(x)\Big]-\frac{2}{3}F(U^1(x)+U^2(x),x)=0,$$

so that we also have

$$-\frac{dU^3(x)}{dx}+\frac{2}{3}U^3(x)+\frac{2}{3}F(U^3(x),x)-\frac{1}{3}\Big[U^1(x)+U^2(x)\Big]=0,$$

which implies that the correct equation holds. The boundary condition is also satisfied as a supersolution because $U^3(L)=U^2(L)+U^1(L)\ge U^2(L)$.

To build a supersolution to (2.42), we choose $U^1=U^2=\frac{1}{2}H$, where $H$ satisfies

$$\frac{dH(x)}{dx}-\frac{1}{3}H(x)-\frac{2}{3}F(H(x),x)=0, \qquad H(0)=2\max(C_0^1,C_0^2). \tag{2.43}$$

We conclude the proof because (2.43) is solved by the Cauchy-Lipschitz theorem. The uniqueness in the Cauchy Lipschitz theorem guarantees the positivity of $H$, because the function constantly equal to 0 is a solution. Note that the boundary condition $H(0)=H^0$ in place of $2\max(C_0^1,C_0^2)$ allows us to find $U^1$ and $U^2$ (and thus $U^3$) as large as we want. □

**Second step. Uniform $L^\infty$ bounds on** $C^i(x,0)$. From the comparison principle (2.13), we conclude that $C(x,t)\le U^i(x)$ choosing, as indicated above, $U^i(x)\ge C^i(x,0)$. This proves (2.16).

From this uniform a priori bound, we also deduce (2.17) which improves (2.38). □

### 2.3.5 Proof of Theorem 2.2.4 (existence of a solution to the stationary problem)

We prove the existence of a solution to (2.8). To do so, we use an auxiliary boundary value problem which is studied in Appendix B,

$$\begin{cases} \dfrac{dC^1(x)}{dx}+\dfrac{2}{3}C^1(x) = \dfrac{1}{3}\Big[C^2(x)+C^3(x)+F(C^3(x),x)\Big], \\ \dfrac{dC^2(x)}{dx}+\dfrac{2}{3}C^2(x) = \dfrac{1}{3}\Big[C^1(x)+C^3(x)+F(C^3(x),x)\Big], \\ -\dfrac{dC^3(x)}{dx}+\dfrac{2}{3}\Big[C^3(x)+F(C^3(x),x)\Big] = \dfrac{1}{3}\Big[C^1(x)+C^2(x)\Big], \\ \qquad C^1(0)=C_0^1>0, \qquad C^2(0)=C_0^2>0, \qquad C^3(L)=C_L^3\geq 0. \end{cases} \tag{2.44}$$

For Theorem 2.2.4, it is enough to prove that there is a positive value $C_L^3$ such that the solution to (2.44) satisfies $C^3(L)=C^2(L)$. To do so, we define the continuous mapping

$$g : C_L^3 \longmapsto C^2(L)-C^3(L)$$

We claim that $g(0)>0$ and that $g(\infty)<0$, which implies that $g$ vanishes on $\mathbb{R}^+$ and concludes the proof.

• $g(0)>0$. By the maximum principle, the $C^i(\cdot)$ are nonnegative and since $C_0^2$ is positive, so is $C^2(L)$.
• $g(\infty)<0$. We want to prove that for $C_L^3$ large enough $C^2(L)<C_L^3$. It is enough to prove that

$$C^1(L)+C^2(L)<C^3(L). \tag{2.45}$$

Because solutions to (2.44) satisfy

$$\frac{d}{dx}\Big[C^1+C^2-C^3\Big]=0,$$

proving (2.45) is equivalent to proving that

$$C_0^1+C_0^2<C^3(0). \tag{2.46}$$

But this is obvious because, since the $C^i$s are nonnegative, we have $C^3(x)\geq C^3(L)\exp(-2(1+\mu_M)(L-x)/3)$. This concludes the existence proof.

Uniqueness follows again from the contraction property (2.40) which for time independent solutions proves that the three components coincide at $x=0$. □

### 2.3.6 Proof of Theorem 2.2.5 (large time limit)

Our proof is organized as follows. We consider the case where the initial data is a sub- or a supersolution to the steady state equation (2.8); we prove that the solutions are monotonic in time and, because they are bounded as stated in Theorem 2.2.3, they converge to the steady state. This is enough because for any initial data, we can always use Theorem 2.2.2 and find a supersolution $U_0$ such that

$$0\leq C^i(x,0)\leq U_0^i(x) \qquad \forall i,\ \forall x\in[0,L].$$

Calling $V$ and $U$ the solutions to (2.9) with respective initial conditions taken to be $V_0=0$ (a subsolution!) and $U_0$, we obtain according to the comparison principle

$$V^i(x,t)\leq C^i(x,t)\leq U^i(x,t) \qquad \forall i,\ \forall x\in[0,L],\ \forall t>0.$$

As $U$ and $V$ converge toward the steady state, so does $C$.

With this argument we are reduced to proving Theorem 2.2.5 with initial data $C(.,t=0)$ that are supersolution to (2.8); indeed the same argument holds for subsolutions where the only modification consists in replacing the $\left(\frac{\partial C}{\partial t}\right)_+$ with $\left(\frac{\partial C}{\partial t}\right)_-$.

**First step.** In the same way that we established the first inequality of Theorem 2.2.3, we can differentiate (2.9) with respect to $t$, multiply each line $i$ by $\text{sign}_+(\frac{\partial C^i}{\partial t})$ (defined in Section 2.3.3), and sum on the lines. We obtain the variant of (2.15)

$$\frac{d}{dt}\int_0^L \Big[\Big(\frac{\partial C^1}{\partial t}\Big)_+ + \Big(\frac{\partial C^2}{\partial t}\Big)_+ + \Big(\frac{\partial C^3}{\partial t}\Big)_+\Big](x,t)dt \leq 0. \tag{2.47}$$

**Second step.** As $C(.,t=0)$ is a supersolution, we have $\Big(\frac{\partial C^i}{\partial t}(x,0)\Big)_+ = 0$ for all $i$, $x \in [0,L]$. Using (2.47), we conclude that

$$\Big(\frac{\partial C^i}{\partial t}(x,t)\Big)_+ = 0 \qquad \forall i,\ \forall x \in [0,L],\ \forall t > 0,$$

which means that $C(.,t)$ is a supersolution of (2.8) for all $t > 0$ and that each component is monotonically decreasing.

Therefore we can pass to the limit pointwise as $t \to \infty$ and $C^i(x,t)$ converges to a function $\overline{C}^i(x)$. Because time derivatives converge to 0 in the distributional sense, $\overline{C}(x)$ is the stationary solution and thus coincides with that built in Theorem 2.2.4.

This establishes theorem 2.2.5 for initial data which are supersolutions and thus concludes the proof. □

## 2.4 Numerical method

Since, at least for small nonlinearities, the solution to the dynamic problem converges exponentially toward the steady state solution, we propose to approach numerically the solution to (2.8) by computing the solution to (2.9) for large times. For simplicity, we only treat the Michaelis-Menten form of the active transport term (2.3). Also, as is usually done with in transport equations, we use a finite volume method (see [9, 25, 58]). This finite volume scheme is directly adapted from finite volume schemes found in the literature.

### 2.4.1 The finite volume scheme

We use a time step $\Delta t$ and a mesh of size $\Delta x = L/N$ with $N$ the number of cells $Q_k = (x_{k-1/2}, x_{k+1/2})$ (that means $x_{1/2} = 0$ and $x_{N+1/2} = L$). The discrete times are denoted by $t^n = n\Delta t$. To guarantee that the discrete solution remains nonnegative as shown later, we use the CFL condition

$$\Delta t \leq \frac{3\Delta x}{3 + 2\Delta x + 2\Delta x V_m}. \tag{2.48}$$

The principle of finite volumes is to enforce numerical conservation of quantities that are physically conserved and thus to approximate quantities by their average. For instance the discrete initial states are, as before

$$C_k^{i,0} = \frac{1}{\Delta x}\int_{Q_k} C^i(x,0)dx, \qquad i = 1,\ 2,\ 3, \quad k = 1, ..., N. \tag{2.49}$$

We call $C_k^{i,n}$ the discrete solution at time $t^n$ in tube $i$ that approximates equation (2.9), for $k \in [0, N]$. We use the scheme

$$\begin{cases} C_k^{1,n+1} = C_k^{1,n} - \dfrac{\Delta t}{\Delta x}(C_k^{1,n} - C_{k-1}^{1,n}) + \Delta t J_k^{1,n}, \\ C_k^{2,n+1} = C_k^{2,n} - \dfrac{\Delta t}{\Delta x}(C_k^{2,n} - C_{k-1}^{2,n}) + \Delta t J_k^{2,n}, \\ C_k^{3,n+1} = C_k^{3,n} + \dfrac{\Delta t}{\Delta x}(C_{k+1}^{3,n} - C_k^{3,n}) + \Delta t J_k^{3,n}, \end{cases} \tag{2.50}$$

with the notations

$$\begin{cases} C_k^{int,n} = \dfrac{1}{3}\Big[C_k^{1,n} + C_k^{2,n} + C_k^{3,n} + V_m \dfrac{C_k^{3,n}}{1 + C_k^{3,n}}\Big], \\ J_k^{1,n} = C_k^{int,n} - C_k^{1,n}, \qquad J_k^{2,n} = C_k^{int,n} - C_k^{2,n}, \\ J_k^{3,n} = C_k^{int,n} - C_k^{3,n} - V_m \dfrac{C_k^{3,n}}{1 + C_k^{3,n}}. \end{cases} \tag{2.51}$$

For boundary conditions, at each time we choose: $C_0^{1,n} = C_0^1$, $C_0^{2,n} = C_0^2$, $C_{N+1}^{3,n} = C_N^{2,n}$.

Because this is an explicit scheme, departing from (2.49), we obtain directly the solution $C_k^{1,n+1}$ at time $t^{n+1}$ from that at time $t^n$.

**Derivation of the CFL condition.** In order to guarantee that the discrete solution remains nonnegative, under the assumptions that the boundary conditions and the initial conditions are nonnegative, we assume that

$$\forall i \in [1,2,3], \forall k \in [1, N], C_k^{i,n} \geq 0.$$

We seek to have the same property for the following step of time:

$$\forall i \in [1,2,3], \forall k \in [1, N], C_k^{i,n+1} \geq 0.$$

We begin with $C_k^{1,n+1}$ and we write (2.50) as

$$C_k^{1,n+1} = \Big[1 - \frac{2}{3}\Delta t - \frac{\Delta t}{\Delta x}\Big] C_k^{1,n} + \frac{\Delta t}{\Delta x} C_{k-1}^{1,n} + \frac{\Delta t}{3} C_k^{2,n} + \frac{\Delta t}{3} C_k^{3,n} + \frac{\Delta t}{3} V_m \frac{C_k^{3,n}}{1 + C_k^{3,n}}.$$

To insure that $C_k^{1,n+1}$ is a positive combination of positive terms, we have to impose $1 - \dfrac{2}{3}\Delta t - \dfrac{\Delta t}{\Delta x} \geq 0$, that is to say

$$\Delta t \leq \frac{3\Delta x}{2\Delta x + 3}. \tag{2.52}$$

The same argument holds for $C^2$. For $C^3$, we write

$$C_k^{3,n+1} = \Big[1 - \frac{2}{3}\Delta t - \frac{\Delta t}{\Delta x} - \frac{2}{3} V_m \frac{\Delta t}{1 + C_k^{3,n}}\Big] C_k^{3,n} + \frac{\Delta t}{\Delta x} C_{k+1}^{3,n} + \frac{\Delta t}{3} C_k^{2,n} + \frac{\Delta t}{3} C_k^{1,n}.$$

Here we have to impose that
$1 - \frac{2}{3}\Delta t - \frac{\Delta t}{\Delta x} - \frac{2}{3} V_m \frac{\Delta t}{1 + C_k^{3,n}} \geq 0$, that is to say

$$\Delta t \leq \frac{3\Delta x}{3 + 2\Delta x + 2\Delta x V_m} \leq \frac{3\Delta x}{2\Delta x + 3}. \tag{2.53}$$

Finally, to satisfy both (2.52) and (2.53), it is sufficient to impose (2.48). □

The arguments developed for the continuous model can be used at the discrete level to prove that the numerical solutions remain bounded, as we now describe.

**Stability of the scheme.** We want to guarantee, under the CFL condition, the stability of the scheme under the form:

$$0 \leq C_k^{i,n} \leq M, \qquad \forall k \in [1, N], \qquad \forall n \in [0, \infty[, \qquad i = 1,\ 2,\ 3. \tag{2.54}$$

**First step. Existence of a family of discrete supersolutions.** We build a nonnegative vector $U = (U_1^1, \ldots, U_N^1, U_1^2, \ldots, U_N^2, U_1^3, \ldots, U_N^3)$ such that

$$\begin{cases} U_k^1 - U_{k-1}^1 \geq \dfrac{\Delta x}{3}\Big[U_k^2 + U_k^3 - 2U_k^1 + V_m \dfrac{U_k^3}{1+U_k^3}\Big], & k \in [1, N], \\ U_k^2 - U_{k-1}^2 \geq \dfrac{\Delta x}{3}\Big[U_k^1 + U_k^3 - 2U_k^2 + V_m \dfrac{U_k^3}{1+U_k^3}\Big], & k \in [1, N], \\ U_k^3 - U_{k+1}^3 \geq \dfrac{\Delta x}{3}\Big[U_k^1 + U_k^2 - 2U_k^3 - 2V_m \dfrac{U_k^3}{1+U_k^3}\Big], & k \in [1, N], \\ \qquad U_0^1 > C_0^1, \qquad U_0^2 > C_0^2, \qquad U_{N+1}^3 = U_N^2, \end{cases} \tag{2.55}$$

and

$$U_k^i \geq C_k^{i,0}, \qquad \forall k \in [1, N], \qquad i = 1,\ 2,\ 3. \tag{2.56}$$

It is sufficient to find a nonnegative vector $U = (U_1^1, \ldots, U_N^1, U_1^2, \ldots, U_N^2, U_1^3, \ldots, U_N^3)$ such that

$$\begin{cases} U_k^1 - U_{k-1}^1 \geq \dfrac{\Delta x}{3}\Big[U_k^2 + U_k^3 - 2U_k^1 + V_m U_k^3\Big], & k \in [1, N], \\ U_k^2 - U_{k-1}^2 \geq \dfrac{\Delta x}{3}\Big[U_k^1 + U_k^3 - 2U_k^2 + V_m U_k^3\Big], & k \in [1, N], \\ U_k^3 - U_{k+1}^3 \geq \dfrac{\Delta x}{3}\Big[U_k^1 + U_k^2 - 2U_k^3 - 2V_m U_k^3\Big], & k \in [1, N], \\ \qquad U_0^1 > C_0^1, \qquad U_0^2 > C_0^2, \qquad U_{N+1}^3 = U_N^2, \end{cases} \tag{2.57}$$

and

$$U_k^i \geq C_k^{i,0}, \qquad \forall k \in [1, N], \qquad i = 1,\ 2,\ 3. \tag{2.58}$$

A vector $V \geq 0$ if all its elements are nonegative. We define the matrix $A = A_{\Delta x}$ such that solving (2.57) is equivalent to finding $U$ which satisfies

$$AU \geq W, \tag{2.59}$$

where

$${}^tW = (C_0^1, 0, \ldots 0, C_0^2, 0, \ldots 0, 0, \ldots 0) \tag{2.60}$$

The matrix $A$ is written

$$
\begin{pmatrix}
1+2\frac{\Delta x}{3} & -1 & & & & & & & & & & \\
-1 & 1+2\frac{\Delta x}{3} & & & & & & & & & & \\
 & & \ddots & \ddots & & & & & & & & \\
 & & & -1 & 1+2\frac{\Delta x}{3} & & & & & & & \\
-\frac{\Delta x}{3} & & & & & 1+\frac{2\Delta x}{3} & -1 & & & & & \\
 & -\frac{\Delta x}{3} & & & & -1 & 1+\frac{2\Delta x}{3} & & & & & \\
 & & \ddots & & & & \ddots & \ddots & & & & \\
 & & & -\frac{\Delta x}{3} & & & & -1 & 1+\frac{2\Delta x}{3} & & & \\
-\frac{\Delta x}{3} & & & & & -\frac{\Delta x}{3} & & & & 1+\frac{2V\Delta x}{3} & -1 & \\
 & -\frac{\Delta x}{3} & & & & & -\frac{\Delta x}{3} & & & & 1+\frac{2V\Delta x}{3} & \\
 & & \ddots & & & & & \ddots & & & & \ddots \\
 & & & -\frac{\Delta x}{3} & & & & & -\frac{\Delta x}{3} & & & -1 \\
 & & & & -\frac{\Delta x}{3} & & & & & -\frac{\Delta x}{3} & & 1+\frac{2V\Delta x}{3}
\end{pmatrix}
$$

where we denote by $V := V_m + 1$.

The matrix ${}^tA$ is irreducible, is diagonally dominant [82], and satisfies

$$\exists\, i_0 \text{ such as } a_{i_0,i_0} - \sum_{\substack{1\le j\le 3N \\ j\neq i_0}} a_{i_0,j} > 0, \qquad (i_0 = 2).$$

Using the M-matrix theory, ${}^tA$ is invertible and $({}^tA)^{-1}$ is positive (that is to say all its coefficients are positive). Then, $A$ is also invertible and $A^{-1}$ is positive. We then choose $x > 0,\ x \in \mathbb{R}^{3N}$. We have $A^{-1}x = y > 0$, so $Ay = x$. We can choose $\alpha$ such that

$$\alpha y \ge C^0, \qquad \alpha y_1 \ge C_0^1, \qquad \alpha y_{N+1} \ge C_0^2. \tag{2.61}$$

Thus, $U = \alpha y$ satisfies (2.57) and (2.58).

**Second step. The induction.** Assuming that for a given $n$

$$C_k^{i,n} \le U_k^i \qquad \forall k \in [1, N] \qquad i = 1,\ 2,\ 3. \tag{2.62}$$

Then,

$$\begin{aligned}
C_k^{1,n+1} =& \Big[1 - \frac{2}{3}\Delta t - \frac{\Delta t}{\Delta x}\Big] C_k^{1,n} + \frac{\Delta t}{\Delta x} C_{k-1}^{1,n} + \frac{\Delta t}{3} C_k^{2,n} + \frac{\Delta t}{3} C_k^{3,n} + V_m \frac{\Delta t}{3} \frac{C_k^{3,n}}{1 + C_k^{3,n}}, \\
\le& \Big[1 - \frac{2}{3}\Delta t - \frac{\Delta t}{\Delta x}\Big] U_k^{1,n} + \frac{\Delta t}{\Delta x} U_{k-1}^{1,n} + \frac{\Delta t}{3} U_k^{2,n} + \frac{\Delta t}{3} U_k^{3,n} + V_m \frac{\Delta t}{3} \frac{U_k^{3,n}}{1 + U_k^{3,n}}, \\
\le& U_k^1.
\end{aligned}$$

The same calculation holds for $C_k^{2,n+1}$ and $C_k^{3,n+1}$. Since (2.58) holds true, we deduce (2.54) with $M = \max\{U_k^i,\ k \in [1, N], i = 1,\ 2,\ 3\}$.

### 2.4.2 Steady states

We then use this method to compute a numerical solution to (2.8), iterating the scheme for $n$ large enough with the initial data $C^j(x, 0) = 1$ for $j = 1$, 2 and 3.

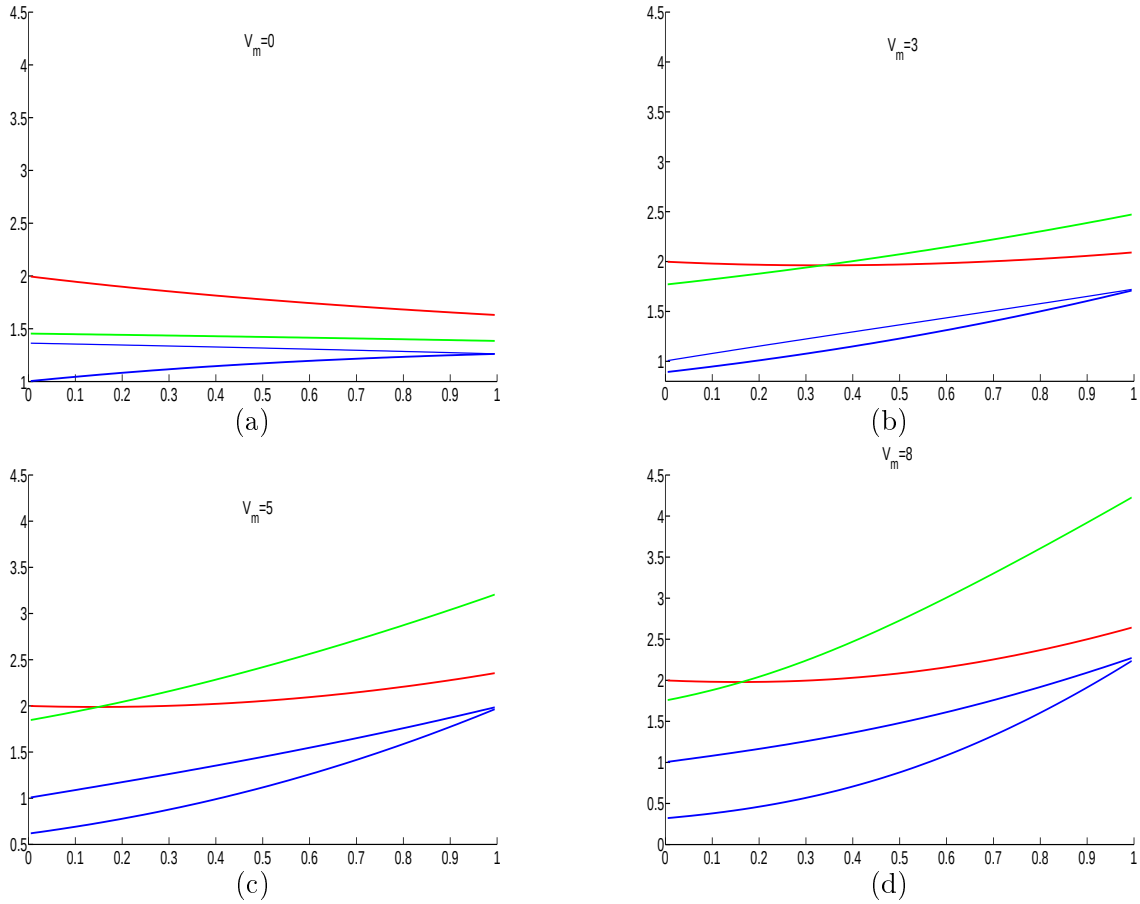


**Figure 2.3:** Concentration profiles at steady state in different tubes. The green curve represents $C^{int}$, the red curve $C^1$, the blue curves $C^2$ and $C^3$. Parameters: $C_0^1 = 2$ and $C_0^2 = 1$, $L = 1$, $\Delta x = 0.01$, $Nc = 0.99$, where $Nc = \frac{\Delta t}{\Delta x}$. The pump velocity $V_m$ is taken as 0 (a), 3 (b), 5 (c), and 8 (d). The profiles are obtained after 1000 time iterations.

Figure 2.3 depicts the concentration profiles at steady state for different values of $V_m$. We observe that if $V_m$ is large enough, there is a longitudinal gradient of concentration, as observed physiologically.

In order to assert the exponential convergence of the algorithm (as predicted by the theory), we define for each time step $n$ the indicator

$$c(n) = \max_{k\in[1,N]} \|C_k^n - C_k^{n-1}\|_\infty.$$

Displayed in Figure 2.4 is the plot of $log(c(n))$ as a function of the number of time iterations $n$. Our results indicate that the exponential convergence holds true even for large values of $V_m$, even though the decay rate is then slower. A physiological interpretation could be that the higher $V_m$, the more significant the concentration gradient, and the longer the time needed to reach equilibrium.

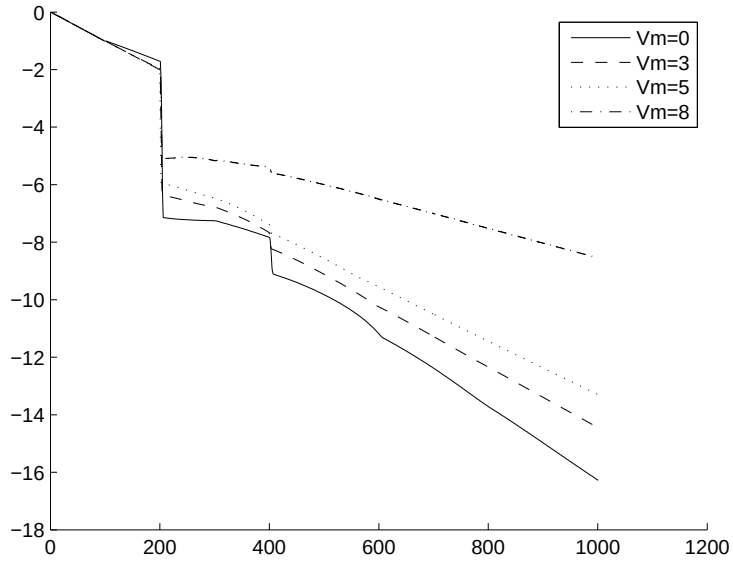


**Figure 2.4:** Log-convergence of the dynamic problem toward the steady state solution, for different values of $V_m$. The parameters are the same as those used in Figure 2.3. The convergence slows down as $V_m$ increases.

### 2.4.3 The linear case $V_m = 0$

If we ignore active transport, the system becomes linear. In this case we prove that the convergence toward the equilibrium state is of order $e^{-\lambda t}$ with $\lambda$ the first eigenvalue as described in Appendix C.

For different values of $L$, on one hand, we calculate the eigenvalue $\lambda$ in (C.1) using the power algorithm, and on the other hand, we compute the logarithmic rate of convergence for the numerical solution to (2.9) as $t$ grows. The theoretical and numerical values are compared in Table 2.2.

## 2.5 Countercurrent exchange across 2 tubes

The counter-current arrangement of tubules and vessels in the kidney has long been known to improve the production of concentrated urine (for a review, see [84]). The concentrating capacity of the kidney is reflected by the increase in fluid osmolality (or concentration) along the

**Table 2.2:** Comparison between the first eigenvalue $\lambda$ of the differential operator (C.1) and the value $\gamma$ of the numerical gradient of the logarithmic convergence. The two values are obtained as described in the text in the linear case $V_m = 0$.

| L | 0.1 | 0.5 | 1 | 2 | 3 | 6 |
|---|---|---|---|---|---|---|
| $\lambda$ | 25.530 | 3.299 | 1.3044 | 0.509 | 0.296 | 0.125 |
| $\gamma$ | 25.166 | 3.234 | 1.3044 | 0.517 | 0.292 | 0.109 |

collecting duct and can therefore be quantified by the interstitial axial concentration gradient. In order to assess the extent to which the counter-arrangement architecture enhances concentration gradients, we then consider a simpler system consisting of two tubes only. Note first that if there were no pump (i.e., no active transport of solute out of one the tubes), the concentration of solute would remain constant, independent of $x$, in both tubes (results not shown). In other words, the pump creates a transversal concentration gradient (referred to as the "single effect"), which in turn generates an axial osmolality gradient [32], [84]. The multiplication of the single effect in the axial direction concentrates the fluid flowing downwards. Our simple 2-tubule model illustrates why multiplication of the single effect is greater in counter-current flows than in cocurrent flows.

### 2.5.1 Countercurrent versus cocurrent exchange

Garner et al. [38] undertook a similar study, in which they solved analytically the time-dependent linear system relative to (2.63), using a Laplace transform which was numerically inverted. In this study, we solve analytically (2.63) and (2.64) to compare the steady state solutions of a countercurrent and a cocurrent architecture, assuming a linear rate for the pump. We then solve numerically the corresponding dynamic system using the finite volume scheme. The advantages of our numerical method are that it can be extended to $n$ tubes ($n \geq 2$), and that we could assume a nonlinear term for active transport.

**Countercurrent flows.** When the tubes are arranged in a counter-current manner, the conservation equations can be written as

$$\begin{cases} \dfrac{dC^1(x)}{dx} = J^1(x), \ -\dfrac{dC^2(x)}{dx} = J^2(x), & x \in [0, L], \\ C^1(0) = C_0^1, \qquad C^2(L) = C^1(L). \end{cases} \tag{2.63}$$

The fluxes are given by

$$J^1(x) = C^{int}(x) - C^1(x), \ J^2(x) = C^{int}(x) - C^2(x) - V_m C^2(x).$$

with the condition

$$J^1 + J^2 = 0.$$

We infer from this condition that

$$C^{int}(x) = \frac{1}{2}\Big[C^1(x) + C^2(x) + V_m C^2(x)\Big], \ C^1(x) - C^2(x) = constant.$$

Knowing that $C^1(L) = C^2(L)$, we conclude that $C^1 = C^2$. Then the system reduces to a single equation

$$\begin{cases} \dfrac{dC^1(x)}{dx} = \dfrac{1}{2} V_m C^1(x), \ C^1(0) = C_0^1. \\ C^2(x) = C^1(x). \end{cases}$$

We can calculate the analytical solution

$$C^1(x) = C_0^1 e^{\frac{V_m}{2} x}.$$

**Cocurrent flows.** In a cocurrent architecture, the equations are

$$\begin{cases} \dfrac{dC^3(x)}{dx} = J^3(x), & \dfrac{dC^4(x)}{dx} = J^4(x), \\ C^3(0) = C_0 = C^4(0). \end{cases} \tag{2.64}$$

The fluxes are still given by

$$J^3(x) = C^{int}(x) - C^3(x), \qquad J^4(x) = C^{int}(x) - C^4(x) - V_m C^4(x).$$

With similar arguments, we obtain the solution

$$\begin{cases} C^3(x) = 2C_0\Big[\dfrac{1+V_m}{2+V_m} - \dfrac{V_m}{2(2+V_m)} e^{(-1-\frac{V_m}{2})x}\Big], \\ C^4(x) = 2C_0\Big[\dfrac{1}{2+V_m} + \dfrac{V_m}{2(2+V_m)} e^{(-1-\frac{V_m}{2})x}\Big]. \end{cases}$$

In both configurations, there is a gradient of concentration in the first tubes (tubes 1 and 3). In the countercurrent configuration, the gradient is exponential in both tubes, with parameter $\frac{V_m}{2}$, where $V_m$ quantifies the single-effect. In the cocurrent configuration, the gradient is lower, and in the best case ($L$ and $V_m$ very large), $C^3(L)$ tends toward $2C_0$ whereas $C^4(L)$ falls near 0.

Shown in figure 2.5 are concentration profiles solution to (2.63) and (2.64).

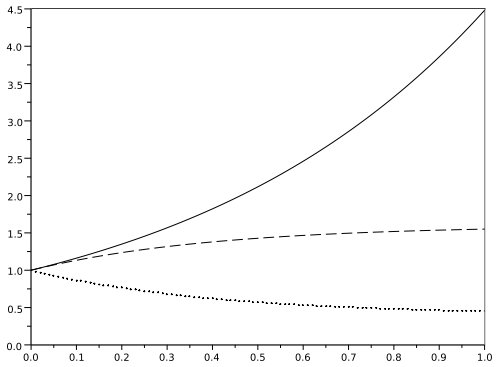


**Figure 2.5:** The solid curve represents the steady state concentration profile ($C^1 = C^2$) for the countercurrent arrangement. The dashed curve ($C^3$) and the dotted curve ($C^4$) represent steady state concentration profiles in the cocurrent arrangement. The pump term is taken to be linear here.

### 2.5.2 Visualization of the dynamic of a countercurrent-flows system

To visualize the evolution of concentration profiles with time, we consider the dynamic problem with countercurrent flows, assuming as the initial condition that the concentration is equal to $C_0$ all along the tubes. We display some curves of concentration profiles at different times and see them evolve toward the equilibrium state. We introduce the equation describing this dynamic problem

$$\begin{cases} \dfrac{\partial C^1}{\partial t}(x,t) + \dfrac{\partial C^1}{\partial x}(x,t) = J^1(x,t), & x \in [0,L],\ t > 0, \\ \dfrac{\partial C^2}{\partial t}(x,t) - \dfrac{\partial C^2}{\partial x}(x,t) = J^2(x,t), & x \in [0,L],\ t > 0, \\ C^1(0,t) = C_0^1, \qquad C^2(L,t) = C^1(L,t). \end{cases} \tag{2.65}$$

which we complete with nonnegative initial concentrations $C^1(x,0), C^2(x,0)$. The fluxes are given by:

$$J^1(x,t) = C^{int}(x,t) - C^1(x,t),$$
$$J^2(x,t) = C^{int}(x,t) - C^2(x,t) - V_m C^2(x,t),$$

with the condition:

$$J^1(x,t) + J^2(x,t) = 0.$$

Shown in Figure 2.6 are concentration profiles at different times in 2 tubes arranged in a counter-current manner, with a pump in the ascending tube, solution to (2.65) obtained using a finite volume scheme.

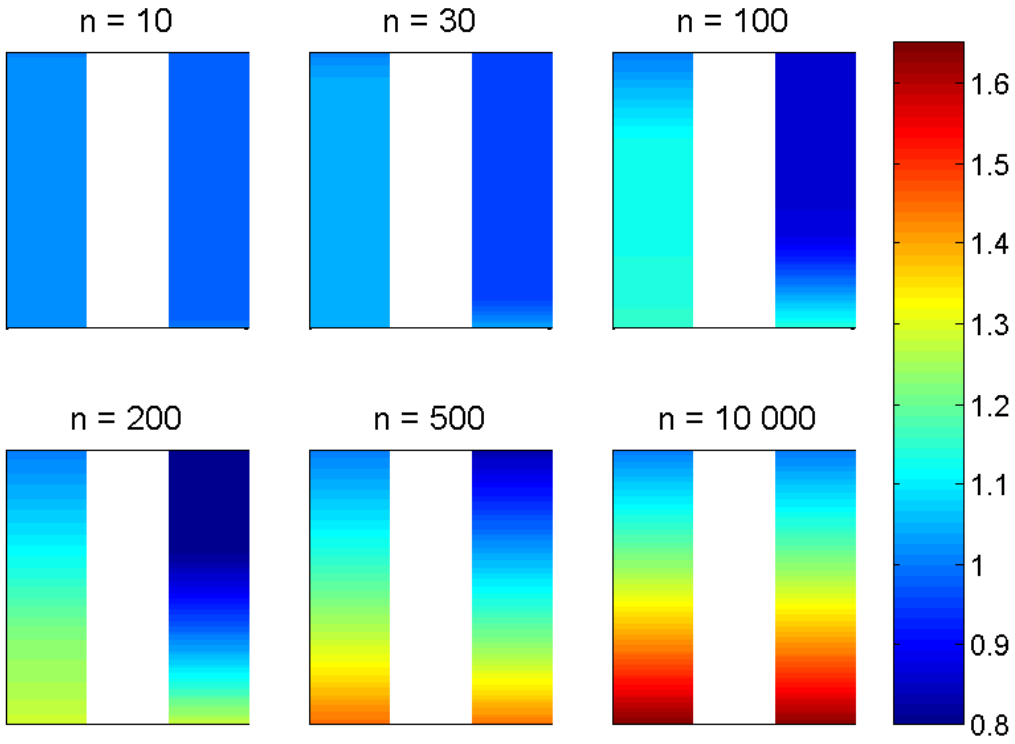


**Figure 2.6:** Concentration profiles at different time iterations $n$ in 2 tubes arranged in a countercurrent manner, with a pump in the ascending one. The pump rate is taken to increase linearly with the concentration $C$, see (2.65). Parameters: $L = 1$, $C^0 = 1$, $V_m = 1$, $\Delta x = 0.01$, $; \Delta t = 0.0099$.

## 2.6 Conclusion and perspectives

Using a simplified model of solute exchange across 3 kidney tubules, in which the latter were taken to all be impermeable to water, we demonstrated the existence and uniqueness of the stationary state. In addition, we showed that the dynamic solution converges toward the steady state solution, and that the convergence is exponential if the maximum rate of the pump mediating active transport in one of the tubes is not too high. Finally, our results illustrate how the counter-current arrangement of tubules enhances the axial concentration gradient, thereby favoring the production of highly concentrated urine.

Under physiological conditions, water and solute flows are tightly coupled in the kidney: osmosis (i.e., transmembrane concentration gradients) is the main driving force for water exchange, and solute movement is partly driven by convection. Hence, the system of nonlinear differential

equations yielding solute and water flows must generally be solved numerically. In this study, we chose to make some simplifying assumptions (such as that of water-impermeable tubules) in order to better characterize this system of differential equations, and to determine the existence and uniqueness of the solution. To the best of our knowledge, there have been few previous attempts to do so in comparable systems [24, 56] . Layton [56] showed that for sufficiently low or sufficiently large rates of NaCl active transport, there exists a unique solution to the Peskin model [?]. The latter model also considers three tubules surrounded by a common interstitium, but it differs significantly from ours in that it assumes that solute concentration is equal in the descending limb (i.e., tube 2 in our representation), the collecting duct (i.e., tube 1), and the interstitium at each level. For the model considered in the present study, we showed that the steady state solution exists and is unique for any given value of $V_m$ (i.e., the maximum rate of NaCl active transport out of the ascending limb). We also demonstrated that the solution to the dynamic model always converges toward the steady state solution. Moreover, if $Vm$ is small enough, namely if condition (13) is satisfied, then the convergence is exponential with time.

It was recognized early on, as reviewed by Stephenson ( [84]), that the formation of a large axial concentration gradient in the kidney is made possible by the fact that tubules (1) exhibit differential permeabilities and (2) are arranged in a counterflow manner. To assess the degree to which the counter-current architecture increases the axial concentration gradient, relative to the cocurrent configuration, we used a 2 tube system and derived an analytical solution for solute concentration profiles. Our results suggest that solute concentration increases exponentially with $x$ in the former case (with an exponential factor that is proportional to $V_m$), whereas it is bounded independently of $V_m$ in the latter case.

A similar exponential concentration increase was predicted for the single loop cycling model with constant water flows [38] . The investigators used Laplace transforms to obtain numerical solutions for two limiting cases: when the pump is either saturated (i.e., the active transport rate is a constant) or very far from saturation (i.e., the rate is a linear function of concentration). Their study cannot be easily extended to account for nonlinear rates, and for more than two tubes, as calculations would then become impracticable. In contrast, the method we developed could be extended to consider more tubules, and could apply to nonlinear rates.

A more realistic representation of kidney function would require accounting for transversal water movement. Whether the existence and uniqueness of steady state solutions to such problems can then be proven remains to be determined.

## Acknowledgments

Funding for this study was provided by the program EMERGENCE (EME 0918) of the Université Pierre et Marie Curie (Paris Univ. 6). We would also like to thank Dr. S. R. Randall for helpful discussions.

# Appendix A

# Definition of weak solutions

A weak solution to (2.9) is a function $C \in C\Big([0,T], L^1[0,L]\Big)^3$ such that for all $\Phi \in V$ defined in (2.34), we have

$$\begin{aligned}
&\int_0^T \int_0^L \frac{\partial \Phi}{\partial t}.C(x,t)dxdt + \int_0^T \int_0^L \frac{\partial \Phi}{\partial x}.(C^1, C^2, -C^3)(x,t)dxdt \\
&= \frac{2}{3}\int_0^T \int_0^L \Phi.C(x,t)dxdt + \frac{2}{3}\int_0^T \int_0^L \Phi^3 F(C^3,x)(x,t)dxdt \\
&- \frac{1}{3}\int_0^T \int_0^L \Big[\Phi^1(C^2 + C^3 + F(C^3,x))(x,t)\Big]dxdt - \frac{1}{3}\int_0^T \int_0^L \Big[\Phi^2(C^1 + C^3 + F(C^3,x))(x,t)\Big]dxdt \\
&- \frac{1}{3}\int_0^T \int_0^L \Big[\Phi^3(C^1 + C^2)(x,t)\Big]dxdt - \int_0^T \Phi^1(0,t)C^1(0,t)dt - \int_0^T \Phi^2(0,t)C^2(0,t)dt \\
&+ \int_0^L \Phi(x,T).C(x,T)dx - \int_0^L \Phi(x,0).C(x,0)dx.
\end{aligned} \tag{A.1}$$

For (2.8), the definition of a weak solution $C \in (L^1[0,L])^3$ uses test functions $\Phi \in W$ with

$$W = \{\Phi \in \Big(C^1([0,L])\Big)^3, \qquad \Phi^1(L) = \Phi^3(0) = 0, \qquad \Phi^3(L) = \Phi^2(L)\},$$

and is written

$$\begin{aligned}
\int_0^L \frac{d\Phi}{dx}.(C^1, C^2, -C^3)(x)dx &= \frac{2}{3}\int_0^L \Phi.C(x,t)dx + \frac{2}{3}\int_0^L \Phi^3 F(C^3,x)(x)dx \\
-\frac{1}{3}\int_0^L \Big[\Phi^1(C^2 + C^3 + F(C^3,x))(x)\Big]dx - \frac{1}{3}\int_0^L \Big[\Phi^2(C^1 + C^3 + F(C^3,x))(x)\Big]dx \\
-\frac{1}{3}\int_0^L \Big[\Phi^3(C^1 + C^2)(x)\Big]dx - \Phi^1(0)C^1(0) - \Phi^2(0)C^2(0).
\end{aligned} \tag{A.2}$$

# Appendix B

# Existence of a solution to the stationary problem

In subsection 2.3.5, we have used the fact that there are nonnegative solutions to

$$\begin{cases} \dfrac{dC^1(x)}{dx}+\dfrac{2}{3}C^1(x) = \dfrac{1}{3}\Big[C^2(x)+C^3(x)+F(C^3(x),x)\Big], \\ \dfrac{dC^2(x)}{dx}+\dfrac{2}{3}C^2(x) = \dfrac{1}{3}\Big[C^1(x)+C^3(x)+F(C^3(x),x)\Big], \\ -\dfrac{dC^3(x)}{dx}+\dfrac{2}{3}\Big[C^3(x)+F(C^3(x),x)\Big] = \dfrac{1}{3}\Big[C^1(x)+C^2(x)\Big], \\ \qquad C^1(0)=C_0^1>0, \qquad C^2(0)=C_0^2>0, \qquad C^3(L)=C_L^3\geq 0. \end{cases} \tag{B.1}$$

and that they are monotonic with respect to the boundary values. We prove these statements here.

**First step. A regularized problem.** For every $\alpha>0$, we prove that the following system has a solution $C$ which is nonnegative

$$\begin{cases} \dfrac{dC^1(x)}{dx}+\dfrac{2}{3}C^1(x)+\alpha C^1(x) = \dfrac{1}{3}\Big[C^2(x)+C^3(x)+F(C^3(x),x)\Big], \\ \dfrac{dC^2(x)}{dx}+\dfrac{2}{3}C^2(x)+\alpha C^2(x) = \dfrac{1}{3}\Big[C^1(x)+C^3(x)+F(C^3(x),x)\Big], \\ -\dfrac{dC^3(x)}{dx}+\dfrac{2}{3}\Big[C^3(x)+F(C^3(x),x)\Big] = \dfrac{1}{3}\Big[C^1(x)+C^2(x)\Big], \\ \qquad C^1(0)=C_0^1>0, \qquad C^2(0)=C_0^2>0, \qquad C^3(L)=C_L^3\geq 0. \end{cases} \tag{B.2}$$

To do so, we use the Banach-Picard theorem in the Banach space

$$X=L^1([0,L],\mathbb{R}^+)\times L^1([0,L],\mathbb{R}^+), \qquad \|(C^1,C^2)\|_X=\int_0^L \Big(C^1(x)+C^2(x)\Big)dx.$$

For $(D^1,D^2)\in X$, we define $(C^1,C^2)$ the solution to

$$\begin{cases} \dfrac{dC^1(x)}{dx}+\dfrac{2}{3}C^1(x)+\alpha C^1(x) = \dfrac{1}{3}\Big[D^2(x)+C^3(x)+F(C^3(x),x)\Big], \\ \dfrac{dC^2(x)}{dx}+\dfrac{2}{3}C^2(x)+\alpha C^2(x) = \dfrac{1}{3}\Big[D^1(x)+C^3(x)+F(C^3(x),x)\Big], \\ -\dfrac{dC^3(x)}{dx}+\dfrac{2}{3}\Big[C^3(x)+F(C^3(x),x)\Big] = \dfrac{1}{3}\Big[D^1(x)+D^2(x)\Big], \\ \qquad C^1(0)=C_0^1>0, \qquad C^2(0)=C_0^2>0, \qquad C^3(L)=C_L^3\geq 0. \end{cases} \tag{B.3}$$

Then, we claim that the operator

$$\mathcal{B}:(D^1,D^2)\longmapsto(C^1,C^2):=\mathcal{B}(D^1,D^2)$$

has a unique fixed point in $X_+$ (the cone of nonnegative functions), which follows from the two properties

$$(a)\ \mathcal{B} : X_+ \longrightarrow X_+, \qquad (b)\ \mathcal{B} \text{ is a strong contraction.}$$

**Second step. The fixed point.** To prove $(a)$, we check that $(C^1, C^2)$ are nonnegative functions. The Cauchy Lipschitz theorem tells us that there is a unique $C^3$, which is a continuous solution to the third equation of (B.3) (here we use assumption (2.10)). Then, we again apply the Cauchy Lipschitz theorem to the first two equations of (B.3) to obtain that $C^1$ and $C^2$ are continuous functions. Thanks to assumption (2.10), we notice that the unique fucntion $V^3$ satisfying

$$\begin{cases} -\dfrac{dV^3(x)}{dx} = -\dfrac{2}{3}(1+\mu)V^3(x) - \dfrac{1}{3}\Big[D^1(x) + D^2(x)\Big], \\ V^3(L) = C^3_L, \end{cases} \tag{B.4}$$

is a sub-solution to the third line of (B.3). The solution of (B.4) is given by

$$V^3(x) = \Big(C^3_L + \frac{D^1(x)+D^2(x)}{2(1+\mu)}\Big)\exp\Big(-\frac{2}{3}(1+\mu)(x-L)\Big) - \frac{D^1(x)+D^2(x)}{2(1+\mu)},$$

which is positive. As the principle of comparison holds for the ordinary differential equation constituted of the third line of (B.3), this proves that $C^3$ is a positive function. As for $C^1$ and $C^2$, we can also exhibit their exact formula which are for $i = 1, 2$ :

$$C^i(x) = C^i_0 \exp\Big(-(\frac{2}{3}+\alpha)x\Big) + \frac{D^2(x) + C^3(x) + F(C^3(x), x)}{2+3\alpha}\Big[1 - \exp\Big(-(\frac{2}{3}+\alpha)x\Big)\Big].$$

Then, $C^1$ and $C^2$ are positive functions.

Now, we check $(b)$. By substractions of solutions, say $(C^1, C^2)$ and $(\overline{C^1}, \overline{C^2})$ for two different $D$, say $(D^1, D^2)$ and $(\overline{D^1}, \overline{D^2})$, we obtain

$$\begin{cases} \dfrac{d(C^1-\overline{C^1})}{dx}(x) + (\dfrac{2}{3}+\alpha)(C^1-\overline{C^1}) = \dfrac{1}{3}\Big[(D^2-\overline{D^2})(x) + (C^3-\overline{C^3})(x) \\ \qquad\qquad + F(C^3(x),x) - F(\overline{C^3}(x),x)\Big], \\ \dfrac{d(C^2-\overline{C^2})}{dx}(x) + (\dfrac{2}{3}+\alpha)(C^2-\overline{C^2}) = \dfrac{1}{3}\Big[(D^1-\overline{D^1})(x) + (C^3-\overline{C^3})(x) \\ \qquad\qquad + F(C^3(x),x) - F(\overline{C^3}(x),x)\Big], \\ -\dfrac{d(C^3-\overline{C^3})}{dx}(x) + \dfrac{2}{3}\Big[(C^3-\overline{C^3})(x) + F(C^3(x),x) - F(\overline{C^3}(x),x)\Big] \\ \qquad\qquad = \dfrac{1}{3}\Big[(D^1-\overline{D^1})(x) + (D^2-\overline{D^2})(x)\Big], \\ (C^1-\overline{C^1})(0) = 0, \qquad (C^2-\overline{C^2})(0) = 0, \qquad (C^3-\overline{C^3})(L) = 0. \end{cases} \tag{B.5}$$

We use the notations

$$\delta^i(x) := (C^i - \overline{C^i})(x), \qquad i = 1,\ 2,\ 3,$$
$$G(x) = |F(C^3(x),x) - F(\overline{C^3}(x),x)|.$$

As in subsection 2.3.3 and using the same notations, we obtain the following inequalities

$$\begin{cases} \dfrac{d|\delta^1|}{dx} + (\dfrac{2}{3}+\alpha)|\delta^1| = \dfrac{1}{3}\operatorname{sign}(\delta^1)(D^2 - \overline{D^2} + \delta^3 + F(C^3) - F(\overline{C^3})), \\ \dfrac{d|\delta^2|}{dx} + (\dfrac{2}{3}+\alpha)|\delta^2| = \dfrac{1}{3}\operatorname{sign}(\delta^2)(D^1 - \overline{D^1} + \delta^3 + F(C^3) - F(\overline{C^3})), \\ -\dfrac{d|\delta^3|}{dx} + \dfrac{2}{3}(|\delta^3| + G) = \dfrac{1}{3}\operatorname{sign}(\delta^3)(D^1 - \overline{D^1} + D^2 - \overline{D^2}). \end{cases} \tag{B.6}$$

Integrating these inequalities, we conclude that

$$\begin{aligned}|\delta^1(L)| + |\delta^2(L)| + |\delta^3(0)| + \int_0^L (\alpha + \frac{2}{3})|\delta^1| + \int_0^L (\alpha + \frac{2}{3})|\delta^2| \\ + \frac{1}{3}\int_0^L \Big[2\,\mathrm{sign}(\delta^3) - \mathrm{sign}(\delta^1) - \mathrm{sign}(\delta^2)\Big](\delta^3 + F(C^3) - F(\overline{C^3})) \\ = \frac{1}{3}\int_0^L \Big[\mathrm{sign}(\delta^2) + \mathrm{sign}(\delta^3)\Big](D^1 - \overline{D^1}) + \frac{1}{3}\int_0^L \Big[\mathrm{sign}(\delta^1) + \mathrm{sign}(\delta^3)\Big](D^2 - \overline{D^2}), \quad \text{(B.7)}\end{aligned}$$

which gives us

$$\int_0^L (\alpha + \frac{2}{3})(|\delta^1| + |\delta^2|) \leq \frac{2}{3}\int_0^L \Big[|D^1 - \overline{D^1}| + |D^2 - \overline{D^2}|\Big]. \quad \text{(B.8)}$$

In terms of the Banach space under consideration, this is to say

$$\|(C^1, C^2) - (\overline{C^1}, \overline{C^2})\|_X \leq \frac{2}{2+3\alpha}\|(D^1, D^2) - (\overline{D^1}, \overline{D^2})\|_X,$$

and we obtain the strong contraction property, and thus the existence of a solution to (B.2).

**Third step. The limit $\alpha = 0$.** From now on, we denote the solution to (B.2) as $C_\alpha = (C^1_\alpha, C^2_\alpha, C^3_\alpha)$; it is Lipschitz continuous because $F$ is. We prove here that the familiy $(C_\alpha)_{\alpha>0}$ is equicontinuous on $[0, L]$. Then we may apply the Ascoli theorem to obtain a strongly convergent subsequence and conclude the proof.

From (B.2), we deduce that

$$\frac{d}{dx}(C^1_\alpha(x) + C^2_\alpha(x) - C^3_\alpha(x)) \leq 0, \quad \text{(B.9)}$$

which tells us that

$$C^1_\alpha(L) + C^2_\alpha(L) + C^3_\alpha(0) \leq C^1_\alpha(0) + C^2_\alpha(0) + C^3_\alpha(L) = C^1_0 + C^2_0 + C^3_L.$$

We deduce that $C^1_\alpha(L), C^2_\alpha(L)$ and $C^3_\alpha(0)$ are uniformly bounded in $\alpha$. Then, using the fact that the endpoints are controlled, (B.9) tells us that the function $h$ defined as

$$h(x) = C^1_\alpha(x) + C^2_\alpha(x) - C^3_\alpha(x) \quad \text{(B.10)}$$

is uniformly bounded in $\alpha$ too. Inserting this in the third line of (B.2), we write

$$-\frac{d}{dx}C^3_\alpha + \frac{2}{3}\Big(C^3_\alpha + F(C^3_\alpha)\Big) = \frac{C^3_\alpha + h}{3},$$

so that $C^3_\alpha$ is uniformly bounded in $\alpha$. Using the first and second lines of (B.2), we also conclude that $(C^1_\alpha + C^2_\alpha)$ are uniformly bounded in $\alpha$, and so are $C^1_\alpha$ and $C^2_\alpha$.

**Fourth step. The comparison principle.** As it was done in the Second step, and using again the argument of subsection 2.3.3 (replacing the absolute value by the positive part), one obtains that if $C^1_0 \geq \overline{C}^1_0$, $C^2_0 \geq \overline{C}^2_0$ and $C^3_L \geq \overline{C}^3_L$, then $C^i(x) \geq \overline{C}^i(x)$ for all $x \in [0, L]$ and $i = 1$, 2 and 3.

# Appendix C

# Existence of eigenelements

As often in nonlinear problems, the eigenelements for the linear problem play an important role in the understanding of nonlinear effects. We state the first eigenelement problem and recall some properties here. For a given continuous function $\mu(x) > 0$, this consists in finding $\big(\lambda(\mu), N(x;\mu) \geq 0, \phi(x,\mu) \geq 0\big)$ solutions to the direct and dual problems defined as

$$\begin{cases} \dfrac{dN^1(x)}{dx} = \dfrac{1}{3}\big[N^2(x) + (1+\mu(x))N^3(x)\big] + (\lambda - \dfrac{2}{3})N^1, \\ \dfrac{dN^2(x)}{dx} = \dfrac{1}{3}\big[N^1(x) + (1+\mu(x))N^3(x)\big] + (\lambda - \dfrac{2}{3})N^2, \\ -\dfrac{dN^3(x)}{dx} = \dfrac{1}{3}\big[N^1(x) + N^2(x)\big] + \big(\lambda - \dfrac{2}{3}(1+\mu(x))\big)N^3, \\ N^1(0) = 0, \qquad N^2(0) = 0, \qquad N^3(L) = N^2(L), \end{cases} \tag{C.1}$$

and

$$\begin{cases} -\dfrac{d\phi^1(x)}{dx} = \dfrac{1}{3}\big[\phi^2(x) + \phi^3(x)\big] + (\lambda - \dfrac{2}{3})\phi^1, \\ -\dfrac{d\phi^2(x)}{dx} = \dfrac{1}{3}\big[\phi^1(x) + \phi^3(x)\big] + (\lambda - \dfrac{2}{3})\phi^2, \\ \dfrac{d\phi^3(x)}{dx} = \dfrac{1+\mu(x)}{3}\big[\phi^1(x) + \phi^2(x)\big] + \big(\lambda - \dfrac{2}{3}(1+\mu(x))\big)\phi^3, \\ \phi^1(L) = 0, \qquad \phi^3(0) = 0, \qquad \phi^2(L) = \phi^3(L). \end{cases} \tag{C.2}$$

It is also standard to normalize the eigenfunctions as

$$\int_0^L (N^1 + N^2 + N^3) = 1, \qquad \int_0^L (N^1\phi^1 + N^2\phi^2 + N^3\phi^3) = 1. \tag{C.3}$$

Finally we use the notation $k(\mu)$:

$$k := k(\mu) \text{ is the biggest real number such that } \qquad \phi^1 + \phi^2 \geq k\phi^3. \tag{C.4}$$

The standard result *à la* Krein-Rutman is

**Proposition C.0.1.** *For $\mu > 0$ there is a (smooth) solution with $\lambda(\mu) > 0$. Moreover we have: $N^1(x) > 0$, $N^2(x) > 0$ for $x > 0$, $N^3 > 0$ and $\phi^1(x) > 0$ for $x < L$, $\phi^3(x) > 0$ for $x > 0$, $\phi^2 > 0$.*

**Strategy for the proof.** We consider the implicit scheme with space step $h$ associated with (C.1). We call $A_h$ the matrix of the scheme. We can prove that $A_h$ is invertible and that its inverse is positive. Thus, the Perron Frobenius theorem yields the existence of $\lambda_h > 0, N_h \geq 0, \phi_h \geq 0$, solution to the eigenproblem

$$A_h N_h = \lambda_h N_h, \ {}^tA_h\phi_h = \lambda_h\phi_h.$$

Since $(\lambda_h)_h$ is bounded by $1 + spec(A)$, there is a subsequence $(\lambda_h)$ such that

$$\lim_{h\to 0} \lambda_h = \lambda > 0.$$

From the discrete functions $N_h$ and $\phi_h$ we build, as in Section 2.3, continuous piecewise functions. Applying the Ascoli theorem to the bounded and equicontinuous families $(N_h)_h$ and $(\phi_h)_h$, we also prove that there are subsequences $(\lambda_h), (\phi_h)$ such as

$$\lim_{h\to 0} N_h = N \geq 0, \ \lim_{h\to 0} \phi_h = \phi \geq 0,$$

with $N$ and $\phi$ satisfying the condition (C.3). Then, we prove that $\lambda, N, \phi$ satisfy (C.1), (C.2).

**Proof of the exponential convergence.** We define, with the notation of Section 2.2.2

$$M(t) = \int_0^L \Big[ d^1(x,t)\phi_1(x) + d^2(x,t)\phi_2(x) + d^3(x,t)\phi_3(x) \Big] dx.$$

The usual duality argument (see [72]) gives, with $G$ defined in Section 2.3.3

$$\begin{aligned} \frac{d}{dt}M(t) &\leq -\lambda M(t) + \frac{1}{3}\int_0^L (G - \mu(x)\ d^3)(\phi_1(x) + \phi_2(x) - 2\phi_3(x))dx \\ &\leq -\lambda M(t) + \frac{(k-2)}{3}\int_0^L (G - \mu(x)\ d^3)\phi_3(x)dx \end{aligned}$$

because $G \leq \mu(x)\ d^3$.

If, in (C.4), $k(\mu) \geq 2$, the result follows from the Gronwall lemma.

Otherwise $k - 2 < 0$ and we write, treating only the case $C^3 \leq \overline{C^3}$ to simplify

$$(2-k)[\mu(x)d^3 - G] = (2-k)\int_{C^3}^{\overline{C^3}} [\mu(x) - \frac{\partial F}{\partial C}(c,x)]dc \leq d^3[\lambda - \delta]$$

with $\delta > 0$ given by the difference between the right and left hand sides in (2.18). From this we conclude that

$$\frac{d}{dt}M(t) \leq -\delta M(t)$$

and the exponential convergence again follows from the Gronwall lemma. □

# Chapter 3

# The role of $V_m$ in countercurrent exchanger models - an asymptotic analysis

This chapter is taken from the paper

M. Tournus. An asymptotic study to explain the role of active transport in models with countercurrent exchangers. *SeMA Journal: Boletín de la Sociedad Española de Matemática Aplicada*, 59:19–35, 2012.

*We study a solute concentrating mechanism that can be represented by coupled transport equations with specific boundary conditions. Our motivation for considering this system is urine concentrating mechanism in nephrons. The model consists in 3 tubes arranged in a countercurrent manner. Our equations describe a countercurrent exchanger, with a parameter $V_m$ which quantifies the active transport. In order to understand the role of active transport in the mechanism, we consider the limit $V_m \to \infty$. We prove that when $V_m$ goes to infinity, the system converges to a profile which stays uniformly bounded in $V_m$ and which presents a boundary layer at the border of the domain. The effect is that the solute is concentrated at a specific point in the tubes. When considering urine concentration, this is physilogically optimal because the composition of final urine is determined at this point.*

## 3.1 Motivation

Here, we study a model of a countercurrent exchanger combined with an active transport pump [32]. Countercurrent exchanges accross parallel tubes can be used for building up concentration or heat gradient. Our equations come from the modelisation of kidney nephrons, in which a concentration gradient is amplified by an active transport pump [84], which plays a fundamental role for urine concentration [63]. In this particular study, we investigate the effects of active transport using a limiting case.

The model consists in a fluid circulating at a constant velocity in 3 tubes arranged in a countercurrent architecture. The 3 tubes are bathing in a common bath in which no solute can accumulate. Each tube can exchange solute with the bath and solute transport accross tubes wall is driven by diffusion in all tubes and by an active pump in tube 3. This active pump extracts solute from tube 3 and carries it into the bath and is assumed to follow Michaelis-Menten kinetics. We call $V_m$ the maximum rate achieved by the pump at saturating concentrations. We call $C^i(x)$ the solute concentration in tube $i$ at depth $x$. The nonlinearity $V_m \dfrac{C^3_{V_m}}{1+C^3_{V_m}}$ represents the effect of active pumps along tube 3. The fluid enters tube 1 with a concentration value $C^1_0$ and tube 2 with a concentration value $C^2_0$. The outlet of tubes 1 and 3 are open at $x = L$ and we have $C^2(L) = C^3(L)$. See Figure 3.1 for a drawing of the system. The stationary state is of particular interest in renal physiology, given that the kidney acts to preserve homeostasis.

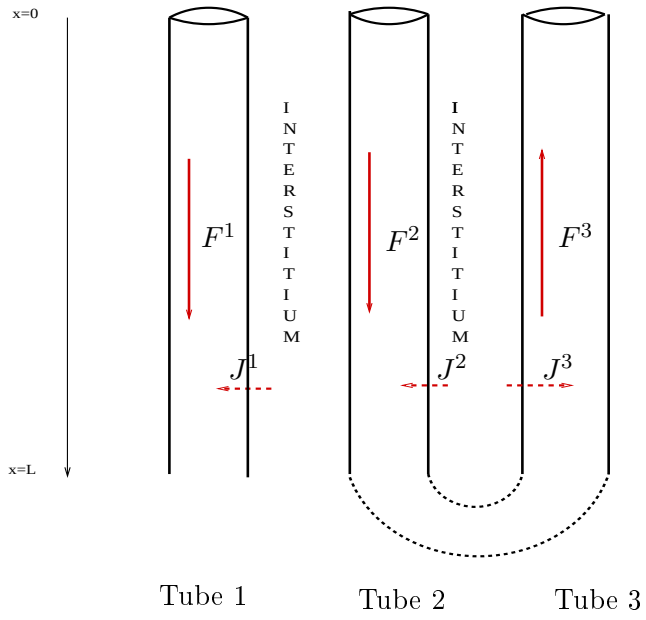


**Figure 3.1:** Representation of the 3-tube architecture in which the fluid circulates. Tubes are water-impermeable but can exchange solutes with the bath.

The differential system satisfied by $C^1, C^2, C^3$ is written as

$$\begin{cases} \dfrac{dC^1(x)}{dx} = \dfrac{1}{3}\Big[C^1(x)+C^2(x)+C^3(x)+V_m\dfrac{C^3(x)}{1+C^3(x)}\Big] - C^1(x), \\ \dfrac{dC^2(x)}{dx} = \dfrac{1}{3}\Big[C^1(x)+C^2(x)+C^3(x)+V_m\dfrac{C^3(x)}{1+C^3(x)}\Big] - C^2(x), \\ -\dfrac{dC^3(x)}{dx} = \dfrac{1}{3}\Big[C^1(x)+C^2(x)+C^3(x)+V_m\dfrac{C^3(x)}{1+C^3(x)}\Big] - C^3(x) - V_m\dfrac{C^3(x)}{1+C^3(x)}, \\ C^1(0) = C^1_0, \qquad C^2(0) = C^2_0, \qquad C^3(L) = C^2(L). \end{cases} \tag{3.1}$$

The specific boundary conditions relate the solutions at different points and make this system not a mere ordinary differential equation. We call $C_{V_m} = (C^1_{V_m}, C^2_{V_m}, C^3_{V_m})$ the solution of (3.1). We wish to explain through the analysis of the system for large values of $V_m$, why this combination of active pump and boundary conditions (tube arrangement) is performing well the task of concentrating the solute at $x = L$, where the composition of final urine is determined. We already know [91] that each $C^i_{V_m}$ is continuous and nonnegative on $[0, L]$. The question we want to answer is : How do the solutions of (3.1) behave when $V_m$ tends to $\infty$?

Other asymptotic studies have been done for similar systems in the context of hyperbolic relaxation where a parameter is assumed to be small in comparison to the typical size of the problem [36, 43, 65]. This approach comes from the concept of mean free path in Boltzmann equation [13]. For example, in [22], the length of the domain is large, and they establish the asymtotic behavior of the solution in the limiting case of an infinite domain. In our case, for answering our question, we prove that $C_{V_m}$ converges toward a limit $C = (C^1, C^2, C^3)$ that we calculate. Our analysis uses only direct a priori estimates and weak limits obtained by compact injections which do not use the specific smooth form of the non-linearity and makes it very general. We identify completely the limit as $V_m \longrightarrow \infty$ including boundary layers. Compact injections give us the convergence of some particular subsequences, but as we point out that the limit only depends on the problem data, we are able to prove that the whole sequence converges. The boundary layers are coming from the particular boundary conditions in the model, which can be seen as reflection conditions and make the problem specific and interesting.

We state our main results in next section. Section 3.3 and 3.4 are devoted to the proofs of the asymptotic results. Numerical illustrations are given in section 3.5.

## 3.2 The limit profiles

It is possible to identify completely the profiles of the limiting values for the solutions $C^1, C^2, C^3$ almost everywhere as $V_m \longrightarrow \infty$. This is stated in the

**Theorem 3.2.1** (Asymptotics). *Solutions to* (3.1) *satisfy*

$$C^1_{V_m} \underset{V_m \longrightarrow +\infty}{\longrightarrow} C^1, \qquad C^2_{V_m} \underset{V_m \longrightarrow +\infty}{\longrightarrow} C^2, \qquad C^3_{V_m} \underset{V_m \longrightarrow +\infty}{\longrightarrow} C^3, \qquad L^p (1 \leq p < \infty), \ a.e., \tag{3.2}$$

*with*

$$C^1(x) = \frac{C^1_0 + C^2_0}{2} + \frac{C^1_0 - C^2_0}{2} e^{-x}, \qquad C^2(x) = \frac{C^1_0 + C^2_0}{2} + \frac{C^2_0 - C^1_0}{2} e^{-x}, \qquad C^3(x) = 0 \qquad a.e. \tag{3.3}$$

This result is somewhat sharp since we will see that a boundary layer occurs and thus the convergence does not hold in $L^\infty$. To state our next result, we need to define the quantity

$$M = \operatorname{ess\,inf} \{ \frac{1}{C^3_{V_m}(x)} ; x \in [0, L], V_m \in \mathbb{R}^+ \}. \tag{3.4}$$

We prove in the next section that $M > 0$. The second result is more accurate and states that $C^3$ decreases exponentially fast to zero. We describe also the boundary layer that appears at $x = L$.

**Theorem 3.2.2** (The boundary layer). *The limits of the boundary values are*

$$\begin{aligned} C^1_{V_m}(L) &\underset{V_m \longrightarrow +\infty}{\longrightarrow} C^1_0 + C^2_0, \\ C^2_{V_m}(L) = C^3_{V_m}(L) &\underset{V_m \longrightarrow +\infty}{\longrightarrow} C^1_0 + C^2_0 + (C^2_0 - C^1_0) e^{-L}, \end{aligned} \tag{3.5}$$

*The behavior of $C^3_{V_m}$ for $x \simeq L$ is given by the inequalities*

$$C^3_{V_m}(x) \le C^3_{V_m}(L)\exp\Big(-\frac{2}{3}V_m M(L-x)\Big) + \frac{K}{V_m}\Big[1-\exp\Big(-\frac{2}{3}V_m M(L-x)\Big)\Big], \tag{3.6}$$

$$C^3_{V_m}(x) \ge C^3_{V_m}(L)\exp\Big(-\frac{2}{3}V_m (L-x)\Big) + \frac{\overline{K}}{V_m}\Big[1-\exp\Big(-\frac{2}{3}V_m (L-x)\Big)\Big], \tag{3.7}$$

*where $K$ and $\overline{K}$ are two constants which do not depend on $V_m$.*

The next section is dedicated to the proof of these results.

## 3.3 Proof of the asymptotic results (Theorem 3.2.1)

**First step: Uniform bounds on the solution.**

**Lemma 3.3.1.** *There is a constant $K$ depending only on $C^1_0, C^2_0$ but not on $V_m$ such that*

$$C^1_{V_m}(L) \le K, \qquad C^3_{V_m}(0) \le C^1_0 + C^2_0, \tag{3.8}$$

$$\int_0^L C^i_{V_m}(x)dx \le K; \qquad V_m\int_0^L C^3_{V_m}(x)dx \le K; \qquad \int_0^L \Big|\frac{dC^3_{V_m}}{dx}(x)\Big|dx \le K; \qquad 0 \le C^i_{V_m} \le K. \tag{3.9}$$

*Proof.* To prove (3.8), we sum the three lines of (3.1), and we obtain a quantity which does not depend on $x$,

$$C^1_{V_m}(x) + C^2_{V_m}(x) - C^3_{V_m}(x) =: K(V_m). \tag{3.10}$$

Using the boundary values, we find uniform bounds on $K(V_m)$

$$K(V_m) = C^1_0 + C^2_0 - C^3_{V_m}(0) \le C^1_0 + C^2_0, \qquad K(V_m) = C^1_{V_m}(L) + C^2_{V_m}(L) - C^3_{V_m}(L) = C^1_{V_m}(L) \ge 0, \tag{3.11}$$

and thus

$$0 \le K(V_m) \le C^1_0 + C^2_0. \tag{3.12}$$

The combination of (3.11) and (3.12) proves (3.8).

Then, we prove the first two bounds in (3.9). The first equation can be written

$$\frac{dC^1_{V_m}(x)}{dx} + C^1_{V_m}(x) = Q_{V_m}(x) \ge 0, \tag{3.13}$$

with

$$Q_{V_m}(x) = \frac{1}{3}\Big[C^1(x) + C^2(x) + C^3(x) + V_m\frac{C^3(x)}{1+C^3(x)}\Big].$$

Therefore we also have

$$\frac{d}{dx}\Big(C^1_{V_m}(x)e^x\Big) = Q_{V_m}(x)e^x.$$

By integration over $[0, L]$, we obtain

$$\int_0^L Q_{V_m}(x)dx \le \int_0^L Q_{V_m}(x)e^x dx = C^1_{V_m}(L)e^L - C^1_0 \le (C^1_0 + C^2_0)e^L. \tag{3.14}$$

We conclude that

$$\int_0^L V_m \frac{C^3_{V_m}(x)}{1+C^3_{V_m}(x)}dx,\ \int_0^L C^i_{V_m}(x)dx,\ i=1,2,3,\ \text{are uniformly bounded by } (C^1_0+C^2_0)e^L. \tag{3.15}$$

Then, by injecting equation (3.14) in (3.13) and because the $C^i_{V_m}$ are positive, we have

$$\int_0^L |\frac{dC^i_{V_m}}{dx}(s)|ds \leq (C^1_0+C^2_0)e^L \qquad i=1,2,3. \tag{3.16}$$

We finally prove that the functions $\left(C^i_{V_m}(x)\right)_{V_m}$ are uniformly bounded in $V_m$. We write

$$|C^i_{V_m}(x)| = |C^i_{V_m}(0) + \int_0^x \frac{dC^i_{V_m}}{dx}(s)ds| \leq |C^i_{V_m}(0)| + \int_0^L |\frac{dC^i_{V_m}}{dx}(s)|ds.$$

Thanks to (3.16) and (3.8), we conclude

$$\|C^i_{V_m}\|_\infty \leq (C^1_0+C^2_0)(e^L+1). \tag{3.17}$$

□

The upper bound (3.17) on $C^3_{V_m}$ gives us that $M>0$.

**Second step: The behaviour of $C^i_{V_m}$ when $V_m \longrightarrow \infty$**

**Lemma 3.3.2.** *After extraction of a subsequence,*

$$C^1_{V_m} \underset{V_m\longrightarrow+\infty}{\longrightarrow} C^1, \qquad C^2_{V_m} \underset{V_m\longrightarrow+\infty}{\longrightarrow} C^2, \qquad C^3_{V_m} \underset{V_m\longrightarrow+\infty}{\longrightarrow} 0, \qquad L^p(1\leq p<\infty),\ a.e., \tag{3.18}$$

*and $C^1+C^2=K^0$ for some constant $K^0$.*

*Proof.* We know from Lemma 3.3.1 that $\left(C^i_{V_m}\right)_{V_m}$ is bounded in $BV_m$, then, using the Rellich-Kondrachov compact injection [16]

$$C^i_{V_m} \underset{V_m\longrightarrow+\infty}{\longrightarrow} C^i, \qquad \text{in } L^p(1\leq p<\infty) \text{ and } a.e. \tag{3.19}$$

On the other hand, we have thanks to (3.15),

$$\int_0^L \frac{C^3_{V_m}(x)}{1+C^3_{V_m}(x)}dx \underset{V_m\longrightarrow+\infty}{\longrightarrow} 0,$$

and thus

$$C^3 \equiv 0 \qquad a.e. \tag{3.20}$$

Combining (3.10) with (3.20), we have $C^1+C^2=K^0$ for some constant $K^0$. □

**Third step : The behavior of $\frac{dC^3_{V_m}}{dx}$.** We define $\mathcal{M}^1[0,L]$ the set of Radon measures on $[0,L]$, taken with the weak convergence of measures.

**Lemma 3.3.3.** *There exists a constant $B$ such that, after extraction,*

$$C^3_{V_m}(L) \underset{V_m\longrightarrow+\infty}{\longrightarrow} B, \qquad \frac{dC^3_{V_m}}{dx} \underset{V_m\longrightarrow+\infty}{\longrightarrow} B\delta_{x=L} \qquad \text{in } \mathcal{M}^1[0,L],$$

*Proof.* The information (3.16) implies that $\Big(\frac{dC^3_{V_m}}{dx}\Big)_{V_m}$ is bounded in $L^1[0,L]$, then [11] there exists $\mu \in \mathcal{M}^1[0,L]$ a Radon measure so that, after extraction,

$$\frac{dC^3_{V_m}}{dx} \underset{V_m \longrightarrow +\infty}{\longrightarrow} \mu \qquad \text{in the sense of measures.} \tag{3.21}$$

For all functions $\phi \in C^1[0,L]$ such as $\phi(0) = \phi(L) = 0$, we have using (3.18)

$$\int_0^L \phi(x) \frac{dC^3_{V_m}}{dx}(x)dx = \int_0^L C^3_{V_m}(x) \frac{d\phi}{dx}(x)dx \underset{V_m \longrightarrow +\infty}{\longrightarrow} 0, \tag{3.22}$$

which means,

$$\mu = 0 \qquad \text{on } ]0,L[. \tag{3.23}$$

Therefore, we can write in the sense of measures

$$\frac{dC^3_{V_m}}{dx} \underset{V_m \longrightarrow +\infty}{\longrightarrow} \beta\delta_{x=L} + \alpha\delta_{x=0}. \tag{3.24}$$

It remains to compute $\alpha$ and $\beta$. To do so, we notice that $\Big(C^3_{V_m}(L)\Big)_{V_m}$ and $\Big(C^3_{V_m}(0)\Big)_{V_m}$ are both real value bounded sequences, so, there are two nonnegative real numbers $A, B$ such that, after extraction,

$$\lim_{V_m \to \infty} C^3_{V_m}(L) = B \geq 0, \qquad \lim_{V_m \to \infty} C^3_{V_m}(0) = A \geq 0. \tag{3.25}$$

For $\phi \in C^1\Big([0,L]\Big)$, we compute

$$\int_0^L \phi(x) \frac{dC^3_{V_m}}{dx}(x)dx = C^3_{V_m}(L)\phi(L) - C^3_{V_m}(0)\phi(0) - \int_0^L C^3_{V_m}(x) \frac{d\phi}{dx}(x)dx \underset{V_m \longrightarrow +\infty}{\longrightarrow} B\phi(L) - A\phi(0),$$

which means

$$\frac{dC^3_{V_m}}{dx} \underset{V_m \longrightarrow +\infty}{\longrightarrow} B\delta_{x=L} - A\delta_{x=0} \qquad \text{in the sense of measures.} \tag{3.26}$$

We still have to prove $A = 0$. To do so we use the system of equations (3.1) which gives us

$$\frac{dC^3_{V_m}}{dx} \geq -\frac{1}{3}(C^1_{V_m} + C^2_{V_m}).$$

As we know from Lemma 3.3.1 that $C^i_{V_m}$ is uniformly bounded from above by $K$, we also have,

$$\frac{dC^3_{V_m}}{dx} \geq -\frac{2}{3}K,$$

which implies $A = 0$. □

**Fourth step: The limiting equation.**

**Lemma 3.3.4.** *In the limit $V_m \longrightarrow \infty$, we have*

$$C^1(x) + C^2(x) = C^1_0 + C^2_0, \qquad V_m \frac{C^3_{V_m}}{1 + C^3_{V_m}} - \frac{C^1_{V_m} + C^2_{V_m}}{2} \longrightarrow \frac{3}{2}B\delta_L \qquad \textit{in the sense of measures.}$$

*Proof.* We deduce from (3.19) and (3.26), by injecting in the third line of (3.1) that

$$V_m \frac{C^3_{V_m}}{1+C^3_{V_m}} - \frac{C^1_{V_m}+C^2_{V_m}}{2} - \frac{3}{2}B\delta_L \longrightarrow 0 \qquad \text{in the sense of measures.} \tag{3.27}$$

Reinjecting in the first lines of (3.1), we find the limit equations on $C^1$ et $C^2$

$$\begin{cases} \dfrac{dC^1}{dx} = -\dfrac{1}{2}C^1 + \dfrac{1}{2}C^2 + \dfrac{1}{2}B\delta_L, \\ \dfrac{dC^2}{dx} = -\dfrac{1}{2}C^2 + \dfrac{1}{2}C^1 + \dfrac{1}{2}B\delta_L, \\ C^1(0) = C^1_0, \qquad C^2(0) = C^2_0. \end{cases} \tag{3.28}$$

Then, summing the two lines,

$$\begin{cases} \dfrac{d(C^2+C^1)}{dx} = B\delta_L, \\ (C^1+C^2)(0) = C^1_0 + C^2_0. \end{cases} \tag{3.29}$$

By integrating this differential equation, we deduce [79] that

$$C^1(x) + C^2(x) = C^1_0 + C^2_0 \qquad \text{a.e.}$$

Indeed, the weak formulation of (3.29) is

$$\forall \phi \in \mathcal{C}^1[0,L], \qquad \int_0^L \frac{d\phi}{dx}(x)[C^1+C^2](x)dx + \phi(0)[C^1_0+C^2_0] = 0. \tag{3.30}$$

By choosing $\phi$ such as $\phi(0)=0$, we obtain $C^1+C^2 \equiv \alpha$ a.e., for some constant $\alpha$. and then, by choosing any $\phi \in \mathcal{C}^1[0,L]$, we have that $\alpha = C^1_0 + C^2_0$. □

The limit equation on $C^i$ then becomes

$$\begin{cases} \dfrac{dC^i}{dx}(x) = -C^i(x) + \dfrac{C^1_0+C^2_0}{2} + \dfrac{1}{2}B\delta_L(x), \qquad i=1,2, \\ C^i(0) = C^i_0. \end{cases}$$

**Fifth step: Explicit solution for the limit** Using the variation of parameters, we compute easily $C^1$ and $C^2$. We find

$$C^1(x) = \frac{C^1_0+C^2_0}{2} + \frac{C^1_0-C^2_0}{2}e^{-x}, \qquad C^2(x) = \frac{C^1_0+C^2_0}{2} + \frac{C^2_0-C^1_0}{2}e^{-x}. \tag{3.31}$$

In particular, $(C^1, C^2, C^3)$ are $\mathcal{C}^\infty$ functions.

## 3.4 Proof of theorem 3.2.2

The limiting profiles are $\mathcal{C}^\infty$ in $[0,L]$, nevertheless, the Dirac mass at $x=L$ indicates a boundary layer. The derivatives of the profiles for $V_m = \infty$ are given by

$$\begin{cases} \dfrac{dC^1}{dx} = \dfrac{1}{2}\Big[(C^2_0 - C^1_0)e^{-x} + B\delta_L\Big], \\ \dfrac{dC^2}{dx} = \dfrac{1}{2}\Big[(C^1_0 - C^2_0)e^{-x} + B\delta_L\Big], \qquad \text{in the sense of measures,} \\ \dfrac{dC^3}{dx} = B\delta_L. \end{cases} \tag{3.32}$$

**First Step: The limiting values of $C$ at $x=L$**

**Lemma 3.4.1.**

$$\begin{aligned} C^1_{V_m}(L) &\underset{V_m\longrightarrow+\infty}{\longrightarrow} C^1_0 + C^2_0, \\ C^2_{V_m}(L) = C^3_{V_m}(L) &\underset{V_m\longrightarrow+\infty}{\longrightarrow} C^1_0 + C^2_0 + (C^2_0 - C^1_0)e^{-L}. \end{aligned} \tag{3.33}$$

*Proof.* We already have defined in Lemma 3.3.3

$$B = \lim_{V_m\to\infty} C^2_{V_m}(L) = \lim_{V_m\to\infty} C^3_{V_m}(L).$$

We know that the $C^i_{V_m}(L)$ are bounded real numbers, then we define

$$B' = \lim_{V_m\to\infty} C^1_{V_m}(L).$$

Our first task is to determine $B$. We compute for all $\phi \in \mathcal{C}^1[0,L]$,

$$\int_0^L \phi(x)\frac{dC^2_{V_m}(x)}{dx}(x)dx = \phi(L)C^2_{V_m}(L) - \phi(0)C^2_{V_m}(0) - \int_0^L \frac{\phi}{dx}(x)C^2_{V_m}(x)dx$$

which converges when $V_m \longrightarrow +\infty$ toward

$$\begin{aligned} &B\phi(L) - C^2_0\phi(0) - \int_0^L \frac{\phi}{dx}(x)[\frac{C^1_0 + C^2_0}{2} + \frac{C^2_0 - C^1_0}{2}e^{-x}]dx \\ &= B\phi(L) - C^2_0\phi(0) - \frac{C^1_0 + C^2_0}{2}\phi(L) + \frac{C^1_0 + C^2_0}{2}\phi(0) - \frac{C^2_0 - C^1_0}{2}\Big[e^{-L}\phi(L) - \phi(0) + \int_0^L e^{-x}\phi(x)\Big] \\ &= B\phi(L) - \frac{C^1_0 + C^2_0}{2}\phi(L) + \frac{C^2_0 - C^1_0}{2}e^{-L}\phi(L) + \frac{C^2_0 - C^1_0}{2}\int_0^L e^{-x}\phi(x)dx. \end{aligned} \tag{3.34}$$

On the other hand, thanks to (3.32)

$$\int_0^L \phi(x)\frac{dC^2_{V_m}(x)}{dx}(x)dx \underset{V_m\longrightarrow+\infty}{\longrightarrow} \frac{C^2_0 - C^1_0}{2}\int_0^L e^{-x}\phi(x)dx + \frac{B}{2}\phi(L). \tag{3.35}$$

By equalizing (3.34) and (3.35), we find

$$B = C^1_0 + C^2_0 + (C^2_0 - C^1_0)e^{-L}, \tag{3.36}$$

which is the unique limit of $C^2_{V_m}(L)$ and $C^3_{V_m}(L)$. In particular, $B > 0$. Our second task is to obtain B'. We perform the same computation for $C^1_{V_m}$. On the one hand, for all $\phi \in \mathcal{C}^1[0,L]$,

$$\int_0^L \phi(x)\frac{dC^1_{V_m}(x)}{dx}(x)dx = \phi(L)C^1_{V_m}(L) - \phi(0)C^1_{V_m}(0) - \int_0^L \frac{\phi}{dx}(x)C^1_{V_m}(x)dx$$

which converges when $V_m \longrightarrow +\infty$ toward

$$= B'\phi(L) - \frac{C^1_0 + C^2_0}{2}\phi(L) + \frac{C^1_0 - C^2_0}{2}e^{-L}\phi(L) + \frac{C^1_0 - C^2_0}{2}\int_0^L e^{-x}\phi(x)dx, \tag{3.37}$$

and on the other hand,

$$\int_0^L \phi(x)\frac{dC^1_{V_m}(x)}{dx}(x)dx$$

converges toward

$$\frac{C^2_0 - C^1_0}{2}\int_0^L e^{-x}\phi(x)dx + \frac{B}{2}\phi(L). \tag{3.38}$$

This gives us

$$B' = C^1_0 + C^2_0, \tag{3.39}$$

and ends the proof of Lemma 3.4.1. □

We proved in passing that the limits of the subsequences we deal with are only determined by the problem data and do not depend on the subsequence we choose. Thus, the whole sequences converge.

**Second step: The boundary layer.**

**Lemma 3.4.2.** *For all $x \in [0, L]$ the inequalities hold*

$$C^3_{V_m}(x) \le C^3_{V_m}(L) exp\Big( -\frac{2}{3} V_m M(L-x)\Big) + \frac{K}{V_m}\Big[1 - exp\Big( -\frac{2}{3} V_m M(L-x)\Big)\Big], \tag{3.40}$$

$$C^3_{V_m}(x) \ge C^3_{V_m}(L) exp\Big( -\frac{2}{3} V_m (L-x)\Big) + \frac{\overline{K}}{V_m}\Big[1 - exp\Big( -\frac{2}{3} V_m (L-x)\Big)\Big], \tag{3.41}$$

*which means that $C^3_{V_m}(x)$ relaxes exponentially fast with $V_m$ to zero, away from the boundary layer at $X = L$.*

*Proof.* We can write the third line of (3.1) as

$$-\frac{dC^3_{V_m}(x)}{dx} + \frac{2}{3} V_m \frac{C^3_{V_m}(x)}{1 + C^3_{V_m}(x)} = \frac{1}{3}\Big[C^1(x) + C^2(x) - 2C^3(x)\Big]. \tag{3.42}$$

We multiply this equation by the exponential factor

$$F(x) = \exp\Big( -\frac{2}{3} V_m \int_L^x \frac{1}{1 + C^3_{V_m}(s)} ds\Big), \tag{3.43}$$

$$-\frac{dC^3_{V_m}(x)}{dx} F(x) + \frac{2}{3} V_m \frac{C^3_{V_m}(x)}{1 + C^3_{V_m}(x)} F(x) = \frac{1}{3}\Big[C^1_{V_m}(x) + C^2_{V_m}(x) - 2C^3_{V_m}(x)\Big] F(x), \tag{3.44}$$

and we obtain

$$\frac{d}{dx}\Big[C^3_{V_m}(x) F(x)\Big] = -\frac{1}{3}\Big[C^1_{V_m}(x) + C^2_{V_m}(x) - 2C^3_{V_m}(x)\Big] F(x).$$

Integrating this equation between $L$ and $x$, we find,

$$C^3_{V_m}(x)F(x) - C^3_{V_m}(L) = -\int_L^x \frac{1}{3}\Big[C^1_{V_m}(x) + C^2_{V_m}(x) - 2C^3_{V_m}(x)\Big] \exp\Big(-\frac{2}{3} V_m \int_L^u \frac{1}{1 + C^3_{V_m}(s)} ds\Big) du.$$

By Lemma 3.3.1, we have,

$$C^3_{V_m}(x) \exp\Big( -\frac{2}{3} V_m \int_L^x \frac{1}{1 + C^3_{V_m}(s)} ds\Big) \le C^3_{V_m}(L) + K' \int_x^L \exp\Big( -\frac{2}{3} V_m \int_L^u \frac{1}{1 + C^3_{V_m}(s)} ds\Big) du.$$

We can now complete our calculation. We estimate

$$\begin{aligned}
C^3_{V_m}(x) \le & C^3_{V_m}(L) \exp\Big( -\frac{2}{3} V_m \int_x^L \frac{1}{1 + C^3_{V_m}(s)} ds\Big) \\
& + K'\Big[\int_x^L \exp\Big( -\frac{2}{3} V_m \int_L^u \frac{1}{1 + C^3_{V_m}(s)} ds\Big) \exp\Big( -\frac{2}{3} V_m \int_x^L \frac{1}{1 + C^3_{V_m}(s)} ds\Big)\Big] du \\
= & C^3_{V_m}(L) \exp\Big( -\frac{2}{3} V_m \int_x^L \frac{1}{1 + C^3_{V_m}(s)} ds\Big) + K' \int_x^L \exp\Big( -\frac{2}{3} V_m \int_x^u \frac{1}{1 + C^3_{V_m}(s)} ds\Big) du \\
\le & C^3_{V_m}(L) \exp\Big( -\frac{2}{3} V_m \int_x^L \frac{1}{1 + C^3_{V_m}(s)} ds\Big) + K' \int_x^L \exp\Big( -\frac{2}{3} V_m M(u-x)\Big) du \\
& \qquad \Big(\text{using } 0 < M < \frac{1}{1 + C^3_{V_m}}\Big) \\
= & C^3_{V_m}(L) \exp\Big( -\frac{2}{3} V_m \int_x^L \frac{1}{1 + C^3_{V_m}(s)} ds\Big) + \frac{K}{V_m}\Big[1 - \exp\Big( -\frac{2}{3} V_m M(L-x)\Big)\Big].
\end{aligned}$$

and (3.40) is proved.

We can prove in the same way the second part of Lemma 3.4.2. □

## 3.5 Numerics

### 3.5.1 The numerical algorithm

Numerical simulations illustrate the solute concentration mechanism at $x = L$ that is proved in the theoretical result. We use the scheme we describe page 43. The stability condition which ensures the positivity of the scheme is given by

$$\Delta t \leq \frac{3\Delta x}{3 + 2\Delta x(1 + V_m)}, \tag{3.45}$$

This CFL condition becomes a tough constraint on $\Delta t$ when we choose $V_m$ large. The constraint on $\Delta x$ also depends on $V_m$ because it is function of the size of the boundary layer. For each $V_m$, to be accurate enough around the boundary layer point $L$, we discretize the space in $N_{V_m}$ cells and we validate a posteriori that this number of cells is high enough since we know from the analytical solution the behaviour of the solution for large values of $V_m$.

### 3.5.2 Concentration profiles for different $V_m$

We present in Figure 3.2 concentration profiles for $V_m = 1, V_m = 10, V_m = 50$ and $V_m = 100$. When the value of the rate $V_m$ has the same order of magnitude as the parameters of (3.1),

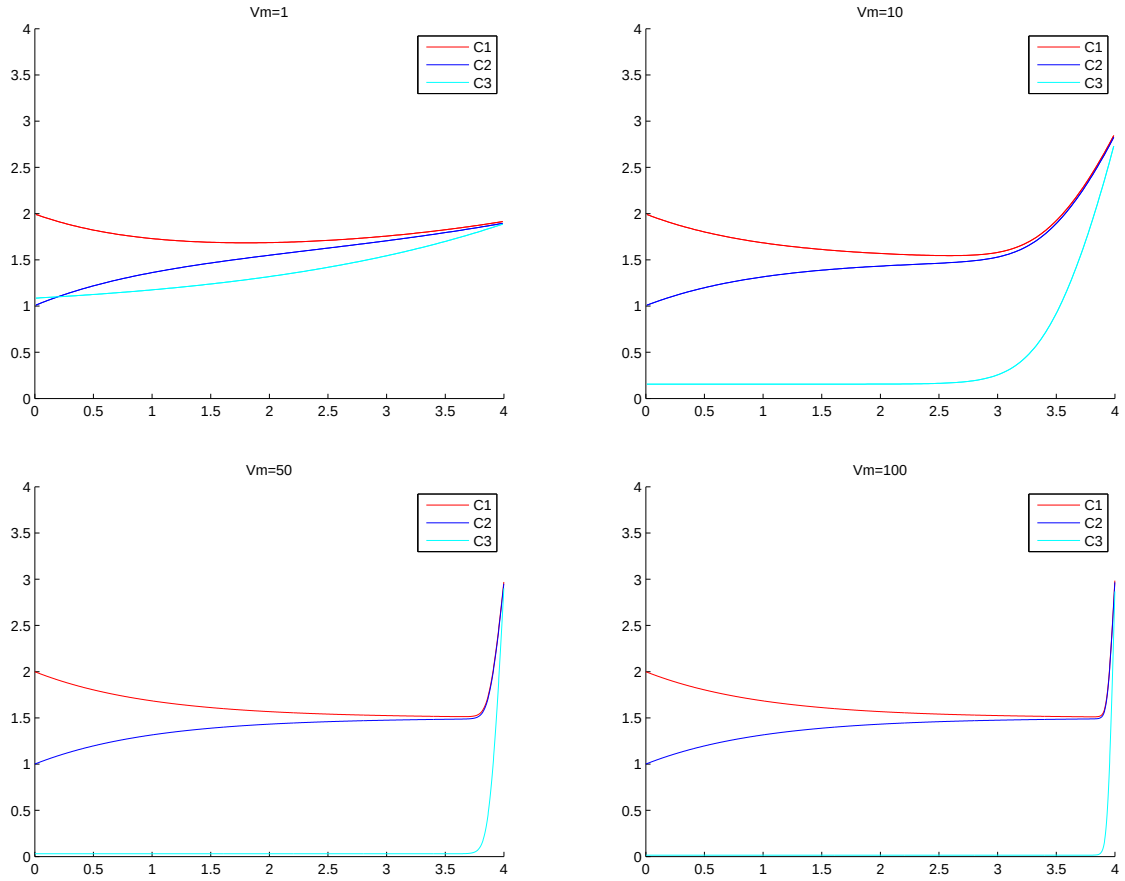


**Figure 3.2:** Concentration profiles for $V_m = 1, 10, 50, 100$, on a domain of length $L = 4$.

concentration is hardly increasing in tubes 2 and 3, but decreasing in tube 1. It comes from the

fact that we chose $C_0^1 > C_0^2$, but it would have been the contrary in the opposite case. With low values of $V_m$, the diffusive part of the system (3.1) is paramount and concentrations tend to homogenize along the tubes. If we increase the pump rate by a factor 10, the concentration tends to approach zero in tube 3 and is abruptly increasing from $L = 3$ and it achieves at $L = 4$ a value greater than $\max(C_0^1, C_0^2)$. We clearly observe the limit profiles and the boundary layer appear for $V_m \geq 50$.

**Illustration of Theorem 3.2.2.** We want to illustrate that the bounds from above and from below found in Theorem 3.2.2 give an accurate descrition of the qualitative behavior of $C^3$.

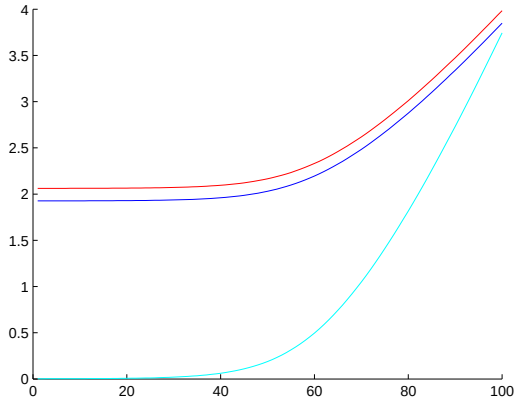


**Figure 3.3:** Zoom on the interval $[0.99L, L]$ of Figure 3.2 for $V_m = 1000$.

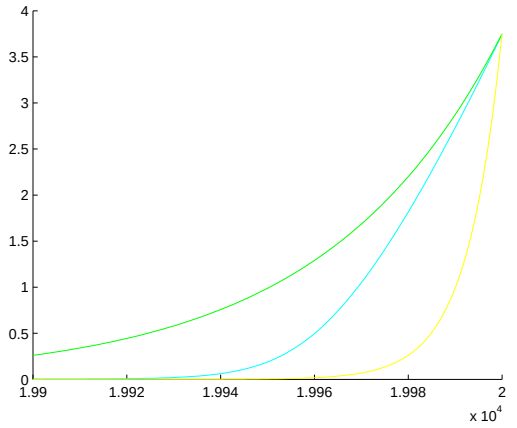


**Figure 3.4:** The curve in the middle represents $C^3_{1000}$ on $[0.99L, L]$. The upper curve represents the upperbound $f$ for $C^3$ found in Lemma 3.4.2 and the the lower curve represents $g$, the bound from below.

Figure 3.3 displays a zoom of the numerical aproximation of $C^3_{1000}(L)$ that we will denote $C^3_{num,1000}(L)$. This approximative value enables us to define $M_{num} = \dfrac{1}{C^3_{num,1000}(L)}$. To illustrate Lemma 3.4.2, we define

$$f(x) = C^3_{num,1000}(L) \exp\Big( - \frac{2 \times 1000}{3} M_{num}(L - x)\Big)$$

and

$$g(x) = C^3_{num,1000}(L) \exp\Big( - \frac{2}{3} \times 1000(L - x)\Big).$$

In Figure 3.4, we depict $C^3_{1000}$ on the interval $[\frac{99L}{100}, L]$ and the profiles of the two functions $f$ and $g$ which control $C^3_{1000}$. We observe that $g \leq C^3_{num,1000} \leq f$, as expected in theorem 3.2.2, and then that the component $C^3_{V_m}$ decreases exponentially to zero.

## 3.6 Conclusion

Motivated by renal flows, we have studied a concentration mechanism with an active pump characterized by a parameter $V_m$. As expected, for $V_m$ large enough, a large axial solute concentration gradient appears in all tubes. The result of our analysis is that the concentrations are uniformly bounded in $V_m$ for all $x \in [0, L]$, and so are their derivatives, except at $x = L$. In the limit $V_m = \infty$, the concentration gradient converges to a Dirac profile at $x = L$. We obtain a limit concentration profile in all tubes which presents a boundary layer at $x = L$. In the urine concentrating model, we are mostly interested on the behaviour at $x = L$, because it is at this depth that the composition of final urine is determined. Therefore, our analysis explains why active transport plays a very specific role, which is to increase solute concentration at $x = L$ and only at $x = L$.

# Chapter 4

# Hyperbolic relaxation of a $2 \times 2$ system with specific boundary conditions

*We consider a kinetic model with two velocities and reflexion boundary conditions. We proves that the model converges to a scalar conservation law we determine. Using the Bardos-Leroux-Neldelec formulation, we identify rigorously the boundary conditions at the limit.The specificity of the model is the spatial heterogeneity of the source term, which gives birth to an heterogeneous flux.*

## 4.1 Motivation

Many physical phenomenons can be described by an hyperbolic system containing a small parameter. In the historical case of the Boltzmann equation, describing a gas by the movement of a density of particules colliding, the small parameter represents the mean free path, which is the order of magnitude of the distance covered by a particule before it meets another particule [6,13]. In some regimes, for example when the gas becomes very dense, the mean free path is very close to zero. Asymptotic expansions on these small parameters give us a new equation usually called the averaged equation, the equilibrium equation, the macroscopic equation or merely the limit equation depending on the context and on the meaning of the small parameter $\varepsilon$.

We are interested in understanding the behavior of the system introduced in [90,91], which describes the concentration of a solute dissolved in a fluid which flows in 1-D tubes with a specific architecture, when the tube permeability $\varepsilon$ to the solute is small. In this context, we can see the system of [91] as a perturbation of a stable equilibrium state given by the equilibrium equation. One motivation of this study is to replace the hyperbolic system of [91] by a scalar equation, which can be solved numerically with usual tools [9,25], in order to get an initial guess on the solution near equilibrium.

To derive the equilibrium equation, we introduce a baby-model, even simpler than the simplified model we study in Chapter 5. The purpose is to present the analytical study with simple notations, intended that there is no additional difficulty for larger systems. This work fits into the scheme of hyperbolic relaxation problems. A survey on this topic can be found in [66]. We start with a $2 \times 2$ linear hyperbolic system and we get at the limit a non linear scalar hyperbolic equation.

Due to non-linearity, an entropic formulation of the hyperbolic limit equation is needed. A study close to what is done here is performed in [36], where the author deals with a system arising in chromatography. The idea is to find an entropic structure of the system at the level $\varepsilon$ and to pass to the limit. Other types of scaling have been performed on similar systems. For example, in [76], [27] a diffusive limit is studied. The specific feature of this work stems from the space dependency of the source term and the specific boundary conditions we handle.

### 4.1.1 A simplified urine concentration model

In our context, the model is interpreted as particules of a same chemical species dissolved in a fluid moving along the $x - axis$ $[0, L]$ in a countercurrent exchanger (see Figure 4.1). Fluid

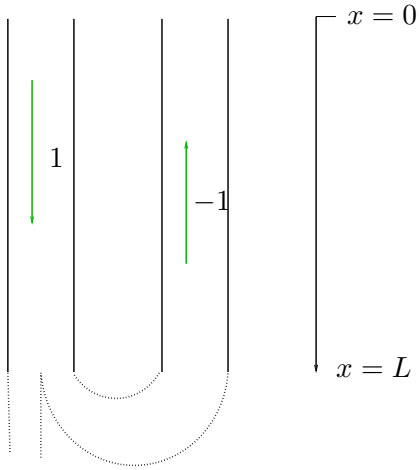


**Figure 4.1:** A countercurrent exchanger

moving with a positive speed 1 have a concentration denoted by $u(x,t)$, and fluid moving at a negative speed $-1$ have a concentration denoted by $v(x,t)$.

The model is written for $t \geq 0$ and $x \in [0, L]$,

$$\begin{cases} \dfrac{\partial u_\epsilon}{\partial t}(x,t) + \dfrac{\partial u_\epsilon}{\partial x}(x,t) = \dfrac{1}{\epsilon}\Big[h(v_\epsilon(x,t),x)) - u_\epsilon(x,t)\Big], \\ \dfrac{\partial v_\epsilon}{\partial t}(x,t) - \dfrac{\partial v_\epsilon}{\partial x}(x,t) = \dfrac{1}{\epsilon}\Big[u_\epsilon(x,t) - h(v_\epsilon(x,t),x))\Big], \\ u_\epsilon(0,t) = u_0, \qquad v_\epsilon(L,t) = \alpha u_\epsilon(L,t), \qquad \alpha \in (0,1), \\ u_\varepsilon(x,0) = u^0(x), \qquad v_\varepsilon(x,0) = v^0(x). \end{cases} \tag{4.1}$$

where $h$ is a function which quantifies the exchanges of solute between the two tubes. The parameter $\alpha$ is the proportion of solute which, at the end $x = L$ of the tube on the left is reinjected in the tube on the right. The system is rescaled with the parameter $\epsilon$.

This scaling, which makes transversal equilibrium $u = h(v, x)$ become instantaneous when $\varepsilon \to 0$, is usually called "hyperbolic scaling", because the finite speed is preserved at the limit by the change of variables $(x, t) \mapsto (\frac{x}{\varepsilon}, \frac{t}{\varepsilon})$.

Initial ($t = 0$) solute concentrations are positive. We also assume that there are uniform (on $\varepsilon$) bounds

$$\begin{array}{lll} u_\epsilon(t=0) \geq 0, & u_\epsilon(t=0) \in L^1(0,L), & \dfrac{d}{dx}u_\epsilon(t=0) \in L^1(0,L), \\ v_\epsilon(t=0) \geq 0, & v_\epsilon(t=0) \in L^1(0,L), & \dfrac{d}{dx}v_\epsilon(t=0) \in L^1(0,L). \end{array} \tag{4.2}$$

We impose the following conditions on the nonlinearity, conditions which are discussed in [91]:

$$\begin{array}{c} h(0,x) = 0, \qquad 1 < \beta \leq \dfrac{\partial h}{\partial v}(v,x) \leq \mu(x) \leq \mu_M, \\ \sup\limits_v \displaystyle\int_0^L |\frac{\partial h}{\partial x}(v,x)|dx \leq C, \qquad h(.,x) \text{ is strictly concave}, \end{array} \tag{4.3}$$

where $C$, $\beta$ and $\mu_M$ are some positive constant, and $\mu$ is a smooth function.

In our particular case where there are 2 tubes (whereas the other study deals with a 3-tube problem), we have the condition $\beta > 1$, instead of $\beta \geq 1$. The third condition means that $h(v, .)$ is $BV$, and that uniformly in $v$. More precisely, this condition can be written

$$\forall \phi \in \mathcal{C}^1_C[0,L], \qquad \sup_v \int_0^L h(v,x)\phi'(x)dx \leq C \tag{4.4}$$

We notice that the $x$-dependence for $h$ can be as stiff as a discontinuity. We denote $h^{-1}(., x)$ the inverse of $v \mapsto h(v, x)$.

We can easily adapt the proof of [91] and obtain the

**Theorem 4.1.1** (Existence and uniqueness). *With assumptions* (4.2) *and* (4.3) *, there is a weak solution (defined in [91]) to the initial value problem* (4.1)*, which lies in* $BV([0,L]\times[0,T])$*. For two initial data* $u(x,0), v(x,0)$ *and* $\widetilde{u}(x,0), \widetilde{v}(x,0)$*, the weak solutions satisfy the weak contraction property and the comparison principle*

$$\int_0^L \big[\, |u-\widetilde{u}| + |v-\widetilde{v}| \,\big](x,t)dx \leq \int_0^L \big[\, |u-\widetilde{u}| + |v-\widetilde{v}| \,\big](x,0)dx, \tag{4.5}$$

$$\int_0^L \big[\, |u-\widetilde{u}|_+ + |v-\widetilde{v}|_+ \,\big](x,t)dx \leq \int_0^L \big[\, |u-\widetilde{u}|_+ + |v-\widetilde{v}|_+ \,\big](x,0)dx. \tag{4.6}$$

*For the latter inequality, we can assume that* $(\widetilde{u}, \widetilde{v})$ *is only a supersolution. The contraction property implies the uniqueness of the solution.*

This solution to (4.1) satisfies the following conservation law associated to (4.1)

$$\frac{\partial}{\partial t}[\, u_\epsilon + v_\epsilon \,] + \frac{\partial}{\partial x}[\, u_\epsilon - v_\epsilon \,] = 0. \tag{4.7}$$

We are interested in the behavior of the functions $u_\varepsilon$ and $v_\varepsilon$ when $\epsilon$ vanishes. What makes system (4.1) peculiar are the specific boundary conditions, and the non-linearity $h$ which is $BV$ and space heterogeneous.

**Proposition 4.1.2.** *There exists $v \in L^\infty([0,L]\times[0,T])$ such that*

$$u_\epsilon(x,t) \underset{\epsilon\to 0}{\longrightarrow} h(v(x,t),x), \qquad v_\epsilon(x,t) \underset{\epsilon\to 0}{\longrightarrow} v(x,t),\ a.e.$$

**Notations.** The conservative quantity $\rho$ and the flux $A$ are defined by

$$\rho(x,t) := h(v(x,t),x) + v(x,t), \tag{4.8}$$

$$A(\rho,t) := h(v(x,t),x) - v(x,t). \tag{4.9}$$

We also set

$$a_0 = h^{-1}(u_0, 0). \tag{4.10}$$

The main result of this paper is

**Theorem 4.1.3** (Limit $\varepsilon \to 0$). *The quantity $\rho(x,t)$ is an entropy solution (as defined in [3]) to*

$$\begin{cases} \dfrac{\partial}{\partial t}\rho(x,t) + \dfrac{\partial}{\partial x}A(\rho(x,t),x) = 0, \qquad t>0,\ x\in[0,L], \\ \rho(0,t) = a_0 + h(a_0,0), \qquad t>0, \\ \rho(x,0) = \rho^0(x), \qquad \rho^0(x) := v^0(x) + h(v^0(x),x), \qquad x\in[0,L]. \end{cases} \tag{4.11}$$

**Some properties of $A$.**

i) For all $x\in[0,L]$, the functions $\rho$ and $A(.,x)$ are non-decreasing functions of $v$, therefore $v$ is a non-decreasing function of $\rho$, which makes $A(.,x)$ a non decreasing function of $\rho$, which justifies that we can define $A$ as a function of $\rho$.

ii) Since $h$ is a concave function of $v$, the flux $A$ is concave in $\rho$.

iii) The explicit expression of $A$ is $A(\rho,x) = h\Big((Id + h(.,x))^{-1}(\rho), x\Big) - (Id + h(.,x))^{-1}(\rho)$.

iv) After some calculations, we establish that

$$0 \le \frac{\partial A}{\partial \rho}(\rho,x) \le \frac{\beta-1}{\beta+1} < 1. \tag{4.12}$$

Indeed, because $r \mapsto \dfrac{r-1}{r+1}$ is non decreasing,

$$\frac{\partial A}{\partial \rho} = \frac{\dfrac{\partial A}{\partial v}}{\dfrac{\partial \rho}{\partial v}} = \frac{\dfrac{\partial h}{\partial v} - 1}{\dfrac{\partial h}{\partial v} + 1} \le \frac{\beta-1}{\beta+1}.$$

In the particular case when $h$ does not depend on $x$, we consider $u_\varepsilon$ and $v_\varepsilon$ close to equilibrium, and denote $\rho_\varepsilon = u_\varepsilon + v_\varepsilon$. A Chapman-Enskog development gives us

$$\frac{\partial}{\partial t}\rho_\varepsilon + \frac{\partial}{\partial x}A(\rho_\varepsilon) = -\varepsilon\frac{\partial}{\partial x}\left[\frac{\left[\frac{\partial A}{\partial \rho}(\rho_\varepsilon)\right]^2 - 1}{\frac{\partial h}{\partial \rho}\Big(\frac{\rho_\varepsilon - A(\rho_\varepsilon)}{2}\Big)}\frac{\partial \rho_\varepsilon}{\partial x}\right] + O(\varepsilon^2). \tag{4.13}$$

In this context, the inequality (4.12) is usually called the Whitham subcharacteristic condition [60]. The equation (4.13) is a viscous approximation of the conservation law (4.11) since (4.12) is satisfied.

Our work is divided in the following way : In part 4.2, we derive the limit equation of (4.1). More precisely, in Section 4.2.1, we give uniform a priori bound on the solution, in Section 4.2.2, we develop the dissipative structure of the system and exhibit an entropy family. In Section 4.2.3, we pass to the limit the equation (4.7) and obtain a conservation law with boundary conditions we determine. Section 4.3 is devoted to establish $BV$ a priori bounds when initial conditions are at equilibrium, pointing that in that specific case, we do not need to use compensated compactness to pass non linear quantities to the limit. In Section 4.4, we perform a numerical illustration. In Section 4.5, we describe the behavior of the convergence near the boundaries by studying the boundary layer occurring.

### 4.1.2 Notations

We will deal with functions of type

$$f : (y, x) \mapsto f(y, x)$$

where $y$ can itself be a $x$-dependent function. Therefore we distinguish

$\frac{\partial f}{\partial x}(y(x), x)$ is the derivative of $f$ with respect to its second variable,
$\frac{d}{dx}f(y(x), x)$ is the derivative with respect to $x$ of the function $x \mapsto f(y(x), x)$.

We also use the notations

$$u_+ = \begin{cases} u & \text{for } u > 0, \\ 0 & \text{else }, \end{cases}$$
$$I(a, b) = [\min(a, b), \max(a, b)].$$

## 4.2 Derivation of the hyperbolic limit

### 4.2.1 Supersolution and uniform a priori bounds

In order to study the limit in (4.1), the first step is to prove uniform estimates.

**Proposition 4.2.1.** *The solution to* (4.1) *satisfies the uniform estimate*

$$\|u_\epsilon\|_{L^\infty([0,L]\times[0,T])} \le K(\beta, u_0, u^0, v^0), \qquad \|v_\epsilon\|_{L^\infty([0,L]\times[0,T])} \le K(\beta, u_0, u^0, v^0). \tag{4.14}$$

*Proof.* To obtain an $L^\infty$ bound on the time-dependent solution, we follow the approach of [3] and use the comparison principle with appropriate supersolution. Indeed, because of the $x-$dependence of $h$, constant functions are not super-solution of the stationary problem.

We introduce the stationary system related to (4.1)

$$\begin{cases} \dfrac{dU_\epsilon}{dx}(x) = \dfrac{1}{\epsilon}\Big[h(V_\epsilon(x),x)) - U_\epsilon(x)\Big], \\ -\dfrac{dV_\epsilon}{dx}(x) = \dfrac{1}{\epsilon}\Big[U_\epsilon(x) - h(V_\epsilon(x),x))\Big], \\ \\ \quad U_\epsilon(0) = U_0, \qquad V_\epsilon(L) = \alpha U_\epsilon(L). \end{cases} \tag{4.15}$$

**Lemma 4.2.2.** *There exists a smooth super solution $(U_\epsilon, V_\epsilon)$ of the stationary problem (4.15), and a constant $K(u_0,\beta) > 0$ such that*

$$\|U_\epsilon\|_\infty \le K(u_0,\beta), \qquad \|V_\epsilon\|_\infty \le K(u_0,\beta). \tag{4.16}$$

*Proof.* We first notice in a mundane way that a solution to (4.15)

where $U_0 \ge u_0$, is a super-solution to (4.15). It remains to find a solution of (4.15) which satisfies $U_0 \ge u_0$ and to prove that it is uniformly bounded in $\epsilon$. It has been proved [91] that (4.15) admits a unique solution (fixed point argument for the existence and contraction for the uniqueness).

Adding the two lines of (4.15), we obtain a quantity which does not depend on $x$,

$$U_\epsilon(x) - V_\epsilon(x) =: K_\epsilon. \tag{4.17}$$

Using the boundary values, we find uniform bounds on $K_\epsilon$

$$K_\epsilon = U_0 - V_\epsilon(0) \le U_0 \qquad K_\epsilon = U_\epsilon(L) - V_\epsilon(L) = (1-\alpha)U_\epsilon(L) \ge 0, \tag{4.18}$$

and thus

$$0 \le K_\epsilon \le U_0, \qquad U_\varepsilon(L) \le \frac{U_0}{1-\alpha}. \tag{4.19}$$

Thus, we just have to prove that $U_\epsilon$ is uniformly bounded in $L^\infty$, knowing that $U_0$ and $U_\epsilon(L)$ are uniformly bounded in $\mathbb{R}$.

For that, we use a maximum principle type argument. Indeed, if $U_\epsilon$ reaches its maximal value on the boundary, the result follows. Now, if $U_\epsilon$ reaches its maximal value at $x_0 \in ]0, L[$, then,

$$0 = \frac{dU_\epsilon}{dx}(x_0) = \frac{1}{\epsilon}\Big(h(U_\epsilon(x_0) - K_\epsilon, x_0) - U_\epsilon(x_0)\Big), \tag{4.20}$$

and thus

$$U_\epsilon(x_0) = h(U_\epsilon(x_0) - K_\epsilon, x_0) \ge \beta U_\epsilon(x_0) - \beta K_\epsilon \tag{4.21}$$

then,

$$U_\epsilon(x_0) \le \frac{\beta}{\beta - 1} K_\epsilon \tag{4.22}$$

and Lemma 4.2.2 is proved. □

Now we combine this uniform supersolution with the contraction principle. Using the classical comparison principle [91]

$$\int_0^L [(u_\epsilon - U_\epsilon)_+ + (v_\epsilon - V_\epsilon)_+](x,t)dx \le \int_0^L [(u_\epsilon - U_\epsilon)_+ + (v_\epsilon - V_\epsilon)_+](x,0)dx, \tag{4.23}$$

which means that if the initial conditions lie under the supersolution, the solution stays bounded for all time $t$, and proves the second part of the lemma.

□

### 4.2.2 Entropies

The purpose of this section is to give the elements of the proof of the Proposition 4.1.2. To that purpose, after we have obtained $L^\infty$ bounds, our next step is to study the dissipative structure for (4.1) through a family of entropies, close to what has been done in [36].

**Definition 4.2.3** (A general family of entropies)**.** *We call an entropy pair for the system* (4.1) *a couple of continuous functions* $(S,\Sigma):\mathbb{R}^+\times[0,L]\mapsto\mathbb{R}^2$ *which satisfies*

$$\begin{aligned} &S(.,x) \text{ and } \Sigma(.,x) \text{ are convex,}\\ &\frac{\partial S}{\partial v}(h(v,x),x)=\frac{\partial \Sigma}{\partial v}(v,x). \end{aligned} \tag{4.24}$$

Now, in order to get rid of the terms containing $x$-derivatives at the limit, and based on Propositions 4.2.5 and 4.2.6 and we define homogeneous entropies

**Definition 4.2.4** (An homogeneous entropy family)**.** *We say that a couple of continuous functions* $(S,\Sigma):\mathbb{R}^+\times[0,L]\mapsto\mathbb{R}^2$*, is an homogeneous entropy pair for the system* (4.1) *if it satisfies the conditions of Definition 4.2.3 and if*

$$-\frac{\partial S}{\partial x}(h(v,x),x)+\frac{\partial \Sigma}{\partial x}(v,x)=0,\qquad \forall v \tag{4.25}$$

**Proposition 4.2.5.** *For a general family of entropies, for* $u_\varepsilon$ *and* $v_\varepsilon$ *solutions to* (4.1)*, the following dissipation law holds*

$$\frac{d}{dt}[\,S(u_\epsilon,x)+\Sigma(v_\epsilon,x)\,]+\frac{d}{dx}[\,S(u_\epsilon,x)-\Sigma(v_\epsilon,x)\,]\leq\frac{\partial S}{\partial x}(u_\epsilon,x)-\frac{\partial \Sigma}{\partial x}(v_\epsilon,x). \tag{4.26}$$

*Proof.* We multiply each line respectively by $\dfrac{\partial S}{\partial v}(u_\epsilon,x)$ and $\dfrac{\partial \Sigma}{\partial v}(v_\epsilon,x)$, we sum the three lines and integrate over $[0,L]$, we then obtain,

$$\begin{aligned} \frac{d}{dt}[\,S(u_\epsilon,x)+\Sigma(v_\epsilon,x)\,]+\frac{d}{dx}[\,S(u_\epsilon,x)-\Sigma(v_\epsilon,x)\,]&\\ =\frac{1}{\epsilon}\Big(\frac{\partial S}{\partial v}(u_\epsilon,x)-\frac{\partial \Sigma}{\partial v}(v_\epsilon,x)\Big)\Big(h(v_\epsilon,x)-u_\epsilon\Big)&\\ +\frac{\partial S}{\partial x}(u_\epsilon,x)-\frac{\partial \Sigma}{\partial x}(v_\epsilon,x).& \end{aligned}$$

Now we use the fact that $\dfrac{\partial S}{\partial v}(h(v,x),x)=\dfrac{\partial \Sigma}{\partial v}(v,x)$ to write

$$\begin{aligned} \frac{d}{dt}[\,S(u_\epsilon,x)+\Sigma(v_\epsilon,x)\,]+\frac{d}{dx}[\,S(u_\epsilon,x)-\Sigma(v_\epsilon,x)\,]&\\ =\frac{1}{\epsilon}\Big(\frac{\partial S}{\partial v}(u_\epsilon,x)-\frac{\partial S}{\partial v}(h(v_\varepsilon,x),x)\Big)\Big(h(v_\epsilon,x)-u_\epsilon\Big)&\\ +\frac{\partial S}{\partial x}(u_\epsilon,x)-\frac{\partial \Sigma}{\partial x}(v_\epsilon,x).& \end{aligned}$$

Now, we know that $S$ is convex with respect to its first variable, then $\dfrac{\partial S}{\partial v}$ is non decreasing with respect to its first variable, which means that $\Big(\dfrac{\partial S}{\partial v}(u_\epsilon,x)-\dfrac{\partial S}{\partial v}(h(v_\varepsilon,x),x)\Big)\Big(h(v_\epsilon,x)-u_\epsilon\Big)$ is non-positive.

$$\frac{d}{dt}[\,S(u_\epsilon,x)+\Sigma(v_\epsilon,x)\,]+\frac{d}{dx}[\,S(u_\epsilon,x)-\Sigma(v_\epsilon,x)\,]\leq\frac{\partial S}{\partial x}(u_\epsilon,x)-\frac{\partial \Sigma}{\partial x}(v_\epsilon,x).$$

□

By choosing a particular entropy, we prove the following $L^2$ convergence.

**Proposition 4.2.6.** *For $u_\varepsilon$ and $v_\varepsilon$ solutions to (4.1), we have the convergence*

$$u_\epsilon - h(v_\epsilon, x) \underset{\epsilon \longrightarrow 0}{\longrightarrow} 0, \qquad L^2\Big([0,L]\times[0,T]\Big). \tag{4.27}$$

*Proof.* We choose $S(u) = \dfrac{u^2}{2}$ and $\Sigma(u,x) = \int_0^u h(s,x)ds$. These functions are consistent with Definition 4.2.3. Indeed, they are convex, $\dfrac{\partial S}{\partial v}(h(v,x),x) = \dfrac{\partial \Sigma}{\partial v}(v,x)$, and $S$ does not depend on $x$ and $\Sigma$ is decreasing with $x$ as $h$ is. Thus, according to proposition (4.2.5),

$$\begin{aligned}\frac{d}{dt}[\, S(u_\epsilon,x) + \Sigma(v_\epsilon,x)\,] + \frac{d}{dx}[\, S(u_\epsilon,x) - \Sigma(v_\epsilon,x)\,] \\ = -\frac{1}{\epsilon}\Big(h(v_\epsilon,x) - u_\epsilon\Big)^2 + \frac{\partial h}{\partial x}(v_\epsilon,x).\end{aligned} \tag{4.28}$$

We integrate this equality on $[0,L]\times[0,T]$. The left hand side terms

$$\int_0^L \Big[S(u_\epsilon(x,T)) + \Sigma(v_\epsilon(x,T)) - S(u_\epsilon(x,0)) - \Sigma(v_\epsilon(x,0))\Big]dx,$$

$$\int_0^T \Big[S(u_\epsilon^1(L,T)) - \Sigma(v_\epsilon(L,T),L) - S(u_0) + \Sigma(v_\epsilon(0,T),0)\Big]dt$$

are uniformly bounded in $\epsilon$ because $u_\varepsilon$ and $v_\varepsilon$ are, and

$$\int_0^T\int_0^L \frac{\partial h}{\partial x}(v_\epsilon,x)dxdt$$

is also uniformly bounded in $\epsilon$ because $h$ is $BV$. Thus,

$$\frac{1}{\epsilon}\int_0^T\int_0^L \Big(h(v_\epsilon,x) - u_\epsilon\Big)^2 dxdt \le K,$$

and the result holds. □

We now have all the ingredients to prove Theorem 4.2.7, which states that the weak-* $L^\infty$-convergence is in fact a strong convergence. That allows us to pass non linear quantities to the limit, and in particular the entropy dissipation laws, which gives us the entropy formulation of a conservation law. As it is standard, we do not give the proof of the theorem. It is based on the compensated compactness method introduced in [64] and developed in [85] [81]. For that kind of specific system, more details can be found in [36]. We also present two alternatives proofs on Section 4.3, which require that the initial conditions are at equilibrium. We point out that for the proof, we need the technical assumption on $h$ (4.3), which implies that the limit flux is non-degenerate.

**Theorem 4.2.7.** *There exists $v \in L^\infty\Big([0,L]\times[0,T]\Big)$ such that*

$$u_\epsilon \underset{\epsilon\longrightarrow 0}{\longrightarrow} h(v,x), \qquad v_\epsilon \underset{\epsilon\longrightarrow 0}{\longrightarrow} v, \qquad L^2,\ a.e., \tag{4.29}$$

### 4.2.3 An entropy formulation for the limit equation

Now that we are able to pass non linear quantities to the limit, we will state an entropy formulation of the conservation law satisfied by the limit of $v_\varepsilon + u_\varepsilon$, which is $v + h(v, x)$. We will state Proposition 4.2.12 and Theorem 4.2.14, which are a more precise version of Theorem 4.1.3.

As $h$ can have spatial heterogeneities, the conservation law we get is also heterogeneous. For these types of conservative laws, an adapted entropy formulation à la Kružkov was developed in [3]. We use this formulation. For dealing with the boundary conditions, we use the formulation à la Bardos-Leroux-Nedelec (BLN) introduced in [7]. This formulation is easier to work with than that developed by Otto in [69], but the price to pay is to assume the existence of traces. In our case, the flux $A$ is strictly concave, and is thus non-degenerate in the sense of [59], and we have the existence of traces thanks to [93].

**Definition 4.2.8.** *For $p \in \mathbb{R}$, we define uniquely the function $k_p$ as*

$$A(k_p(x), x) = p. \tag{4.30}$$

It is well-defined because $A$ is one-to-one with respect to its first variable. That makes $k_p$ be a stationary solution of the limit equation (4.11). This is equivalent to say

$$h(k_p(x), x) - k_p(x) = p,$$

and

$$\frac{d}{dx}\Big[h(k(x), x) - k(x)\Big] = 0 \Leftrightarrow k'(x) = -\frac{\dfrac{\partial h}{\partial x}(k(x), x)}{\dfrac{\partial h}{\partial v}(k(x), x)) - 1}, \qquad x \in [0, L]. \tag{4.31}$$

**Proposition 4.2.9.** *For all $x \in [0, L]$, $p \mapsto k_p(x)$ is increasing and lipschitz, and $k_0(x) = 0$, $k_{+\infty}(x) = +\infty$.*

As a consequence, for all $x_0$, $k_p(x_0)$ can take every positive desired value.

**Definition 4.2.10** (Adapted Kružkov entropies)**.** *We define the adapted Kružkov entropies relatively to the system* (4.1) *as*

$$S_p(u, x) = |u - h(k_p(x), x)|, \qquad \Sigma_p(v, x) = |v - k_p(x)|. \tag{4.32}$$

As we prove it later in Section 4.2.5, these are special cases of homogeneous entropies. We then state the main proposition. It states the following entropy inequality in the sense of distributions

$$\frac{\partial}{\partial t}\Big|\rho(x,t) - \Big(k_p(x) + h(k_p(x), x)\Big)\Big| + \frac{\partial}{\partial x}\Big|A(\rho, x) - A\Big(k_p(x) + h(k_p(x), x), x\Big)\Big| \leq 0, \tag{4.33}$$

where $\rho$ is defined in (4.8).

**Definition 4.2.11.** *The couple $(u_\varepsilon, v_\varepsilon)$ is called an entropic solution of* (4.1) *if for all $\phi \in$*

$\mathcal{C}^1\Big([0,L]\times[0,T]\Big)$ *such that* $\phi\geq 0$ *and* $\phi(.,T)=0$, *and for all* $k_p$ *defined in* (4.30),

$$\begin{aligned}
&-\int_0^T\int_0^L\Big[|u_\varepsilon-h(k_p(x),x)|+|v_\varepsilon-k_p(x)|\Big]\frac{\partial\phi}{\partial t}dxdt\\
&\qquad-\int_0^T\int_0^L\Big[|u_\varepsilon-h(k_p(x),x)|-|v_\varepsilon-k_p(x)|\Big]\frac{\partial\phi}{\partial x}dxdt\\
&\qquad-\int_0^L\Big[|u_\varepsilon(x,0)-h(k_p(x),x)|+|v_\varepsilon(x,0)-k_p(x)|\Big]\phi(x,0)dx\\
&\qquad+\int_0^T\Big[|u_\varepsilon(L,t)-h(k_p(L),L)|-|\alpha u_\varepsilon(L,t)-k_p(L)|\Big]\phi(L,t)dt\\
&\qquad-\int_0^T\Big[|u_0-h(k_p(0),0)|-|v_\varepsilon(0,t)-k_p(0)|\Big]\phi(0,t)dt\leq 0.
\end{aligned}\tag{4.34}$$

**Proposition 4.2.12.** *For all* $\phi\in\mathcal{C}^1\Big([0,L]\times[0,T]\Big)$ *such that* $\phi\geq 0$ *and* $\phi(0,.)=\phi(L,.)=\phi(.,T)=0$, *for all* $k_p$ *defined in* (4.30) *the function* $\rho$ *satisfies*

$$\begin{aligned}
&\int_0^T\int_0^L|\rho-h(k_p(x),x)-k_p(x)|\frac{\partial\phi}{\partial t}\\
&\qquad+\Big(A(\rho,x)-(h(k_p(x),x)-k_p(x))\Big)\,\mathrm{sign}\,\Big(\rho-h(k_p(x),x)-k_p(x)\Big)\frac{\partial\phi}{\partial x}dxdt\\
&\qquad+\int_0^L|\rho(x,0)-h(k_p(x),x)-k_p(x)|\phi(x,0)dx\geq 0,
\end{aligned}\tag{4.35}$$

This proposition is an explicit formulation of the statement in Theorem 4.1.3. This is a definition of the unique solution of the conservation law (4.11) in the sense of the solutions defined by Kru*mb̌oxz*zkov [46].

*Proof.* We write the Definition (4.2.11) for different well chosen $\phi$. We choose $\phi$ which vanishes at $x=0$ and $x=L$, and we pass to the limit to obtain

$$\begin{aligned}
&-\int_0^T\int_0^L\Big[|h(v,x)-h(k_p(x),x)|+|v-k_p(x)|\Big]\frac{\partial\phi}{\partial t}dxdt\\
&\qquad-\int_0^T\int_0^L\Big[|h(v,x)-h(k_p(x),x)|-|v-k_p(x)|\Big]\frac{\partial\phi}{\partial x}dxdt\\
&\qquad-\int_0^L\Big[|h(v(x,0),x)-h(k_p(x),x)|+|v(x,0)-k_p(x)|\Big]\phi(x,0)dx\leq 0.
\end{aligned}$$

We notice the two identities

$$|h(v)-h(k_p)|+|v-k_p|=|h(v)+v-h(k_p)-k_p|,$$

$$|h(v)-h(k_p)|-|v-k_p|=\Big[(h(v)-v)-(h(k_p)-k_p)\Big]\,\mathrm{sign}\,\Big(h(v)+v-h(k_p)-k_p\Big),$$

then the first assertion of the theorem holds true. □

### 4.2.4 The boundary conditions for the limit equation

We use the following theorem based on a theorem stated in [93] and on a lemma stated in [7]. We use the notation of [2]. It enables us to define strong traces for $BV$ functions.

**Theorem 4.2.13.** *We consider* $z \in L^\infty\Big([0,L]\times[0,T]\Big)$,

- *if* $z \in BV\Big([0,L]\times[0,T]\Big)$,
  *or*
- *if* $z$ *is an entropy solution of* $\dfrac{\partial z}{\partial t}z + \dfrac{\partial z}{\partial x}f(z) = 0$ *in* $[0,L]\times\mathbb{R}^+$ *where* $f$ *is a continuous function which is non constant on any non-degenerate interval,*

*then there exists strong traces* $\gamma^0 uz$ *and* $\gamma^L u$ *on the boundaries* $\{x=0\}$ *and* $\{x=L\}$, *in the sense*

$$\lim_{h\downarrow 0}\frac{1}{h}\int_0^{+\infty}\int_0^h |z(x,t)-\gamma^0 z(t)|\xi(t)dxdt, \qquad \forall \xi \in \mathcal{C}_C^\infty([0,+\infty)),$$
$$\lim_{h\downarrow 0}\frac{1}{h}\int_0^{+\infty}\int_{L-h}^L |z(x,t)-\gamma^L z(t)|\xi(t)dxdt, \qquad \forall \xi \in \mathcal{C}_C^\infty([0,+\infty)).$$

For all $\varepsilon$, the solutions $u_\varepsilon$ and $v_\varepsilon$ to (4.1) admit traces on the boundaries $\{x=0\}$ and $\{x=L\}$ because they are $BV$ [91]. We denote by $u_\varepsilon(0,t)$ and $v_\varepsilon(L,t)$ the respective strong traces of $u_\varepsilon$ and $v_\varepsilon$ on $\{x=0\}$ and $\{x=L\}$. We denote by $w_0(t) = \lim_{\varepsilon\longrightarrow 0} v_\varepsilon(0,t)$ and by $w_L(t) = \lim_{\varepsilon\longrightarrow 0} u_\varepsilon(L,t)$. We also denote $a_L = h^{-1}(w_L)$.

**Theorem 4.2.14.** *The function* $\rho$ *satisfies*

*i) The boundary condition at* $x=0$ *: For all* $k_p(0) \in I\Big(\rho(0,t), a_0 + h(a_0,0)\Big)$,

$$\operatorname{sign}\Big(\rho(0,t) - a_0 - h(a_0,0)\Big)\Big(A(\rho(0,t),0) - (h(k_p(0),0)+k_p(0))\Big) \le 0 \tag{4.36}$$

*ii) The boundary condition at* $x=L$ *: For all* $k_p(L) + h(k_p(L),L) \in I\Big(\rho(L,t), a_L + h(a_L,L)\Big)$,

$$\operatorname{sign}\Big(\rho(L,t) - a_L - h(a_L,L)\Big)\Big(A(\rho(L,t),L) - (h(k_p(L),L)-k_p(L))\Big) \ge 0 \tag{4.37}$$

**First Step: The boundary conditions at $x=0$.** Thanks to Theorme 4.2.13, we know that the function $\rho$, as solution of a non degenerate conservation law in the sense of [70], admits some traces on the boundary $\{0,L\}$. We merely denote by $\rho(0,t)$ and $\rho(L,t)$ the traces of $\rho$ on $\{0\}\times[0,T]$ and on $\{L\}\times[0,T]$. We choose in (4.34) $\phi(x,t) = g(t)\max(0,1-\dfrac{x}{\eta}) * j_a(x)$ where $j_a$ is kernel function, $g$ is any test function, and let $a$ and $\eta$ go to zero. Formally, it boils down to take in (4.34) $\phi(0,t) = g(t)$ and $\dfrac{\partial\phi}{\partial x}(x,t) = -\delta(x-0)g(t)$.

We obtain

$$\begin{aligned}\Big[A(\rho(0,t),0) - (h(k_p(0),0)-k_p(0))\Big]\operatorname{sign}\Big(\rho(0,t) - (h(k_p(0),0)-k_p(0))\Big)\\ \le |u_0 - h(k_p(0),0)| - |w_0 - k_p(0)|.\end{aligned} \tag{4.38}$$

To convert this formulation into a formulation à la BLN, we follow the method developed in [65]. From (4.38), we deduce that

$$A(\rho(0,t),0) = u_0 - w_0. \tag{4.39}$$

Indeed, choosing $k_p(0)$ such that $\rho(0,t) \leq h(k_p(0),0) + k_p(0)$ and $u_0 \leq h(k_p(0),0)$ and $w_0(t) \leq k_p(0)$, we obtain

$$A(\rho(0,t),0) \geq u_0 - w_0,$$

and choosing $k_p(0)$ such that $\rho(0,t) \geq h(k_p(0),0)+k_p(0)$ and $u_0 \geq h(k_p(0),0)$ and $w_0(t) \geq k_p(0)$, we obtain

$$A(\rho(0,t),0) \leq u_0 - w_0.$$

Without loss of generality, we choose values of $k_p(0)$ such that $k_p(0)+h(k_p(0),0) \in I(\rho(0,t), a_0+h(a_0,0))$. Now, we distinguish two cases.

**First case** We assume that $\rho(0,t) \leq a_0 + h(a_0)$.

To obtain (4.36), we want to prove that $A(\rho(0,t)) \geq h(k_p(0),0) - k_p(0)$. We know that $k_p(0) + h(k_p(0),0) \in [\rho(0,t), a_0 + h(a_0,0)]$, which implies that $k_p(0) \leq a_0$ which is $h(k_p(0),0) \leq u_0$ We distinguish two cases :

-If $w_0 \geq k_p(0)$,then

$$\begin{aligned} -A(\rho(0,t),0) + h(k_p(0),0) - k_p(0) &\leq u_0 - h(k_p(0),0) - w_0 + k_p(0) \\ &= A(\rho(0,t),0) - h(k_p(0),0) + k_p(0) \end{aligned}$$

which yields the conclusion.

-If $w_0 \leq k_p(0)$, then, from (4.39), $A(\rho(0,t),0) = u_0 - w_0 \geq h(k_p(0),0) - k_p(0)$.

**Second case** We assume that $\rho(0,t) \geq a_0 + h(a_0,0)$.

In that case, to obtain (4.36), we want to prove that $A(\rho(0,t)) \leq h(k_p(0),0) - k_p(0)$. We know that $k_p(0) + h(k_p(0),0) \in [a_0 + h(a_0,0), \rho(0,t)]$, which implies that $h(k_p(0),0) \geq u_0$.

-If $w_0 \geq k_p(0)$, the conclusion follows directly from (4.39).

-If $w_0 \leq k_p(0)$, then

$$\begin{aligned} A(\rho(0,t)) - h(k_p(0),0) + k_p(0) &\leq -u_0 + h(k_p(0),0) + w_0 - k_p(0) \\ &= -A(\rho(0,t)) + h(k_p(0),0) - k_p(0), \end{aligned}$$

which ends the proof for the boundary conditions at $x = 0$.

**Second Step: The boundary conditions at $x = L$.**

The outline is the same that for the boundary condition $x = 0$. We do not give so much details. We formally choose in (4.34) $\phi(L,t) = g(t)$ and $\dfrac{\partial \phi}{\partial x}(x,t) = \delta(x-L)g(t)$ where $g$ is again any test function, which gives us

$$\begin{aligned} \Big[A(\rho(L,t),L) - (h(k_p(L),L) - k_p(L))\Big] \operatorname{sign}\Big(\rho(L,t) - (h(k_p(L),L) - k_p(L))\Big) \\ \geq |w_L - h(k_p(L),L)| - |\alpha w_L - k_p(L)|, \end{aligned} \tag{4.40}$$

and

$$A(\rho(L,t),L) = (1-\alpha)w_L. \tag{4.41}$$

From (4.40) and (4.41), we deduce (4.37).

The combination of Proposition 4.2.12 and Theorem 4.2.14 defines a unique $\rho$. We remark that the parameter $\alpha$ does not occur in the limit equation. We also point out that, as we used the BLN formulation, we had to guess the boundary conditions of the limit equation before proving they were the right boundary conditions. By opposition, a straightforward proof which would enable us to derive the boundary conditions from the original system would be more desirable in order to extend this result to more general boundary conditions.

### 4.2.5 The link between adapted Kružkov entropies and homogeneous entropies

The adapted Kružkov entropies we define in Definition 4.2.10 based on [3] coincide with homogeneous entropies (Definition 4.2.4) we defined in Section 4.2.2 regarding the dissipative structure.

**Proposition 4.2.15.** *The adapted Kružkov entropies*

$$\Sigma(v,x) = |v - k_p(x)|, \qquad S(v,x) = |v - h(k_p(x),x)|, \tag{4.42}$$

*are homogeneous entropies.*

*Proof.* Let $(\Sigma(v,x), S(v,x)) = (|v-k_p(x)|, |v-h(k_p(x),x)|)$ be adapted entropies for the system (4.1). We prove here that $(\Sigma, S)$ are homogeneous entropies. We compute

$$\frac{\partial \Sigma}{\partial v}(v,x) = \begin{cases} +1 & \text{if } k(x) < v, \\ -1 & \text{else,} \end{cases}$$

and beause $h$ is on decreasing with respect to its first variable, we also have

$$\frac{\partial S}{\partial v}(h(v,x),x) = \begin{cases} +1 & \text{if } h(k(x),x) < h(v,x), \\ -1 & \text{else,} \end{cases} = \begin{cases} +1 & \text{if } k(x) < v, \\ -1 & \text{else.} \end{cases}$$

From this we conclude that

$$\frac{\partial \Sigma}{\partial v}(v,x) = \frac{\partial S}{\partial v}(h(v,x),x),$$

and thus

$$\begin{aligned} -\frac{\partial S}{\partial x}(h(v,x),x) + \frac{\partial \Sigma}{\partial x}(h(v,x),x) &= \Big[ -\frac{\partial h}{\partial x}(k_p(x),x) - k_p'(x)\frac{\partial h}{\partial v}(k_p(x),x)\Big] \operatorname{sign}\Big(h(v,x) - h(k_p(x),x)\Big) \\ &\qquad + k_p'(x) \operatorname{sign}\Big(v - k_p(x)\Big) \\ &= \Big[ -\frac{\partial h}{\partial x}(k_p(x),x) + k_p'(x)(1 - \frac{\partial h}{\partial v}(k_p(x),x))\Big] \operatorname{sign}\Big(v - k_p(x)\Big) \\ &= 0. \end{aligned}$$

as we replace $k_p'(x)$ by its expression (4.31). According to Definition 4.2.4, this ends the proof. □

## 4.3 Well-prepared initial conditions, and compactness properties

In the specific case where the initial condition is at equilibrium and has bounded variations, we have two additional proofs to the compensated compactness method. We make the following assumption

$$v(x,0) \in BV([0,L]), \qquad u(x,0) = h(v(x,0),x), \qquad x \in [0,L]. \tag{4.43}$$

Because of the hypotheses made on $h$, this assumption implies that $u(x,0)$ belongs to $BV([0,L])$.

We have the two propositions. Proposition 4.3.1 states that we can prove BV estimates under more assumptions on $h$. These BV estimates lead to the strong compactness of $(u_\varepsilon, v_\varepsilon)$. Proposition 4.3.2 states the strong compactness of $(u_\varepsilon, v_\varepsilon)$ without any BV estimate.

**Proposition 4.3.1.** *Under assumptions* (4.2), (4.3) *and* (4.43), *we have the following BV estimate on the solution*

$$\int_0^L [\, |\frac{\partial}{\partial t} u_\epsilon| + |\frac{\partial}{\partial t} v_\epsilon|\,](x,t)dx \le K_1(u^0) + K_2(v^0), \tag{4.44}$$

*and if moreover, $h$ does not depend on $x$, we have the spatial BV estimate*

$$\int_0^L [\,|\frac{\partial}{\partial x}u_\epsilon| + |\frac{\partial}{\partial x}v_\epsilon|\,](x,t)dx \leq K_3(u^0,v^0), \tag{4.45}$$

**Proposition 4.3.2.** *Under assumptions* (4.2), (4.3) *and* (4.43) *and without any restriction on the spatial dependance of $h(v,.)$, there exists $v \in L^\infty\Big([0,L]\times[0,T]\Big)$ such that*

$$u_\epsilon \underset{\epsilon\longrightarrow 0}{\longrightarrow} h(v,x), \qquad v_\epsilon \underset{\epsilon\longrightarrow 0}{\longrightarrow} v, \qquad L^2,\ a.e. \tag{4.46}$$

*Proof. A bound on the time derivative at $t=0$.* We start by claiming the following estimate

$$\int_0^L |\frac{\partial u_\epsilon}{\partial t}(x,0)|dx \leq K_1(u^0), \qquad \int_0^L |\frac{\partial v_\epsilon}{\partial t}(x,0)|dx \leq K_2(v^0). \tag{4.47}$$

Indeed, because initial conditions are at equilibrium, we have

$$\frac{\partial v_\epsilon}{\partial t}(x,0) - \frac{\partial v_\epsilon}{\partial x}(x,0) = 0.$$

We multiply it by $\text{sign}\Big(\frac{\partial}{\partial t}v_\epsilon\Big)(x,0)$ and integrate over $[0,L]$ to get

$$\int_0^L \Big|\frac{\partial v_\epsilon}{\partial t}(x,0)\Big|dx = \int_0^L \Big|\frac{\partial v_\epsilon}{\partial x}(x,0)\Big|dx, \tag{4.48}$$

Then, thanks to assumption (4.43), we have

$$\int_0^L |\frac{\partial v_\epsilon}{\partial x}(x,0)|dx \leq K_2(v^0)$$

which gives the first inequality of estimates (4.47). It is the same argument for $u$.

**First step. The time BV estimate.**

To obtain (4.44), we differentiate each line of (4.1) and we multiply it respectively by $\text{sign}\Big(\frac{\partial}{\partial t}u_\epsilon\Big)$ and $\text{sign}\Big(\frac{\partial}{\partial t}v_\epsilon\Big)$. Adding the two lines, we obtain

$$\begin{aligned}\frac{d}{dt}\int_0^L [\,|\frac{\partial}{\partial t}u_\epsilon| + |\frac{\partial}{\partial t}v_\epsilon|\,](x,t)dx &\leq |\frac{\partial}{\partial t}u_0| - |\frac{\partial}{\partial t}u_\epsilon(L,t)| + |\frac{\partial}{\partial t}v_\epsilon(L,t)| - |\frac{\partial}{\partial t}v_\epsilon(0,t)| \\ &= -\frac{1}{2}|\frac{\partial}{\partial t}u_\epsilon(L,t)| - |\frac{\partial}{\partial t}v_\epsilon(0,t)| \leq 0,\end{aligned} \tag{4.49}$$

which implies

$$\int_0^L [\,|\frac{\partial}{\partial t}u_\epsilon| + |\frac{\partial}{\partial t}v_\epsilon|\,](x,t)dx \leq \int_0^L [\,|\frac{\partial}{\partial t}u_\epsilon| + |\frac{\partial}{\partial t}v_\epsilon|\,](x,0)dx.$$

Thus, using estimate (4.47), the first statement of Proposition 4.3.1 holds.

*A bound on the edges.* Before we start the second step, we point out the following a priori bounds

$$\int_0^T |\frac{\partial}{\partial t}u_\epsilon(L,t)|dt \leq K_1(u^0) + K_2(v^0), \qquad \int_0^T |\frac{\partial}{\partial t}v_\epsilon(0,t)|dt \leq 2\Big(K_1(u^0) + K_2(v^0)\Big). \tag{4.50}$$

These estimates are obtained by integrating the last right hand side of (4.49) over $[0,T]$ and by using (4.44).

**Second step. The BV estimate in space (only in the case when h is not space-dependant).**

Even if this method merely enables us to obtain BV estimates in the homogeneous case, we find interesting to put it forward here. The arguments we use were found in [65].

By doing the same computation, and using that $h$ does not depend on $x$, we obtain the inequality on the space derivatives :

$$\frac{\partial}{\partial t}\Big[|\frac{\partial u_\epsilon}{\partial x}| + |\frac{\partial v_\epsilon}{\partial x}|\Big](x,t) + \frac{\partial}{\partial x}\Big[|\frac{\partial u_\epsilon}{\partial x}| - |\frac{\partial v_\epsilon}{\partial x}|\Big](x,t) \leq 0. \tag{4.51}$$

We integrate this inequality on the square $[0,T]\times[0,L]$ and we get

$$\begin{aligned}\int_0^L \Big[|\frac{\partial u_\epsilon}{\partial x}| + |\frac{\partial v_\epsilon}{\partial x}|\Big](x,T)dx \leq &\int_0^L \Big[|\frac{\partial u_\epsilon}{\partial x}| + |\frac{\partial v_\epsilon}{\partial x}|\Big](x,0)dx \\ &+ \int_0^T \Big[|\frac{\partial u_\epsilon}{\partial x}| - |\frac{\partial v_\epsilon}{\partial x}|\Big](0,t)dt \\ &+ \int_0^T \Big[|\frac{\partial u_\epsilon}{\partial x}| - |\frac{\partial v_\epsilon}{\partial x}|\Big](L,t)dt\end{aligned} \tag{4.52}$$

and we need to control the three terms in the right hand side of this inequality.

For the first term, we have immediately thanks to (4.43)

$$\int_0^L \Big[|\frac{\partial u_\epsilon}{\partial x}| + |\frac{\partial v_\epsilon}{\partial x}|\Big](x,0)dx \leq K_1(u^0) + K_2(v^0). \tag{4.53}$$

For second and third terms, we write

$$\begin{aligned}\Big||\frac{\partial u_\epsilon}{\partial x}| - |\frac{\partial v_\epsilon}{\partial x}|\Big|(0,t) &\leq \Big|\frac{\partial u_\epsilon}{\partial x} - \frac{\partial v_\epsilon}{\partial x}\Big|(0,t) \\ &= \Big|\frac{\partial u_\epsilon}{\partial t} + \frac{\partial v_\epsilon}{\partial t}\Big|(0,t) \text{ (by reporting in} \\ &\leq |\frac{\partial}{\partial t}u_0| + |\frac{\partial}{\partial t}v_\epsilon(0,t)| \\ &= |\frac{\partial}{\partial t}v_\epsilon(0,t)|.\end{aligned} \tag{4.54}$$

Thus, by integrating (4.54) and using (4.50), we control the second term.

The term $\displaystyle\int_0^T \Big[|\frac{\partial u_\epsilon}{\partial x}| - |\frac{\partial v_\epsilon}{\partial x}|\Big](L,t)dt$ is treated the same way. □

*Proof.* We prove here Proposition 4.3.2. This proof is applicable without any restriction on the space dependance of $h$. We add the two lines of (4.1) and obtain

$$\Big(\frac{\partial}{\partial x}(u_\varepsilon - v_\varepsilon)\Big)(x,t) = -\Big(\frac{\partial}{\partial t}(u_\varepsilon + v_\varepsilon)\Big)(x,t).$$

Using (4.44), we thus conclude that for all $t \geq 0$

$$\int_0^L \Big|\ \frac{\partial}{\partial x}(u_\epsilon - v_\varepsilon)\ \Big|(x,t)dx \leq K_1(u^0) + K_2(v^0).$$

Therefore we can conclude that

$$u_\varepsilon - v_\varepsilon \qquad \text{is compact in } L^1\Big([0,L]\times[0,T]\Big).$$

Now, thanks to Proposition 5.2.6,

$$h(v_\varepsilon,.) - u_\varepsilon \qquad \text{is compact in } L^1\Big([0,L]\times[0,T]\Big).$$

A combination of these two last compact embeddings gives us that

$$h(v_\varepsilon,.) - v_\varepsilon \qquad \text{is compact in } L^1\Big([0,L]\times[0,T]\Big), \tag{4.55}$$

thus, after extraction,

$$h(v_\varepsilon,.) - v_\varepsilon \underset{\varepsilon\longrightarrow 0}{\longrightarrow} L(x),$$

and because $v \mapsto h(v,x) - v$ is bijective, we conclude that

$$v_\varepsilon \text{ and then } u_\varepsilon \text{ are compact in } L^1\Big([0,L]\times[0,T]\Big). \tag{4.56}$$

□

## 4.4 Numerical relaxation

In this section, we illustrate numerically the convergence of $u_\varepsilon + v_\varepsilon$ toward the conservative quantity $\rho$, but for a boundary layer. We chose

$$h(v,x) = 2V\frac{v}{1+v} + 2v, \qquad \alpha = \frac{1}{2},$$

with $V$ a positive constant. In this section $h$ does not depend on $x$, for this section, and this makes the numerical scheme more readable. Finite volumes are well adapted to the hyperbolic equations however we need to adapt them in order to treat the limit $\varepsilon \to 0$.

### 4.4.1 An asymptotic preserving scheme

We build here a scheme which is stable and consistent with (4.1) and which gives rise to a consistent and stable solver for the limit equation. Such schemes are called AP schemes (Asymptotic Preserving) and a review on this topic can be found in [41]. In our context, a first necessary condition is to build a scheme which is unconditionally stable in $\varepsilon$. More precisely, that means that the CFL condition associated with the scheme does not go to zero with $\varepsilon$. A naive explicit scheme, due to the stiff right hand side in (4.1) will be stable under a CFL condition

$$\Delta t \leq \frac{\varepsilon\Delta x}{\Delta x + \varepsilon} \tag{4.57}$$

which becomes expensive as $\varepsilon$ becomes small.

This leads to treat implicitly the right hand sides which are responsible for (4.57). Among the many ways to do so, we present a simple variant which preserves the structure

$$\frac{\partial(u+v)}{\partial t} + \frac{\partial(u-v)}{\partial x} = 0.$$

We use the following scheme

$$\begin{cases} \dfrac{u_{\epsilon,k}^{n+1} - u_{\epsilon,k}^{n}}{\Delta t} + \dfrac{u_{\epsilon,k}^{n} - u_{\epsilon,k-1}^{n}}{\Delta x} = \dfrac{1}{\epsilon}\Big[2V\dfrac{v_{\epsilon,k}^{n+1}}{1+v_{\epsilon,k}^{n}} + 2v_{\epsilon,k}^{n+1} - u_{\epsilon,k}^{n+1}\Big], \\ \dfrac{v_{\epsilon,k}^{n+1} - v_{\epsilon,k}^{n}}{\Delta t} + \dfrac{v_{\epsilon,k}^{n} - v_{\epsilon,k+1}^{n}}{\Delta x} = \dfrac{1}{\epsilon}\Big[u_{\epsilon,k}^{n+1} - 2V\dfrac{v_{\epsilon,k}^{n+1}}{1+v_{\epsilon,k}^{n}} - 2v_{\epsilon,k}^{n+1}\Big], \end{cases} \tag{4.58}$$

with the boundary conditions

$$u^n_{\epsilon,0} = u_0, \qquad v^n_{\epsilon,N+1} = v_I = \frac{1}{2}u^n_{\epsilon,N}. \tag{4.59}$$

We detail the algorithm that allows us to compute step by step the $u^{n+1}, v^{n+1}$. In this description, we omit the indexes $\varepsilon$. We know $(u^n_k)_k$ and $(v^n_k)_k$ for a given $n$ and we want to determine $(u^{n+1}_k)_k$ and $(v^{n+1}_k)_k$ We notice that, whereas the source term is partially implicit, the quantity $\rho^{n+1}_k := u^{n+1}_k + v^{n+1}_k$ is equal to $u^n_k + v^n_k + \dfrac{\Delta t}{\Delta x}\Big[u^n_{k-1} - u^n_k - v^n_k + v^n_{k+1}\Big]$.

*First Step : We compute* $\rho^{n+1}_k$

$$\rho^{n+1}_k = u^n_k + v^n_k + \frac{\Delta t}{\Delta x}\Big[u^n_{k-1} - u^n_k - v^n_k + v^n_{k+1}\Big], \qquad \forall k \in [1, N].$$

*Second Step : We compute* $v^{n+1}_k$

$$\begin{aligned} v^n_{N+1} &= \frac{1}{2}u^n_N, \\ v^{n+1}_k &= \frac{1}{1 + \dfrac{2\Delta t}{\epsilon} + \dfrac{2V\Delta t}{\varepsilon(1+v^n_k)} + \dfrac{\Delta t}{\varepsilon}}\Big[v^n_k(1 - \frac{\Delta t}{\Delta x}) + v^n_{k+1}\frac{\Delta t}{\Delta x} + \frac{\Delta t}{\varepsilon}\rho^{n+1}_k\Big], \qquad \forall k \in [1, N]. \end{aligned}$$

*Third Step : We compute* $u^{n+1}_k$

$$\begin{aligned} u^{n+1}_0 &= u_0, \\ u^{n+1}_k &= \rho^{n+1}_k - v^{n+1}_k, \qquad \forall k \in [1, N]. \end{aligned}$$

**Proposition 4.4.1.** *Under the CFL condition*

$$\Delta t \leq \Delta x, \tag{4.60}$$

*then* $u^n_{\varepsilon,k}$ *and* $v^n_{\varepsilon,k}$ *are non negative and are uniformly bounded in k,n and* $\varepsilon$.

The CFL condition (4.60) is not surprising since the velocity in the limiting equation is less than 1, as expressed in condition (4.12).

### 4.4.2 The conservation law

We formally determine the fluxes of the conservation law, that we write under the form

$$\frac{\partial}{\partial t}\rho + \frac{\partial}{\partial x}A(\rho) = 0. \tag{4.61}$$

We have

$$\frac{\partial}{\partial t}\Big[3v + 2V(x)\frac{v}{1+v}\Big] + \frac{\partial}{\partial x}\Big[v + 2V(x)\frac{v}{1+v}\Big] = 0. \tag{4.62}$$

Writing $\rho = 3v + 2V(x)\dfrac{v}{1+v}$, and $A(\rho) = v + 2V(x)\dfrac{v}{1+v}$, we find

$$A(\rho) = \frac{1}{3}\Big(2\rho + 3 + 2V - \sqrt{(3 + 2V - \rho)^2 + 12\rho}\Big). \tag{4.63}$$

Thus, the conservation law satisfied by the the limit $v + h(v) =: \rho$ is

$$\begin{cases} \dfrac{\partial}{\partial t}\rho + \dfrac{\partial}{\partial x}\dfrac{1}{3}\Big(2\rho + 3 + 2V - \sqrt{(3 + 2V - \rho)^2 + 12\rho}\Big) = 0, & t > 0, x \in [0, L], \\ \rho(0,t) = a_0 + 2h(a_0, 0), & t > 0, \\ \rho(0,x) = u(0,x) + v(0,x), & x \in [0, L]. \end{cases} \tag{4.64}$$

### 4.4.3 Comparison between $u_\varepsilon + v_\varepsilon$ and $\rho$

Because we have proved that $u_\varepsilon(x,t) + v_\varepsilon(x,t)$ converges to $\rho(x,t)$ as $\varepsilon \to 0$, we expect the same behavior for the scheme. The Figure 4.2 illustrates the convergence, which is effective inside the domain. The difference between the $\rho$ and $u_\varepsilon + v_\varepsilon$ on the domain is purely numerical and is due to the fact that we use an upwind scheme to compute the solution of the theoretical limit equation, whereas the AP scheme give rise to a Rusanov type scheme at the limit $\varepsilon = 0$, which is more diffusive. However, we observe a boundary layer that occurs at $x = L$, which appears at $T = 1$ and 2. We study this boundary layer in the next section.

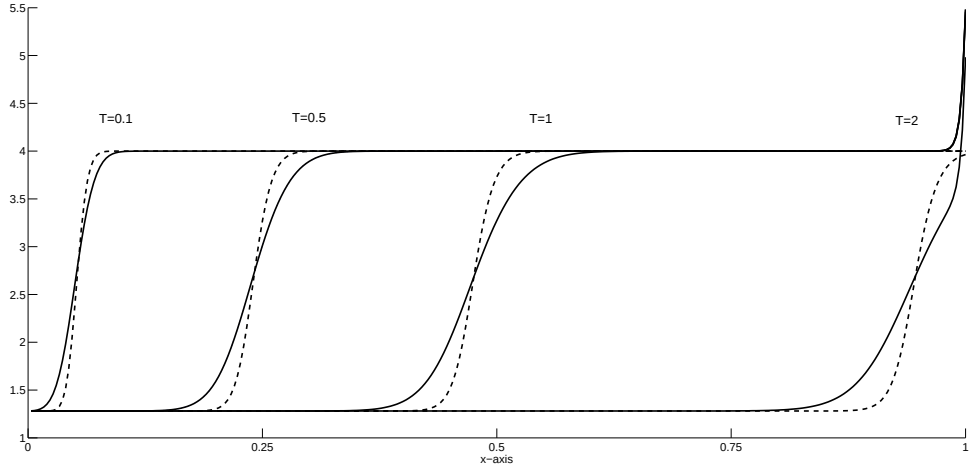


**Figure 4.2:** The numerical solution of the conservation law (4.64) $\rho$ for $T = 0.1$, $T = 0.5$, $T = 1$ and $T = 2$ is plotted in dotted line. It is obtained with an upwind scheme. In full line, we plot $u_\epsilon + v_\epsilon$ at the same times $T$, where $u_\varepsilon$ and $v_\varepsilon$ are the numerical solutions of (4.1), for $\varepsilon = 10^{-3}$ using the scheme in Section 4.4.

## 4.5 The boundary layer

At the boundary $x = L$, two equilibrium are competing with each other. The couple $(u, v)$ tends to belong to two manifolds defined as

$$M_b = \{(u, v) \in \mathbb{R}^2 | v = \alpha u\}, \tag{4.65}$$

$$M_{eq} = \{(u, v) \in \mathbb{R}^2 | u = h(v, L)\}, \tag{4.66}$$

which are disconnected in the generic case. In the neighborhood of $x = L$, a boundary layer occurs, as illustrated on Figure 4.2. We state the proposition

**Proposition 4.5.1** (Existence of the boundary layer). *We assume that $h(\alpha u_0, L) \neq u_0$ and that $h(v, .)$ is continuous at $x = L$. Then, there exists $D > 0$, $\eta > 0$ such that*

$$\forall t > 0, \forall x \in [L - \eta\varepsilon, L], \qquad |h(v_\varepsilon(x, t), x) - u_\varepsilon(x, t)| > D. \tag{4.67}$$

To avoid technicalities, we just explain formally the result and restrict ourselves to the case when $h$ does not depend on $x$. In order to investigate the boundary layer at $x = L$, and as we postulate that its size is of the same order of magnitude as $\varepsilon$, we make the following change of variables

$$y = \frac{x - L}{\varepsilon}, \tag{4.68}$$

as illustrated in Figure 4.3.

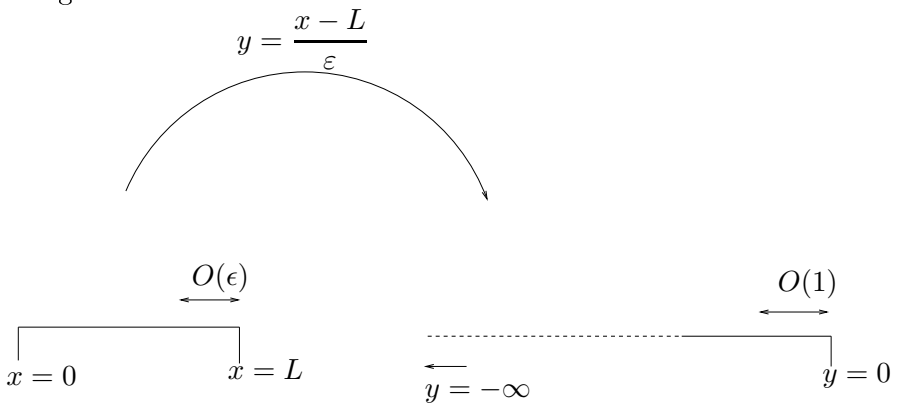


**Figure 4.3:** A boundary layer of size $\varepsilon$ for (4.1) becomes a boundary layer of size 1 for (4.70)

The system (4.1) becomes

$$\begin{cases} \varepsilon \dfrac{\partial u_\epsilon}{\partial t}(y, t) + \dfrac{\partial u_\epsilon}{\partial y}(y, t) = \Big[h(v_\epsilon(y, t)) - u_\epsilon(y, t)\Big], \\ \varepsilon \dfrac{\partial v_\epsilon}{\partial t}(y, t) - \dfrac{\partial v_\epsilon}{\partial y}(y, t) = \Big[u_\epsilon(y, t) - h(v_\epsilon(y, t))\Big], \\ \\ u_\epsilon(-\infty, t) = u_0, \qquad v_\epsilon(0, t) = \alpha u_\epsilon(0, t). \end{cases} \tag{4.69}$$

When $\varepsilon$ tends to zero, solutions to (4.69) behave like solutions to

$$\begin{cases} \dfrac{du}{dy}(y) = h(v(y)) - u(y), \\ -\dfrac{dv}{dy}(y) = u(y) - h(v(y)), \\ \\ u(-\infty) = u_0, \qquad v(0) = \alpha u(0). \end{cases} \tag{4.70}$$

We are left to study the system (4.70). We assume that the solutions are smooth. Through two lemmas, we first state that equilibrium $M_{eq}$ is reached at $y = -\infty$, then that equilibrium $M_{eq}$ is not reached at $y = 0$, and finally prove that to connect these two states, a boundary later of size 1 is necessary.

**Lemma 4.5.2.**

$$\lim_{y\to-\infty}\Big(u(y) - h(v(y))\Big) = 0 \tag{4.71}$$

*Proof.* First, we derive $L^\infty$ bounds on $u$ and $v$, as performed in Section 4.2.1. We sum the two lines of (4.70) and notice that

$$u(y) - v(y) = K, \tag{4.72}$$

with $K$ which satisfies

$$K = u(0) - v(0) = (1-\alpha)u(0) \geq 0, \qquad K = u(-\infty) - v(-\infty) \leq u_0.$$

That gives us the existence of the limit $\lim_{y\to-\infty} v(y)$, and uniform bounds on $u(0)$ and $v(-\infty)$. Using the same maximum principle as in lemma 5.2.2, we prove that $u(y) \leq \dfrac{K}{\beta - 1}$. As a consequence,

$$\|u\|_\infty \leq C, \qquad \|v\|_\infty \leq C.$$

We end the proof by arguing by contradiction. Let us assume that

$$\lim_{y\to-\infty}\Big(u(y) - h(v(y))\Big) = l > 0. \tag{4.73}$$

Reporting in (4.70),

$$\lim_{y\to-\infty}\frac{du}{dy}(y) = l,$$

thus, we can find $M$ such that, for $y < -M$, $\dfrac{du}{dy}(y) > \dfrac{l}{2}$, then $\lim_{y\to-\infty} u(y) = -\infty$, which is absurd. The same argument holds if $l < 0$. That proves (4.71). □

**Lemma 4.5.3.** *Except in the specific case where $h(\alpha u_0) = u_0$, we have*

$$u(0) - h(v(0)) \neq 0. \tag{4.74}$$

*Proof.* We first assume that there exists $y_0$ such that $u(y_0) \neq h(v(y_0))$. If for example $u(y_0) - h(v(y_0)) > 0$ (we reason the same way if it is negative), then

$$\frac{d}{dy}\Big(u - h(v)\Big)(y_0) = \Big(\frac{\partial h}{\partial v}(v) - 1\Big)\Big(u - h(v)\Big)(y_0) > 0. \tag{4.75}$$

Then, as soon, as $u(y) - h(v(y)) > 0$, $u(y) - h(v(y))$ is increasing. Then, $u(0) - h(v(0)) > 0$.

If the assumption we made at the beginning is not true, then $u \equiv h(v)$, which means that $\dfrac{du}{dy} = \dfrac{dv}{dy} = 0$, thus

$$\begin{cases} u \equiv u_0, \\ v \equiv \alpha u_0, \end{cases}$$

which implies $h(\alpha u_0) = u_0$. □

Now, we denote

$$M := \Big(h(v) - u\Big).$$

We assume $M > 0$. Here again, we could have assumed $M < 0$ and performed the same type of reasoning. The computation (4.75) implies that

$$(\beta - 1)M < \frac{d}{dy}\Big(h(v) - u)\Big)(y) < (\mu_M - 1)M.$$

Thus, as long as $h(v) - u > 0$,

$$0 < \frac{d}{dy}\Big(h(v) - u)\Big)(y) < (\mu_M - 1)M.$$

The equilibrium $u = h(v)$ is not reached at least on a neighborhood of 0 of a size of order of magnitude 1, which means for the system (4.1) that the equilibrium $u = h(v)$ is not reached at least on a neighborhood of $L$ of a size of order of magnitude $\varepsilon$

## 4.6 Conclusion

We derived an entropic formulation and the boundary conditions of the limit equation of our hyperbolic system. The tools we use are a priori estimates, compensated compactness and entropic formulations. The flux of the limit equation is increasing for every initial conditions, thus, we only had to specify the boundary conditions at $x = 0$. For this reason, neither the boundary conditions at equilibrium, nor the limit equation make occur the parameter $\alpha$. The convergence toward equilibrium occurs on the whole domain $(0, L)$. However, we noticed after performing a numerical illustration the occurrence of a boundary layer in the neighborhood of $x = L$. We then pointed out that this boundary layer is not an artificial numerical effect but well and truly a phenomenon occurring at the continuous level when $\varepsilon$ goes to zero. In a future work, we would like to get rid of this boundary layer, at least numerically, by building an asymptotic preserving scheme which makes it vanish at the limit $\varepsilon = 0$. Also left to a future work is the consideration of a more generic function $h$ (not necessarily monotonous) and of more generic boundary conditions for the original system, and the understanding of the limit boundary conditions at equilibrium.

# Chapter 5

# Hyperbolic relaxation of the $3 \times 3$ system for the kidney model

This chapter is a complement to Chapter 4 and concerns the complete $3\times3$ system. We extend our asymptotic analysis in this case.

## 5.1 The rescaled $3 \times 3$ kidney

### 5.1.1 A simplified urine concentration model

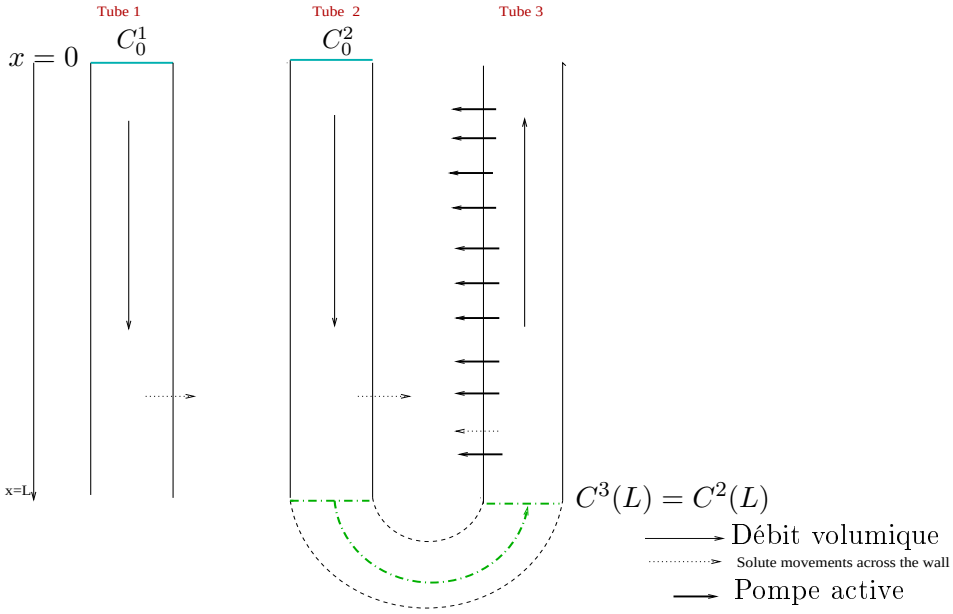


**Figure 5.1:** A 3-tube countercurrent exchanger

We write the system (1.15) with non-dimensional variables, using the parameter $\epsilon$ which measures the ratio between ionic exchanges and flow along the tubules. For $t \geq 0$ and $x \in [0, L]$,

$$\begin{cases} \dfrac{\partial C_\epsilon^1}{\partial t}(x,t) + \dfrac{\partial C_\epsilon^1}{\partial x}(x,t) = \dfrac{1}{3\epsilon}\Big[C_\epsilon^2(t,x) + h(C_\epsilon^3(x,t),x)) - 2C_\epsilon^1(t,x)\Big], \\ \dfrac{\partial C_\epsilon^2}{\partial t}(x,t) + \dfrac{\partial C_\epsilon^2}{\partial x}(x,t) = \dfrac{1}{3\epsilon}\Big[C_\epsilon^1(t,x) + h(C_\epsilon^3(x,t),x)) - 2C_\epsilon^2(t,x)\Big], \\ \dfrac{\partial C_\epsilon^3}{\partial t}(x,t) - \dfrac{\partial C_\epsilon^3}{\partial x}(x,t) = \dfrac{1}{3\epsilon}\Big[C_\epsilon^1(t,x) + C_\epsilon^2(t,x) - 2h(C_\epsilon^3(x,t),x))\Big], \\ C_\epsilon^1(0,t) = C_0^1, \qquad C_\epsilon^2(0,t) = C_0^2, \qquad C_\epsilon^3(L,t) = C_\epsilon^2(L,t), \qquad t > 0. \end{cases} \tag{5.1}$$

Initial ($t = 0$) solute concentrations are positive and we assume the uniform bounds on $\varepsilon$

$$\begin{aligned} &C_\epsilon^1(t=0) \geq 0, \qquad C_\epsilon^1(t=0) \in W^{1,1}(0,L), \\ &C_\epsilon^2(t=0) \geq 0, \qquad C_\epsilon^2(t=0) \in W^{1,1}(0,L), \\ &C_\epsilon^3(t=0) \geq 0, \qquad C_\epsilon^3(t=0) \in W^{1,1}(0,L). \end{aligned} \tag{5.2}$$

We make the usual assumptions on $h$ (Chapter 4)

$$\begin{aligned} &h(0,x) = 0, \qquad 1 \leq \frac{\partial h}{\partial v}(v,x) \leq \mu(x) \leq \mu_M, \\ &\sup_v \int_0^L |\frac{\partial h}{\partial x}(v,x)|dx \leq C, \qquad h(.,x) \text{ is not affine on any sub-interval,} \end{aligned} \tag{5.3}$$

where $C$ and $\mu_M$ are some positive constant, and $\mu$ is a smooth function. With assumptions (5.3) and (5.2), we proved in [91] that there is a weak solution $(C_\epsilon^1, C_\epsilon^2, C_\epsilon^3)$ to the initial value problem (2.9), which lies in $BV([0,L]\times[0,T]) \cap \mathcal{C}\Big([0,T], L^1[0,L]\Big)^3$ and is nonnegative. This solution satisfies the following conservation property

$$\frac{\partial}{\partial t}[\, C_\epsilon^1 + C_\epsilon^2 + C_\epsilon^3 \,] + \frac{\partial}{\partial x}[\, C_\epsilon^1 + C_\epsilon^2 - C_\epsilon^3 \,] = 0. \tag{5.4}$$

We denote by $h^{-1}(.,x)$ the inverse of $h$ with respect to its first variable at point $x$.

### 5.1.2 Results

**Notations.** The conservative quantity $\rho$ is defined by

$$\rho(x,t) := 2h(C(x,t),x) + C(x,t), \tag{5.5}$$

and the flux $B$ is defined by

$$B(\rho,t) := 2h(C(x,t),x) - C(x,t). \tag{5.6}$$

**Theorem 5.1.1** (Limit $\varepsilon \to 0$). *The quantity $\rho(x,t)$ is an entropy solution (as defined in [3]) to*

$$\begin{cases} \dfrac{\partial}{\partial t}\rho(x,t) + \dfrac{\partial}{\partial x}B(\rho(x,t),x) = 0, \qquad t>0,\ x\in[0,L], \\ \\ \rho(0,t) = C_0^1 + C_0^2 + h^{-1}(\dfrac{C_0^1+C_0^2}{2},0), \qquad t>0, \\ \\ \rho(x,0) = \rho^0(x), \qquad \rho^0(x) := C^0(x) + 2h(C^0(x),x), \qquad x\in[0,L]. \end{cases} \tag{5.7}$$

**Heuristic on the boundary conditions at $x = 0$.**

The boundary condition at $x = 0$ is the main difficulty in the limit equation. For the two tube case (Chapter 4), we could argue as follows; we had the strong convergence

$$\begin{aligned} &u_\epsilon(x,t) \underset{\epsilon\to 0}{\longrightarrow} h(v(x,t),x), \\ &v_\epsilon(x,t) \underset{\epsilon\to 0}{\longrightarrow} v(x,t), \\ &\overline{\rho}(x,t) = v(x,t) + h(v(x,t),x). \end{aligned}$$

Assume that equilibrium propagates at boundary $x = 0$, we write formally the following equation on quantity $v(0,t)$

$$h(v(0,t),0) = u_0,$$

which gives us $v(0,t) = h^{-1}(u_0,0)$ and thus $\rho(0,t) = u_0 + h^{-1}(u_0,0)$. This is the boundary condition we derived rigorously. Let us try the same argument for the 3-tube case, based on the strong convergence

$$\begin{aligned} &C_\epsilon^1(x,t) \underset{\epsilon\to 0}{\longrightarrow} h(C(x,t),x), \\ &C_\epsilon^2(x,t) \underset{\epsilon\to 0}{\longrightarrow} h(C(x,t),x), \\ &C_\epsilon^3(x,t) \underset{\epsilon\to 0}{\longrightarrow} C(x,t), \\ &\rho(x,t) = C(x,t) + 2h(C(x,t),x). \end{aligned}$$

If we assume again that the propagation of equilibrium reaches the boundary $x = 0$, the formal quantity $C(0,t)$ has to satisfy

$$\begin{cases} h(C(0,t),0) = C_0^1, \\ h(C(0,t),0) = C_0^2. \end{cases}$$

If $C_0^1 \neq C_0^2$, these conditions are contradictory. It means that such a simple analysis does not enable us to determine the boundary conditions in the three tube case, and that the rigorous proof based on the Bardos-Leroux-Nedelec formulation is needed.

**Definition 5.1.2.** *For $p \in \mathbb{R}$, we define uniquely the function $k_p$ as*

$$B(k_p(x), x) = p. \tag{5.8}$$

We define $w_L(t) := \lim_{\varepsilon \longrightarrow 0} C_\varepsilon^1(L,t)$

**Theorem 5.1.3** (Entropic formulation of the boundary conditions)**.** *The function $\rho$ satisfies*

*i) The boundary condition at $x = 0$ :*

*For all $k_p$ such that $k_p(0) + 2h(k_p(0),0) \in I\Big(\rho(0,t), h^{-1}(\frac{C_0^1 + C_0^2}{2}, 0) + C_0^1 + C_0^2\Big)$,*

$$\operatorname{sign}\Big(\rho(0,t) - h^{-1}(\frac{C_0^1 + C_0^2}{2}, 0) - C_0^1 - C_0^2\Big)\Big(B(\rho(0,t),0) - (2h(k_p(0),0) - k_p(0))\Big) \leq 0 \tag{5.9}$$

*ii) The boundary condition at $x = L$ :*

*For all $k_p(L) + 2h(k_p(L),L) \in I\Big(\rho(L,t), 2w_L + h^{-1}(w_L, L)\Big)$,*

$$\operatorname{sign}\Big(\rho(L,t) - 2w_L - h^{-1}(w_L,L)\Big)\Big(B(\rho(L,t),L) - (2h(k_p(L),L) - k_p(L))\Big) \geq 0 \tag{5.10}$$

This theorem is a rigorous formulation of what is stated in Theorem 5.1.1 concerning the boundary conditions. There is no boundary condition to impose at $x = L$, and the boundary condition at $x = 0$ is $\rho(0,t) = C_0^1 + C_0^2 + h^{-1}(\frac{C_0^1 + C_0^2}{2}, 0)$ for $t > 0$. We now sketch the proof and only give details when the techniques are sufficiently different from those of Chapter 4.

## 5.2 Proof rudiments

### 5.2.1 Uniform a priori bounds

In this section we establish uniform a priori bounds with respect to $\varepsilon$.

**Proposition 5.2.1.** *The solution to* (5.1) *satisfies the uniform estimate*

$$\|C_\epsilon^i\|_{L^\infty[0,L]\times[0,T]} \leq K(C_0^1, C_0^2, C^0) \qquad i = 1,2,3, \tag{5.11}$$

*Proof.* Following the same method as in Chapter 4, we first prove $L^\infty$ bound on the time-dependent solution. We introduce the stationary system related to (5.1)

$$\begin{cases} \dfrac{dU^1_\epsilon}{dx}(x) = \dfrac{1}{3\epsilon}\Big[U^2_\epsilon(x) + h(U^3_\epsilon(x),x)) - 2U^1_\epsilon(x)\Big], \\ \dfrac{dU^2_\epsilon}{dx}(x) = \dfrac{1}{3\epsilon}\Big[U^1_\epsilon(x) + h(U^3_\epsilon(x),x)) - 2U^2_\epsilon(x)\Big], \\ -\dfrac{dU^3_\epsilon}{dx}(x) = \dfrac{1}{3\epsilon}\Big[U^1_\epsilon(x) + U^2_\epsilon(x) - 2h(U^3_\epsilon(x),x))\Big], \\ \quad U^1_\epsilon(0) = C^1_0, \qquad U^2_\epsilon(0) = C^2_0, \qquad U^3_\epsilon(L) = U^2_\epsilon(L). \end{cases} \tag{5.12}$$

**Lemma 5.2.2.** *There exists a super solution $(U^1_\epsilon, U^2_\epsilon, U^3_\epsilon)$ of the stationary problem (5.12), and a constant $K > 0$ such that*

$$\|U^i_\epsilon\|_\infty \leq K, \qquad i = 1,2,3. \tag{5.13}$$

*Proof.* We first notice that a solution to

$$\begin{cases} \dfrac{dU^1_\epsilon}{dx}(x) = \dfrac{1}{3\epsilon}\Big[U^2_\epsilon(x) + h(U^3_\epsilon(x),x)) - 2U^1_\epsilon(x)\Big], \\ \dfrac{dU^2_\epsilon}{dx}(x) = \dfrac{1}{3\epsilon}\Big[U^1_\epsilon(x) + h(U^3_\epsilon(x),x)) - 2U^2_\epsilon(x)\Big], \\ -\dfrac{dU^3_\epsilon}{dx}(x) = \dfrac{1}{3\epsilon}\Big[U^1_\epsilon(x) + U^2_\epsilon(x) - 2h(U^3_\epsilon(x),x))\Big], \\ \quad U^1_\epsilon(0) = U^2_\epsilon(0) = C_0 := max(C^1_0, C^2_0), \qquad U^3_\epsilon(L) = U^2_\epsilon(L). \end{cases} \tag{5.14}$$

is a super-solution to (5.12). It remains to find a solution of (5.14) and to prove that it is uniformly bounded in $\epsilon$. It has been proved [91] that (5.14) admits a unique solution (fixed point argument for the existence and contraction for the uniqueness). By symmetry, as the solution is unique, we have $U^1_\epsilon = U^2_\epsilon$. We are left to solve

$$\begin{cases} \dfrac{dU^1_\epsilon}{dx}(x) = \dfrac{1}{3\epsilon}\Big(h(U^3_\epsilon(x),x) - U^1_\epsilon(x)\Big), \\ -\dfrac{dU^3_\epsilon}{dx}(x) = \dfrac{2}{3\epsilon}\Big(U^1_\epsilon(x) - h(U^3_\epsilon(x),x)\Big), \\ \quad U^1_\epsilon(0) = C_0, \qquad U^3_\epsilon(L) = U^1_\epsilon(L). \end{cases} \tag{5.15}$$

By combination of the two lines of (5.15), we obtain a quantity which does not depend on $x$,

$$2U^1_\epsilon(x) - U^3_\epsilon(x) =: K_\epsilon,$$

$$K_\epsilon = 2C_0 - U^3_\epsilon(0) \leq 2C_0, \qquad K_\epsilon = 2U^1_\epsilon(L) - U^3_\epsilon(L) = U^1_\epsilon(L) \geq 0,$$

and thus

$$0 \leq K_\epsilon \leq 2C_0, \qquad U^3_\varepsilon(0) \leq 2C_0 \qquad U^1_\varepsilon(L) \leq C^0.$$

Thus, we just have to prove that $U^1_\epsilon$ is uniformly bounded in $L^\infty$, knowing that $U^1_\epsilon(0)$ and $U^1_\epsilon(L)$ are uniformly bounded in $\mathbb{R}$. For that, we use a maximum principle type argument. Indeed, if $U^1_\epsilon$ reaches its maximal value on the boundary, the result follows. Now, if $U^1_\epsilon$ reaches its maximal value at $x_0 \in ]0, L[$, then,

$$\frac{dU^1_\epsilon}{dx}(x_0) = \frac{1}{3\epsilon}\Big(h(2U^1_\epsilon(x_0) - K_\epsilon, x_0) - U^1_\epsilon(x_0)\Big),$$

and thus

$$U^1_\epsilon(x_0) = h(2U^1_\epsilon(x_0) - K_\epsilon, x_0) \geq 2U^1_\epsilon(x_0) - K_\epsilon$$

then

$$U_\epsilon^1(x_0) \leq K_\epsilon$$

and then Lemma 5.2.2 is proved.

□

We write in the same way

$$\begin{aligned}\int_0^L [(C_\epsilon^1 - U_\epsilon^1)_+ + (C_\epsilon^2 - U_\epsilon^2)_+ + (C_\epsilon^3 - U_\epsilon^3)_+](x,t)dx \\ \leq \int_0^L [(C_\epsilon^1 - U_\epsilon^1)_+ + (C_\epsilon^2 - U_\epsilon^2)_+ + (C_\epsilon^3 - U_\epsilon^3)_+](x,0)dx,\end{aligned} \tag{5.16}$$

which means that if the initial conditions lie under the supersolution, the solution stays below for all time $t$, and proves Proposition 5.11. □.

□

### 5.2.2 Entropies

The entropies we define are similar to those introduced in Chapter 4

**Definition 5.2.3** (A general family of entropies). *A triplet of continuous functions* $(S^1, S^2, S^3)$ *which satisfies*

$$\begin{aligned}&\text{The } S^i(.,x) \text{ are convex and continuous,} \\ &\frac{\partial S^1}{\partial C}(h(C,x),x) = \frac{\partial S^2}{\partial C}(h(C,x),x) = \frac{\partial S^3}{\partial C}(C,x), \\ &\forall \phi \in \mathcal{C}_C^1[0,L], \qquad \sup_v \int_0^L S^i(v,x)\phi'(x)dx \leq K,\end{aligned} \tag{5.17}$$

*is called an entropy for the system* (5.1)

**Definition 5.2.4** (An homogeneous entropy family). *We define* $S : \mathbb{R}^3 \times \mathbb{R} \mapsto \mathbb{R}$, *a continuous function as an homogeneous entropy if it satisfies the conditions of Definition 5.2.3 and if*

$$-\frac{\partial S^1}{\partial x}(h(C,x),x) - \frac{\partial S^2}{\partial x}(h(C,x),x) + \frac{\partial S^3}{\partial x}(C,x) = 0, \qquad \forall C \in \mathbb{R} \tag{5.18}$$

**Proposition 5.2.5.** *For a general family of entropies, the following dissipation law holds*

$$\begin{aligned}\frac{\partial}{\partial t}[\, S^1(C_\epsilon^1,x) + S^2(C_\epsilon^2,x) + S^3(C_\epsilon^3,x)\,] + \frac{\partial}{\partial x}[\, S^1(C_\epsilon^1,x) + S^2(C_\epsilon^2,x) - S^3(C_\epsilon^3,x)\,] \\ \leq \frac{\partial S^1}{\partial x}(C_\epsilon^1,x) + \frac{\partial S^2}{\partial x}(C_\epsilon^2,x) - \frac{\partial S^3}{\partial x}(C_\epsilon^3,x).\end{aligned} \tag{5.19}$$

From the entropy dissipation, we immediately conclude the following proposition

**Proposition 5.2.6.** *We have the convergences*

$$C_\epsilon^1 - h(C_\epsilon^3,x) \underset{\epsilon \longrightarrow 0}{\longrightarrow} 0, \qquad C_\epsilon^2 - h(C_\epsilon^3,x) \underset{\epsilon \longrightarrow 0}{\longrightarrow} 0, \qquad L^2\Big([0,L]\times[0,T]\Big). \tag{5.20}$$

### 5.2.3 Strong convergence

In this section, we settle for our estimates and we prove that the convergence of $C_\epsilon^3$ to its limit is strong enough to obtain an entropic formulation at the limit. As it is classical, we did not detail this part in Chapter 4. In order to have a self-contained work, we detail here the method for the three tube case.

**Proposition 5.2.7.** *There exists* $C \in L^\infty\Big([0,L]\times[0,T]\Big)$ *such that*

$$C_\epsilon^1 \underset{\epsilon\longrightarrow 0}{\longrightarrow} h(C,x), \qquad C_\epsilon^2 \underset{\epsilon\longrightarrow 0}{\longrightarrow} h(C,x), \qquad C_\epsilon^3 \underset{\epsilon\longrightarrow 0}{\longrightarrow} C, \qquad L^2,\ a.e., \tag{5.21}$$

From the $L^\infty$ estimates (and the Banach-Alaoglu-Bourbaki theorem [11]), we have

**Lemma 5.2.8.** *There exists* $\overline{C}^i, \overline{h}, \overline{S}$ *and* $\overline{S^i}, i=1,2$ *such that after extraction of a subsequence,*

$$C_\epsilon^i \underset{\epsilon\longrightarrow 0}{\rightharpoonup} \overline{C}^i, \qquad h(C_\epsilon^3,x) \underset{\epsilon\longrightarrow 0}{\rightharpoonup} \overline{h}, \qquad S^i(h(C_\epsilon^3,x),x) \underset{\epsilon\longrightarrow 0}{\rightharpoonup} \overline{S^i}, \qquad S^3(C_\epsilon^3,x) \underset{\epsilon\longrightarrow 0}{\rightharpoonup} \overline{S}, \qquad L^\infty - w*. \tag{5.22}$$

We call $\nu_{x,t}$ the Young measure associated with the sequence $(C_\epsilon^3)_\epsilon$ at $(x,t)$ [5, 16, 86]. When no confusion can be made, we merely write $\nu = \nu_{x,t}$. We have, for every continuous function $\alpha$,

$$\alpha(C_\epsilon^3) \rightharpoonup \overline{\alpha} = \int_{\mathbb{R}} \alpha(\xi) d\nu(\xi) =: < \nu, \alpha > . \tag{5.23}$$

In particular, we write

$$\begin{aligned}
\overline{C^3} &=< \nu, \xi >= \int_{\mathbb{R}} \xi d\nu(\xi),\\
\overline{h} &=< \nu, h(\xi,x) >= \int_{\mathbb{R}} h(\xi,x) d\nu(\xi),\\
\overline{S} &=< \nu, S^3(\xi,x) >= \int_{\mathbb{R}} S^3(\xi,x) d\nu(\xi),\\
\overline{S^i} &:=< \nu, S^i(h(\xi,x),x) >= \int_{\mathbb{R}} S^i(h(\xi,x),x) d\nu(\xi), \qquad i=1,2.
\end{aligned} \tag{5.24}$$

Next we prove that for all $(x,t)$, $\nu_{x,t}$ reduces to a Dirac mass $\delta_{\xi=A}$. Then, we have

$$\overline{C}^3(x,t) = \int_{\mathbb{R}} \xi \delta_{\xi=A},$$

therefore, for all $(x,t) \in [0,L]\times\mathbb{R}$

$$\nu_{x,t} = \delta_{\xi=\overline{C}^3(x,t)} \tag{5.25}$$

and so

$$\begin{aligned}
&\overline{h}(x,t) = \int_{\mathbb{R}} h(x,\xi)\delta_{\xi=\overline{C}^3(x,t)} = h(\overline{C^3}(x,t),x),\\
&\overline{S} = S^3(\overline{C^3}(x,t),x).
\end{aligned} \tag{5.26}$$

**Lemma 5.2.9.** *The* $L^\infty$ *weak limits satisfy*

$$\overline{C^3\Big[S^2(h(C^3,x)) + S^1(h(C^3,x))\Big]} - \overline{C^3S^2 + S^1} = 2\overline{h(C^3,x)S^3(C^3,x)} - 2\overline{h}\ \overline{S} \qquad L^\infty - w*. \tag{5.27}$$

**Lemma 5.2.10.** *The Young measure $\nu_{x,t}$ associated with the sequence $(C^3_\epsilon(x,t))_\epsilon$ reduces to a Dirac mass for all $(x,t)$.*

**First step : Proof of Lemma 5.2.9**

*Proof.* We use the div-curl lemma [87] to prove Lemma 5.2.9. We define

$$\begin{aligned} U_\epsilon &= \Big(C^3_\epsilon + 2h(C^3_\epsilon,x), 2h(C^3_\epsilon,x) - C^3_\epsilon\Big) \\ V_\epsilon &= \Big(S^1(h(C^3_\epsilon,x),x) + S^2(h(C^3_\epsilon,x),x) - S^3(C^3_\epsilon,x), \\ &\quad - S^1(h(C^3_\epsilon,x),x) - S^2(h(C^3_\epsilon,x),x) - S^3(C^3_\epsilon,x)\Big) \end{aligned} \tag{5.28}$$

We recall that for $(a,b) : \mathbb{R}^2 \mapsto \mathbb{R}^2$,

$$\operatorname{div}(a,b) = \frac{\partial a}{\partial t} + \frac{\partial b}{\partial x}, \qquad \operatorname{curl}(a,b) \quad = \frac{\partial a}{\partial x} - \frac{\partial b}{\partial t}. \tag{5.29}$$

We now define

$$S_\epsilon = \operatorname{div}(U_\epsilon), \qquad T_\epsilon = \operatorname{curl}(V_\epsilon). \tag{5.30}$$

Their expression are given by

$$\begin{aligned} S_\epsilon &= \frac{\partial}{\partial t}\Big[C^3_\epsilon + 2h(C^3_\epsilon,x)\Big] + \frac{\partial}{\partial x}\Big[2h(C^3_\epsilon,x) - C^3_\epsilon\Big], \\ T_\epsilon &= \frac{\partial}{\partial t}\Big[S^1(h(C^3_\epsilon,x),x) + S^2(h(C^3_\epsilon,x),x) + S^3(C^3_\epsilon,x)\Big] \\ &\quad + \frac{\partial}{\partial x}\Big[S^1(h(C^3_\epsilon,x),x) + S^2(h(C^3_\epsilon,x),x) - S^3(C^3_\epsilon,x)\Big]. \end{aligned} \tag{5.31}$$

For the hypotheses of the div-curl lemma [64] to be satisfied, , we are left to prove that $S_\epsilon$ and $T_\epsilon$ lie in a compact of $H^{-1}\Big([0,L]\times[0,T]\Big)$. It is sufficient to prove this property for $T_\epsilon$ because $S_\epsilon$ is equal to $T_\epsilon$ with the choice of the specific entropies $S^1(C,x) = S^2(C,x) = S^3(C,x) = C$. We expand $T_\epsilon$ as follows

$$T_\epsilon = \mu_\epsilon + w_\epsilon + z_\epsilon \tag{5.32}$$

with

$$\begin{aligned} \mu_\epsilon &= \frac{\partial}{\partial t}\Big[S^1(C^1_\epsilon,x) + S^2(C^2_\epsilon,x) + S^3(C^3_\epsilon,x)\Big] + \frac{\partial}{\partial x}\Big[S^1(C^1_\epsilon,x) + S^2(C^2_\epsilon,x) - S^3(C^3_\epsilon,x)\Big], \\ w_\epsilon &= \frac{\partial}{\partial t}\Big[S^1(h(C^3_\epsilon,x)) - S^1(C^1_\epsilon,x)\Big] + \frac{\partial}{\partial x}\Big[S^1(h(C^3_\epsilon,x)) - S^1(C^1_\epsilon,x)\Big], \\ z_\epsilon &= \frac{\partial}{\partial t}\Big[S^2(h(C^3_\epsilon,x)) - S^2(C^2_\epsilon,x)\Big] + \frac{\partial}{\partial x}\Big[S^2(h(C^3_\epsilon,x)) - S^2(C^2_\epsilon,x)\Big]. \end{aligned}$$

(5.33)

We have,

$$C^1_\epsilon - h(C^3_\epsilon,x) \underset{\epsilon\longrightarrow 0}{\longrightarrow} 0, \qquad L^2\Big([0,L]\times[0,T]\Big),$$

then, as $S^1$ is continuous,

$$S^1(C^2_\epsilon) - S^1(h(C^3_\epsilon,x)) \underset{\epsilon\longrightarrow 0}{\longrightarrow} 0, \qquad L^2\Big([0,L]\times[0,T]\Big).$$

As $\frac{\partial}{\partial t}$ and $\frac{\partial}{\partial x}$ are continuous from $L^2$ to $H^{-1}$, then,

$$w_\epsilon \underset{\epsilon \longrightarrow 0}{\longrightarrow} 0, \qquad H^{-1}\Big([0,L]\times[0,T]\Big). \tag{5.34}$$

A fortiori, $w_\epsilon$ (and with the same argument $z_\epsilon$) lie in a compact of $H^{-1}\Big([0,L]\times[0,T]\Big)$.

Since $(x,t) \mapsto S^i(C^i_\varepsilon(x,t),x) \in BV\Big([0,L]\times[0,T]\Big)$, then, $(x,t) \mapsto \frac{\partial}{\partial t}S^i(C^i_\varepsilon(x,t),x)$ and $(x,t) \mapsto \frac{\partial}{\partial t}S^i(C^i_\varepsilon(x,t),x)$ are Radon measures. We cannot bound each of these quantities separately from the other, because it would mean that we can find uniform $BV$ estimates on the $C^i_\varepsilon$, which is not the case. We use the following equality

$$\begin{aligned}
\frac{\partial}{\partial t}[\, S^1(C^1_\epsilon,x)+S^2(C^2_\epsilon,x)+S^3(C^3_\epsilon,x)\,]+\frac{\partial}{\partial x}[\, S^1(C^1_\epsilon,x)+S^2(C^2_\epsilon,x)-S^3(C^3_\epsilon,x)\,] \\
=\frac{1}{3\epsilon}\Big[\Big(\frac{\partial S^1}{\partial C}(C^1_\epsilon,x)-\frac{\partial S^1}{\partial C}(C^2_\epsilon,x)\Big)\Big(C^2_\epsilon-C^1_\epsilon\Big) \\
+\Big(\frac{\partial S^1}{\partial C}(C^1_\epsilon,x)-\frac{\partial S^1}{\partial C}(h(C^3_\epsilon,x),x)\Big)\Big(h(C^3_\epsilon,x)-C^1_\epsilon\Big) \\
+\Big(\frac{\partial S^1}{\partial C}(C^2_\epsilon,x)-\frac{\partial S^1}{\partial C}(h(C^3_\epsilon,x)\Big)\Big(h(C^3_\epsilon,x)-C^2_\epsilon\Big)\Big] \\
+\frac{\partial S^1}{\partial x}(C^1_\epsilon,x)+\frac{\partial S^2}{\partial x}(C^2_\epsilon,x)-\frac{\partial S^3}{\partial x}(C^3_\epsilon,x).
\end{aligned} \tag{5.35}$$

Thanks to the assumption on the $x$ derivative of $S^i$, $\frac{\partial S^1}{\partial x}(C^1_\epsilon,x)+\frac{\partial S^2}{\partial x}(C^2_\epsilon,x)-\frac{\partial S^3}{\partial x}(C^3_\epsilon,x)$ is bounded in $\mathcal{M}^\infty[0,L]\times[0,T]$. The other term of the right hand side of equality (5.35) is a non-positive measure. then $\mu_\varepsilon$ is uniformly bounded in $W^{-1,\infty}_{loc}$, thanks to Murat's lemma [86], it is compact in $H^{-1}\Big([0,L]\times[0,T]\Big)$. We conclude that $\operatorname{div}(U_\epsilon)$ and $\operatorname{curl}(V_\epsilon)$ lie in a compact of $H^{-1}\Big([0,L]\times[0,T]\Big)$. We can now apply the div-curl lemma

$$U_\epsilon.V_\epsilon \rightharpoonup U.V \qquad L^\infty - w*, \tag{5.36}$$

which is the result announced. □ □

**Second step: Proof of Lemma 5.2.10**

*Proof.* We consider $\nu_{x,t}$ the Young measure associated with the sequence $\Big(C_\epsilon(x,t)\Big)_\epsilon$. We write

$$<\nu,(\xi-\overline{C}^3(x,t))\Big[S^1(h(\xi,x),x)+S^2(h(\xi,x),x)\Big]-2\Big[h(\xi,x)-\overline{h(C^3(x,t),x)}\Big]\overline{S}\xi>=0 \tag{5.37}$$

We introduce the following Kruzkov-like entropies

$$\begin{aligned}
S^1(C,x)&=|C-h(k,x)|,\\
S^2(C,x)&=|C-h(k,x)|,\\
S^3(C,x)&=|C-k|
\end{aligned} \tag{5.38}$$

with $k$ a real parameter

Clearly, $(S^1,S^2,S^3)$ is an entropy in the sense of definition 5.2.3. Indeed, they are convex and continuous with respect to their first variable and using assumption (5.3)

$$\frac{\partial S^1}{\partial x}(h(C,x),x)=\frac{\partial h}{\partial x}(h(C,x),x)\operatorname{sign}(C-h(x),x)\le K. \tag{5.39}$$

Equality (5.37) thus becomes

$$< \nu, (\xi - \overline{C^3}(x))2|h(\xi,x) - h(\overline{C^3}(x),x)| - 2\Big[h(\xi,x) - \overline{h(C^3(x),x)}\Big]|\xi - \overline{C^3}(x)| >= 0, \quad (5.40)$$

$h$ is non increasing, then,

$$< \nu, 2|\xi - \overline{C}^3(x)|(h(\xi,x) - h(\overline{C^3}(x),x)) - 2\Big[h(\xi,x) - \overline{h(C^3(x),x)}\Big]|\xi - \overline{C^3}(x)| >= 0, \quad (5.41)$$

thus,

$$2\Big(h(\overline{C^3}(x),x) - \overline{h(C^3(x),x)}\Big) < \nu, |\xi - \overline{C^3}(x)| >= 0. \quad (5.42)$$

If $h$ is non-affine on any sub-interval, this implies thanks to Jensen strict inequality

$$< \nu, |\xi - \overline{C^3}(x)| >= 0, \quad (5.43)$$

and then

$$supp(\nu) = \{\xi | \xi - \overline{C^3(x)} = 0\}$$

thus

$$\nu_{x,t} = \delta_{\overline{C^3}(x,t)}. \quad (5.44)$$

For all $x$, the Young measure associated with the sequence $C^3_\epsilon(x)$ is a Dirac mass. We conclude that for all $\alpha$ continuous,

$$\alpha(C^3_\epsilon) \underset{\epsilon \longrightarrow 0}{\longrightarrow} \alpha(\overline{C^3}), \qquad L^p, 1 \leq p < \infty, \ a.e.$$

We end the proof of Proposition 5.2.7 by using Proposition 5.2.6. □

# Chapter 6

# An asymptotic targeting scheme

*We develop a class of asymptotic preserving schemes for the system we study in Chapter 4. The asymptotic preserving schemes obtained thanks to a splitting method give rise to a boundary layer at the neighborhood of $x = L$. Based on well balanced schemes methods, we build an asymptotic preserving scheme which becomes an upwind scheme at the limit.*

## 6.1 Introduction

### 6.1.1 The continuous problem

We consider the following hyperbolic relaxation system. For $t \geq 0$ and $x \in [0, L]$ :

$$\begin{cases} \dfrac{\partial u_\epsilon}{\partial t}(x,t) + \dfrac{\partial u_\epsilon}{\partial x}(x,t) = \dfrac{1}{\epsilon}\Big[h(v_\epsilon(x,t)) - u_\epsilon(x,t)\Big], \\ \dfrac{\partial v_\epsilon}{\partial t}(x,t) - \dfrac{\partial v_\epsilon}{\partial x}(x,t) = \dfrac{1}{\epsilon}\Big[u_\epsilon(x,t) - h(v_\epsilon(x,t))\Big], \\ u_\epsilon(0,t) = u_0, \qquad v_\epsilon(L,t) = \alpha u_\epsilon(L,t), \qquad \alpha \in (0,1), \\ u_\varepsilon(x,0) = u^0(x), \qquad v_\varepsilon(x,0) = v^0(x), \qquad u^0, v^0 \in W^{1,1}[0,L] \end{cases} \tag{6.1}$$

where $\varepsilon$ is the relaxation parameter and $h$ is a non linear function which satisfies

$$h(0) = 0, \qquad 1 < \beta \leq h'(v) \leq \mu, \qquad h \text{ is not affine on any sub-interval}, \tag{6.2}$$

where $\alpha$, $\beta$ and $\mu$ positive constants.

As proved in Chapter 4, under assumptions (6.2), the solution $(u_\varepsilon, v_\varepsilon)$ to (6.1) converges to $(u, v)$ solution to

$$\begin{cases} \dfrac{\partial}{\partial t}\Big(v + h(v)\Big)(x,t) + \dfrac{\partial}{\partial x}\Big(h(v) - v\Big) = 0, \qquad t > 0,\ x \in [0,L], \\ v(0,t) = h^{-1}(u_0), \qquad t > 0, \\ v(x,0) = v^0(x), \qquad x \in [0,L], \end{cases} \tag{6.3}$$

and

$$u = h(v). \tag{6.4}$$

The mathematical study of the system (6.1) and its convergence toward (6.3) are performed in Chapter 4.

### 6.1.2 An asymptotic preserving scheme compatible with the boundary conditions

An asymptotic preserving scheme is defined as a stable, in the sense that its CFL condition is independant of $\varepsilon$, and consistent numerical scheme $(S_\varepsilon)$ for the system (6.1) which converges as $\varepsilon$ goes to zero to a numerical scheme $(S)$ for systems (6.3),(6.4).

Several AP have been proposed [20] [21], and we also proposed one in Chapitre 4, based on a splitting method. We notice that the limit scheme $(S)$ we obtain is diffusive, and generates a boundary layer at $x = L$ due to the boundary conditions $v_\epsilon(L,t) = \alpha u_\epsilon(L,t)$ which are not at equilibrium. We wish to build an asymptotic preserving scheme which enables us to get rid of the boundary layer, as it has no real meaning in the limit $\varepsilon = 0$. To this purpose, we build here a numerical scheme which becomes an upwind scheme when $\varepsilon = 0$. When considering the conservative law

$$\frac{\partial z}{\partial t} + \frac{\partial z}{\partial x} f(z) = 0$$

and in the case wher $f'(z) > 0$, $\forall z$, we define an explicit upwind scheme as a scheme which can be written

$$z_k^{n+1} = z_k^n + \frac{\Delta t}{\Delta x}\Big(g_{k+\frac{1}{2}} - g_{k-\frac{1}{2}}\Big),$$

where $g_{k+\frac{1}{2}}$ only depends on $z_k^n$ (and not on $z_{k+1}^n$). This work fits into the more general problem of building AP schemes with constraint on the limit scheme $(S)$. In [8], the authors developed a method to make optional the choice of the numerical scheme in the asymptotic regime $\varepsilon$ tends to zero. They provide a Riemann solver coming from a well balanced Godunov scheme, by choosing a clever way to approximates the source term, which concentrates on the interfaces. We build here an AP scheme by a specific choice of correction terms. At the limit, we do not obtain the standard upwind scheme. It could be done, but it would require to invert a function. The drawback our method is that we then have to analyze the scheme properties by hand, whereas properties of stability or convergence are automatically given with the construction used in [8], as their scheme can be seen as a convex combination of well-known schemes. The advantage is that we obtain a larger class of AP schemes, parametrized by a real value $b$, and that we do not have to invert a function. We consider a class of schemes under the form

$$\begin{cases} u_k^{n+1} = u_k^n - \dfrac{\Delta t}{\Delta x}\Big[u_k^n - u_{k-1}^n\Big] + \dfrac{\Delta t}{\varepsilon + \Delta x} S^u(u^n, v^n), \\ v_k^{n+1} = v_k^n - \dfrac{\Delta t}{\Delta x}\Big[-v_{k+1}^n + v_k^n\Big] - \dfrac{\Delta t}{\varepsilon + \Delta x} S^v(u^n, v^n), \end{cases} \tag{6.5}$$

where $S^u$ and $S^v$ are two discretizations of the source term. We point out that the term

$$\frac{\Delta t}{\varepsilon + \Delta x} \tag{6.6}$$

behaves like $\dfrac{\Delta t}{\varepsilon}$ when $\Delta x$ goes to zero, and like $\dfrac{\Delta t}{\Delta x}$ when $\varepsilon$ goes to zero. We impose both the scheme to be consistent with the system (6.1) and to become an upwind scheme when $\varepsilon = 0$. Our two constraints are written as

i) $S^u$ and $S^v$ are consistent with $h(v) - u$,

ii) $u_k^n - u_{k-1}^n + v_k^n - v_{k+1}^n - S^u + S^v = h(v_k^n) - v_k^n - (h(v_{k-1}^n) - v_{k-1}^n)$.

We restrict ourselves to linear schemes with a 3 point stencil

$$\begin{cases} S^u = h(v_{k-1}^n) - u_{k-1}^n - a v_{k+1}^n + b v_k^n - c v_{k-1}^n, \\ S^v = h(v_k^n) - u_k^n + (1-a) v_{k+1}^n + (b-2) v_k^n + (1-c) v_{k-1}^n, \end{cases} \tag{6.7}$$

where $a, b, c$ are real numbers. Stability constraints on the scheme impose constraints on $a, b, c$.

## 6.2 Results

In the context of the finite volume schemes framework, we consider a mesh of $N$ disjoint cells. Let $\Delta x$ be the size of each cell and $\Delta t$ the size of the time step. The final time is denoted by $T$, and the number of iterations is denoted by $n_f$, so that $n_f \Delta t = T$.

**Proposition 6.2.1.** *In the class* (6.5), (6.7) *of numerical asymptotic preserving schemes* $(S_\varepsilon)$ *whose limiting scheme* $(S)$ *coincide with the upwind scheme, the scheme which are stable in* $L^\infty \cap BV$ *and those where* $a$, $b$ *and* $c$ *are constant which satisfy*

$$a = 0, \qquad b = c, \qquad 1 \leq b, \tag{6.8}$$

*and thus are written*

$$\begin{cases} \dfrac{u_k^{n+1} - u_k^n}{\Delta t} + \dfrac{u_k^n - u_{k-1}^n}{\Delta x} = \dfrac{1}{\varepsilon + \Delta x}\Big(h(v_{k-1}^n) - u_{k-1}^n + b v_k^n - b v_{k-1}^n\Big), \\ \dfrac{v_k^{n+1} - v_k^n}{\Delta t} + \dfrac{v_k^n - v_{k+1}^n}{\Delta x} = -\dfrac{1}{\varepsilon + \Delta x}\Big(h(v_k^n) - u_k^n + v_{k+1}^n + (b-2) v_k^n + (1-b) v_{k-1}^n\Big), \\ u_0^n = u_0, \qquad v_0^n = h^{-1}(u_0), \qquad v_{N+1}^n = \alpha u_N^n. \end{cases} \tag{6.9}$$

### 6.2.1 Stability of the scheme

**Proposition 6.2.2** (Conservation, Monotony and Positivity). *Let* $\left(u_k^n, v_k^n\right)_{k\in[0,N],n\geq 0}$ *denote the finite volume approximation solution defined by* (6.8),(6.9).

*i) The quantity* $u_k^n + v_k^n$ *is conserved, which means that there exists a numerical flux* $G$ *such that*

$$u_k^{n+1} + v_k^{n+1} = u_k^n + v_k^n - \frac{\Delta t}{\Delta x}(G_{k+\frac{1}{2}}^n - G_{k-\frac{1}{2}}^n).$$

*Under the Courant-Friedrichs-Levy condition*

$$\Delta t \leq \frac{\Delta x}{\mu - 1 + b}, \tag{6.10}$$

*ii) the scheme is monotone, which means that we can write*

$$\begin{cases} u_k^{n+1} = G(u_{k-1}^n, u_k^n, u_{k+1}^n, v_{k-1}^n, v_k^n, v_{k+1}^n) \\ v_k^{n+1} = H(u_{k-1}^n, u_k^n, u_{k+1}^n, v_{k-1}^n, v_k^n, v_{k+1}^n), \end{cases}$$

*where* $G$ *and* $H$ *are non-decreasing functions with respect to each of their variables,*

*iii) and the scheme preserves positivity :*

$$\text{If } \forall k \in [1,N], \qquad u_k^0 \geq 0, v_k^0 \geq 0, \qquad \text{then} \qquad \forall n \geq 0, \forall k \geq 0, \qquad u_k^n \geq 0, \qquad v_k^n \geq 0. \tag{6.11}$$

**Proposition 6.2.3** ($L^\infty$ estimate). *Under the CFL condition* (6.10), *there exists two vectors* $U(\varepsilon) \in \mathbb{R}^n, V(\varepsilon) \in \mathbb{R}^n$ *depending on* $\varepsilon$, *such that*

$$\forall n \geq 0, \forall k \geq 0, \qquad u_k^n \leq U_k(\varepsilon), \qquad v_k^n \leq V_k(\varepsilon).$$

**Proposition 6.2.4** ($BV$ estimate). *We define*

$$|u^n|_{BV} = \sum_{k=1}^{N-1} |u_{k+1}^n - u_k^n|, \qquad |v^n|_{BV} = \sum_{k=1}^{N} |v_{k+1}^n - v_k^n|.$$

*Under the CFL condition* (6.10), *there exists* $K(\varepsilon)$ *such that*

$$|u^n|_{BV} + |v^n|_{BV} \leq K(\varepsilon).$$

### 6.2.2 Relaxation toward the equilibrium

We denote here by $\left(u_k^n, v_k^n\right)_{k\in[0,N],n\geq 0}$ the finite volume approximation solution defined by (6.8), (6.9) for $\varepsilon = \mathbf{0}$. As it could be ambiguous, we point out that in the previous sections, we denoted the same manner the solution defined by (6.8), (6.9) for all $\varepsilon > 0$. In this part, we made the following assumption

$$\sum_{k=1}^{N-1} |v_{k+1}^n - v_k^n| \leq K, \qquad \text{where } K \text{ does not depend on } \Delta x. \tag{6.12}$$

**Lemma 6.2.5.** *Under the assumption* (6.12)*, we have*

$$\|u_k^n - h(v_k^n)\|_{L^1} \underset{\Delta x \longrightarrow 0}{\longrightarrow} 0 \tag{6.13}$$

Our main result is the

**Proposition 6.2.6.** *Under the assumption* (6.12)*, for* $\varepsilon = 0$*, the scheme we obtain on* $\rho_k^n := u_k^n + v_k^n$ *is*

## 6.3 Proofs

### 6.3.1 Monotony and positivity

We prove here Proposition 6.2.2. We first write the scheme under the following conservative form

$$\begin{aligned}
u_k^{n+1} = u_k^n - \frac{\Delta t}{\Delta x}\Big[u_k^n - u_k^{n-1} + \frac{\Delta x}{2(\Delta x+\varepsilon)}\Big((h(v_k^n) - u_k^n + v_{k+1}^n - v_k^n) - (h(v_{k-1}^n) - u_{k-1}^n + v_k^n - v_{k-1}^n)\Big)\Big] \\
+ \frac{\Delta x}{2(\Delta x+\varepsilon)}\Big[h(v_k^n) + h(v_{k-1}^n) - (u_k^n + u_{k-1}^n) + (2b-2)v_k^n + v_{k+1}^n + (1-2b)v_{k-1}^n\Big], \\
v_k^{n+1} = v_k^n - \frac{\Delta t}{\Delta x}\Big[v_k^n - v_k^{n+1} + \frac{\Delta x}{2(\Delta x+\varepsilon)}\Big((h(v_k^n) - u_k^n + v_{k+1}^n - v_k^n) - (h(v_{k-1}^n) - u_{k-1}^n + v_k^n - v_{k-1}^n)\Big)\Big] \\
- \frac{\Delta x}{2(\Delta x+\varepsilon)}\Big[h(v_k^n) + h(v_{k-1}^n) - (u_k^n + u_{k-1}^n) + (2b-2)v_k^n + v_{k+1}^n + (1-2b)v_{k-1}^n\Big],
\end{aligned}$$

so that the quantity $u_k^n + v_k^n$ appears in a conservative way. To prove the monotony, we write the scheme under the form

$$\begin{aligned}
u_k^{n+1} &= \Big[1 - \frac{\Delta t}{\Delta x}\Big]u_k^n + \Big[\frac{\Delta t}{\Delta x} - \frac{\Delta t}{\Delta x+\varepsilon}\Big]u_{k-1}^n + \frac{\Delta t}{\Delta x+\varepsilon}\Big[h(v_{k-1}^n) - bv_{k-1}^n\Big] \\
&\quad + b\frac{\Delta t}{\Delta x+\varepsilon}v_k^n := G, \\
v_k^{n+1} &= \Big[1 - \frac{\Delta t}{\Delta x} + \frac{(2-b)\Delta t}{\Delta x+\varepsilon}\Big]v_k^n + \Big[\frac{\Delta t}{\Delta x} - \frac{\Delta t}{\Delta x+\varepsilon}\Big]v_{k+1}^n - \frac{\Delta t}{\Delta x+\varepsilon}h(v_k^n) + \frac{\Delta t}{\Delta x+\varepsilon}u_k^n \\
&\quad + (b-1)\frac{\Delta t}{\Delta x+\varepsilon}v_{k-1}^n := H.
\end{aligned} \tag{6.14}$$

To guarantee the monotony of the scheme, we state that the derivatives of $G$ and $H$ with respect to each of their variables are nonnegative under the CFL condition. The only derivative whose positivity is not obvious is

$$\begin{aligned}
\frac{\partial H(u_{k-1}^n, u_k^n, u_{k+1}^n, v_{k-1}^n, v_k^n, v_{k+1}^n)}{\partial v_k^n} &= \frac{\partial}{\partial v_k^n}\Big[1 - \frac{\Delta t}{\Delta x} + (2-b)\frac{\Delta t}{\Delta x+\varepsilon}\Big]v_k^n - \frac{\Delta t}{\Delta x+\varepsilon}h(v_k^n) \\
&\geq \Big[1 - \frac{\Delta t}{\Delta x} + (2-b)\frac{\Delta t}{\Delta x+\varepsilon} - \mu\frac{\Delta t}{\Delta x+\varepsilon}\Big]v_k^n \\
&\geq \Big[1 - \frac{\Delta t}{\Delta x}(\mu - 1 + b)\Big]v_k^n \\
&\geq 0 \qquad \text{as soon as } \Big[1 - \frac{\Delta t}{\Delta x}(\mu - 1 + b)\Big] \geq 0.
\end{aligned}$$

We notice that $G(0,0,0,0,0,0) = H(0,0,0,0,0,0) = 0$, and the positivity follows from the monotony.

### 6.3.2 The $L^\infty$ stability

We want to prove uniform $L^\infty$ estimates with respect to $\Delta t, \Delta x$ on the solution of the numerical schemes.

**Lemma 6.3.1.** *For all $M > u_0$, there exists a pair of vectors $(U, V)$ of size $N$ which depend on $\varepsilon$ such that*

$$\begin{cases} U_k - U_{k-1} \geq \dfrac{\Delta x}{\Delta x + \varepsilon}\Big[h(V_{k-1}) - U_{k-1} + bV_k - bV_{k-1}\Big], \\ V_k - V_{k+1} \geq \dfrac{\Delta x}{\Delta x + \varepsilon}\Big[ - h(V_k) + U_k - V_{k+1} + (2-b)V_k + (b-1)V_{k-1}\Big], \\ \qquad U_0 \geq u_0, \qquad V_0 = h^{-1}(u_0), \qquad V_{N+1} \geq \alpha U_N. \end{cases} \tag{6.15}$$

*and*

$$\inf_{k\in[0,N]} U_k > M, \qquad \inf_{k\in[0,N]} V_k > M.$$

The last condition expresses that $(U, V)$ can be chosen as large as desired, in particular larger than the initial state.

We assume the existence of $(U, V)$ as defined in Lemma 6.3.1 with $M \geq \sup_{k\in[1,N]} u_k^0$ and $M \geq \sup_{k\in[1,N]} v_k^0$. We state that

$$\forall n \geq 0, \forall k \in [1, N], \qquad u_k^n \leq U_k, \qquad v_k^n \leq V_k. \tag{6.16}$$

Indeed, if for a given $n$, $u_k^n \leq U_k$ and $v_k^n \leq V_k$, then, using the monotony of the scheme, we have

$$\begin{cases} u_k^{n+1} = G(u_{k-1}^n, u_k^n, u_{k+1}^n, v_{k-1}^n, v_k^n, v_{k+1}^n) \leq G(U_{k-1}, U_k, U_{k+1}, V_{k-1}, V_k, V_{k+1}) \\ v_k^{n+1} = H(u_{k-1}^n, u_k^n, u_{k+1}^n, v_{k-1}^n, v_k^n, v_{k+1}^n) \leq H(U_{k-1}, U_k, U_{k+1}, V_{k-1}, V_k, V_{k+1}). \end{cases} \tag{6.17}$$

We write $G$ and $H$ under the form

$$\begin{cases} G(U_{k-1}, U_k, U_{k+1}, V_{k-1}, V_k, V_{k+1}) = U_k - \dfrac{\Delta t}{\Delta x}\Big(U_k - U_{k-1} - \dfrac{\Delta x}{\Delta x + \varepsilon}\Big[h(V_{k-1}) - U_{k-1} + bV_k - bV_{k-1}\Big]\Big) \\ H(U_{k-1}, U_k, U_{k+1}, V_{k-1}, V_k, V_{k+1}) = V_k - \dfrac{\Delta t}{\Delta x}\Big(V_k - V_{k+1} \\ \qquad\qquad - \dfrac{\Delta x}{\Delta x + \varepsilon}\Big[ - h(V_k) + U_k - V_{k+1} + (2-b)V_k + (b-1)V_{k-1}\Big]\Big). \end{cases}$$

That implies, according to (6.15)

$$\begin{cases} G(U_{k-1}, U_k, U_{k+1}, V_{k-1}, V_k, V_{k+1}) \leq U_k \\ H(U_{k-1}, U_k, U_{k+1}, V_{k-1}, V_k, V_{k+1}) \leq V_k, \end{cases}$$

which combined with (6.17) leads to

$$u^{n+1} \leq U, \qquad v^{n+1} \leq V,$$

and the $L^\infty$ bound follows by induction. We now prove Lemma 6.3.1.

We are looking for two vectors $U$, $V$ which satisfy (6.15). We claim that it is sufficient to find $U, V$ such that

**Lemma 6.3.2.** *There exists a couple of vectors $(U, V)$ satisfying*

$$\begin{cases} U_k - U_{k-1} = \dfrac{\Delta x}{\Delta x + \varepsilon}\Big[h(V_{k-1}) - U_{k-1} + bV_k - bV_{k-1}\Big], \\ V_k - V_{k+1} = \dfrac{\Delta x}{\Delta x + \varepsilon}\Big[-h(V_k) + U_k - V_{k+1} + (2-b)V_k + (b-1)V_{k-1}\Big], \\ \qquad U_0 \geq u_0, \qquad V_{N+1} \geq \alpha U_N, \end{cases} \tag{6.18}$$

*are they are given by the formula*

$$\begin{cases} U_k = V_k + (b-1)\dfrac{\Delta x}{\Delta x + \varepsilon}\Big(V_k - V_{k-1}\Big) + K(\varepsilon, \Delta x), \qquad k = 1..N, \\ V_k = V_{k-1} + \dfrac{\Delta x}{\varepsilon}\Big(h(V_{k-1}) - V_{k-1}\Big) - \dfrac{\Delta x}{\varepsilon}K(\varepsilon, \Delta x) + (b-1)\dfrac{\Delta x}{\varepsilon}\dfrac{2\Delta x + \varepsilon}{\Delta x + \varepsilon}\Big(V_{k-1} - V_{k-2}\Big), \end{cases} \tag{6.19}$$

*where*

$$V_1 > V_0 > u_0, \qquad 0 < K(\varepsilon, \Delta x) \leq \min\Big((\beta - 1)V_0, \frac{1-\alpha}{\alpha}V_0\Big). \tag{6.20}$$

*Proof.* We denote by $U$ and $V$ the vectors described by (6.19) and (6.20).
**Vectors $U$ and $V$ satisfy (6.18).**

We have, by replacing $K(\varepsilon, \Delta x)$ by its value given by the first line of (6.19),

$$\begin{aligned} V_k = V_{k-1} + \frac{\Delta x}{\varepsilon}\Big(h(V_{k-1}) - V_{k-1}\Big) - \frac{\Delta x}{\varepsilon}\Big(U_k - V_k - (b-1)\frac{\Delta x}{\Delta x + \varepsilon}\Big(V_k - V_{k-1}\Big)\Big) \\ + (b-1)\frac{\Delta x}{\varepsilon}\frac{2\Delta x + \varepsilon}{\Delta x + \varepsilon}\Big(V_{k-1} - V_{k-2}\Big) \end{aligned}$$

We multiply the upper line by $1 - \dfrac{\Delta x}{\Delta x + \varepsilon} = \dfrac{\varepsilon}{\Delta x + \varepsilon}$ and we obtain

$$\begin{aligned} \Big(1 - \frac{\Delta x}{\Delta x + \varepsilon}\Big)V_k = \Big(1 - \frac{\Delta x}{\Delta x + \varepsilon}\Big)V_{k-1} + \frac{\Delta x}{\Delta x + \varepsilon}\Big(h(V_{k-1} - V_{k-1} - U_{k-1} + V_{k-1}\Big) \\ + (b-1)\Big[\frac{\Delta x(2\Delta x + \varepsilon)}{(\Delta x + \varepsilon)^2} - \frac{(\Delta x)^2}{(\Delta x + \varepsilon)^2}\Big]\Big(V_{k-1} - V_{k-2}\Big) \end{aligned}$$

thus

$$V_k = V_{k-1} + \frac{\Delta x}{\Delta x + \varepsilon}\Big(h(V_{k-1}) - V_{k-1} - U_{k-1} - V_k + V_{k-1} - \frac{b-1}{\Delta x + \varepsilon}\Big(V_{k-1} - V_{k-2}\Big)\Big)$$

which proves the second line of (6.18). According to the second line of (6.19), $U$ satisfy

$$U_k - U_{k-1} = V_k - V_{k-1} + (b-1)\frac{\Delta x}{\Delta x + \varepsilon}\Big(V_k - (2-b)V_{k-1} - (b-1)V_{k-2}\Big),$$

which is, using the expression of $V$

$$\begin{aligned} U_k - U_{k-1} = \frac{\Delta x}{\varepsilon}\Big(h(V_{k-1}) - U_{k-1} + V_k - (2-b)V_{k-1} - (b-1)V_{k-2}\Big) \\ + (b-1)\frac{\Delta x}{\Delta x + \varepsilon}\Big(V_k - (2-b)V_{k-1} - (b-1)V_{k-2}\Big), \end{aligned}$$

and then

$$U_k - U_{k-1} = \frac{\Delta x}{\Delta x + \varepsilon}\Big[h(V_{k-1}) - U_{k-1} + bV_k - bV_{k-1}\Big].$$

**Positivity of $U$ and $V$**

From assumption (6.20), we deduce that

$$V_2 > \frac{\Delta x}{\varepsilon}\Big(h(V_1) - V_1\Big) - \frac{\Delta x}{\varepsilon}K(\varepsilon, \Delta x),$$

and then

$$V_2 > \frac{\Delta x}{\varepsilon}(\beta - 1)V_1 - \frac{\Delta x}{\varepsilon}K(\varepsilon, \Delta x)$$

which implies $V_2 > 0$ thanks to the assumption on $K(\varepsilon, \Delta x)$. Reasonning the same way for all $k$, we prove that $V_k > V_{k-1}$ and $V_k > 0,\ k = 0..N$, and then we conclude that $U_k > 0,\ k = 0..N$. The fact that the sequence $(V_k)_k$ is increasing gives us that

$$0 < K(\varepsilon, \Delta x) \leq \min\Big((\beta - 1)V_k, \frac{1-\alpha}{\alpha}V_k\Big), \qquad k = 0..N. \tag{6.21}$$

**The boundary conditions** We first compute

$$\begin{aligned} V_{N+1} - \alpha V_N = (1-\alpha)V_N + \frac{\Delta x}{\varepsilon}\Big(h(V_N) - V_N - K(\varepsilon, \Delta x)\Big) + (b-1)\frac{\Delta x}{\Delta x + \varepsilon}(\frac{2\Delta x + \varepsilon}{\varepsilon} - \alpha) \\ - \alpha K(\varepsilon, \Delta x), \end{aligned}$$

then

$$V_{N+1} - \alpha V_N > \frac{\Delta x}{\varepsilon}\Big(h(V_N) - V_N - K(\varepsilon, \Delta x)\Big) - \alpha K(\varepsilon, \Delta x),$$

and $thus V_{N+1} > \alpha V_N$ as soon as $\frac{1-\alpha}{\alpha}V_0 < \frac{1-\alpha}{\alpha}V_0$, which is (6.21).

The expression of $U_k$ gives us immediately that

$$U_0 > V_0 > u_0.$$

□

### 6.3.3 The BV estimates

We start with a preliminary lemma.

**Lemma 6.3.3.** *For all $n > 0$, there are two constants $(C_\varepsilon, D_\varepsilon)$ uniformly bounded in $(\Delta t, \Delta x)$ such that*

$$\|u^n\|_{BV} + \|v^n\|_{BV} \leq \Big(1 + C_\varepsilon\Big)^n\Big[\|u^0\|_{BV} + \|v^0\|_{BV}\Big] + \frac{D_\varepsilon}{C_\varepsilon}\Big(1 - (1 + C_\varepsilon \Delta t)^n\Big).$$

*Proof.* Using the numerical scheme (6.9), we first state that

$$\begin{aligned} &\sum_{k=0}^{N-1} |u_{k+1}^{n+1} - u_k^{n+1}| + \sum_{k=0}^{N} |v_{k+1}^{n+1} - v_k^{n+1}| \\ &= \sum_{k=1}^{N-1} \Big|(1 - \frac{\Delta t}{\Delta x})(u_{k+1}^n - u_k^n) + (\frac{\Delta t}{\Delta x} - \frac{\Delta t}{\Delta x + \varepsilon})(u_k^n - u_{k-1}^n) \\ &+ \frac{\Delta t}{\Delta x + \varepsilon}\Big[h(v_k^n) - h(v_{k-1}^n) - b(v_k^n - v_{k-1}^n)\Big] + \frac{b\Delta t}{\Delta x + \varepsilon}(v_{k+1}^n - v_k^n)\Big| \\ &+ \sum_{k=1}^{N-1} \Big|(1 - \frac{\Delta t}{\Delta x} + (2-b)\frac{\Delta t}{\Delta x + \varepsilon})(v_{k+1}^n - v_k^n) \\ &+ (\frac{\Delta t}{\Delta x} - \frac{\Delta t}{\Delta x + \varepsilon})(v_{k+2}^n - v_{k+1}^n) - \frac{\Delta t}{\Delta x + \varepsilon}(h(v_{k+1}^n) - h(v_k^n)) \\ &\qquad + \frac{\Delta t}{\Delta x + \varepsilon}(u_{k+1}^n - u_k^n) + (b-1)\frac{\Delta t}{\Delta x + \varepsilon}(v_k^n - v_{k-1}^n)\Big| \\ &\qquad + \Big|u_1^{n+1} - u_0\Big| + \Big|v_1^{n+1} - v_0\Big| \qquad + \qquad |v_{N+1}^{n+1} - v_N^{n+1}|. \end{aligned}$$

We split the three terms of the sum. We denote by $A$ the term corresponding to $k$ going from 1 to $N-1$ and we treat separately the terms corresponding to $k=0$ and to $k=N$. We use assumption (6.2) and the positivity under the CFL condition to obtain

$$\begin{aligned}A \leq &\sum_{k=1}^{N-1}(1-\frac{\Delta t}{\Delta x}+\frac{\Delta t}{\Delta x+\varepsilon})|u_{k+1}^n-u_k^n|+\sum_{k=0}^{N-2}(\frac{\Delta t}{\Delta x}-\frac{\Delta t}{\Delta x+\varepsilon})|u_{k+1}^n-u_k^n|\\&+\sum_{k=1}^{N-1}(1-\frac{\Delta t}{\Delta x}+(2-\beta)\frac{\Delta t}{\Delta x+\varepsilon})|v_{k+1}^n-v_k^n|\\&+\sum_{k=0}^{N-2}(\mu-1)\frac{\Delta t}{\Delta x+\varepsilon}|v_{k+1}^n-v_k^n|+\sum_{k=2}^{N}(\frac{\Delta t}{\Delta x}-\frac{\Delta t}{\Delta x+\varepsilon})|v_{k+1}^n-v_k^n|.\end{aligned}$$

We obtain our first estimate

$$\begin{aligned}A \leq &\Big(1+(\mu+1-\beta)\frac{\Delta t}{\Delta x+\varepsilon}\Big)\sum_{k=2}^{N-2}\Big[|u_{k+1}^n-u_k^n|+|v_{k+1}^n-v_k^n|\Big]\\&+|u_2^n-u_1^n|+|(1-\frac{\Delta t}{\Delta x}+(\mu+1-\beta)\frac{\Delta t}{\Delta x+\varepsilon})|v_2^n-v_1^n|\\&+(1-\frac{\Delta t}{\Delta x}+\frac{\Delta t}{\Delta x+\varepsilon})|u_N^n-u_{N-1}^n|+(1+(1-\beta)\frac{\Delta t}{\Delta x+\varepsilon})|v_N^n-v_{N-1}^n|\\&+(\frac{\Delta t}{\Delta x}-\frac{\Delta t}{\Delta x+\varepsilon})|u_1^n-u_0|+(\mu-1)\frac{\Delta t}{\Delta x+\varepsilon}|v_1^n-v_0|\\&+(\frac{\Delta t}{\Delta x}-\frac{\Delta t}{\Delta x+\varepsilon})|\alpha u_N^n-v_N^n|.\end{aligned}\tag{6.22}$$

The term corresponding to $k=0$ is treated in the following way

$$\begin{aligned}|u_1^{n+1}-u_0|+|v_1^{n+1}-v_0| =&\Big|(1-\frac{\Delta t}{\Delta x})u_1^n+(\frac{\Delta t}{\Delta x}-\frac{\Delta t}{\Delta x+\varepsilon})u_0+\frac{\Delta t}{\Delta x+\varepsilon}\Big[h(v_0)-bv_0\Big]\\&+\frac{b\Delta t}{\Delta x+\varepsilon}v_1^n-u_0\Big|\\&+\Big|(1-\frac{\Delta t}{\Delta x}+(2-b)\frac{\Delta t}{\Delta x+\varepsilon})v_1^n+(\frac{\Delta t}{\Delta x}-\frac{\Delta t}{\Delta x+\varepsilon})v_2^n-\frac{\Delta t}{\Delta x+\varepsilon}h(v_1^n)\\&+\frac{\Delta t}{\Delta x+\varepsilon}u_1^n+(b-1)\frac{\Delta t}{\Delta x+\varepsilon}v_0-v_0\Big|,\end{aligned}$$

we now use the equality $u_0=h(v_0)$, we obtain

$$\begin{aligned}|u_1^{n+1}-u_0|+|v_1^{n+1}-v_0| \leq &\Big|(1-\frac{\Delta t}{\Delta x})(u_1^n-u_0)+\frac{\Delta t}{\Delta x+\varepsilon}(v_1^n-v_0)\Big|\\&+\Big|(\frac{\Delta t}{\Delta x}-\frac{\Delta t}{\Delta x+\varepsilon})(v_2^n-v_1^n)+(1-\frac{\Delta t}{\Delta x+\varepsilon}+(2-b)\frac{\Delta t}{\Delta x+\varepsilon})(v_1^n-v_0)\\&-\frac{\Delta t}{\Delta x+\varepsilon}(h(v_1^n)-h(v_0))+\frac{\Delta t}{\Delta x+\varepsilon}(u_1^n-u_0)\Big|.\end{aligned}$$

Using estimate (6.2) again and rearranging the terms

$$\begin{aligned}|u_1^{n+1}-u_0|+|v_1^{n+1}-v_0| \leq &(1-\frac{\Delta t}{\Delta x}+\frac{\Delta t}{\Delta x+\varepsilon})|u_1^n-u_0|+(\frac{\Delta t}{\Delta x}-\frac{\Delta t}{\Delta x+\varepsilon})|v_2^n-v_1^n|\\&+(1+(2-b-\beta)\frac{\Delta t}{\Delta x+\varepsilon})|v_1^n-v_0|.\end{aligned}\tag{6.23}$$

The term $k=N$ is treated as

$$|v_{N+1}^{n+1}-v_N^{n+1}|=|\alpha u_N^{n+1}-v_N^{n+1}|,$$

then, using the scheme (6.9),

$$\begin{aligned}|v_{N+1}^{n+1}-v_N^{n+1}| = \Big|&\alpha(1-\frac{\Delta t}{\Delta x})u_N^n+\alpha(\frac{\Delta t}{\Delta x}-\frac{\Delta t}{\Delta x+\varepsilon})u_{N-1}^n+\alpha\frac{\Delta t}{\Delta x+\varepsilon}\Big[h(v_{N-1}^n)-bv_{N-1}^n\Big]\\&+\alpha\frac{b\Delta t}{\Delta x+\varepsilon}v_N^n-(1-\frac{\Delta t}{\Delta x}+(2-b)\frac{\Delta t}{\Delta x+\varepsilon})v_N^n-\alpha(\frac{\Delta t}{\Delta x}-\frac{\Delta t}{\Delta x+\varepsilon})u_N^n\\&+\frac{\Delta t}{\Delta x+\varepsilon}h(v_N^n)-\frac{\Delta t}{\Delta x+\varepsilon}u_N^n-(b-1)\frac{\Delta t}{\Delta x+\varepsilon}v_{N-1}^n\Big|,\end{aligned}$$

by rearranging the terms

$$\begin{aligned}|v_{N+1}^{n+1}-v_N^{n+1}| =\Big|&(1-\frac{\Delta t}{\Delta x}-\frac{\Delta t}{\alpha(\Delta x+\varepsilon)})\alpha u_N^n+\alpha(\frac{\Delta t}{\Delta x}-\frac{\Delta t}{\Delta x+\varepsilon})(u_{N-1}^n-u_N^n)\\&-(1-\frac{\Delta t}{\Delta x}-\frac{\Delta t}{\alpha(\Delta x+\varepsilon)})v_N^n\\&+\frac{\Delta t}{\Delta x+\varepsilon}\Big[(-b-\alpha b-1)v_{N-1}^n+\alpha h(v_{N-1}^n)+(\alpha b+b-2+\frac{1}{\alpha}v_N^n+h(v_N^n)\Big]\Big|.\end{aligned}$$

From the boundary condition, we may replace $\alpha u_N^n$ by $v_{N+1}^n$ to get

$$|v_{N+1}^{n+1}-v_N^{n+1}| \le (1-\frac{\Delta t}{\Delta x}-\frac{\Delta t}{\alpha(\Delta x+\varepsilon)})\alpha|v_{N+1}^n-v_N^n|+\alpha(\frac{\Delta t}{\Delta x}-\frac{\Delta t}{\Delta x+\varepsilon})|u_{N-1}^n-u_N^n|+D_\varepsilon, \tag{6.24}$$

with

$$D_\varepsilon = \max_{\Delta t,\Delta x}\frac{\Delta t}{\Delta x+\varepsilon}\Big[(-b-\alpha b-1)v_{N-1}^n+\alpha h(v_{N-1}^n)+(\alpha b+b-2+\frac{1}{\alpha})v_N^n+h(v_N^n)\Big]. \tag{6.25}$$

According to proposition 6.2.3, $D_\varepsilon$ is a constant which is uniformly bounded in $(\Delta t,\Delta x)$.

We combine now (6.22), (6.23) and (6.24) and obtain

$$\sum_{k=0}^{N-1}|u_{k+1}^{n+1}-u_k^{n+1}|+\sum_{k=0}^{N}|v_{k+1}^{n+1}-v_k^{n+1}| \le (1+C_\varepsilon\Delta t)\Big[\sum_{k=0}^{N-1}|u_{k+1}^n-u_k^n|+\sum_{k=0}^{N}|v_{k+1}^n-v_k^n|\Big]+D_\varepsilon, \tag{6.26}$$

with

$$C_\varepsilon = \frac{\mu+1-\beta}{\Delta x+\varepsilon}, \tag{6.27}$$

which ends the proof of Lemma 6.3.3. □

From (6.26) we obtain

$$|u^{n+1}|_{BV}+|v^{n+1}|_{BV} \le \Big(1+C_\varepsilon\Delta t\Big)^n\Big[|u^n|_{BV}+|v^n|_{BV}\Big]+\frac{D_\varepsilon}{C_\varepsilon}\Big(1-(1+C_\varepsilon\Delta t)^n\Big). \tag{6.28}$$

We notice that

$$(1+C_\varepsilon\Delta t)^n = \exp(n\log(1+C_\varepsilon\Delta t)) = \exp(C_\varepsilon T)+o(1),$$

and then Proposition 6.2.4 is proved.

## 6.4 Proof of the relaxation toward equilibrium

We prove Lemma 6.2.5.
We define

$$e_k^n = |u_k^n - h(v_k^n)|. \tag{6.29}$$

We compute

$$e_k^{n+1} = \Big|u_k^{n+1} - h(v_k^{n+1})\Big| = \Big|\Big(1 - \frac{\Delta t}{\Delta x}\Big)u_k^n + \frac{\Delta t}{\Delta x}\Big(h(v_{k-1}^n) + b(v_k^n - v_{k-1}^n)\Big) - h(v_k^{n+1})\Big|,$$

which we can write

$$e_k^{n+1} = \Big|\Big(1 - \frac{\Delta t}{\Delta x}\Big)\Big(u_k^n - h(v_k^n)\Big) + \frac{\Delta t}{\Delta x}\Big(h(v_{k-1}^n) - h(v_k^n)\Big) + b\frac{\Delta t}{\Delta x}\Big(v_k^n - v_{k-1}^n\Big) + \Big(h(v_k^n) - h(v_k^{n+1})\Big)\Big|.$$

Hence

$$e_k^{n+1} \le \Big(1 - \frac{\Delta t}{\Delta x}\Big)e_k^n + \frac{\Delta t}{\Delta x}(b-\beta)\Big|v_k^n - v_{k-1}^n\Big| + \mu\Big|v_k^{n+1} - v_k^n\Big|,$$

and then

$$e_k^{n+1} \le \Big(1 - \frac{\Delta t}{\Delta x}\Big)e_k^n + \frac{\Delta t}{\Delta x}(b-\beta)\Big|v_k^n - v_{k-1}^n\Big| + \mu(b-1)\frac{\Delta t}{\Delta x}\Big|v_k^n - v_{k-1}^n\Big| + \mu\frac{\Delta t}{\Delta x}\Big|h(v_k^n) - u_k^n\Big|.$$

We multiply by $\Delta x$ and we sum over $k \in [1, N]$ to obtain

$$\|e_k^{n+1}\|_1 \le \Big(1 - \frac{\Delta t}{\Delta x}\Big)\|e_k^n\|_1 + \text{Cste}\Delta t|v^n|_{BV}.$$

Under assumption (6.12) which guarantees that $|v^n|_{BV}$ is uniformly bounded by $K$ with $\Delta x$, and thus,

$$\|e_k^{n+1}\|_1 \le \Big(1 - \frac{\Delta t}{\Delta x}\Big)\frac{T}{\Delta t}\Big(\|e_k^0\|_1 - (1 - \frac{\Delta t}{\Delta x})\Big) + K\Delta t,$$

which proves Lemma 6.2.5.

## 6.5 Numerical illustrations

For the numerical illustrations, as in Chapter 4, we choose

$$h(v) = 2\frac{v}{1+v} + 2v, \qquad \alpha = \frac{1}{2},$$

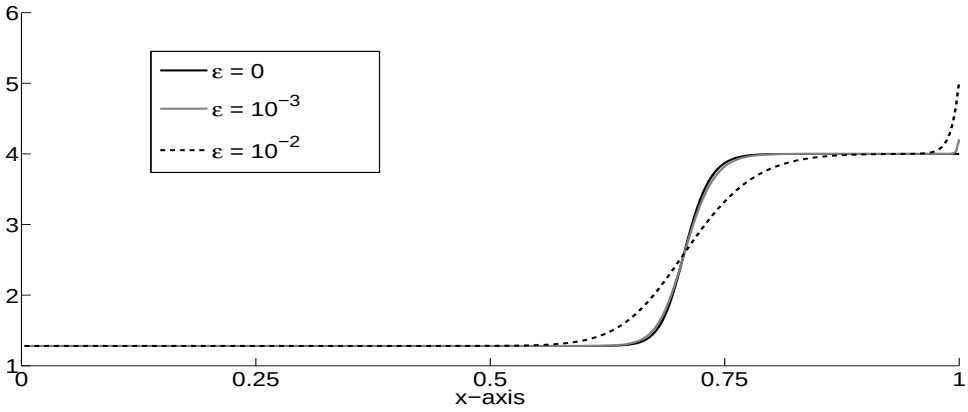


**Figure 6.1:** We plot $u_\varepsilon + v_\varepsilon$ solution to (6.1) for $L = 1$, taken at $t = 1.5$, using the numerical scheme (6.9), for $\varepsilon = 10^{-3}$, $\varepsilon = 10^{-2}$ and $\varepsilon = 0$. We notice that the boundary layer tends to vanish as $\varepsilon \longrightarrow 0$.

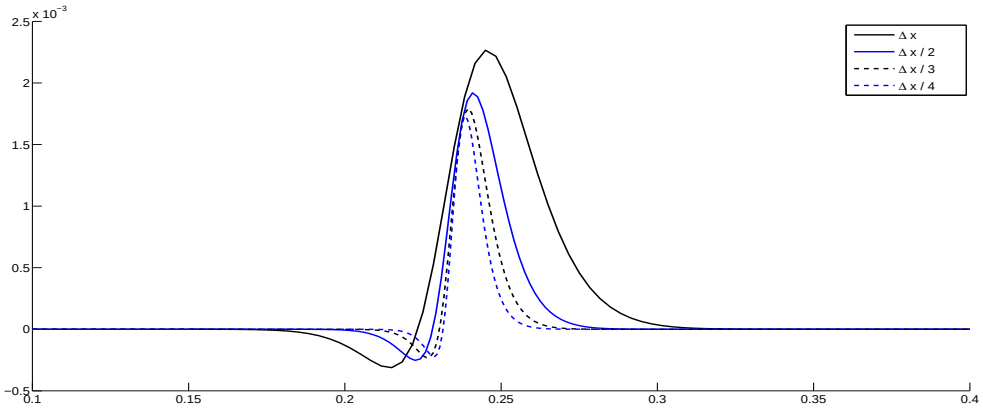


**Figure 6.2:** The error to equilibrium $u - h(v)$ for $(u_\varepsilon, v_\varepsilon)$ solution to (6.1) for $L = 1$ taken at time $t = 0.5$, zoomed on $x \in [0.1, 0.4]$, U scheme (6.9) with $\varepsilon = 0$. The three curves correspond to different values of $\Delta x$.

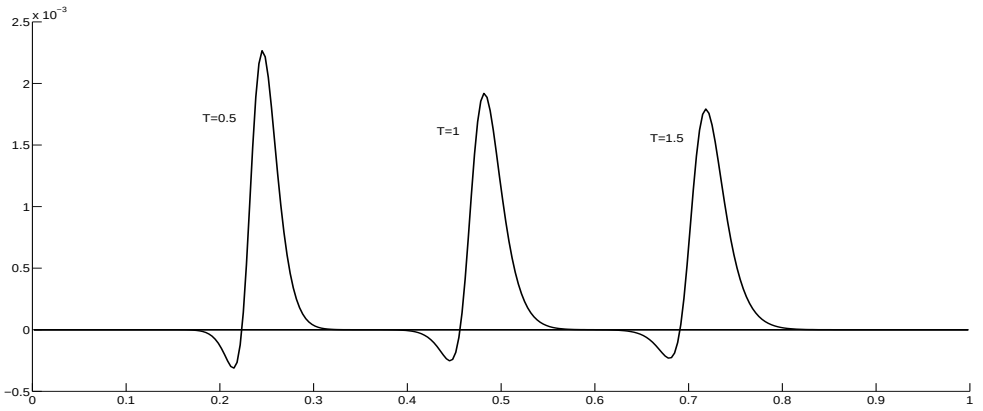


**Figure 6.3:** The error to equilibrium $u - h(v)$ for $(u_\varepsilon, v_\varepsilon)$ solution to (6.1) using the numerical scheme (6.9) with $\varepsilon = 0$. The three curves correspond to different time values $t$.

# Part II

# A more realistic model

# Chapter 7

# Description of the model

This chapter is inspired from the first part of the paper

M. Tournus, N. Seguin, B. Perthame, S.R. Thomas, and A. Edwards. A Model of Calcium Transport along the Rat Nephron. *Accepted in the American Journal of Physiology*, 2013.

*We developed a mathematical model of calcium ($Ca^{2+}$) transport along the rat nephron to investigate the factors that promote hypercalciuria. The model is an extension of the flat medullary model of Hervy and Thomas (Am J Physiol Renal Physiol 284: F65-F81, 2003). It explicitly represents all the nephron segments beyond the proximal tubules, and distinguishes between superficial and deep nephrons. It is a set of dynamic conservation equations to determine NaCl, urea, and $Ca^{2+}$ concentration profiles in tubules, vasa recta, and the interstitium.*

## Introduction

In this chapter, we describe precisely the model we study and from which we draw conclusions. It is a model of a rat kidney. The conclusions we draw from that model are at least as far from the reality as the model is far from the real kidney. We also introduce in this part some specific vocabulary, in order to have a common language with biologists and nephrologists. We recall that what drives our interest is the prediction of calcium reabsorption rates along the nephron, and calcium concentration profiles in vasa recta, tubules and the interstitum.

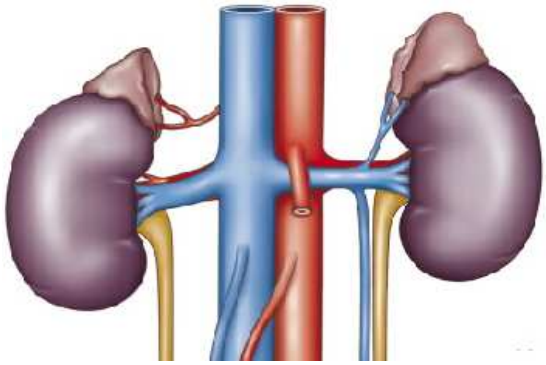

**Figure 7.1:** Representation of the two kidneys of one individual. This picture is taken from [35].

## 7.1 Physical representation

### 7.1.1 The renal architecture

We distinguish two domains in the kidney : the cortex and the medulla.

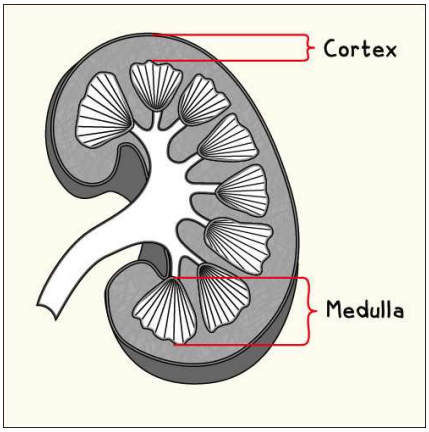


**Figure 7.2:** The cortex and and the medulla are two domains of the kidney.

The renal medulla is divided into the outer medulla (OM) and the inner medulla (IM), as illustrated in Figure 7.3. The outer medulla itself consists of an outer stripe (OS) and an inner stripe (IS). The inner medulla is also subdivided into an upper part (UIM) and lower part (LIM). Whereas the cortical interstitium is taken to be everywhere isosmotic with plasma, solute concentrations in the renal medullary interstitium vary along the cortico-medullary axis (which is the $x$-axis).

Our model of tubular and vascular transport takes into account the different tubes in the medulla and in the cortex. It first contains the descending and ascending vasa recta (DVR and AVR), which are blood vessels. Blood arrives to the descending vasa recta from the renal artery

(in red on Figure 7.1 ), it flows in the descending vasa recta and is finally evacuated by the renal vein (in blue in Figure 7.1). The model also includes nephron segments, including the descending limbs (DL) and the ascending limbs (AL) which constitute the loop of Henle, and the collecting ducts (CD). All of these tubes are immersed in a common interstitium. This is a 1-D model, which means that all physical quantities depend only on the depth $x$ and on the tube. In contrast with the HT model which specifies steady state boundary conditions at the inlet of the outer medullary collecting duct (OMCD) as an algebraic function of the outlet of the medullary thick ascending limb, we explicitly represent the cortical distal tubules that connect the medullary thick ascending limb (mTAL) outlet to the OMCD inlet. The four cortical segments include the cortical thick ascending limb (cTAL), the distal convoluted tubule (DCT), the connecting tubule (CNT) and the cortical collecting duct (CCD). The cortical segments are immersed in the cortex. The cortex is taken to be an infinite medium. The concentration of each solute in the cortex is equal to the concentration entering the vasa recta. We also distinguish between long and short limbs: the short ones do not penetrate into the inner medulla. As depicted in Figure 7.3, the short-looped nephrons have a longer cTAL and a shorter CNT, relative to the long loops. We assume that short- and long-looped nephrons (hereafter referred to as short and long nephrons) connect at the CCD entrance.

To simplify the notation, tubes (i.e., tubules and vasa recta) are numbered as follows in the medulla: 1= DVR, 2= AVR, 3= long DL (or LDL), 4= long AL (or LAL), 5 = short DL (or SDL), 6 = short AL (or SAL), 7= CD. In addition, the superscript "d" and "int" respectively denote the cortical distal tubules and the interstitium. The physical properties (e.g., permeability and radius) of a given class of tubules or vasa recta are identical, and may vary with depth. Finally, the model explicitly represents 3 solutes, NaCl (denoted "Na"), urea ("U"), and $Ca^{2+}$ ("Ca").

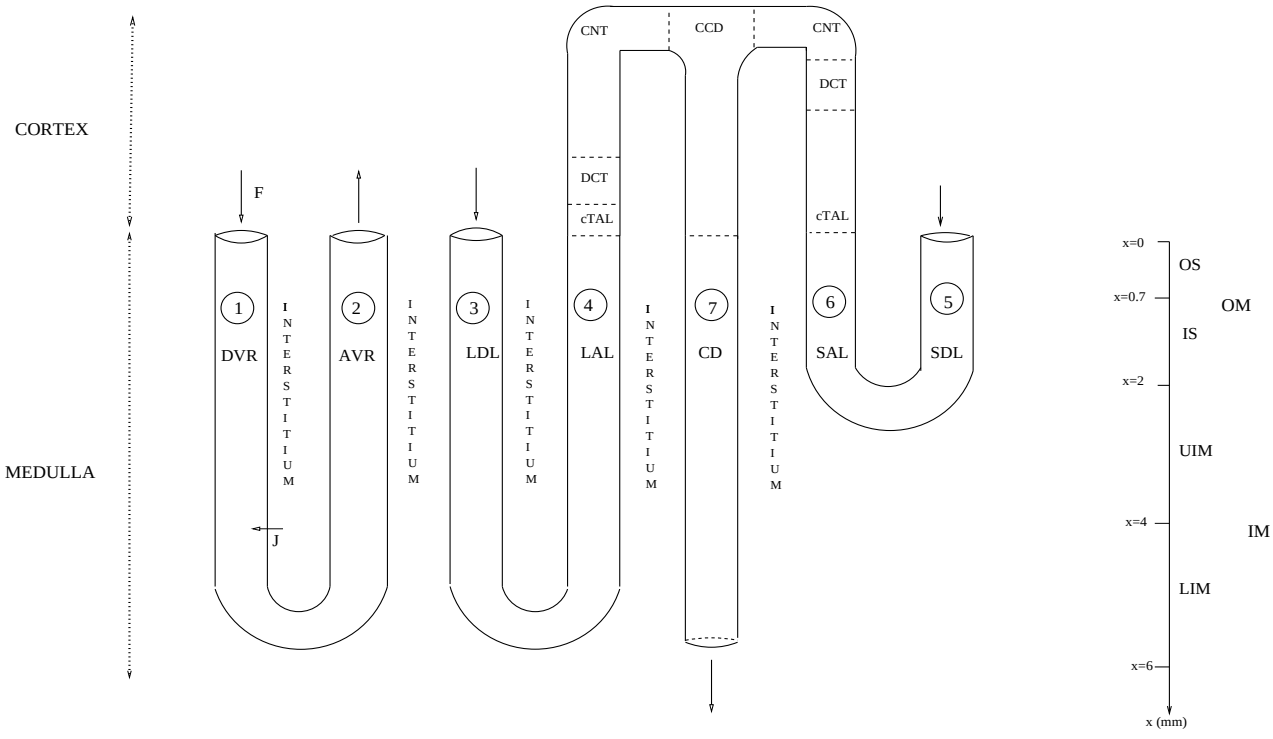


**Figure 7.3:** Model representation of the renal architecture

### 7.1.2 Number and length of vessels and tubules

The loops of Henle and vasa recta turn back at varying distances from the cortex as depicted in Figure 7.3. Let $N^j(x)$ denote the total number of tubes of type $j$ at depth $x$; $L$ denotes

the total length of the medulla (6 mm). The abscissa $x_{OS/IS}$ (0.7 mm) and $x_{OM/IM}$ (2 mm) respectively represent the spatial coordinate at the boundary between the outer and inner stripe, and between the outer and inner medulla. The DCT and CCD are taken to be 0.7 and 3.0 mm long, respectively. As noted above, the length of the cTAL and CNT varies between short- and long-looped nephrons. These segments are taken to be, respectively, 2.5 and 1.0 mm long in short nehrons, and 0.5 and 3.0 mm long in long nephrons. The combined length of the cTAL, DCT, and CNT (denoted $L_{CTDC}$) is therefore equal to 4.2 mm in both short and long nephrons. We denote by $y_L$ the spatial coordinate at the boundary between the cTAL and DCT in long nephrons, by $y_S$ that in short nephrons, and by $L_d$ the total length of the cortical distal tubules (7.2 mm). These values correspond to rat values.

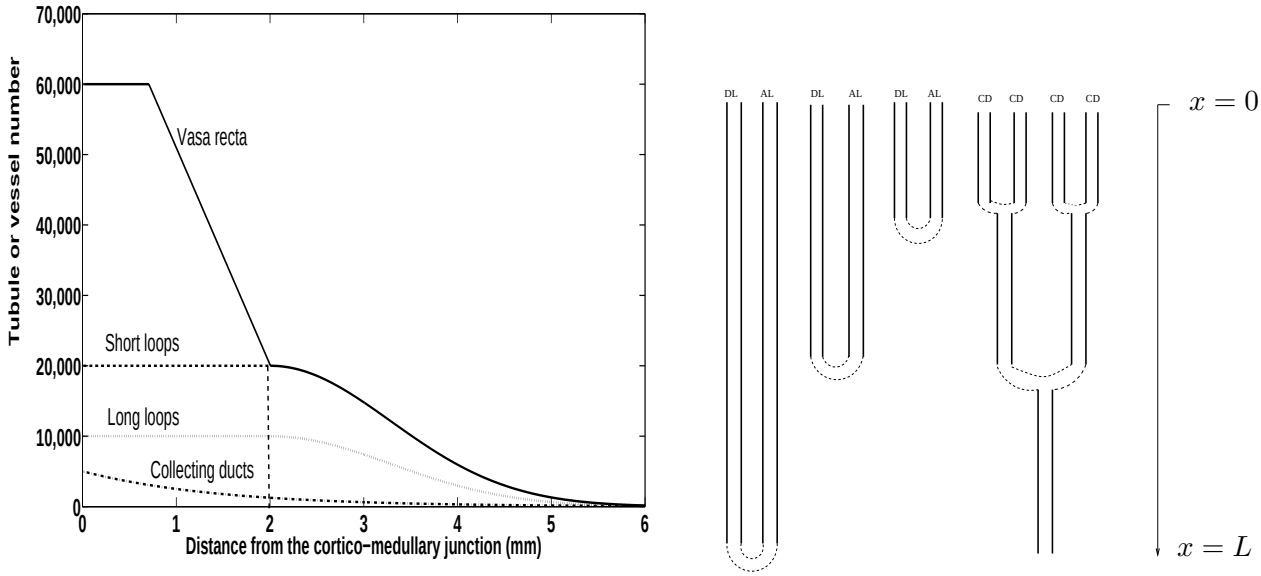


**Figure 7.4:** The left-side panel represents the number of descending vasa recta ($N^1$), descending loops of Henle (short and long) ($N^5$and $N^3$), and collecting ducts ($N^7$) as a function of depth. As an illustration, we draw on the right-side panel a representation of tubules and vessels of varying length. The architecture of tubes 3 and 4 (DL and AL) is the same as that of tubes 1 and 2 (DVR and AVR) and the architecture of distal tubules is similar to that of collecting ducts.

We now describe the number of tubules as a function of depth. The total number of nephrons is taken as 30 000. These parameter values are not fundamental for understanding the rest of this chapter and the next chapter.

**Vessels.**

The number of long descending vasa recta ($N_L^1$) is taken to decrease exponentially in the IM:

$$\begin{aligned} N_L^1(x) &= 20\,000 && 0 \le x \le x_{OM/IM}, \\ N_L^1(x) &= 20\,000\ \exp(-k^1(x - x_{OM/IM})) && x_{OM/IM} \le x. \end{aligned}$$

The number of short descending vasa recta ($N_S^1$) is taken to be constant in the OS and to linearly decrease in the IS

$$\begin{aligned} N_S^1(x) &= 40\,000 \qquad 0 \le x \le x_{OS/IS} \\ N_S^1(x) &= 40\,000 \times \Big[1 - \frac{x - x_{OS/IS}}{x_{OM/IM} - x_{OS/IS}}\Big] \qquad x_{OS/IS} \le x \le x_{OM/IM}. \end{aligned}$$

Note that by continuity, the number of ascending vasa recta (or loops of Henle) at a given level is equal to that of descending vasa recta (or loops of Henle) at that level.

**Loops of Henle.**
The number of long descending limbs $N^3$ is given by

$$\begin{aligned} N^3(x) =& 10\,000 \qquad 0 \le x \le x_{OM/IM}, \\ N^3(x) =& 10\,000\ \exp(-k^3(x - x_{OM/IM})), \qquad x_{OM/IM} \le x. \end{aligned}$$

The number of short descending limbs ($N^5$) is taken to be constant in the OM

$$N^5(x) = 20\,000 \qquad 0 \le x \le x_{OM/IM}.$$

**Cortical distal tubules.**
We distinguish between the cTAL, DCT and CCD of long-looped (superscript "dL") and short-looped (superscript "dS") nephrons. In both short and long nephrons, the number of cTAL and DCT remains constant, and the number of CNT is taken to decrease exponentially

$$\begin{aligned} N^{dL}(y) =& N^{dL}(0), \qquad y \in [0, y_L], \\ N^{dL}(y) =& N^{dL}(0) \exp(-k^d(y - 1.2)), \qquad y \in [V, L_{CTDC}], \end{aligned}$$

where $N^{dL}(0)$ is the number of long loops at the CM junction, i.e. $N^3(0)$.

$$\begin{aligned} N^{dS}(y) =& N^{dS}(0), \qquad y \in [0, y_S], \\ N^{dS}(y) =& N^{dS}(0) \exp(-k^d(y - 1.2)), \qquad y \in [y_S, L_{CTDC}], \end{aligned}$$

where $N^{dS}(0)$ is the number of short loops at the CM junction, i.e. $N^5(0)$.

We assume that long- and short-looped nephrons meet at the CCD entrance. The number of CCD ($N^{CCD}$) is taken to decrease exponentially

$$N^{CCD}(y) = (N^{dL}(L_{CTDC}) + N^{dS}(L_{CTDC})) \exp(-k^d(y - L_{CTDC})), \qquad y \in [L_{CTDC}, L_d],$$

**Medullary collecting ducts.** The number of medullary collecting ducts ($N^7$) decreases as they coalesce, and we assume the following distribution [**?**]:

$$N^7(x) = 5\,000 \exp(-k^7 x), \qquad x \in [0, L].$$

For medullary tubules and vessels, $k^j$ (j $= 1, 3, 7$) is a constant computed such that the number of a given class of tubules is $\approx 75$ at $x = L$. We also make the assumption that the parameter $k^d$ which characterizes the exponential decrease of tubules in the cortex is the same for long- and short-looped nephrons. Then, $k^d$ is ajusted so that the number of CDs leaving the cortex is equal to that entering the medulla (that is, 5 000). With these assumptions, $k^1 = k^3 = 1.22\ mm^{-1}$ , $k^7 = 0.7\ mm^{-1}$, $k^d = 0.4\ mm^{-1}$.

## 7.2 Physical variables

### 7.2.1 The unknowns

The unknowns to be determined are defined for all time $t > 0$, for all $x \in [0, L]$ for tubes $1, 2, 3, 4, 7, int$, for all $x \in [0, \frac{L}{3}]$ for tubes $5, 6$, and for all $y \in [0, L_d]$ for the distal tubule. The superscript $j$ denotes a given type of tube ($j = 1 - 7, d$), and the subscript $i$ denotes a given solute (i= Na, U, Ca).

- $F^j(t, x)$ $(m^3.s^{-1})$ is the water flow in one representative tube of the set of tubes $j$ at depth $x$ and time $t$. It represents the volume of water passing through the area centered in $x$ in 1 second. The variable $N^j(x)F^j(t, x)$ represents the total water flow of the set of tubes $j$ at depth $x$ and at time $t$. Note that in ascending tubes, $F^j$ is a negative number.

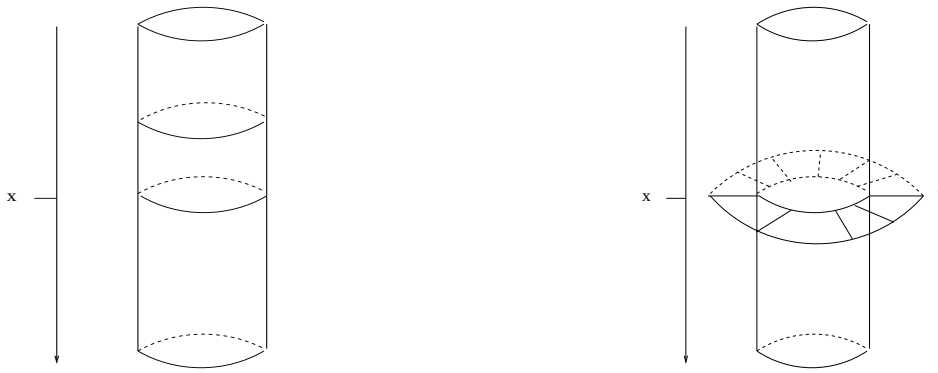


**Figure 7.5:** The water flow $F(t,x)$ is the volume of water passing through the area centered in $x$ in 1 second. The water flux $J_V(t,x)$ is the signed surface of water entering tube $j$ at depth $x$ in 1 second.

- $C_i^j(t,x)(mol.m^{-3})$ is the concentration of solute $i$ in one representative tube $j$. The product $F^j(t,x)C_i^j(t,x)(mol.s^{-1})$ represents the number of moles of solute $i$ passing through the area centered in $x$ in 1 second.
- $J_V^j(t,x)$ $(m^2.s^{-1})$ is the algebraic water flux across the wall of tube $j$. It represents the signed surface of water entering tube $j$ across the wall at depth $x$ in 1 second. $N^j(x)J_V^j(t,x)$ represents the total water flux entering the set of tubes $j$.
- $J_i^j(t,x)(mol.m^{-1}.s^{-1})$ is the algebraic flux of solute $i$ entering tube. It represents the number of moles entering tube $j$ across the wall at depth $x$ in 1 second. $N^j(x)J_i^j(t,x)$ represents the total water flux entering the set of tubes $j$.

With our convention, the fluxes $J^j$ are positive when they go from the interstitium to the tube $j$, and negative in the other case. In the interstitium, both cortical and medullary, we assume that there is no axial water flow ($F^{int}(t,x) = 0$). This assumption is made in all nephron models, and is justified by the fact that interstitial cells are organized in layers perpendicular to the cortico-medullary axis, which prevents any flow in the $x$-direction.

### 7.2.2 Physical phenomena included in the model

We describe here exchanges across tube wall. The luminal membrane is the side of the membrane which is inside the tube, whereas the basolateral membrane is the other side.

Water transport across the tube walls is driven by osmosis. In a region where there are $n$ solutes of concentration $(C_1, C_2, ..., C_n)$ with osmotic coefficients $(\Phi_1, \Phi_2, ..., \Phi_n)$, we define the osmotic pressure as

$$\Pi = RT \sum_{i=1}^{n} \Phi_i C_i. \tag{7.1}$$

This expression is only valid for small solutes The osmotic coefficient $\Phi_i$ of a solute $i$ is a weight that only depends on the solute.

- **Osmosis**: When the wall of a tube is permeable to water, water moves from the side with the lower osmotic pressure to the side with the higher osmotic pressure.

There are also solute exchanges throughout tube walls.

- **Diffusion**: When the wall of a tube is permeable to a solute, that solute moves from the more concentrated side to the less concentrated side.
- **Convection**: The water transport due to osmosis can drive solute transport, if the pathway used by water is permeable to the given solute.

- **Active transport**: There are active pumps in some epithelial layers (such as those of the AL, CD and distal tubules) which pump solute against the electrochemical potential gradient.
- **Electrodiffusion**: The transport of charged solutes such as calcium is also driven by electric potential differences. Here we assume that the electric potentials are fixed everywhere.

### 7.2.3 The parameters

**Table 7.1:** Parameters depending on $x$, $(0 \leq x \leq L)$.

| Parameter | Description |
|---|---|
| $R^j$ | Radius of tube $j$ |
| $L_P^j RT$ | Water permeability of tube $j$ |
| $P_i^j$ | Permeability to solute $i$ of tube $j$ |
| $\sigma_i^j$ | Reflection coefficient of tube $j$ to solute $i$ |
| $V_m^j$ | Rate of active transport across tube $j$ |
| $\Delta V_{TE}$ | Electric potential difference between the lumen and the interstitium |

As written earlier, model parameters are estimated based on measurements in rats.

Water and solute permeability values are summarized in Table 7.2. Also given in Table 7.2 are radius values for each set of tubules and vessels. As for size of the interstitium, we calculate its equivalent radius $R^{int}$ (see Eq.(7.6)) by assuming that at a given depth $x$, the cross-sectional area of the interstitium is 40% that of tubules [62]. It gives

$$R^{int}(x) = \sqrt{0.4 \sum_{j=3}^{7} N^j(x)(R^j)^2}. \tag{7.2}$$

Parameter values for water, NaCl and urea in the medulla are those of the HT model. As the HT model does not take into account the cortical distal tubules, water permeability values for the CCD, and for the DCT and CNT of short nephrons, are respectively taken from references [95–97]. Other parameter values for the distal tubules are taken from reference [63], and rescaled for compatibility with medullary values (i.e., so that the properties of cTAL and mTAL are identical). However, as this is the first model at the macroscopic scale incorporating calcium, calcium parameters have to be determined. $\Delta V_{TE}$ values come from references [80] and [40]. Other parameters ($\sigma_{Ca}$ and vasa recta $P_{Ca}$) are estimated. The permeability of the rat cTAL to $Ca^{2+}$ is taken as $5 \times 10^{-5}$ cm/s, i.e., an intermediate value between the value of $8.4 \times 10^{-5}$ cm/s measured in the laboratory of "Génomique, Physiologie et Physiopathologies Rénales, Centre de Recherche des Cordeliers, Paris" [73] and a lower value of $1 \times 10^{-5}$ cm/s estimated from the study of Mandon et al. [83]. That study suggested that the permeability of the rat mTAL to $Ca^{2+}$ is 10 times lower than that of the cTAL; the former is thus taken as $0.5 \times 10^{-5}$ cm/s here. To our knowledge, the permeability of the thin ascending limb to $Ca^{2+}$ has not been measured in rats. In rabbits, it is similar to that of the mTAL [80]. Thus, we take it to be equal to $0.5 \times 10^{-5}$ cm/s here.

The rat descending limb was found to transport $Ca^{2+}$ [37], but permeability values could not be inferred from the latter study. Based on measurements in rabbits [74,75], the DL permeability to $Ca^{2+}$ is taken as $0.7 \times 10^{-5}$ cm/s. We did not find any estimates of the permeability of vasa recta to $Ca^{2+}$. The latter is chosen as $1 \times 10^{-5}$ cm/s.

Shown in Table 7.3 are active transport parameters for $NaCl$ and $Ca^{2+}$. The $NaCl$ parameter values are comparable to those of the HT model. They were slightly modified so that approximately 25% of the calcium filtered load is reabsorbed in the ascending limbs of short nephrons. The $Ca^{2+}$ parameters were chosen so that (1) the $Ca^{2+}$ concentration in the final urine (i.e., at

| | | $R$ $\mu m$ | $L_P RT$ $cm^4.s^{-1}.mol.^{-1}$ | $P_{Na}$ $10^{-5}cm.s^{-1}$ | $P_U$ $10^{-5}cm.s^{-1}$ | $P_{Ca}$ $10^{-5}cm.s^{-1}$ | $\sigma_{Na}$ $\emptyset$ | $\sigma_U$ $\emptyset$ | $\sigma_{Ca}$ $\emptyset$ | $\Delta V_{TE}$ $mV$ |
|---|---|---|---|---|---|---|---|---|---|---|
| DVR | OS | 9. | 6.7 | 80 | 360 | 1.0 | 0.5 | 0.5 | 0.5 | 0 |
| | IS | | 2.5 | 80 | 360 | 1.0 | 0.5 | 0.5 | 0.5 | 0 |
| | IU | | 3.3 | 80 | 120 | 1.0 | 0.5 | 0.5 | 0.5 | 0 |
| | IL | | 3.3 | 80 | 120 | 1.0 | 0.5 | 0.5 | 0.5 | 0 |
| AVR | OS | 10 | / | 120 | 120 | 1.0 | 0 | 0 | 0 | 0 |
| | IS | | / | 120 | 120 | 1.0 | 0 | 0 | 0 | 0 |
| | IU | | / | 120 | 120 | 1.0 | 0 | 0 | 0 | 0 |
| | IL | | / | 120 | 120 | 1.0 | 0 | 0 | 0 | 0 |
| LDL | OS | 10 | 6.7 | 20 | 2.0 | 0.7 | 0.9 | 1 | 1 | 0 |
| | IS | | 6.3 | 20 | 2.0 | 0.7 | 0.9 | 1 | 1 | 0 |
| | IU | | 5.8 | 1.0 | 12 | 0.7 | 0.9 | 1 | 1 | 0 |
| | IL | | 5.8 | 0.5 | 12 | 0.7 | 0.9 | 1 | 1 | 0 |
| AL | OS | 10 | 0 | 2.0 | 4.5 | 0.5 | 1 | 1 | 1 | 15 |
| | IS | | 0 | 2.0 | 4.5 | 0.5 | 1 | 1 | 1 | 15 |
| | IU | | 0 | 0.8 | 23 | 0.5 | 1 | 1 | 1 | 0 |
| | IL | | 0 | 0.8 | 23 | 0.5 | 1 | 1 | 1 | 0 |
| CD | OS | 15 | 1.0 | 0 | 0.5 | 0.01 | 1 | 1 | 1 | $-10$ |
| | IS | | 0.53 | 0 | 0.5 | 0.01 | 1 | 1 | 1 | $-10$ |
| | IU | | 0.27 | 0 | 1.0 | 0.01 | 1 | 1 | 1 | $-10$ |
| | IL | | 0.33 | 0 | 70 | 0.01 | 1 | 1 | 1 | $-10$ |
| DT | cTAL | 12 | 0 | 2.0 | 4.5 | 5 | 1 | 1 | 1 | 15 |
| | DCT | | 0.2/0.05* | 1.0 | 0.8 | 0.1 | 1 | 1 | 1 | $-5$ |
| | CNT | | 0.72/0.18* | 1.0 | 0.8 | 0.1 | 1 | 1 | 1 | $-40$ |
| | CCD | | 1.8 | 1.0 | 0.8 | 0.01 | 1 | 1 | 1 | $-30$ |

**Table 7.2:** Tubule and vessel parameters. $R$: inner radius, $L_P$ : water permeability, $P_{Na}, P_U$, $P_{Ca}$ : permeability to sodium, urea, and calcium, $\sigma_{Na}, \sigma_U$, $\sigma_{Ca}$: reflection coefficient to sodium, urea, and calcium. $\Delta V_{TE}$: lumen-to-interstitium electrical potential difference. * Short-looped/long-looped nephrons.

the CD outlet) is about 2.0 mM [12] and (2) the percentage of calcium reabsorption in the DCT and CNT is about 10 % .

| | | $V_{m,Na}$ $nmol.mm^{-2}.s^{-1}$ | $K_{m,Na}$ $mM$ | $V_{m,Ca}$ $nmol.mm^{-2}.s^{-1}$ | $K_{m,Ca}$ $mM$ |
|---|---|---|---|---|---|
| SAL | OS | 0.20 | 50 | 0 | 0 |
| | IS | 0.20 | 50 | 0 | 0 |
| LAL | OS | 0.14 | 50 | 0 | 0 |
| | IS | 0.14 | 50 | 0 | 0 |
| | IU | 0 | 50 | 0 | 0 |
| | IL | 0 | 50 | 0 | 0 |
| CD | OS | $1.4 \times 10^{-3}$ | 50 | 0 | 0 |
| | IS | $1.4 \times 10^{-3}$ | 150 | 0 | 0 |
| | IU | $1.4 \times 10^{-3}$ | 50 | 0 | 0 |
| | IL | $1.4 \times 10^{-3}$ | 50 | 0 | 0 |
| Long-looped nephrons | cTAL | $2.8 \times 10^{-2}$ | 0.5 | 0 | 0 |
| | DCT | $4.6 \times 10^{-3}$ | 0.5 | $3.1 \times 10^{-3}$ | 5 |
| | CNT | $4.6 \times 10^{-3}$ | 0.5 | $3.1 \times 10^{-3}$ | 5 |
| | CCD | 0 | 0.5 | 0 | 0 |
| Short-looped nephrons | cTAL | $2.3 \times 10^{-3}$ | 0.5 | 0 | 0 |
| | DCT | $5.9 \times 10^{-3}$ | 0.5 | $3.1 \times 10^{-3}$ | 5 |
| | CNT | $5.9 \times 10^{-3}$ | 0.5 | $3.1 \times 10^{-3}$ | 5 |
| | CCD | 0 | 0.5 | 0 | 0 |

**Table 7.3:** Active transport parameters. Parameter values were selected as described in the text.

## 7.3 The equations

### 7.3.1 Conservation equations

The variables are related by conservation equations which we derive. It is the first dynamic model which takes into account the varying number of tubes with the depth.

For tubes $j = 1 - 6$ and for each solute $i$, the equations are written as

$$\begin{cases} \dfrac{\partial}{\partial x}\Big(N^j(x)F^j(t,x)\Big) = N^j(x)J_V^j(t,x) + \dfrac{dN^j}{dx}(x)F^{j'}(t,x), \\ \pi N^j(x)(R^j)^2\dfrac{\partial}{\partial t}C_i^j(t,x) + \dfrac{\partial}{\partial x}\Big(N^j(x)F^j(t,x)C_i^j(t,x)\Big) = N^j(x)J_i^j(t,x) + \dfrac{dN^j}{dx}(x)F^{j'}(t,x)C_i^j(t,x), \end{cases} \tag{7.3}$$

where $R^j$ is the radius of tube $j$, and $j' = 1$ if $j = 1$ or 2, $j' = 3$ if $j = 4$ or 3, $j' = 5$ if $j = 5$ or 6.

For tubes 7 and $d$ we have

$$\begin{cases} \dfrac{\partial}{\partial x}\Big(N^j(x)F^j(t,x)\Big) = N^j(x)J_V^j(t,x), \qquad j = 7, d, \\ \pi N^j(x)(R^j)^2\dfrac{\partial}{\partial t}C_i^j(t,x) + \dfrac{\partial}{\partial x}\Big(N^j(x)F^j(t,x)C_i^j(t,x)\Big) = N^j(x)J_i^j(t,x), \qquad j = 7, d. \end{cases} \tag{7.4}$$

We further explain the form of the equations. We point out that the conservative variables we work with are $NF$ and $NFC$, which represent the total water flow and molar flow in a given

class of tubes at depth $x$. Then, we interpret the variables $F$ and $FC$ as the water flow and the molar flow at depth $x$ per tube. In that sense, the model is an averaged model. We also point out that by imposing the values of $j'$ as we did, we tacitly assume that the fluid flows in the positive direction in the tubes 1, 3, 5, $d$ and 7 and in the negative direction in tubes 2, 4 and 6. Depending on the initial conditions and on the parameter values, flow reversal could occur. In that case, to have a pertinent model, for $j = 1$ or 2 for example, to compute the term corresponding to $\dfrac{dN^j}{dx}(x)F^{j'}(t,x)$, we have to distinguish four cases depending on the signs of $F^1$ and $F^2$. We do not build such a model, because in the numerical simulations, we find that there is no flow reversal. As presented, our model is only valid in the case where there is no flow reversal. We build later in this chapter a model that would deal with flow reversal. We complete equations (7.3) and (7.4) with two closure conditions. Assuming that the interstitium is rigid and does not accumulate water, we have

$$\sum_{j=1}^{7} J_V^j(t,x) = 0 \qquad \forall t > 0, \qquad \forall x \in [0, L]. \tag{7.5}$$

This is compatible with the fact that there is no axial water flow in the interstitium. Solute conservation in the interstitium is written as

$$\pi(R^{int})^2(x)\frac{\partial}{\partial t}C_i^{int}(t,x) = J_i^{int}(t,x), \qquad i = Na, U, Ca. \tag{7.6}$$

**Formal derivation of volume and mass conservation equations**

We derive here the equations for descending and ascending vasa recta (tubes 1 and 2). We assume that $F^1 \geq 0$ and that $F^2 \leq 0$. The difference in the total water flow in the DVR between depths $x$ and $x + dx$ can be expressed as

$$N^1(x + dx)F^1(x + dx) - N^1(x)F^1(x). \tag{7.7}$$

Conservation of water implies that this difference equals the amount of water entering DVR across vessel walls between $x$ and $x + dx$, minus the amount of water that is shunted to AVR. The latter corresponds to the water flow at the end of the tubes that turn back between $x$ and $x + dx$. These two terms are written as

$$\int_x^{x+dx} N^1(s)J_V^1(s)ds + \int_x^{x+dx} -\Big( - \frac{dN^1}{dx}(s)F^1(s)ds\Big) \tag{7.8}$$

Note that $-\dfrac{dN^1}{dx}(x)$ represents the number of DVR that end at depth $x$. Setting (7.7) equal to (7.8):

$$N^1(x + dx)F^1(x + dx) - N^1(x)F^1(x) = \int_x^{x+dx} N^1(s)J_V^1(s)ds + \int_x^{x+dx} -\Big( - \frac{dN^1}{dx}(s)F^1(s)ds\Big)$$

The differential form of this equation is

$$\frac{\partial}{\partial x}\Big(N^1(x)F^1(x)\Big) = N^1(x)J_V^1(x) + \frac{dN^1}{dx}(x)F^1(x), \tag{7.9}$$

Following the same reasoning, the conservation equation for AVR is written as:

$$\frac{\partial}{\partial x}\Big(N^1(x)F^2(x)\Big) = N^1(x)J_V^2(x) - \frac{dN^1}{dx}(x)F^1(x). \tag{7.10}$$

The water conservation equations for tubules are obtained in the same manner. Note that there are no shunt terms for medullary collecting ducts (tubes 7) and cortical distal tubules, hence the form of Eq (7.4).

The total amount of solute in the DVR domain comprised between depth $x$ and $x+dx$ at time $t$ is

$$M(t) := \int_x^{x+dx} \pi (R^1)^2 N^1(y) C^1(t,y) dy.$$

The time evolution of $M$ between time $t$ and $t+dt$ is due to

- the difference between the amount of solute entering the infinitesimal volume and the amount of solute leaving the volume between time $t$ and $t+dt$

$$-\int_t^{t+dt} \Big( N^1 F^1 C^1(s, x+dx) - N^1 F^1 C^1(s,x) \Big) ds,$$

- the amount of solute entering DVR across vessel walls between $x$ and $x+dx$ and time $t$ and $t+dt$

$$\int_t^{t+dt} \int_x^{x+dx} N^1(s) J^1(s,y) dy ds,$$

- and the solute that flows at the end of the tubes turning back between $x$ and $x+dx$

$$\int_t^{t+dt} \int_x^{x+dx} -\Big( -\frac{dN^1}{dx}(s) F^1(s,y) C^1(s,y) \Big) dy ds.$$

We obtain the equality.

$$\begin{aligned} M(t+dt) - M(t) = &-\int_t^{t+dt} \Big( N^1 F^1 C^1(s, x+dx) - N^1 F^1 C^1(s,x) \Big) ds \\ &+ \int_t^{t+dt} \int_x^{x+dx} N^1(s) J^1(s,y) dy ds + \int_t^{t+dt} \int_x^{x+dx} +\Big( \frac{dN^1}{dx}(s) F^1(s,y) C^1(s,y) \Big) dy ds. \end{aligned}$$

The differential form gives us the second equation of (7.3).

### 7.3.2 Flux equations

The water flux is given by

$$J_V^j(t,x) = 2\pi R^j L_P^j(x) RT \Big[ \sum_{i=1}^{I} \sigma_i^j(x) \Big( C_i^j(t,x) - C_i^{int}(t,x) \Big) - \delta^j E(x) \Big], \qquad I = \{Na, U, Ca\}, \tag{7.11}$$

where $L_p^j$ is the water permeability of tube $j$, $\sigma_i^j$ is the reflection coefficient of tube $j$ to solute $i$, and $\delta^j$ is 1 in tubules and zero in vasa recta. Equation (7.11) implicitly assumes that hydrostatic pressures are negligible relative to osmotic pressures.

To date, the mechanisms underlying the formation of the axial osmolality gradient in the inner medulla remain to be fully elucidated, as discussed below. To reproduce the observed gradient, we follow the approach of Thomas and Wexler ( [89]) and add an external osmotic driving force in the inner medullary interstitium. Thus, $E$ is the concentration of external osmolytes in the interstitium, taken as zero in the outer medulla, and 80 mM in the inner medulla.

Note that the water permeability of AVR is so large that the corresponding water flux is calculated based on water conservation Eq. (7.5) instead. Solute transport is driven by electro-diffusion, convection and active transport. The fluxes of uncharged solutes (NaCl and urea), are

written as

$$J_i^j(t,x) = -2\pi R^j P_i^j(x)\Big(C_i^j(t,x) - C_i^{int}(t,x)\Big) + J_V^j(t,x)(1-\sigma_i^j(x))C_i^\alpha(t,x) - 2\pi R^j V_{m,i}^j(x)\frac{C_i^j(t,x)}{K_{m,i}^j + C_i^j(t,x)}, \tag{7.12}$$

with

$$C_i^\alpha(t,x) = \begin{cases} C_i^{int}(t,x) & \text{for } J_V^j(t,x) > 0, \\ C_i^j(t,x) & \text{for } J_V^j(t,x) \leq 0. \end{cases} \tag{7.13}$$

The first term represents diffusive transport; $P_i^j$ is the permeability of tube $j$ to solute $i$. The second term, which represents convective transport, is formulated differently than in other kidney models [34,63], where it is expressed as:

$$J_{conv}^j = J_V^j(t,x)(1-\sigma_i^j(x))\frac{C_i^{int}(t,x) + C_i^j(t,x)}{2}, \tag{7.14}$$

In the latter formulation, the amount of solute carried by convection is independent of the direction of the water flux. To insure that our system of equation is well-posed and positive, we use instead an upwind term. The theoretical problem we raise is the following. Imagine a model with only one solute. Imagine that at depth $x$, the interstitium has a concentration in this solute which is zero, and that it is not the case in the tube. Then, the model would take solute from the interstitium to carry it to the tube, making the solute concentration in the interstitium negative. As we are interested in the mathematical properties of our model such as the positivity of the solution [91], we suggest an other way to compute the convective term. At each depth, depending on the sign of $J_V$, which means depending on whether water goes from the interstitium to the tube or from the tube to the interstitium, we compute the solute flux differently. For example, if $J_V^j(t,x) > 0$ which means that water goes from the interstitium to tube $j$, we compute the solute flux based upon its concentration in the interstitium. The third term represents active transport, with Michaelis-Menten kinetics.

For a charged solute such as $Ca^{2+}$, the flux is written as

$$\begin{aligned} J_{Ca}^j(t,x) = -2\pi R^j P_{Ca}^j(x)\Big[\Big(C_{Ca}^j(t,x) - C_{Ca}^{int}(t,x)\Big) + \frac{2F}{RT}\Delta V_{TE}^j(x) C_{Ca}^\beta(t,x)\Big] \\ + J_V^j(t,x)(1-\sigma_{Ca}^j(x))C_{Ca}^\alpha(t,x) - 2\pi R^j V_{m,Ca}^j(x)\frac{C_{Ca}^j(t,x)}{K_{m,Ca}^j + C_{Ca}^j(t,x)}, \end{aligned} \tag{7.15}$$

with

$$C_{Ca}^\alpha(t,x) = \begin{cases} C_{Ca}^{int}(t,x) & \text{for } J_V^j(t,x) > 0, \\ C_{Ca}^j(t,x) & \text{for } J_V^j(t,x) \leq 0. \end{cases} \tag{7.16}$$

and

$$C_{Ca}^\beta(t,x) = \begin{cases} C_{Ca}^j(t,x) & \text{for } \Delta V_{TE}(x) > 0, \\ C_{Ca}^{int}(t,x) & \text{for } \Delta V_{TE}(x) \leq 0. \end{cases} \tag{7.17}$$

Solute conservation implies that

$$J_i^{int}(t,x) = -\sum_j J_i^j(t,x) \qquad \forall t > 0, \forall x \in [0,L]. \tag{7.18}$$

This last equation, which closes the system, expresses the fact that the net flux of solute into the interstitium ($J_i^{int}$) is the opposite of the net flux from the interstitium into surrounding tubules and vessels.

### 7.3.3 Boundary conditions

Water and solute flows are specified at the inlet of DVR (tube 1) and DL (tubes 3 and 5) for all times:

$$\begin{aligned}
&F^1(t,0) = 3.25 \text{ nl/min/vessel},\ F^3(t,0) = F^5(t,0) = 10 \text{ nl/min/tubule},\\
&C^1_{Na}(t,0) = C^3_{Na}(t,0) = C^5_{Na}(t,0) = 139 \text{ mM},\\
&C^1_U(t,0) = 5 \text{ mM},\ C^3_U(t,0) = C^5_U(t,0) = 10 \text{ mM},\\
&C^1_{Ca}(t,0) = C^3_{Ca}(t,0) = C^5_{Ca}(t,0) = 1.2 \text{ mM},
\end{aligned} \tag{7.19}$$

In addition, by continuity between adjacent tubes, we have:

$$\begin{cases}
F^2(t,L) = -F^1(t,L), \qquad F^4(t,L) = -F^3(t,L), \qquad F^{dL}(t,0) = -F^4(t,0), \qquad F^{dS}(t,0) = -F^6(t,0),\\
C^2_i(t,L) = C^1_i(t,L), \qquad C^4_i(t,L) = C^3_i(t,L), \qquad C^{dL}_i(t,0) = C^4_i(t,0), \qquad C^{dS}_i(t,0) = C^6_i(t,0),\\
\qquad F^7(t,0) = F^{CCD}(t,L_d) \qquad C^7_i(t,0) = C^{CCD}_i(t,L_d),\\
\qquad F^6(t,\frac{L}{3}) = -F^5(t,\frac{L}{3}), \qquad C^6(t,\frac{L}{3}) = C^5(t,\frac{L}{3}),\\
N^{dS}(t,L_{CTDC})F^{dS}(t,L_{CTDC}) + N^{dL}(t,L_{CTDC})F^{dL}(t,L_{CTDC}) = N^{CCD}(t,0)F^{CCD}(t,0),\\
N^{dS}(t,L_{CTDC})F^{dS}(t,L_{CTDC})C^{dS}(t,L_{CTDC}) + N^{dL}(t,L_{CTDC})F^{dL}(t,L_{CTDC})C^{dL}(t,L_{CTDC})\\
\qquad\qquad = N^{CCD}(t,0)F^{CCD}(t,0)C^{CCD}(t,0).
\end{cases}$$

The last two equations express the fact that the total water and molar flows are conserved when short and long nephrons merge at the CCD inlet.

## 7.4 Flow reversal

Based on the analysis made on Chapter 2, we infer that the concentrations $C$ are positive for all time $t$. But nothing can guarantee that during the transient regime, the flow $F$ keeps the sign expected at stationary state. It can happen that, for example, for a given $(t,x)$, $F^1(t,x)$ becomes negative and $F^2(t,x)$ becomes positive. This phenomenon is called "flow reversal" in the literature. If it occurs at a time $t$, as the conservation equations are derived under assumptions on the sign on $F$, the model is no more valid. Happily, it does not happen for physiological initial conditions. In this part, we suggest a way to deal with this phenomenon, in order to obtain a model that is well-posed for any set of initial conditions. To include flow reversal in our model, we should for example modify the equations for the vasa recta flow as follows :

$$\begin{cases}
\dfrac{\partial}{\partial x}\Big(N^1(x)F^1(t,x)\Big) = N^1(x)J^1_V(t,x) + \dfrac{dN^1}{dx}(x)F^{shunt}(t,x),\\
\pi N^j(x)(R^1)^2\dfrac{\partial}{\partial t}C^1(t,x) + \dfrac{\partial}{\partial x}\Big(N^1(x)F^1(t,x)C^1(t,x)\Big) = N^j(x)J^1(t,x) + \dfrac{dN^1}{dx}(x)(FC)^{shunt}(t,x),
\end{cases} \tag{7.20}$$

where

$$F^{shunt}(t,x) = \begin{cases}
F^1(t,x) & \text{if } F^1 \geq 0 \text{ and } F^2 \leq 0,\\
F^2(t,x) & \text{if } F^2 \geq 0 \text{ and } F^1 \leq 0,\\
F^1(t,x) - F^2(t,x) & \text{if } F^1 \geq 0 \text{ and } F^2 \geq 0,\\
F^2(t,x) - F^1(t,x) & \text{if } F^1 \leq 0 \text{ and } F^2 \leq 0,
\end{cases}$$

and

$$(FC)^{shunt}(t,x) = \begin{cases} F^1(t,x)C^1(t,x) & \text{if } F^1 \geq 0 \text{ and } F^2 \leq 0, \\ F^2(t,x)C^2(t,x) & \text{if } F^2 \geq 0 \text{ and } F^1 \leq 0, \\ F^1(t,x)C^1(t,x) - F^2(t,x)C^2(t,x) & \text{if } F^1 \geq 0 \text{ and } F^2 \geq 0, \\ F^2(t,x)C^2(t,x) - F^1(t,x)C^1(t,x) & \text{if } F^1 \leq 0 \text{ and } F^2 \leq 0. \end{cases}$$

Such an approach cannot be found in any modeling study.

## 7.5 The coalescing effect and the shunting effect

Before we start our analysis, we want to draw attention to the quantities we are interested in and which we plot on the figures. A typical quantity we will plot is $F(t,x)C_{Ca}(t,x)$ at equilibrium. It will be described as the calcium molar flow "per tube". In the CD for example, since the tubes are coalescing, if we put the calcium permeability to zero, then, the calcium molar flow per tube will rise with depth, as illustrated on the figure on the right. Thus, a tube can be calcium impermeable, which means that there is no calcium flux between this tube and the interstitum, and yet the calcium molar flow can vary with the depth along this tube. Afterwards, we will call this effect the coalescing effect.

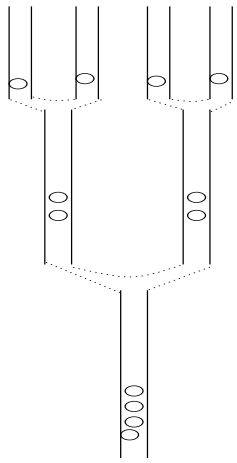

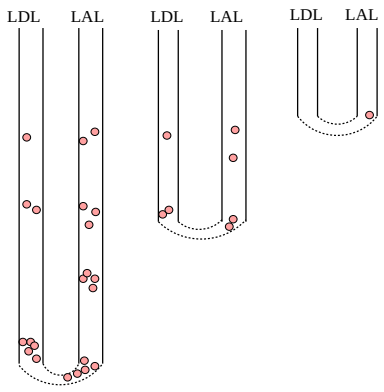


In the tubes which are not coalescing, for example the LDL and the LAL, we notice another phenomenon. Imagine that the amount of calcium is increasing with depth in the LDL and that the LAL is impermeable to calcium. The number of LDL varies. That means that at each depth $x \in [x_{OM/IM}, L]$, one of the LDL is turning back and an LAL is receiving at its tip the amount of calcium of the LDL that turned back. As the amount of calcium is increasing with depth in the LDL, less and less calcium is reinjected in the ascending limbs as one gets closer to the cortex. The amount of calcium decreases in the LAL as one gets closer to the cortex. Afterwards, we will call this effect the shunting effect.

The coalescing and the shunting effects are phenomena due to the fact that our model is an averaged model.

## Glossary

| | |
|---|---|
| AL | ascending limb of Henle's loop |
| AVR | ascending vasa recta |
| $C_i^j$ | concentration of solute $i$ in vessel or tubule $j$ |
| CCD | cortical collecting duct |
| CD | collecting duct |
| CM | cortico-medullary |
| CNT | connecting tubule |
| cTAL | cortical thick ascending limb |
| DCT | distal convoluted tubule |
| DL | descending limb of Henle's loop |
| DVR | descending vasa recta |
| F | water flow |
| IM | inner medulla |
| IS | inner stripe of outer medulla |
| $K_{m,i}^j$ | Michaelis-Menten constant for active transport of solute $i$ in vessel of tubule $j$ |
| L | total length of medulla |
| $L_{CTDC}$ | combined length of the cTAL, DCT,CNT |
| $L_d$ | total length of cortical distal tubules |
| LIM | lower part of inner medulla |
| $L_p^j$ | permeability of vessel or tubule $j$ to water |
| mTAL | medullary thick ascending limb |
| $N^J$ | number of vessels or tubules of type $j$ |
| OM | outer medulla |
| OS | outer stripe of outer medulla |
| $P_i^j$ | permeability of vessel or tubule $j$ to solute $i$ |
| $R^j$ | radius of vessel or tubule $j$ |
| SAL | short ascending limb |
| SAV | short ascending vasa recta |
| SDL | short descending limb |
| SDV | short descending vasa recta |
| TAL | thick ascending limb |
| UIM | upper part of inner medulla |
| $V_{m,i}^j$ | maximal rate of active transport of solute i in tubule j |
| $x_{OM/IM}$ | spatial coordinate at the OM-IM boundary |
| $x_{OS/IS}$ | spatial coordinate at the OS-IS boundary |
| $\Delta V_{TE}^j$ | electric potential difference between the lumen of tubule $j$ and the interstitium |
| $\sigma_i^j$ | reflection coefficient of vessel or tubule $j$ to solute $i$ |

# Chapter 8

# Numerical Solution - A finite volume scheme

This chapter is inspired from the paper

A. Edwards, N. Seguin, and M. Tournus. A finite-volume scheme for a kidney nephron model. *ESAIM: Proc.*, 35-Congrès National de Mathématiques Appliquées et Industrielles:287–292, 2012.

*We present a finite volume type scheme to solve a transport nephron model. The model consists in a system of transport equations with specific boundary conditions. The transport velocity is driven by another equation that can undergo sign changes during the transient regime. This is the main difficulty for the numerical resolution. The scheme we propose is based on an explicit resolution and is stable under a CFL condition which does not depend on the stiffness of source terms.*

We developed a new finite-volume scheme [9], combined with a splitting method, to solve the dynamic model equations. The purpose we keep in mind is the resolution of the stationary state associated with the dynamic problem we present.

For simplicity, the scheme is presented here for the blood vessels and the collecting duct (tubes 1, 2 and 7), but it can easily be expanded to the renal tubules. The AVR (tube 2) appears specifically in this minimal scheme because its water flux is calculated differently than that of other structures. Tube 7 is also included is this reduced model, because of the specific shape of its conservation equation. We merely present the scheme with one solute ($I = 1$) but it is easily generalized to $I$ solutes, the only differences lying in the computation of water fluxes (which then contain one more term).

Since the 80's, several numerical studies of stationary systems close to the stationary state associated with (7.3), (7.4) have been published. We can divide them into two classes. One class consists in Newton-type methods [34,88]. They solve directly the stationary state and require an initial guess close enough to equilibrium. The second class consists in methods that solve a dynamic system which relaxes toward the stationary state. In [63], the method of lines is used to solve such a dynamic system. Since then, new dynamic numerical methods have been implemented, involving computation of space derivatives upwind along the flow direction. An explicit method for solving hyperbolic PDEs [53] [54] was adapted by Layton and Pitman, but the CFL condition they obtained was a very limiting constraint. To deal with this problem, a semi lagrangian-semi implicit (SLSI) method was implemented [52]. The drawback of this method is the lack of accuracy, thus it is combined with a Newton-type solver, which uses the solution from the SLSI method as an initial guess. More recently, a scheme based on the second order Godunov method was developed [51] for a 3-tube model whose particularity is that the transmural solute flux contains no convective term. The scheme we describe here is a splitting scheme. The transport part is treated thanks to an upwind scheme and the source term is treated implicitly.

## 8.1 Finite volume scheme - A simplified model

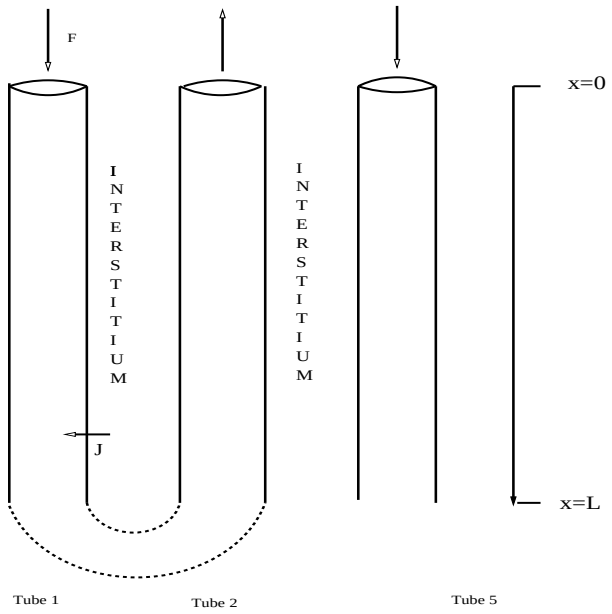


**Figure 8.1:** The reduced model is made of descending vasa recta, ascending vasa recta and collecting ducts.

We first describe a reduced model with which we present the numerical scheme. This reduced model is taken to be as simple as possible, but complex enough to keep all the difficulties and

specificities of the model described in Chapter 7. In order to keep homogeneous notations, we keep on referring to the collecting duct with the number 7. We will then consider tubes 1, 2 and 7. We recall that $N^1$ and $N^7$ are given parameters. The model reduces to

$$\begin{cases} \dfrac{\partial}{\partial x}\Big(N^1(x)F^1(t,x)\Big) = N^1(x)J_V^1(t,x) + \dfrac{dN^1}{dx}(x)F^1(t,x), \\ \dfrac{\partial}{\partial x}\Big(N^1(x)F^2(t,x)\Big) = N^1(x)J_V^2(t,x) - \dfrac{dN^1}{dx}(x)F^1(t,x), \\ \pi N^1(x)(R^1)^2\dfrac{\partial}{\partial t}C^1(t,x) + \dfrac{\partial}{\partial x}\Big(N^1(x)F^1(t,x)C^1(t,x)\Big) = N^1(x)J^1(t,x) + \dfrac{dN^1}{dx}(x)F^1(t,x)C^1(t,x), \\ \pi N^1(x)(R^2)^2\dfrac{\partial}{\partial t}C^2(t,x) + \dfrac{\partial}{\partial x}\Big(N^1(x)F^2(t,x)C^2(t,x)\Big) = N^1(x)J^2(t,x) - \dfrac{dN^1}{dx}(x)F^1(t,x)C^1(t,x), \end{cases} \tag{8.1}$$

$$\begin{cases} \dfrac{\partial}{\partial x}\Big(N^7(x)F^7(t,x)\Big) = N^7(x)J_V^7(t,x), \\ \pi N^7(x)(R^7)^2\dfrac{\partial}{\partial t}C^7(t,x) + \dfrac{\partial}{\partial x}\Big(N^7(x)F^7(t,x)C^7(t,x)\Big) = N^7(x)J^7(t,x), \end{cases} \tag{8.2}$$

with water fluxes in tubes 1 and 7 given by

$$J_V^j(t,x) = 2\pi R^j L_P^j(x)RT\sigma^j(x)\Big(C^j(t,x) - C^{int}(t,x)\Big), \qquad j = 1,7, \tag{8.3}$$

whereas the water flux in tube 2, $J_V^2$ is determined by

$$N^1(x)J_V^1(t,x) + N^2(x)J_V^2(t,x) + N^7(x)J_V^7(t,x) = 0 \qquad \forall t > 0, \qquad \forall x \in [0,L]. \tag{8.4}$$

The solute fluxes are given by

$$J^j(t,x) = -2\pi R^j(x)P^j(x)\Big(C^j(t,x) - C^{int}(t,x)\Big) + J_V^j(t,x)(1-\sigma^j(x))C^{j,\alpha}(t,x) - 2\pi R^j V_m^j\frac{C^j}{K_m^j + C^j}, \tag{8.5}$$

with

$$C^{j,\alpha}(t,x) = \begin{cases} C^{int}(t,x) & \text{for } J_V^j(t,x) > 0, \\ C^j(t,x) & \text{for } J_V^j(t,x) \le 0. \end{cases} \tag{8.6}$$

The interstitial flux is computed as

$$J^{int}(t,x) = -\sum_{j=1,2,7} N^j(x)J^j(t,x) \qquad \forall t > 0, \forall x \in [0,L], \tag{8.7}$$

and the evolution of $C^{int}$ is described by

$$\pi(R^{int}(x))^2\frac{\partial}{\partial t}C^{int}(t,x) = J^{int}(t,x), \tag{8.8}$$

The boundary conditions are the following

$$\begin{cases} F^1(0) = F_0^1, & F^2(L) = -F^1(L), & F^7(0) = F_0^7, \\ C^1(0) = C_0^1, & C^2(L) = C^1(L), & C^7(0) = C_0^7, \end{cases}$$

where $F_0^1, F_0^7, C_0^1, C_0^7$ are four nonnegative given values. We complete the system with the initial conditions

$$C^1(0,x) = C^{1,0}(x), \qquad C^2(0,x) = C^{2,0}(x), \qquad C^7(0,x) = C^{7,0}(x).$$

We notice that

$$\frac{\partial}{\partial x}\Big(N^1(x)F^1(t,x)\Big) - \frac{dN^1}{dx}(x)F^1(t,x) = N^1(x)\frac{\partial}{\partial x}F^1(t,x).$$

Then, the equations for tube 1 can be written as

$$\begin{cases} \dfrac{\partial}{\partial x}\Big(F^1(t,x)\Big) = J_V^1(t,x), \\ \pi(R^1)^2\dfrac{\partial}{\partial t}C^1(t,x) + \dfrac{\partial}{\partial x}\Big(F^1(t,x)C^1(t,x)\Big) = J^1(t,x). \end{cases} \tag{8.9}$$

For the discretization of system (8.1), we directly use this last formulation. We state now a conservation property of our system. This property will be preserved by our scheme, at a discrete level.

**Proposition 8.1.1.** *We have the following conservation properties*

*i)*

$$(N^1F^1 + N^1F^2 + N^7F^7)(t,x) \text{ does not depend on } x. \tag{8.10}$$

*ii) Moreover, a stationary state satisfies*

$$(N^1F^1C^1 + N^1F^2C^2 + N^7F^7C^7)(x) \text{ does not depend on } x. \tag{8.11}$$

This means that there is no water accumulation in the interstitium, and that there is no solute accumulation in the interstitium when equilibrium is reached.

*Proof.* The first statement of proposition 8.11 is obtained by summing the first two lines of (8.1) and the first line of (8.2), which gives us

$$\frac{\partial}{\partial x}(N^1F^1 + N^1F^2 + N^7F^7)(t,x) = N^1(x)J_V^1(t,x) + N^1(x)J_V^2(t,x) + N^7(x)J_V^7(t,x),$$

which proves by using (8.4)

$$\frac{\partial}{\partial x}(N^1F^1 + N^1F^2 + N^7F^7)(t,x) = 0.$$

The second statement is obtained at least formally by noticing that at equilibrium, the quantities does not depend on $t$ anymore. In particular, $\dfrac{\partial}{\partial t}C^{int}(t,x) = 0$ which implies

$$N^1(x)J^1(t,x) + N^1(x)J^2(t,x) + N^7(x)J^7(t,x) = 0.$$

Then, by summing the third and fourth line of system (8.1) and the second line of (8.2), we get

$$\frac{\partial}{\partial x}(N^1F^1C^1 + N^1F^2C^2 + N^7F^7C^7)(t,x) = N^1(x)J^1(t,x) + N^1(x)J^2(t,x) + N^7(x)J^7(t,x) = 0,$$

and the results holds. □

## 8.2 Description of our scheme

### 8.2.1 A finite volume approach

When solving hyperbolic equations, as discontinuous solutions can occur, the finite volume method is well adapted. In this framework, we consider a space-mesh of $N$ disjoint numerical cells $Q_k = (x_{k-1/2}, x_{k+1/2}), k \in [1, N]$. Let $\Delta x = \dfrac{L}{N}$ be the size of each cell and $\Delta t$ the size of the time step. The final time is denoted by $T$, and the number of iterations is denoted by $n_f$, so that $n_f \Delta t = T$. The quantities $C_k^{j,n}, j = 1, 2, 7, int$ and $F_k^{j,n}, j = 1, 2, 7$ respectively represent the values of the concentration and water flow in cell $k$ after $n$ iterations.

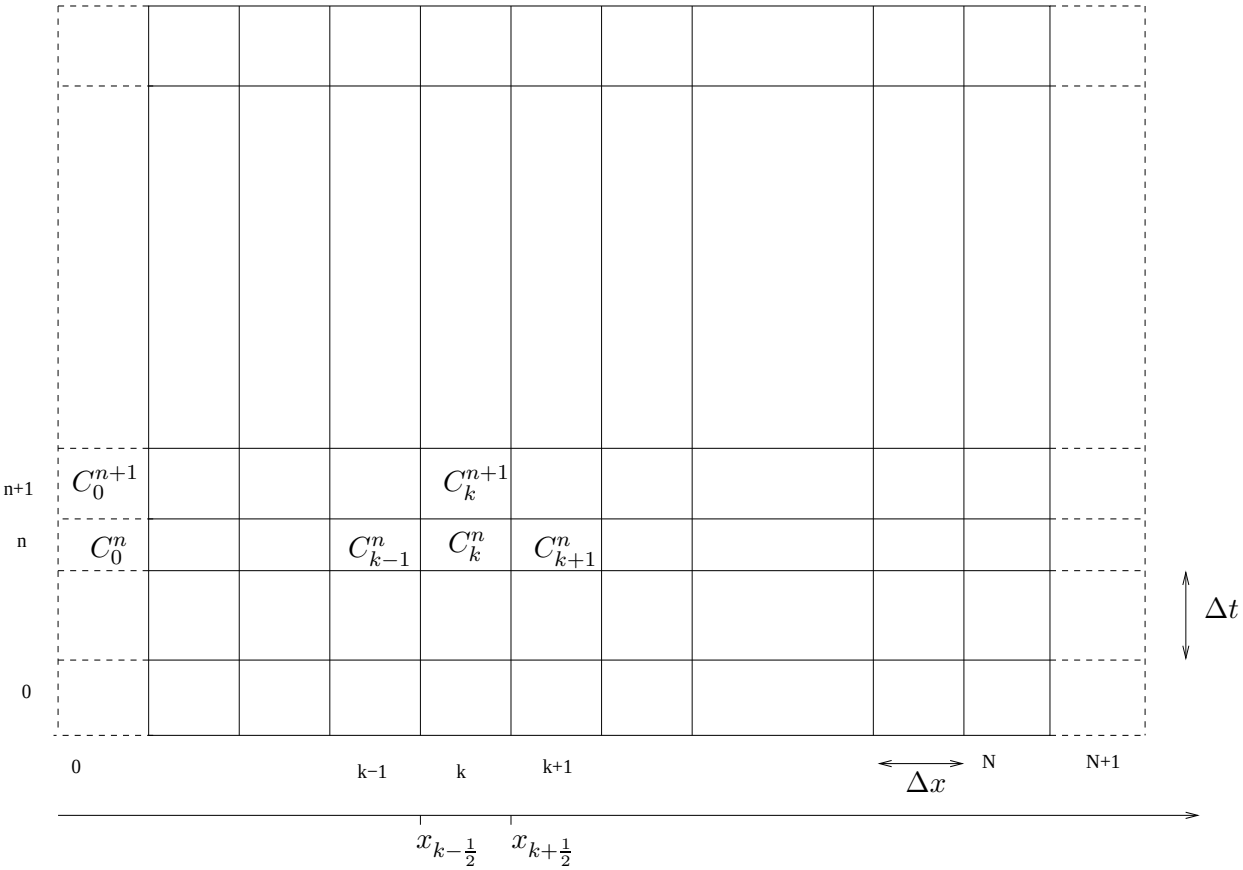


**Figure 8.2:** The domain $[0, L] \times [0, T]$ is divided in cells indexed by $(k, n) \in [1, N] \times [1, n_f]$. To deal with the boundary conditions and the initial condition, we add artificial cells corresponding to $n = 0$, $k = 0$ and $k = N + 1$.

For the initial condition, we define the cell average as

$$C_k^{j,0} = \frac{1}{\Delta x} \int_{Q_k} C^j(x, 0) dx, \qquad j = 1, 2, 7, \quad k = 1, ..., N. \tag{8.12}$$

We discretize every parameter $P(x)$ as

$$P_k^j = \frac{1}{\Delta x} \int_{Q_k} P^j(x) dx, \qquad j = 1,\ 2, 7, \quad k = 1, ..., N. \tag{8.13}$$

This discretization affects particularly $N^j(x)$, the number of tubes of type $j$ at depth $x$. As the other parameters we use are piecewise constant, the way they are discretized in not of real importance. The boundary conditions at the inlet of tubes 1 and 7 yield, $C_0^{1,n} = C_0^1$, $F_0^{1,n} = F_0^1$, $C_0^{7,n} = C_0^7$, $F_0^{7,n} = F_0^7$. By continuity we have $C_{N+1}^{2,n} = C_N^{1,n}$ and $F_{N+1}^{2,n} = -F_N^{1,n}$; in

addition, by symmetry, we have $C^{1,n}_{N+1} = C^{2,n}_N$ and $F^{1,n}_{N+1} = -F^{2,n}_N$ . The scheme we build does not preserve a priori the sign of the flows, however, the boundary conditions and the structure of the model and scheme implicitly assume that $F^1 \geq 0, F^2 \leq 0$, and $F^7 \geq 0$, as expected under most physiological conditions. If by accident, flow reversal occur, this is considered as unphysiological and we stop the simulation and start with another set of initial conditions. Indeed, the community of physiologists believe that flow reversal does not occur under most conditions.

### 8.2.2 The equations on the flow

The equations on the flows $F^1, F^2$ and $F^7$ are ordinary differential equations. The source term is computed at the time iteration $n$ and in cell $k$

$$\begin{cases} J^{1,n}_{V,k} = -2\pi R^1 L^1_{p,k}\sigma^1_k\Big(C^{1,n}_k - C^{int,n}_k\Big), \\ J^{7,n}_{V,k} = -2\pi R^7 L^7_{p,k}\sigma^7_k\Big(C^{7,n}_k - C^{int,n}_k\Big), \\ J^{2,n}_{V,k} = -J^{1,n}_{V,k} - J^{7,n}_{V,k}. \end{cases} \tag{8.14}$$

We solve the differential equations with a finite difference method

$$\begin{cases} \dfrac{F^{1,n}_k - F^{1,n}_{k-1}}{\Delta x} = J^{1,n}_{V,k}, \qquad F^{2,n}_{N+1} = -F^{1,n}_N, \\ \dfrac{N^1_k F^{2,n}_k - N^1_{k+1}F^{2,n}_{k+1}}{\Delta x} = -N^1_{k+1}J^{2,n}_{V,k+1} + \dfrac{N^1_{k+1} - N^1_k}{\Delta x}F^1_k. \end{cases} \tag{8.15}$$

For tube 7 we set

$$\frac{N^7_k F^{7,n}_k - N^7_{k-1}F^{7,n}_{k-1}}{\Delta x} = N^7_k J^{7,n}_{V,k}. \tag{8.16}$$

The way the source term is discretized in the second equation of (8.15) is imposed by the water conservation we have chosen to preserve. We detail it in the properties of the scheme.

### 8.2.3 The splitting method - Concept and application

We now solve numerically the evolution equation for concentration. We treat separately the source term source and the transport part, using a splitting method. We assume we know $(C^{j,n}_k)_{k\in[0,N]}$ and $(F^n_k)_{k\in[0,N]}$. We wish to determine here $(C^{n+1}_k)_{k\in[0,N]}$. For that, we solve the two following split systems one after the other.

$$\begin{cases} \pi N^1(x)(R^1)^2\dfrac{\partial}{\partial t}C^1(t,x) + \dfrac{\partial}{\partial x}\Big(N^1(x)F^1(t,x)C^1(t,x)\Big) = \dfrac{dN^1}{dx}(x)F^1(t,x)C^1(t,x), \\ \pi N^1(x)(R^2)^2\dfrac{\partial}{\partial t}C^2(t,x) + \dfrac{\partial}{\partial x}\Big(N^1(x)F^2(t,x)C^2(t,x)\Big) = -\dfrac{dN^1}{dx}(x)F^1(t,x)C^1(t,x), \\ \pi N^7(x)(R^7)^2\dfrac{\partial}{\partial t}C^7(t,x) + \dfrac{\partial}{\partial x}\Big(N^7(x)F^7(t,x)C^7(t,x)\Big) = 0, \end{cases} \tag{8.17}$$

We define $(C^{n+\frac{1}{2}}_k)_{k\in[0,N]}$ as a numerical approximation to be specified later, of the solution to (8.17) with initial condition $C^j(x,0) = \sum_{k=1,N} C^{j,n}_k \mathbb{1}_{[k\Delta x,(k+1)\Delta x]}$ taken at time $t = \Delta t$.

$$\begin{cases} \pi N^1(x)(R^1)^2\dfrac{\partial}{\partial t}C^1_i(t,x) = N^1(x)J^1_i(t,x), \\ \pi N^1(x)(R^2)^2\dfrac{\partial}{\partial t}C^2_i(t,x)) = N^1(x)J^2_i(t,x), \\ \pi N^7(x)(R^7)^2\dfrac{\partial}{\partial t}C^7_i(t,x) = N^7(x)J^7_i(t,x). \end{cases} \tag{8.18}$$

We then compute $(C_k^n)_{k\in[0,N]}$ as a numerical approximation to be specified in the rest of the solution to 8.18 with initial condition $C^j(x,0) = \sum_{k=1,N} C_k^{j,n+\frac{1}{2}} \mathbb{1}_{[k\Delta x,(k+1)\Delta x]}$ taken at time $t = \Delta t$.

We specify now how we compute the numerical approximation of both systems (8.17) and (8.18).

### 8.2.4 Finite volume scheme on the transport equation

System (8.17) is a system of transport equations whose respective velocity keeps the same sign. In tube 1, the quantity $C^1$ is transported with a velocity $F^1 \geq 0$

$$\pi(R^1)^2 \frac{C_k^{1,n+\frac{1}{2}} - C_k^{1,n}}{\Delta t} + \frac{1}{\Delta x}\Big(F_{k+\frac{1}{2}}^{1,n} C_{k+\frac{1}{2}}^{1,n} - F_{k-\frac{1}{2}}^{1,n} C_{k-\frac{1}{2}}^{1,n}\Big) = 0.$$

We use an upwind scheme and then define the numerical fluxes as

$$F_{k+1/2}^{1,n} C_{k+1/2}^{1,n} = F_k^{1,n} C_k^{1,n}$$

which leads us to the scheme

$$\pi(R^1)^2 \frac{C_k^{1,n+\frac{1}{2}} - C_k^{1,n}}{\Delta t} + \frac{1}{\Delta x}\Big(F_k^{1,n} C_k^{1,n} - F_{k-1}^{1,n} C_{k-1}^{1,n}\Big) = 0. \tag{8.19}$$

We point out that the indexes $k+\frac{1}{2}$ and $n+\frac{1}{2}$ do not have the same meaning. The index $k+\frac{1}{2}$ holds for the finite volume notation. $F_{k+\frac{1}{2}}$ represents the water flow at the interface between cells $k$ and $k+1$. The index $n+\frac{1}{2}$ represents an artificial time step between time steps $n$ and $n+1$. In tubes 2 and 7, the quantities $N^1C^2$ and $N^7C^7$ are respectively transported with a velocity $F^2 \leq 0$ and $F^7 \geq 0$. We use an upwind scheme and then define the numerical fluxes as

$$\begin{aligned} F_{k+1/2}^{2,n} N_{k+1/2}^1 C_{k+1/2}^{2,n} &= F_{k+1}^{2,n} N_{k+1}^1 C_{k+1}^{2,n}, \\ F_{k+1/2}^{7,n} N_{k+1/2}^7 C_{k+1/2}^{7,n} &= F_k^{7,n} N_k^7 C_k^{7,n}, \end{aligned}$$

which yields the expressions

$$\pi(R^2)^2 N_k^1 \frac{C_k^{2,n+\frac{1}{2}} - C_k^{2,n}}{\Delta t} + \frac{1}{\Delta x}\Big(F_{k+1}^{2,n} N_{k+1}^1 C_{k+1}^{2,n} - F_k^{2,n} N_k^1 C_k^{2,n}\Big) = -\frac{N_{k+1}^1 - N_k^1}{\Delta x} F_k^{1,n} C_k^{1,n}, \tag{8.20}$$

and

$$\pi(R^7)^2 N_k^7 \frac{C_k^{7,n+\frac{1}{2}} - C_k^{7,n}}{\Delta t} + \frac{1}{\Delta x}\Big(F_k^{7,n} N_k^7 C_k^{7,n} - F_{k-1}^{7,n} N_{k-1}^7 C_{k-1}^{7,n}\Big) = 0. \tag{8.21}$$

Here again, the way the source term is discretized in (8.20) will be justified later. It is written for a discrete version of Proposition 8.1.1 to be satisfied.

### 8.2.5 Treatment of the source term

In the scheme we built for the simplified model in chapter 2, the source term was an obstacle to the positivity of the solutions. For large values of $V_m$, we had to chose a very small $\Delta t$ in order to ensure the positivity. Using a splitting method, we are left to solve a stiff differential equation. So as to avoid the imitations of a stability condition, we decide here to use an implicit scheme for the terms responsible for the stiffness of the differential equation (i.e. the term with

a sign '-' in the source term). Concerning the source term, since it contains a non linear part (corresponding to the active transport term), making it entirely implicit would lead us to invert a function. To avoid this, we only make implicit part of the source term. Thus, to compute the definitive value of the concentration, we use a semi-implicit scheme, written explicitly as follows

$$\begin{aligned}
\pi(R^1)^2\frac{C_k^{1,n+1}-C_k^{1,n+\frac{1}{2}}}{\Delta t} &= J_k^{1,n},\\
\pi(R^2)^2\frac{C_k^{2,n+1}-C_k^{2,n+\frac{1}{2}}}{\Delta t} &= J_{k+1}^{2,n},\\
\pi(R^7)^2\frac{C_k^{7,n+1}-C_k^{7,n+\frac{1}{2}}}{\Delta t} &= J_k^{7,n},
\end{aligned} \tag{8.22}$$

with

$$J_k^{j,n} = \begin{cases} -2\pi R^j P_k^j (C_k^{j,n+1}-C_k^{int,n}) + J_{V,k}^n(1-\sigma_k^j)C_k^{int,n} - V_{m,k}^j R^j \dfrac{C_k^{j,n+1}}{1+C_k^{j,n+\frac{1}{2}}} & \text{if } J_{V,k}^{j,n}>0\\ -2\pi R^j P_k (C_k^{j,n+1}-C_k^{int,n}) + J_{V,k}^{j,n}(1-\sigma_k^j)C_k^{j,n+1} - V_{m,k}^j R^j \dfrac{C_k^{j,n+1}}{1+C_k^{j,n+\frac{1}{2}}} & \text{if } J_{V,k}^{j,n}<0 \end{cases} \tag{8.23}$$

Then we compute the solute flux entering the interstitium and update the interstitial concentration

$$J_k^{int,n} = -J_k^{1,n} - J_k^{2,n} - J_k^{7,n}, \tag{8.24}$$

$$\pi(R_k^{int})^2\frac{C_k^{int,n+1}-C_k^{int,n}}{\Delta t} = J_k^{int,n}. \tag{8.25}$$

### 8.2.6 Main properties

We denote here $N_k^2 = N_k^1$.

**Proposition 8.2.1.** *The scheme is conservative in the sense that*

*i)*

$$\sum_{j=1,2,7} N_k^j F_k^j \qquad \textit{does not depend on } k. \tag{8.26}$$

*ii) At equilibrium (for large values of $n\Delta t$),*

$$\sum_{j=1,2,7} N_k^j F_k^j C_k^j \qquad \textit{does not depend anymore on } k. \tag{8.27}$$

*Proof.* To demonstrate the conservation property, by adding and subtracting artificially to the first equation the term $\dfrac{N_{k-1}^1}{\Delta x}F_{k-1}^1$, we write the scheme on the flow as

$$\begin{cases} \dfrac{N_k^1F_k^{1,n}-N_{k-1}^1F_{k-1}^{1,n}}{\Delta x} = N_k^1J_{V,k}^{1,n} + \dfrac{N_k^1-N_{k-1}^1}{\Delta x}F_{k-1}^1,\\ \dfrac{N_k^1F_k^{2,n}-N_{k-1}^1F_{k-1}^{2,n}}{\Delta x} = N_k^1J_{V,k}^{2,n} - \dfrac{N_k^1-N_{k-1}^1}{\Delta x}F_{k-1}^1,\\ \dfrac{N_k^7F_k^{7,n}-N_{k-1}^7F_{k-1}^{7,n}}{\Delta x} = N_k^7J_{V,k}^{7,n}. \end{cases}$$

We sum on the lines and obtain

$$\forall k \in [2, N],\ \Big(N_k^1 F_k^{1,n} + N_k^1 F_k^{2,n} + N_k^7 F_k^{7,n}\Big) - \Big(N_{k-1}^1 F_{k-1}^{1,n} + N_{k-1}^1 F_{k-1}^{2,n} + N_{k-1}^7 F_{k-1}^{7,n}\Big) = 0$$

and (8.26) holds.

Using a similar approach, it can be shown that the scheme satisfies solute conservation (8.27) at steady state (for large t values). This property represents mass conservation at the discrete level and can be used as a criterion to determine when the system has reached steady state. □

We now state a stability result under a CFL condition and a stability condition.

**Proposition 8.2.2.** *Under the CFL [15] condition*

$$\Delta t \leq \Delta x \min_{j=1,2,7} \Big(\frac{\pi (R^j)^2}{\max_k |F_k^{j,n}|}, \tag{8.28}$$

*and the stability condition*

$$\Delta t \leq \min_k \left(\frac{1}{\sum_{j=1,2,7} \Big(2\pi R^j P_k^j + |J_{V,k}^j|(1-\sigma_k^j)\Big)}\right), \tag{8.29}$$

*the scheme preserves the positivity of the concentrations.*

The condition on the time step is divided in two parts. Condition (8.28) corresponds to the CFL [15] condition, which is the condition coming from the transport part of the system. It means that the discrete velocity $\dfrac{\Delta x}{\Delta t}$ has to be larger than the longitudinal (i.e. in the $x$ direction) fluid velocity which is $\dfrac{F^j}{\pi (R^j)^2}$, expressed in m.s$^{-1}$.

*Proof.* We prove that for any $n$,

$$\Big(\forall j = 1,2,7, int,\ \forall k \in [1,N],\ C_k^{j,n} \geq 0\Big) \ \Rightarrow\ \Big(\forall j = 1,2,7, int,\ \forall k \in [1,N],\ C_k^{j,n+1} \geq 0\Big).$$

We already know that, because of the semi-implicit scheme,

$$\Big(\forall j = 1,2,7, int,\ \forall k \in [1,N],\ C_k^{j,n+\frac{1}{2}} \geq 0\Big) \ \Rightarrow\ \Big(\forall j = 1,2,7, int,\ \forall k \in [1,N],\ C_k^{j,n+1} \geq 0\Big).$$

We are then left to prove that the scheme on the transport equation preserves positivity.

To guarantee the positivity of $C_k^{j,n+\frac{1}{2}}$, we write it as combination of $C_{k-1}^{j,n}, C_k^{j,n}$ and $C_k^{j,n}$ and we make sure the coefficient of each term is nonnegative.

**First step.** The concentration inside the tubes.

We have

$$C_k^{1,n+\frac{1}{2}} = \Big(1 - \frac{\Delta t}{\Delta x}\frac{F_k^{1,n}}{\pi (R^1)^2}\Big) C_k^{1,n} + \frac{\Delta t}{\Delta x}\frac{F_k^{1,n}}{\pi (R^1)^2} C_{k-1}^{1,n}.$$

Thus we impose

$$\forall k \in [1,N], \qquad \Delta t \leq \Delta x \frac{\pi (R^1)^2}{F_k^{1,n}} \tag{8.30}$$

For tube 2,

$$C_k^{2,n+\frac{1}{2}} = \Big(1 + \frac{\Delta t}{\Delta x}\frac{F_k^{2,n}}{\pi (R^2)^2}\Big) C_k^{2,n} - \frac{\Delta t}{\Delta x}\frac{N_{k+1}^2 F_{k-1}^{2,n}}{N_k^2 \pi (R^2)^2} C_{k+1}^{2,n} - \frac{\Delta t}{\Delta x}\frac{(N_{k+1}^1 - N_k^1) F_k^{1,n}}{N_k^1 \pi (R^2)^2} C_k^{1,n}.$$

Since $F_k^2 \leq 0$ for all $k \in [1, N]$, we obtain the condition

$$\forall k \in [1, N], \qquad \Delta t \leq \Delta x \frac{\pi (R^2)^2}{|F_k^{2,n}|}. \tag{8.31}$$

For tube 7,

$$C_k^{7,n+\frac{1}{2}} = \Big(1 - \frac{\Delta t}{\Delta x} \frac{F_k^{7,n}}{\pi (R^7)^2}\Big) C_k^{7,n} + \frac{\Delta t}{\Delta x} \frac{N_{k-1}^7 F_{k-1}^{7,n}}{N_k^7 (R^7)^2} C_{k-1}^{7,n}.$$

Thus we impose

$$\forall k \in [1, N], \qquad \Delta t \leq \Delta x \frac{\pi (R^7)^2}{F_k^{7,n}}. \tag{8.32}$$

Combining the constraints (8.30), (8.31) and (8.32) gives (8.28).

**Second step.** The interstitial concentration.

We write

$$C_k^{int,n+1} = \Big(1 - \Delta t \Big( \sum_{j=1,2,7} 2\pi R^j P_k^j + \sum_{j | J_{V,k}^{j,n} > 0} J_{V,k}^{j,n} (1 - \sigma_k^j) \Big) \Big) C_k^{int,n} + \text{ positive terms}$$

and then $C_k^{int,n+1}$ is positive under the stability condition (8.29). □

## Flow reversal

Moore and Marsh [63] raised the issue of the instability of usual schemes for realistic parameter values. Indeed, the high permeability to water in some tube segments can result in very large water movements across those segments. If enough water is extracted from the tube, water flow can reverse direction during the dynamic process thereby rendering the numerical method unstable. The method they were using did not deal with this problem and forced them to consider lower values of the water permeability $L_P$. To avoid numerical instabilities arising from reversal of flow, other authors [88] prevent this phenomenon from appearing by diminishing the water flux when it becomes so high that a flow reversal occurs. To deal with flow reversal, we have to consider a model which takes it into account, and not a model which tacitly assumes that water always flows in the same direction. Such a model is described in Chapter 7. Thus, to compute the shunted water flow and the shunted solute flow between the descending vasa recta and the ascending vasa recta, we must take into account the direction of water flow in both DVR and AVR. Numerically, to compute $F^{DVR}$, we must know at least the sign of $F^{AVR}$. We cannot anymore compute $F^{DVR}$ from $x = 0$ to $L$ and then compute $F^{AVR}$ from $x = L$ to 0, but instead, we have to compute directly and simultaneously the entire vectors $F^{DVR}$ and $F^{AVR}$. And they are solutions to a N-dimensional non linear operator, where $N$ is the size of the space discretization. In our case, when flow reversal occurs, even if by any chance the scheme remains stable, the dynamic solution we get has no real meaning, because we are out of the bounds of the model. However, for a certain set of initial conditions, we notice that flow reversal can occur. In that case, we stop the simulation and start with other initial conditions.

# Chapter 9

# Results and physiological conclusions

This chapter is inspired from the last part of the paper

M. Tournus, N. Seguin, B. Perthame, S.R. Thomas, and A. Edwards. A Model of Calcium Transport along the Rat Nephron. *Accepted in the American Journal of Physiology*, 2013.

*Calcium is known to be reabsorbed passively in the thick ascending limb, and actively in the distal convoluted (DCT) and connecting (CNT) tubules. Our model predicts that the passive diffusion of $Ca^{2+}$ from the loop of Henle generates a significant axial $Ca^{2+}$ concentration gradient in the medullary interstitium. In the base case, the urinary $Ca^{2+}$ concentration and fractional excretion are predicted as 2 mM and 0.5%, respectively. Urinary $Ca^{2+}$ excretion is found to be strongly modulated by water and NaCl reabsorption along the nephron. Our simulations also suggest that $Ca^{2+}$ molar flow and concentration profiles differ significantly between superficial and deep nephrons, such that the latter deliver less $Ca^{2+}$ to the collecting duct. Finally, our results suggest that the DCT and CNT can act to counteract upstream variations in $Ca^{2+}$ transport, but not always sufficiently to prevent hypercalciuria.*

We present here and analyze the results we obtain from the numerical scheme described in Chapter 8 when steady state is reached.

## 9.1 Results on the osmolality profiles

Base case steady state profiles of sodium concentration, urea concentration, and total osmolality in medullary segments are similar to those of the HT model. The osmolality of the tubular fluid at the outlet of the collecting duct is predicted as 1280 mosM (with an external osmole concentration of 80 mM in the IM). Shown in Figure 9.1 is the osmolality profile of the tubular fluid in cortical distal segments. The fluid exiting the mTAL is significantly hypo-osmotic relative to plasma, following the massive reabsorption of NaCl that occurs in that water-impermeable segment. In the cTAL, which is similarly water-impermeable, the osmolality of the fluid is predicted to remain nearly constant, as the passive secretion of urea approximately counterbalances the active reabsorption of NaCl. The reabsorption of water resumes in the DCT, along which the tubular fluid osmolality rises accordingly. It increases more steeply in the CNT, the water permeability of being greater than that of the DCT. Osmotic equilibration is predicted to occur very early in the CCD. Note that osmolality profiles differ significantly between the superficial and deep nephrons (9.2), since the latter have a shorter cTAL, and a longer CNT. We assumed that the water permeability of the DCT and CNT is 4 times lower in deep nephrons than in superficial ones (Table 7.2), so as to avoid luminal fluid depletion in the former. Along the CCD, the tubular fluid osmolality is predicted to be stable.

As we mentioned in the Introduction, the urinary concentrating mechanism is not completely elucidated yet, and the predicted gradient in the inner medulla is due to the external osmole we add in the interstitium. Since we are interested in calcium profiles and since calcium profiles are determined by the profiles of other solutes, we keep the hypothesis of the external osmole. We plot the osmolarity profile without considering the exteranl osmole on Figure 9.3.

## 9.2 Results concerning calcium

We first examined $Ca^{2+}$ flow and concentration profiles along the nephron under baseline conditions. We then simulated scenarios under which $Ca^{2+}$ handling by specific segments is altered, to investigate how our kidney model overall responds to such changes.

### 9.2.1 Base case $Ca^{2+}$ concentration profiles

Medullary and cortical calcium concentration ($[Ca^{2+}]$) profiles at steady state are shown in Figure 9.4.

In the longest descending limb, the predicted $[Ca^{2+}]$ increases several-fold between the cortico-medullary (CM) junction and the papillary tip, because of massive water reabsorption. The permeability of the DL to $Ca^{2+}$ is small but not negligible ($0.7 \times 10^{-5}$ cm/s), allowing for some passive diffusion of $Ca^{2+}$ into the interstitium, but the latter is too small to counteract the effect of water abstraction. Along the water-impermeable ascending limb, $[Ca^{2+}]$ decreases due to passive $Ca^{2+}$ reabsorption. In the thick portion of the limb, the lumen-positive transepithelial voltage gradient ($\Delta V_{TE} = +15$ mV) greatly increases the driving force for $Ca^{2+}$ transport. Overall, the luminal concentration of $Ca^{2+}$ in the ascending limb is predicted to decrease by 40% between the papillary tip and the CM junction, and then more abruptly in the cTAL because this segment is significantly more permeable to $Ca^{2+}$. Note that the concentration of $[Ca^{2+}]$ decreases more in the cTAL of superficial nephrons, since the latter is taken to be 5 times longer than that of deep nephrons.

In the DCT, even though passive diffusion favors $Ca^{2+}$ secretion (since $\Delta V_{TE} < 0$ and $[Ca^{2+}]$ is lower in the lumen than in the interstitium), active transport mechanisms predominate and

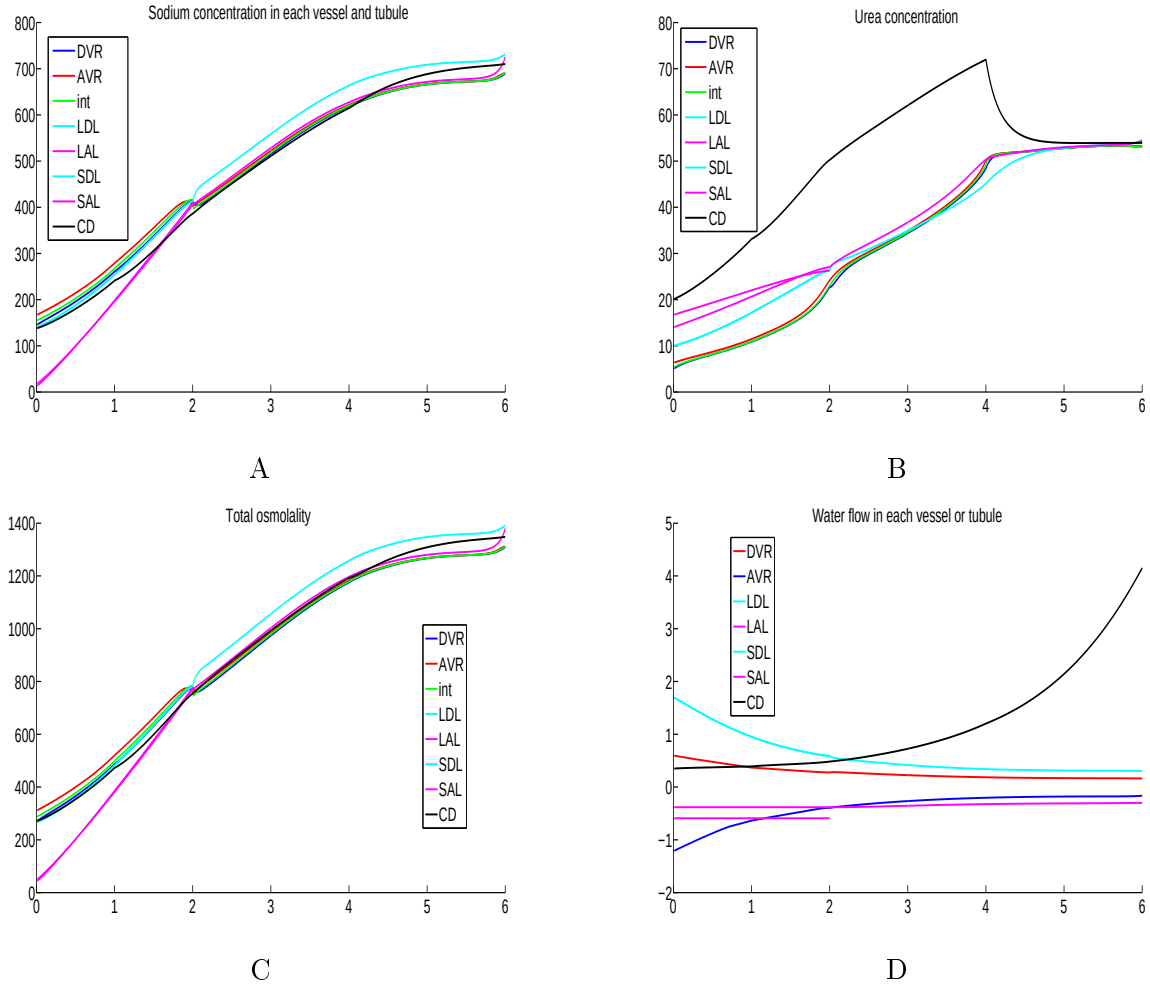


**Figure 9.1:** A : Sodium concentration is the medulla, B: Urea concentration in the medulla, C: Total osmolarity in the medulla, D: Water flows in the medulla. The x-axis represents the depth along the medulla, in $mm$. Concentration are plotted in $mM$, and water flows are plotted in $m`3.s^{-1}$

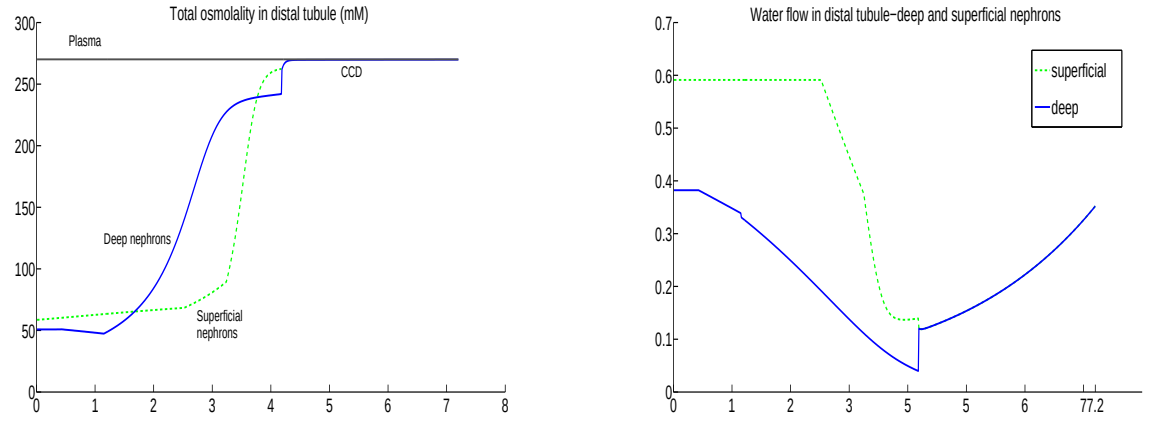


**Figure 9.2:** The $x-$axis represents the length along the distal tubule, in $mm$. Left : Osmolarity in distal, in $mM$. Right : Water flow in distal, in $m^3.s^{-1}$.

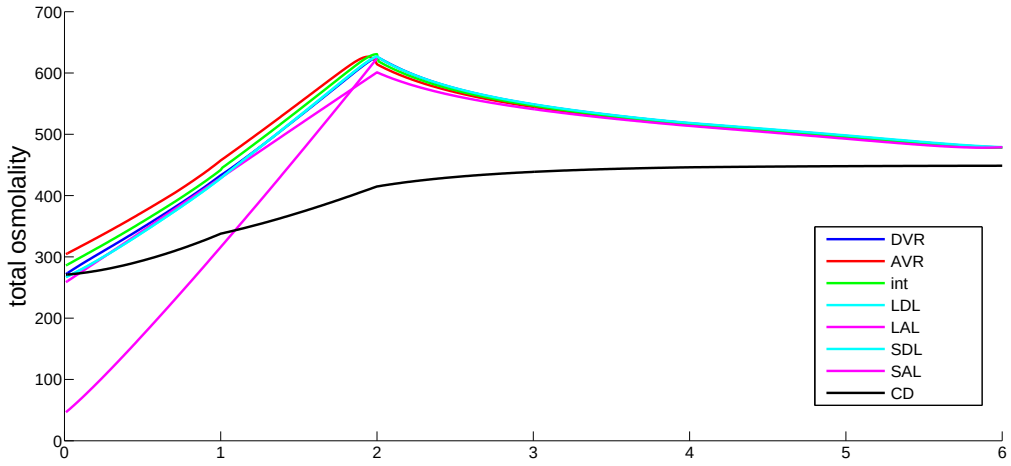


**Figure 9.3:** Total osmolarity in the medulla without the external osmole ($E = 0$), in $mM$. The $x-$axis represents the depth along the medulla in $mm$.

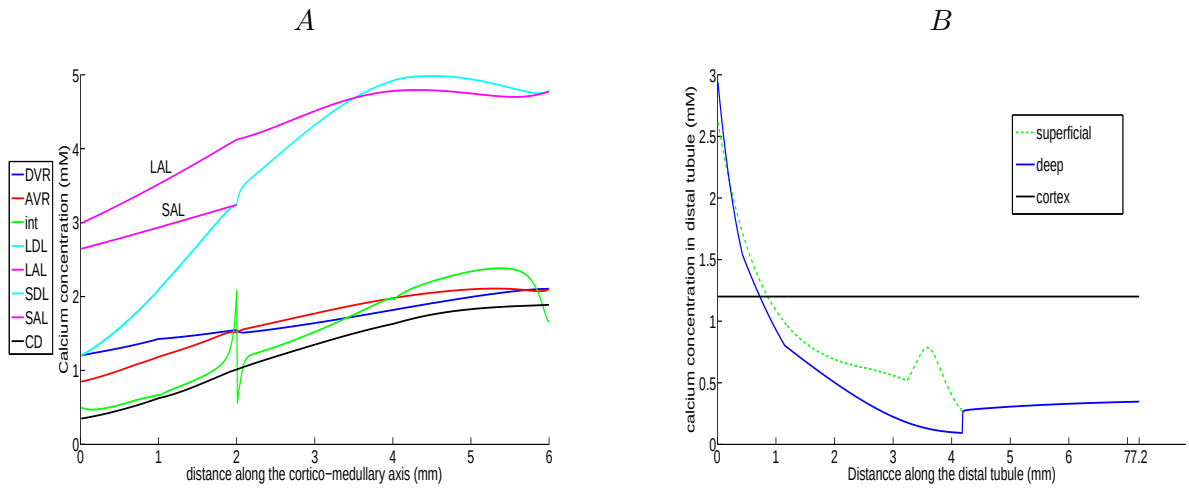


**Figure 9.4:** Left : Calcium concentration in medullary tubules, vessels and in the interstitium. Right : Calcium concentration in the cortical distal tubules emanating from long and short limbs.

[$Ca^{2+}$] decreases at rate that is similar in deep and superficial nephrons. In the CNT, [$Ca^{2+}$] continues to be actively reabsorbed. As described above, the fluid entering the cortical distal tubules is significantly hypo-osmotic. In superficial nephrons, the model predicts a significant increase in [$Ca^{2+}$] in the first half of the CNT (in spite of active reabsorption), because of massive water abstraction. Beyond the mid-point, the rate of water reabsorption decreases and [$Ca^{2+}$] resumes its downward trajectory. In the CNT of deep nephrons, where water is reabsorbed less rapidly, [$Ca^{2+}$] is predicted to decrease monotonically.

In the model configuration, the superficial and deep nephrons meet at the CCD entrance. Solute concentrations at the CCD inlet are therefore a weighted average between the CNT outlet concentrations of deep and superficial nephrons. The collecting duct (cortical and medullary) reabsorbs very little $Ca^{2+}$ passively, and none actively. The predicted [$Ca^{2+}$] increase along the medullary collecting duct is solely due to water abstraction.

We assumed that the vasa recta are permeable to $Ca^{2+}$. The model predicts that [$Ca^{2+}$] increases along DVR, even though there is some passive $Ca^{2+}$ diffusion into the interstitium, because of water reabsorption (as in descending limbs). Similarly, the predicted [$Ca^{2+}$] decrease in AVR is predominantly driven by water uptake.

### 9.2.2 Base case $Ca^{2+}$ molar flow

The molar flow rate of $Ca^{2+}$ at steady state is displayed in Figure 9.5.

Note that the molar flow per tubule can vary solely as a result of variations in tubule number, that is, even when there is no transmembrane solute transport. Such effects are particularly manifest in the collecting ducts, which exchange very little $Ca^{2+}$ with the interstitium; yet, because the model represents 64 CDs that converge to a single CD in the inner medulla [34], the $Ca^{2+}$ molar flow per tubule increases steeply along the IMCD. A similar phenomenon occurs in those vessels and tubules that turn at varying depths along the medullary axis. In the thin ascending limbs for instance, the $Ca^{2+}$ molar flow per tubule increases in the direction of the flow largely because the descending limbs that turn back at different levels reinject $Ca^{2+}$ into the AL lumen. We refer to this factor hereafter as the "coalescing" or "shunting" effect.

As shown in Figure 9.5, the $Ca^{2+}$ load diminishes from 12 to 9 pmol/min/tubule along the longest descending limb. In the outer medulla, where the number of DL does not vary, this decrease results from passive diffusion into the interstitium. In the inner medulla, a fraction of long DL turns back at each depth, and the shunting effect contributes significantly to the decrease in the $Ca^{2+}$ load per tubule.

In the thin ascending limb, the concentration gradient of $Ca^{2+}$ favors passive $Ca^{2+}$ reabsorption. Nevertheless, the $Ca^{2+}$ load per tubule rises, as a result of the shunting effect described above. This effect is absent in mTALs, the number of which remains constant. In addition, the driving force for passive $Ca^{2+}$ reabsorption is enhanced by the lumen-positive voltage gradient. As a result, the $Ca^{2+}$ load per tubule decreases significantly in mTALs. As mentioned above, the rate of passive $Ca^{2+}$ reabsorption rises further along cTALs, since they are several-fold more permeable to $Ca^{2+}$ than mTALs.

In deep nephrons, the load of $Ca^{2+}$ entering the DCT is predicted as 4 pmol/min/tubule. Following active reabsorption, it drops to 0.0017 pmol/min/tubule at the CNT outlet. In superficial nephrons, whose cTAL is much longer, the $Ca^{2+}$ load at the DCT entrance is lower (about 2.5 pmol/min/tubule). Conversely, the $Ca^{2+}$ molar flow does not decrease as much along the DCT and CNT (relative to deep nephrons), because the latter segment is much shorter.

Along the collecting duct, a very small amount of $Ca^{2+}$ is reabsorbed, so that the total $Ca^{2+}$ molar flow rate diminishes slightly. However, the $Ca^{2+}$ load per tubule increases steeply because the collecting ducts merge (i.e., the coalescing effect).

Base results are summarized in Table 9.1. The concentration of $Ca^{2+}$ at the CD outlet ($C_{out}$) is predicted to be 2.0 mM and the $Ca^{2+}$ molar flow at that point represents 0.46% of the filtered load.

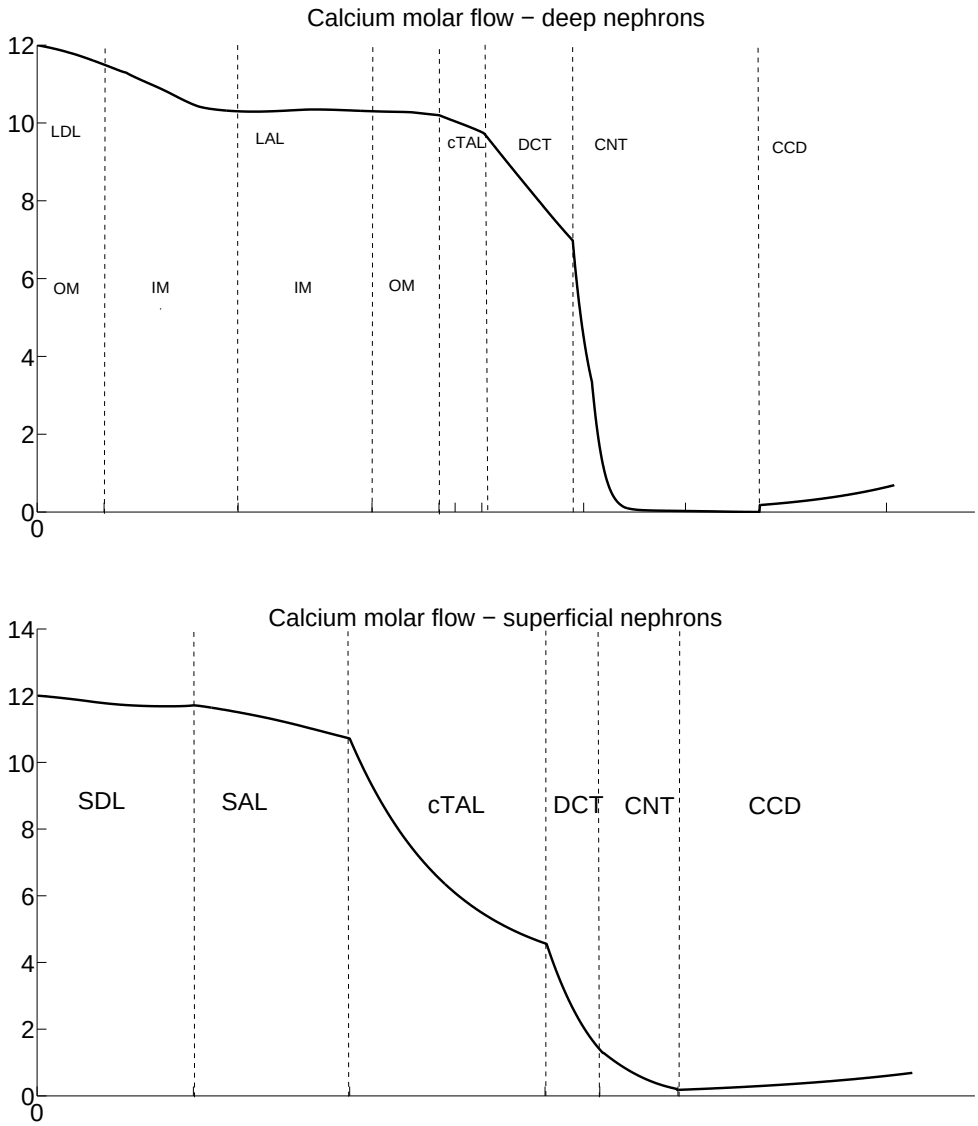


**Figure 9.5:** Predicted $Ca^{2+}$ molar flow per tubule at steady-state. in deep (upper panel) and superficial (bottom panel) nephrons, from the descending limb to the end of the cortical collecting duct. Calcium molar flow is expressed in $mol.s^{-1}$.

| | Superficial nephrons Fractional $Ca^{2+}$ load delivered to | | | | Deep nephrons Fractional $Ca^{2+}$ load delivered to | | | |
|---|---|---|---|---|---|---|---|---|
| | mTAL | cTAL | DCT | CCD | mTAL | cTAL | DCT | CCD |
| Base case | 31.07 | 25.62 | 6.28 | 0.61 | 25.93 | 19.23 | 10.32 | 0.01 |
| Filtered load of $Ca^{2+}$ × 2 | 31.13 | 25.94 | 6.72 | 1.04 | 26.61 | 20.45 | 11.80 | 0.035 |
| No $Ca^{2+}$ transport in mTAL | 30.78 | 30.78 | 6.54 | 0.66 | 25.70 | 25.69 | 13.23 | 0.02 |
| No $Ca^{2+}$ transport in cTAL | 31.07 | 25.63 | 25.62 | 4.39 | 25.97 | 19.30 | 19.30 | 0.02 |
| No $Ca^{2+}$ transport in mTAL and cTAL | 30.80 | 30.78 | 30.78 | 6.37 | 25.76 | 25.75 | 25.75 | 0.030 |
| No active $Ca^{2+}$ transport in DCT-CNT | 31.07 | 25.65 | 6.33 | 6.63 | 26.05 | 19.42 | 10.54 | 9.21 |
| No voltage gradient in DCT-CNT | 31.07 | 25.62 | 6.28 | 0.48 | 25.93 | 19.23 | 10.32 | 0.00 |
| No passive $Ca^{2+}$ transport in DCT-CNT | 31.07 | 25.62 | 6.28 | 0.44 | 25.93 | 19.23 | 10.32 | 0.00 |
| No $Ca^{2+}$ transport in cortical CD | 31.07 | 25.62 | 6.28 | 0.61 | 25.93 | 19.23 | 10.32 | 0.01 |
| No $Ca^{2+}$ transport in medullary CD | 31.07 | 25.62 | 6.29 | 0.62 | 25.94 | 19.24 | 10.32 | 0.01 |
| No external osmolytes in IM ($E = 0$) | 31.29 | 26.84 | 8.33 | 1.64 | 31.27 | 27.62 | 21.58 | 7.47 |

**Table 9.1:** Effects of perturbations in $Ca^{2+}$ transport on $Ca^{2+}$ reabsorption along the nephron. Note that the fractional load reabsorbed along a given segment is the difference between the fractional load delivered to that segment and that delivered to the one immediately downstream.

### 9.2.3 Sensitivity analysis

Most parameter values were taken from experimental studies, except the following: the permeability of vasa recta to $Ca^{2+}$, which has not been measured to our knowledge, and the macroscopic parameters that describe the rate of active $Ca^{2+}$ transport in the DCT-CNT. Table 9.2 illustrates the model sensitivity to selected values.

| | Fractional urinary $Ca^{2+}$ excretion | Urinary $Ca^{2+}$ concentration (mM) | CD fluid osmolality at papillary tip (mosM) |
|---|---|---|---|
| Base case | 0.46 | 2.03 | 1300 |
| Calcium permeability of vasa recta | | | |
| VR permeability × 2 | 0.45 | 2.05 | 1300 |
| VR permeability × 0.5 | 0.46 | 2.01 | 1300 |
| Active calcium reabsorption in DCT/CNT | | | |
| $V^d_{m,Ca}$ × 2 | 0.12 | 0.53 | 1320 |
| $V^d_{m,Ca}$ × 0.5 | 1.47 | 6.36 | 1320 |
| $K^d_{m,Ca}$ × 2 | 1.31 | 5.69 | 1320 |
| $K^d_{m,Ca}$ × 0.5 | 0.12 | 0.56 | 1320 |
| External osmolyte in inner medullary interstitium | | | |
| E × 1.1 | 0.42 | 2.43 | 1480 |
| E × 0.9 | 0.60 | 1.63 | 1110 |

**Table 9.2:** Sensitivity analysis

**Active transport.** Our model represents the epithelial layer as a single barrier, and we used Michaelis-Menten equations to describe the active transport of $Ca^{2+}$. The corresponding parameters, that is, the maximal rate of active $Ca^{2+}$ reabsorption in the DCT/CNT ($V^d_{m,Ca}$) and the $Ca^{2+}$ concentration at which the rate is half its maximal value ($K_{m,Ca}$) were fitted so that the urinary concentration of calcium would be on the order of 2 mM, as observed experimentally [12]. Not surprisingly, model results are very sensitive to $V_{m,Ca}$ and $K_{m,Ca}$. A 2-fold increase in $V^d_{m,Ca}$ would reduce the fractional $Ca^{2+}$ excretion by a factor of 4 (to 0.12%), and $C_{out}$ to a similar extent (to 0.53 mM). Conversely, a 2-fold decrease in $V^d_{m,Ca}$ would raise the fractional $Ca^{2+}$ excretion and $C_{out}$ approximately 3-fold. In addition, a 2-fold decrease in $K^d_{m,Ca}$ would have comparable effects on $Ca^{2+}$ transport as a 2-fold decrease in $V^d_{m,Ca}$, and vice-versa.

**External osmole.** The concentration of the external osmole in the inner medulla ($E$) has a large impact on the IM osmolality gradient, which is subsequently reflected in the $Ca^{2+}$ concentration at the CD outlet. As shown in Table 9.2, a 10% increase in $E$ would raise $C_{out}$ by 20% without affecting much the fractional $Ca^{2+}$ excretion. In contrast, a 10% decrease in $E$ would raise the fractional $Ca^{2+}$ excretion by 25% and lower $C_{out}$ by 20%.

### 9.2.4 Interstitial $Ca^{2+}$ concentration gradient

At steady-state, $Ca^{2+}$ diffuses from the loops of Henle and DVR into the interstitium, from which it is carried into AVR by convection. Our model thus predicts a significant interstitial [$Ca^{2+}$] gradient along the medullary axis. If the permeability of all vessels and tubules to $Ca^{2+}$ were zero, the gradient would vanish (results not shown). To assess the relative contribution of each structure, we computed the average interstitial [$Ca^{2+}$] in the OM and IM following a 2-fold increase in the $Ca^{2+}$ permeability of selected tubules and vessels. As illustrated in Figure 9.4, interstitial [$Ca^{2+}$] values are mostly determined by the $Ca^{2+}$ permeability of the descending and ascending limbs, and by that of the vasa recta to a lesser extent. The contribution of the CD is negligible.

As displayed in Figure 9.6, the predicted interstitial [$Ca^{2+}$] profile exhibits a sharp spike at the OM-IM boundary. This spike stems from abrupt changes in several parameter values at that point (especially in the transepithelial voltage gradient), in combination with the manner in which the interstitial $Ca^{2+}$ concentration ($C_{Ca}^{int}$) is computed. As opposed to other variables, $C_{Ca}^{int}$ is determined by an equation that does not contain a spatial derivative, which would act to smooth variations; as a result, the interstitial $C_{Ca}^{int}$ profile echoes spatial discontinuities in model parameters.

### 9.2.5 Effects of local perturbations

We then sought to investigate the specific contribution of each nephron segment in maintaining the renal $Ca^{2+}$ balance. For this purpose, we simulated alterations in the $Ca^{2+}$-transport properties of tubules and examined their impact on urinary $Ca^{2+}$ excretion. Corresponding results are summarized in Tables 9.1 and 9.3.

| | Fractional $Ca^{2+}$ load delivered to CCD | Fractional urinary $Ca^{2+}$ excretion | Urinary $Ca^{2+}$ concentration (mM) | CD fluid osmolality at papillary tip (mosM) |
|---|---|---|---|---|
| Base case | 0.59 | 0.46 | 2.03 | 1240 |
| Filtered load of $Ca^{2+}$ ×2 | 1.16 | 0.81 | 4.71 | 1050 |
| No $Ca^{2+}$ transport in mTAL | 0.64 | 0.49 | 2.05 | 1300 |
| No $Ca^{2+}$ transport in cTAL | 4.21 | 2.96 | 12.55 | 1300 |
| No $Ca^{2+}$ transport in mTAL and cTAL | 6.10 | 4.26 | 16.8 | 1250 |
| No voltage gradient in DCT-CNT | 0.46 | 0.37 | 1.62 | 1300 |
| No passive $Ca^{2+}$ transport in DCT-CNT | 0.43 | 0.34 | 1.53 | 1250 |
| No active $Ca^{2+}$ transport in DCT-CNT | 10.56 | 7.36 | 29.57 | 1300 |
| No $Ca^{2+}$ transport in cortical CD | 0.59 | 0.42 | 1.85 | 1300 |
| No $Ca^{2+}$ transport in medullary CD | 0.59 | 0.46 | 2.02 | 1300 |
| No external osmolytes in IM | 5.07 | 3.59 | 1.08 | 550 |

**Table 9.3:** Effects of perturbations in $Ca^{2+}$ transport on the composition of the CD luminal fluid at the papillary tip.

**Calcium handling along the nephron**

The base case assumes that the filtered load of calcium equals 36 pmol/min/tubule, two-thirds of which are reabsorbed in the proximal tubule. Thus, 12 pmol/min are delivered to each descending limb. If the latter amount is increased by a factor of 2, the fractional $Ca^{2+}$ load at the mTAL entrance is predicted to remain approximately unchanged (Table 9.1), which means

that in absolute terms, the DL and thin AL reabsorb twice as much calcium as in the base case. The mTAL and cTAL also reabsorb about the same proportion of the $Ca^{2+}$ load as in the base case. Hence, the fractional $Ca^{2+}$ load at the DCT-CNT entrance is less than 2% higher than in the base case. In absolute terms, however, the $Ca^{2+}$ load and concentration at that point remain about 2-fold higher.

The DCT and CNT adapt to this increased load by increasing the rate at which $Ca^{2+}$ is actively reabsorbed. Yet, they are not able to fully adjust, and the fractional $Ca^{2+}$ load that is delivered to the CCD is predicted to double relative to the base case (Table 9.3). In the absence of compensating mechanisms in the collecting duct, the urinary concentration of $Ca^{2+}$, as reflected by $C_{out}$, increases more than 2-fold.

**Calcium handling by the TAL**

The mTAL is generally thought to reabsorb insignificant amounts of $Ca^{2+}$ relative to the cTAL [40]. Based on flux measurements [83], we assumed that the mTAL is 10 times less permeable to $Ca^{2+}$ than the cTAL. We found that this is sufficient to mediate some passive $Ca^{2+}$ reabsorption in the mTAL (6% of the filtered load in the base case), given the large, lumen-positive $\Delta V_{TE}$. When the mTAL permeability to $Ca^{2+}$ was set to zero, the cTAL, DCT and CNT each acted to compensate for the absence of $Ca^{2+}$ reabsorption in the mTAL, as shown in Table 9.1, and $C_{out}$ was very close to its base case value (Table 9.3).

When the cTAL permeability to $Ca^{2+}$ was set to zero, the DCT and CNT also increased the active reabsorption of $Ca^{2+}$, but not enough to fully offset the absence of reabsorption in the cTAL. In superficial nephrons, whose CNT is relatively short, the $Ca^{2+}$ load at the CNT outlet was more than 7 times higher than in the base case. As a consequence, $C_{out}$ was predicted to be $>$ 10 mM (Table 9.3). When the entire TAL was made impermeable to $Ca^{2+}$, the predicted hypercalciuria was even more severe. Even though the DCT and CNT together reabsorbed 2-4 times more $Ca^{2+}$ than in the base case (Table 9.1), this did not suffice to compensate for the absence of reabsorption upstream, and the fractional excretion of $Ca^{2+}$ was 10 times higher.

**Calcium handling by the DCT-CNT**

The renal excretion of $Ca^{2+}$ is fine-tuned in the DCT and CNT, wherein $Ca^{2+}$ reabsorption is an active process that is mediated apically by transient receptor potential vanilloid 5 (TRPV5) channels, and basolaterally by type 1 $Na^{+}$-$Ca^{2+}$ exchangers and plasma membrane $Ca^{2+}$ pumps. Assuming that the passive permeability of the rat DCT and CNT to $Ca^{2+}$ is $0.1\times10^{-5}$ cm/s [80], the model predicts that the backflux of $Ca^{2+}$ into these segments is not negligible, as the lumen-negative transepithelial voltage gradient favors $Ca^{2+}$ secretion into the lumen. To assess the importance of this backflux, we set $\Delta V_{TE}$ to zero in the DCT and CNT. As shown in Table9.3, the fractional $Ca^{2+}$ load delivered to the CCD then decreased from 0.59% to 0.46%, and $C_{out}$ from 2.0 to 1.5 mM. When passive diffusion was fully abolished in the DCT and CNT (i.e., when the $Ca^{2+}$ permeability of these segments was set to zero), the delivery of $Ca^{2+}$ to the CCD and $C_{out}$ decreased slightly more (Table 9.3). These results indicate that the back-flux of $Ca^{2+}$ into the DCT and CNT lumen may not negligible, and that it is predominantly driven by the transepithelial electric potential difference.

We next simulated the full inhibition of active $Ca^{2+}$ transport in the DCT and CNT, by setting $Vm^{d}_{Ca}$ to zero. Owing to water abstraction, the luminal concentration of $Ca^{2+}$ then increased continuously downstream from the cTAL, and the model predicted a massive increase in urinary $Ca^{2+}$ excretion in the absence of compensating mechanisms along the CD (Table 9.3).

**Calcium handling by the CD**

The luminal concentration of $Ca^{2+}$ increases by a factor of $\sim$ 10 along the collecting duct, primarily as a result of water reabsorption. In the base case, the exchange of $Ca^{2+}$ between the CD and the interstitium is negligible; as shown in Figure 9.6, setting the $Ca^{2+}$ permeability of the cortical or medullary CD to zero has a minimal impact on urinary $Ca^{2+}$ excretion. It should be noted that one experimental study suggested the existence of an active $Ca^{2+}$ reabsorption mechanism in the medullary collecting duct. Magaldi et al. [61] measured a $Ca^{2+}$ flux in the

IMCD in the absence of significant chemical and electric potential gradients, and showed that $Ca^{2+}$ reabsorption was $Na^+$-dependent. Based upon their results, we estimated the $Ca^{2+}$ flux to be on the order of 2 pmol/min/mm tubule in the IMCD, which is comparable to measured values in the CNT [14]. We thus performed simulations in which the rate of active $Ca^{2+}$ transport in the IMCD was taken to be equal to (case 1), of double that (case 2) in the DCT and CNT. All else being equal, the predicted $C_{out}$ was 1.40 mM in case 1, and 0.95 mM in case 2.

To examine whether active $Ca^{2+}$ transport in the IMCD could act to compensate for dysfunctions upstream, we then eliminated the reabsorption of $Ca^{2+}$ in the DCT and CNT. Under these conditions, $C_{out}$ was computed as 24.8 mM in case 1, and 20.1 mM in case 2. These results suggest that if $Ca^{2+}$ reabsorption could indeed be induced in the IMCD, it would only counterbalance slightly $Ca^{2+}$ transport defects upstream.

## 9.3 Conclusion

**Calcium transport in deep versus superficial nephrons**

Our model distinguishes between superficial and deep nephrons, and predicts distinct flow and concentration profiles in each type. In regards to $Ca^{2+}$ transport specifically, our results suggest that not only the amount of $Ca^{2+}$ that is delivered to the medullary thick ascending limb, but also the fractional load of $Ca^{2+}$ that is reabsorbed along the downstream segments, vary significantly between deep and superficial nephrons. The model predicts that 19% of the filtered $Ca^{2+}$ load reaches the cTAL in deep nephrons (vs. 26% in superficial nephrons), and that the cTAL and DCT-CNT each reabsorb 9% and 10% of the load in deep nephrons (vs. 19% and 6% in superficial nephrons). Thus, the $Ca^{2+}$ molar flow and concentration profiles differ significantly in the distal segments emanating from long and short mTALs, up until the point where they merge. Whether this is indeed the case in vivo remains to be determined experimentally.

**Calcium reabsorption in the mTAL**

It is generally thought that $Ca^{2+}$ reabsorption is negligible in the mTAL under base conditions [40]. Interestingly, one study showed that the presence of bicarbonate enhances the mTAL $Ca^{2+}$ flux [99], whereas most perfusion studies are performed in the absence of $HCO_3^-$. Based on flux measurements, we assumed here that the mTAL permeability to $Ca^{2+}$ is one tenth that of the cTAL. Despite the 1:10 permeability ratio, in deep nephrons, the mTALs are predicted to reabsorb almost as much $Ca^{2+}$ as the cTALs (6% of the filtered load of, vs. 8%). This is because (a) the longest mTAL is taken to be 4 times longer than the cTAL in deep nephrons, and (b) the transepithelial $Ca^{2+}$ concentration gradient is more favorable to reabsorption in the medulla than in the cortex. However, we also found that in the absence of $Ca^{2+}$ reabsorption in the mTAL, the cTAL reabsorbs a significantly higher fraction of the filtered load. Since the DCT and CNT also do so, the concentration of $Ca^{2+}$ at the CD outlet is not much affected (Table 9.3). These results suggest that $Ca^{2+}$ transport dysfunctions in the mTAL may not, per se, significantly affect the urinary excretion of $Ca^{2+}$.

**Role of the DCT and CNT**

Our model predicts that the DCT and CNT are able to adjust to changes in $Ca^{2+}$ transport upstream, but not always finely enough to prevent hypercalciuria. For instance, these two segments cannot fully counterbalance the abolition of $Ca^{2+}$ reabsorption along the entire TAL: under these conditions, the model predicts a 8-fold increase in urinary $Ca^{2+}$ excretion. It is difficult to compare these predictions with experimental data, since manoeuvers that abolish the passive reabsorption of $Ca^{2+}$ in the TAL (such as the administration of furosemide) typically affect the transport of NaCl as well, thereby altering the interstitial osmolality gradient and changing the driving force for $Ca^{2+}$ exchange across other nephron segments (see below).

It should be noted that in the absence of significant $Ca^{2+}$ transport across the CD epithelium, the concentration of $Ca^{2+}$ in the CD fluid increases approximately 10-fold from the CM junction

to the papillary tip, due to massive water reabsorption along that segment; this amplification means that seemingly small changes in the $Ca^{2+}$ load at the CCD entrance have a large impact on the urinary concentration of $Ca^{2+}$. As an illustration, when the filtered load of $Ca^{2+}$ is increased 2-fold, the fractional amounts of $Ca^{2+}$ reabsorbed along the TAL, DCT and CNT are very similar to base case values, and the fractional $Ca^{2+}$ load that is delivered to the CCD increases by 0.6% only (Table 5). This variation nevertheless represents a 2-fold increase relative to the base case, and the predicted $C_{out}$ increases by a similar factor, from 2.0 to 4.7 mM.

**Interstitial $Ca^{2+}$ concentration gradient**

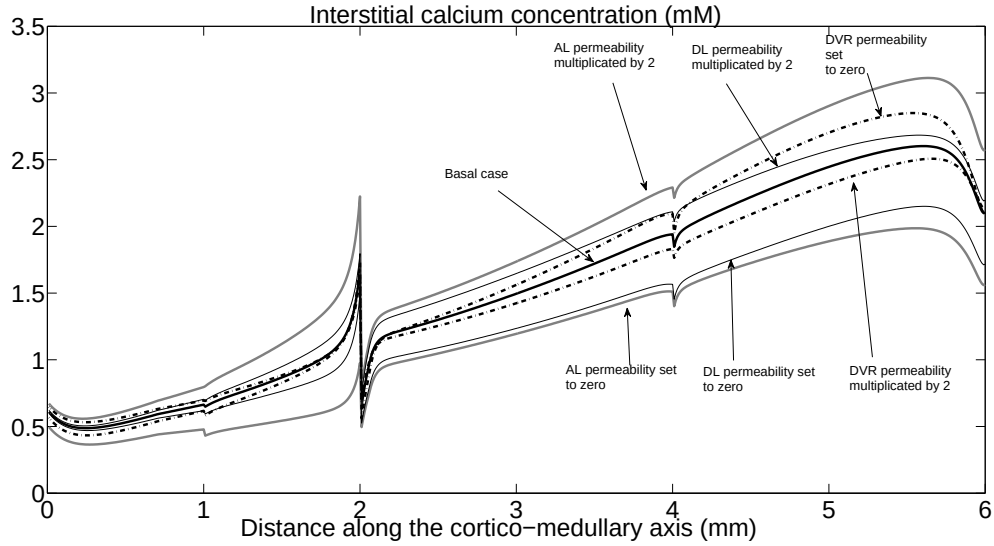


**Figure 9.6:** Predicted $Ca^{2+}$ interstitial concentration

In the base case, the average interstitial $Ca^{2+}$ concentration is predicted as 0.74 mM in the OM, and 1.78 mM in the IM (Figure 9.6). These results suggest that a significant interstitial $[Ca^{2+}]$ gradient develops along the medullary axis, if the limbs of Henle and vasa recta are not fully impermeable to $Ca^{2+}$. As described above, we estimated the thin limb permeability to $Ca^{2+}$ in rats by extrapolating rabbit data, but there may be significant inter-species differences. The resulting values are small compared to the $Ca^{2+}$ permeability of the proximal tubules and cTALs, yet they are sufficient to allow some $Ca^{2+}$ to passively diffuse from the thin descending and ascending limbs to the interstitium. A similar amount of $Ca^{2+}$ is predicted to diffuse from the DVR as well. The interstitial $[Ca^{2+}]$ increases overall along the medullary axis because as water is reabsorbed from the descending limb, the concentration of $Ca^{2+}$ in the DL lumen rises, thereby increasing that in the interstitium as well.

Axial interstitial concentration gradients can be maintained because axial transport is negligible in the medullary interstitium: interstitial cells are stacked like the rungs of a ladder and their orientation impedes axial diffusion [57]. Likewise, we assumed no exchanges between the cortical and medullary interstitium, and the model therefore predicts a sharp discontinuity in the interstitial $[Ca^{2+}]$ at the CM junction. It is likely, however, that the change is more gradual in vivo.

**Interstitial osmolality gradient**

Our results suggest that the contribution of $Ca^{2+}$ to the axial osmolality gradient is generally negligible relative to that of NaCl and urea. As described above, the driving force behind the urinary concentrating mechanism in the inner medulla remains to be completely understood. None of the hypotheses that have been proposed in the last decades has been fully validated [17]. A recent model of the urinary concentrating mechanism that accounts for preferential interactions among tubules and vessels and for new permeability data was able to predict a substantial

urea gradient in the IM, but failed to reproduce the observed increase in sodium concentration along the IM axis [50]. Reasoning that the IM osmolality gradient could be important for $Ca^{2+}$ transport, we generated this gradient by adding an external osmolyte (Eq. (7.11)), a hypothesis initially proposed by Hargitay and Kuhn [33], revived by Jen and Stephenson [39] and subsequently probed by Wexler and Thomas [88] [89]. The HT model demonstrated that in principle, the accumulation of lactate (via anaerobic glycolysis) in the IM could drive water out of descending limbs and thereby amplify the IM osmolality gradient. This hypothesis has yet to be confirmed, and we did not include the transport of glucose and lactate in the current model. Our results indicate that the IM osmolality gradient has indeed a significant impact on $Ca^{2+}$ transport in the kidney. In the absence of such a gradient, the luminal fluid remains much more dilute, and the passive reabsorption of $Ca^{2+}$ along the loop of Henle is reduced (Table 9.1). Consequently, even though the DCT and CNT actively reabsorb slightly more $Ca^{2+}$ than in the base case, the fractional load delivered to the CCD equals 5.1% (vs. 0.6% in the base case). Nevertheless, since water abstraction in the CD is greatly diminished, the $Ca^{2+}$ concentration in the CD fluid at the papillary tip is about half its base case value (Table 9.3).

**Novelty of mathematical model**

Most models of solute transport in the medulla do not represent the cortical distal tubules, and instead specify steady state boundary conditions at the entrance to the medullary CD. We chose to explicitly include the cTAL, DCT, CNT, and CCD in our model because the DCT and the CNT are the nephron segments where $Ca^{2+}$ reabsorption is exquisitely regulated. Without their specific inclusion, we would not have been able to investigate the role of these segments in maintaining the $Ca^{2+}$ balance. In addition, adding these segments was necessary to build a dynamic model with arbitrary (i.e., non-steady state) initial conditions. Even though we focused on steady-state results in this study, a dynamic model has several advantages. The finite-volume type scheme that we developed is robust, in that it converges to the steady-state solution no matter what the initial conditions are. It is also relatively fast: reaching steady state usually requires less than 3 minutes of CPU time.

In summary, we have developed the first detailed model of calcium transport in the rat kidney. Our results suggest that $Ca^{2+}$ reabsorption profiles differ between superficial and deep nephrons. Our model also predicts the existence of an axial $Ca^{2+}$ concentration gradient in the medullary interstitium.

# Bibliography


[1] G. Allaire. *Analyse numérique et optimisation.* . Les éditions de l'école polytechnique, 2005.

[2] B. Andreianov, P. Goatin, and N. Seguin. Finite volume schemes for locally constrained conservation laws. *Numer. Math.*, 115(4):609–645, 2010. With supplementary material available online.

[3] E. Audusse and B. Perthame. Uniqueness for scalar conservation laws with discontinuous flux via adapted entropies. *Proc. Roy. Soc. Edinburgh Sect. A*, 135(2):253–265, 2005.

[4] A. Aw and M. Rascle. Resurrection of "second order" models of traffic flow. *SIAM J. Appl. Math.*, 60(3):916–938 (electronic), 2000.

[5] J. M. Ball. A version of the fundamental theorem for Young measures. In *PDEs and continuum models of phase transitions (Nice, 1988)*, volume 344 of *Lecture Notes in Phys.*, pages 207–215. Springer, Berlin, 1989.

[6] C. Bardos, F. Golse, and D. Levermore. Fluid dynamic limits of kinetic equations. I. Formal derivations. *J. Statist. Phys.*, 63(1-2):323–344, 1991.

[7] C. Bardos, A. Y. le Roux, and J.-C. Nédélec. First order quasilinear equations with boundary conditions. *Comm. Partial Differential Equations*, 4(9):1017–1034, 1979.

[8] C. Berthon, C. Chalons, and R. Turpault. Asymptotic-preserving Godunov-type numerical schemes for hyperbolic systems with stiff and non-stiff relaxation terms. *Preprint*, 2012.

[9] F. Bouchut. *Non linear stability of finite volume methods for hyperbolic conservation laws and well balanced schemes for sources.* Birkhaüser-Verlag, 2004.

[10] Y. Brenier, L. Corrias, and R. Natalini. Relaxation limits for a class of balance laws with kinetic formulation. In *Advances in nonlinear partial differential equations and related areas (Beijing, 1997)*, pages 2–14. World Sci. Publ., River Edge, NJ, 1998.

[11] H. Brezis. *Functional Analysis.* Collection of Applied Mathematics for the Master's Degree. Masson, Paris, 1983. Theory and applications.

[12] D. A. Bushinsky, K. J Neumann, J. Asplin, and N. S. Krieger. Alendronate decreases urine calcium and supersaturation in genetic hypercalciuric rats. . *Kidney Int*, 55(4):234–243, 1999.

[13] C. Cercignani. *The Boltzmann equation and its applications*, volume 67 of *Applied Mathematical Sciences.* Springer-Verlag, New York, 1988.

[14] L. S. Costanzo. Comparison of calcium and sodium transport in early and late rat distal tubules: effect of amiloride. *Am J Physiol Renal Physiol*, 246:F937–F945, 1984.

[15] R. Courant, K. Friedrichs, and H. Lewy. On the partial difference equations of mathematical physics. *IBM J. Res. Develop.*, 11:215–234, 1967.

[16] C. M. Dafermos. *Hyperbolic conservation laws in continuum physics*, volume 325 of *Grundlehren der Mathematischen Wissenschaften [Fundamental Principles of Mathematical Sciences].* Springer-Verlag, Berlin, third edition, 2010.

[17] A. Edwards. A possible catalytic role for NH4+ in Na+ reabsorption across the thick ascending limb. *Am. J. Physio.l Renal*, (298):F510–F511, 2010.

[18] A. Edwards, N. Seguin, and M. Tournus. A finite-volume scheme for a kidney nephron model. *ESAIM: Proc.*, 35-Congrès National de Mathématiques Appliquées et Industrielles:287–292, 2012.

[19] L. C. Evans. *Partial differential equations*, volume 19 of *Graduate Studies in Mathematics.* American Mathematical Society, Providence, RI, second edition, 2010.

[20] F. Filbet and S. Jin. A class of asymptotic-preserving schemes for kinetic equations and related problems with stiff sources. *J. Comput.. Phys.*, 229(20):7625–7648, 2010.

[21] F. Filbet and A. Rambaud. Analysis of an Asymptotic Preserving Scheme for Relaxation Systems. *ESAIM: Mathematical Modelling and Numerical Analysis*, 47:609–633.

[22] A. Friedman and G. Craciun. A model of intracellular transport of particles in an axon. *J. Math. Biol.*, 51(2):217–246, 2005.

[23] C. Făciu and M. Mihăilescu-Suliciu. The energy in one-dimensional rate-type semilinear viscoelasticity. *Internat. J. Solids Structures*, 23(11):1505–1520, 1987.

[24] J. B. Garner and R. B. Kellogg. Existence and uniqueness of solutions in general multisolute renal flow problems. *Journal of Mathematical Biology*, 26:455–464, 1988. 10.1007/BF00276373.

[25] E. Godlewski and P.-A. Raviart. *Numerical approximation of hyperbolic systems of conservation laws*, volume 118 of *Applied Mathematical Sciences*. Springer-Verlag, New York, 1996.

[26] F. Golse, P. L. Lions, B. Perthame, and R. Sentis. Regularity of the moments of the solution of a transport equation. *J. Funct. Anal.*, 76(1):110–125, 1988.

[27] F. Golse and F. Salvarani. The nonlinear diffusion limit for generalized Carleman models: the initial-boundary value problem. *Nonlinearity*, 20(4):927–942, 2007.

[28] L. Gosse and G. Toscani. An asymptotic-preserving well-balanced scheme for the hyperbolic heat equations. *C. R. Math. Acad. Sci. Paris*, 334(4):337–342, 2002.

[29] L. Gosse and G. Toscani. An asymptotic-preserving well-balanced scheme for the hyperbolic heat equations. *C. R. Math. Acad. Sci. Paris*, 334(4):337–342, 2002.

[30] L. Gosse and G. Toscani. Space localization and well-balanced schemes for discrete kinetic models in diffusive regimes. *SIAM J. Numer. Anal.*, 41(2):641–658 (electronic), 2003.

[31] J. M. Greenberg and A. Y. Leroux. A well-balanced scheme for the numerical processing of source terms in hyperbolic equations. *SIAM J. Numer. Anal.*, 33(1):1–16, 1996.

[32] B. Hargitay and K. Werner. The Multiplication Principle as the Basis for Concentrating Urine in the Kidney(with comments by Bart Hargitay and S. Randall Thomas). *J Am Soc Nephrol*, 12(7):1566–1586, 2001.

[33] V. B. Hargitay and W. Kuhn. Das multiplikationsprinzip als grundlage der harnkonzentrierung in der niere. *Z Elektrochem*, 55:539–558, 1951.

[34] S Hervy and S. R. Thomas. Inner medullary lactate production and urine-concentrating mechanism: a flat medullary model. *Am J Physiol Renal Physiol*, 284:F65–F8, 2003.

[35] A. Hoznek, S. Larré, L. Salomon, A. De La Taille, and C.-C. Abbou. Néphrectomie partielle par voie laparoscopique. *Annales d'Urologie*, 41(3):134–144, 2007.

[36] F. James. Convergence results for some conservation laws with a reflux boundary condition and a relaxation term arising in chemical engineering. *SIAM J. Math. Anal.*, 29(5):1200–1223 (electronic), 1998.

[37] R.L. Jamison, N.R. Frey, and F.B. Lacy. Calcium reabsorption in the thin loop of Henle. *American Journal of Physiology - Renal Physiology*, 751(6):F227–F745, 1974.

[38] K.S. Crump J.B. Garner and J.L. Stephenson. Transient behaviour of the single loop solute cycling model of the renal medulla. *Bulletin of Mathematical Biology*, 40:273–300, 1978.

[39] J. F. Jen and Stephenson J. L. Externally driven countercurrent multiplication in a mathematical model of the urinary concentrating mechanism of the renal inner medulla. *Bulletin of Mathematical Biology*, 56:491–514, 1994.

[40] Hoenderop J.G., Dimke H., and Bindels R.J. Hereditary tubular transport disorders: implications for renal handling of Ca and Mg. *Clin Sci (Lond)*, 2010.

[41] S. Jin. Asymptotic preserving (AP) schemes for multiscale kinetic and hyperbolic equations: a review. *Riv. Math. Univ. Parma*, 3:177–216, 2012.

[42] S. Jin and Z. P. Xin. The relaxation schemes for systems of conservation laws in arbitrary space dimensions. *Comm. Pure Appl. Math.*, 48(3):235–276, 1995.

[43] M. A. Katsoulakis and A. E. Tzavaras. Contractive relaxation systems and the scalar multidimensional conservation law. *Comm. Partial Differential Equations*, 22(1-2):195–233, 1997.

[44] J. Keener and J. Sneyd. *Mathematical physiology. Vol. II: Systems physiology*, volume 8/ of *Interdisciplinary Applied Mathematics*. Springer, New York, second edition, 2009.

[45] C. Klingenberg and Y. Lu. The Cauchy problem for hyperbolic conservation laws with relaxation terms: a conference report. *Mat. Contemp.*, 11:53–60, 1996. Fourth Workshop on Partial Differential Equations, Part II (Rio de Janeiro, 1995).

[46] S. N. Kružkov. First order quasilinear equations with several independent variables. *Mat. Sb. (N.S.)*, 81 (123):228–255, 1970.

[47] E. W. Larsen and J. E. Morel. Asymptotic solutions of numerical transport problems in optically thick, diffusive regimes. II. *J. Comput. Phys.*, 83(1):212–236, 1989.

[48] E. W. Larsen, J. E. Morel, and Jr. W. F. Miller. Asymptotic solutions of numerical transport problems in optically thick, diffusive regimes. *J. Comput. Phys.*, 69(2):283–324, 1987.

[49] C. Lattanzio and A. E. Tzavaras. Structural properties of stress relaxation and convergence from viscoelasticity to polyconvex elastodynamics. *Arch. Ration. Mech. Anal.*, 180(3):449–492, 2006.

[50] A. T. Layton. A mathematical model of the urine concentrating mechanism in the rat renal medulla: I. Formulation and base-case results. *Am J Physiol Renal Physiol*, (300):F356–F371, 2011.

[51] A.T. Layton. A methodology for tracking solute distribution in a mathematical model of the urine concentrating mechanism. *Journal of Biological System*, 13(4):1–21, 2005.

[52] A.T. Layton and H.E. Layton. A semi-Lagrangian semi-implicit numerical method for models of the urine concentrating mechanism. *SIAM Journal on Scienfic Computing*, 23:1526–1548, 2002.

[53] H. Layton and E. Pitman. A dynamic numerical method for models of renal tubules. *Bulletin of Mathematical Biology*, 56:547–565, 1994.

[54] H. E. Layton, E. Bruce Pitman, and Mark A. Knepper. A dynamic numerical method for models of the urine concentrating mechanism. *SIAM J. Appl. Math.*, 55:1390–1418, October 1995.

[55] H.E. Layton. Distribution of Henle's loops may enhance urine concentrating capability. *Biophysical Journal*, 49(5):1033–1040, 1986.

[56] H.E. Layton. Existence and uniqueness of solutions to a mathematical model of the urine concetrating mechanism. *Mathematical Biosciences*, 84, 1987.

[57] W Lemley and K. V. Kriz. Anatomy of the renal interstitium. *Kidney Int*, (39):370–381, 1991.

[58] R. J. LeVeque. *Finite volume methods for hyperbolic problems*. Cambridge University Press, 2002.

[59] P.-L. Lions, B. Perthame, and E. Tadmor. A kinetic formulation of multidimensional scalar conservation laws and related equations. *J. Amer. Math. Soc.*, 7(1):169–191, 1994.

[60] T.P. Liu. Hyperbolic conservation laws with relaxation. *Comm. Math. Phys.*, 108(1):153–175, 1987.

[61] A. J. Magaldi, A. A. van Baak, and A. S. Rocha. Calcium transport across rat inner medullary collecting duct perfused in vitro. *Am J Physiol Renal Physiol*, November 1:257:F738–F745, 1989.

[62] D.J. Marsh, R. B. Kelman, and H.C. Howard. The theory of urine formation in water diuresis with implications for anti-diuresis. *Bull. Math. Biophysics*, 29:67-89, 1967.

[63] L. C. Moore and D. J. Marsh. How descending limb of Henle's loop permeability affects hypertonic urine formation. *Am.J.Physiol*, (239):F57–F71, 1980.

[64] F. Murat. Compacité par compensation. *Ann. Scuola Norm. Sup. Pisa Cl. Sci. (4)*, 5(3):489–507, 1978.

[65] R. Natalini. Convergence to equilibrium for the relaxation approximations of conservation laws. *Comm. Pure Appl. Math.*, 49(8):795–823, 1996.

[66] R. Natalini. Recent results on hyperbolic relaxation problems. In *Analysis of systems of conservation laws (Aachen, 1997)*, volume 99 of *Chapman & Hall/CRC Monogr. Surv. Pure Appl. Math.*, pages 128–198. Chapman & Hall/CRC, Boca Raton, FL, 1999.

[67] R. Natalini and A. Terracina. Convergence of a relaxation approximation to a boundary value problem for conservation laws. *Comm. Partial Differential Equations*, 26(7-8):1235–1252, 2001.

[68] S. Nishibata and S. H. Yu. The asymptotic behavior of the hyperbolic conservation laws with relaxation on the quarter-plane. *SIAM J. Math. Anal.*, 28(2):304–321, 1997.

[69] F. Otto. Initial-boundary value problem for a scalar conservation law. *C. R. Acad. Sci. Paris Sér. I Math.*, 322(8):729–734, 1996.

[70] B. Perthame. Lecture notes on kinetic formulation of conservation laws. In *Some current topics on nonlinear conservation laws*, volume 15 of *AMS/IP Stud. Adv. Math.*, pages 111–140. Amer. Math. Soc., Providence, RI, 2000.

[71] B. Perthame. *Kinetic formulation of conservation laws*, volume 21 of *Oxford Lecture Series in Mathematics and its Applications*. Oxford University Press, Oxford, 2002.

[72] B. Perthame. *Transport equations in biology*. Frontiers in Mathematics. Birkhäuser Verlag, Basel, 2007.

[73] S. Ramakrishnan, A. Loupy, A. Edwards, D.A. Bushinsky, and P. Houillier. Genetic hypercalciuria stone-forming rats have a decrease in paracellular permeability to calcium in the cortical thick ascending limb . *J Am Soc Nephrol*, 23(43A):641–658 (electronic), 2012.

[74] A. S. and Magaldi J. B. Rocha and J. P. Kokko. Calcium and phosphate transport in isolated segments of rabbit Henle's loop. *The Journal of Clinical Investigation*, 59(5):975–983,, 1977.

[75] D. Rouse, R.C. Ng, and W. N. Suki. Calcium transport in the pars recta and thin descending limb of Henle of the rabbit, perfused in vitro. *The Journal of Clinical Investigation*, 65(4):37–42, 1980.

[76] F. Salvarani. Diffusion limits for the initial-boundary value problem of the Goldstein-Taylor model. *Rend. Sem. Mat. Univ. Politec. Torino*, 57(3):209–220 (2002), 1999.

[77] J. A. Sayer, G. Carr, and N.L. Simmons. Nephrocalcinosis: molecular insights into calcium precipitation within the kidney. *Clinical science*, 106:549–561, 2004.

[78] S.G. Schultz. *Basic Principles Of Membrane Transport*. IUPAB biophysics series 2. Cambridge University Press, 1980.

[79] L. Schwartz. *Théorie des distributions*. . Hermann, Paris, 1966.

[80] D. W. Selden and G. Giebisch. *The kidney: physiology and pathophysiology*. . Raven Press, New York, 1985.

[81] D. Serre. *Systèmes de lois de conservation. II.* Fondations. [Foundations]. Diderot Editeur, Paris, 1996. Structures géométriques, oscillation et problèmes mixtes. [Geometric structures, oscillation and mixed problems].

[82] D. Serre. *Matrices*, volume 216 of *Graduate Texts in Mathematics*. Springer, New York, second edition, 2010. Theory and applications.

[83] N. B. Siga, E. Roinel, and C. Rouffignac. Ca2+, Mg2+, and K+ transport in the cortical and medullary thick ascending limb of the rat nephron: influence of transepithelial voltage. *Pflügers Archiv European Journal of Physiology*, 424(4):558–560, 1993.

[84] J. L. Stephenson. *Urinary concentration and dilution: Models.* Oxford University Press, New-York, 1992.

[85] L. Tartar. Compacité par compensation: résultats et perspectives. In *Nonlinear partial differential equations and their applications. Collège de France Seminar, Vol. IV (Paris, 1981/1982)*, volume 84 of *Res. Notes in Math.*, pages 350–369. Pitman, Boston, MA, 1983.

[86] L. Tartar. The compensated compactness method applied to systems of conservation laws. In *Systems of nonlinear partial differential equations (Oxford, 1982)*, volume 111 of *NATO Adv. Sci. Inst. Ser. C Math. Phys. Sci.*, pages 263–285. Reidel, Dordrecht, 1983.

[87] L. Tartar. *The general theory of homogenization*, volume 7 of *Lecture Notes of the Unione Matematica Italiana*. Springer-Verlag, Berlin, 2009. A personalized introduction.

[88] S. R. Thomas. Inner medullary lactate production and accumlation: a vasa recta model. *Am.J.Physiol*, (279):F468–F481, 2000.

[89] Wexler S. A. Thomas S. R. and. Inner medullary external osmotic driving force in a 3-D model of the renal concentrating mechanism. *Am.J.Physiol*, (269):F159–71, 1995.

[90] M. Tournus. An asymptotic study to explain the role of active transport in models with countercurrent exchangers. *SeMA Journal: Boletín de la Sociedad Española de Matemática Aplicada*, 59:19–35, 2012.

[91] M. Tournus, A. Edwards, N. Seguin, and B. Perthame. Analysis of a simplified model of the urine concentration mechanism. *Network Heterogeneous Media*, 7(7):989 – 1018, 2012.

[92] M. Tournus, N. Seguin, B. Perthame, S.R. Thomas, and A. Edwards. A Model of Calcium Transport along the Rat Nephron. *Accepted in the Am J. Physiol. Renal Physiol*, 2012.

[93] A. Vasseur. Strong traces for solutions of multidimensional scalar conservation laws. *Arch. Ration. Mech. Anal.*, 160(3):181–193, 2001.

[94] W. C. Wang and Z. Xin. Asymptotic limit of initial-boundary value problems for conservation laws with relaxational extensions. *Comm. Pure Appl. Math.*, 51(5):505–535, 1998.

[95] A. M. Weinstein. A mathematical model of rat cortical collecting duct: determinants of the transtubular potassium gradient. *American Journal of Physiology - Renal Physiology*, 280(6):F1072–F1092, 2001.

[96] A. M. Weinstein. A mathematical model of rat distal convoluted tubule. I. Cotransporter function in early DCT. *American Journal of Physiology - Renal Physiology*, 289(4):F699–F720, 2005.

[97] A. M. Weinstein. A mathematical model of rat distal convoluted tubule. II. Potassium secretion along the connecting segment. *American Journal of Physiology - Renal Physiology*, 289(4):F721–F741, 2005.

[98] G.B. Whitham. *Linear and Nonlinear Waves*. Pure and Applied Mathematics: A Wiley Series of Texts, Monographs and Tracts. Wiley, 2011.

[99] M. Wittner, A. Stefano, P. Wangemann, R. Nitschke, R. Greger, C. Bailly, C. Amiel, N. Roinel, and C. Rouffignac. Differential effects of ADH on sodium, chloride, potassium, calcium and magnesium transport in cortical and medullary thick ascending limbs

of mouse nephron. *Pflügers Archiv European Journal of Physiology*, 412:516–523, 1988. 10.1007/BF00582541.

[100] Z. Xin and W. Q. Xu. Stiff well-posedness and asymptotic convergence for a class of linear relaxation systems in a quarter plane. *J. Differential Equations*, 167(2):388–437, 2000.

[101] S. Y. Zhang and Y. G. Wang. Well-posedness and asymptotics for initial boundary value problems of linear relaxation systems in one space variable. *Z. Anal. Anwendungen*, 23(3):607–630, 2004.